Dissertation

submitted to the
Combined Faculties for the Natural Sciences and for Mathematics
of the Ruperto-Carola University of Heidelberg, Germany
for the degree of
Doctor of Natural Sciences

presented by
Dipl.-Biol. Christoph Schiklenk
born in Braunschweig
Oral examination: 29th November 2016

Characterization of *Schizosaccharomyces pombe* chromosome condensation factor Zas1

Referees: Dr. Rainer Pepperkok

Prof. Dr. Michael Knop

Summary

Every second, more than three million cells divide in the human body (Notta et al., 2016). Whenever a cell divides, it segregates its genetic information encoded on its chromosomes to its daughter cells. Failure to successfully segregate chromosomes can compromise viability of the daughter cells or lead to cancer. Therefore, a complex cell division machinery has evolved that first compacts the two meters of human DNA and then distributes it to the cell poles, before the approximately 20-micron-diameter human cell splits into two genetically identical daughter cells. This compaction of chromatin – called chromosome condensation – is one of the least understood processes of cell division. In order to be able to probe chromosome condensation, a microscopy-based chromosome condensation assay had been developed in the fission yeast *S. pombe*, which employs locus-specific labeling. A screen using this assay identified three alleles conferring temperature sensitivity of the poorly characterized gene *zas1* in which chromosome condensation is defective (Petrova, 2012).

In this thesis, I characterize *zas1* and show that its function depends on its zinc finger domains and an E2F-like short linear motif peptide sequence, which had not been reported previously in unicellular organisms. I discover that Zas1 enhances the transcription of the condensin subunit *cnd1*, explaining the condensation defect in *zas1* mutants. This is the first report of a transcription factor for a condensin subunit in *S. pombe*.

In the second part of the thesis, I improve the chromosome condensation assay by creating a computational pipeline for automated image processing and data analysis. These optimizations allow me to probe experiment-to-experiment variability and reveal a positive correlation between chromosome label spacing and condensation rate. This correlation shows that the activity of condensation is distributed along the chromosome arm. Optimization of the microscopy setup and the computational pipeline also allow me to resolve the axial contraction of chromosomes during mitosis at the single cell level. I observe linear compaction and minute-scale oscillations before final compaction. Finally, I establish improved versions of the chromatin labels by adapting non-recombinable tetracyclin operator arrays for *S. pombe*.

Zusammenfassung

Pro Sekunde teilen sich mehr als 3 Millionen Zellen im menschlichen Körper (Notta et al., 2016). Bei jeder dieser Zellteilungen muss die korrekte Verteilung der Chromosomen - die Träger der genetischen Information - gewährleistet werden. Ist die Verteilung der genetischen Information ungleichmäflig, z. B. aufgrund eines fehlenden oder überschüssigen Chromosoms, kommt es zum Tod der betroffenen Tochterzelle oder Krebs. So hat sich eine faszinierend zuverlässige Machinerie entwickelt, die in der Mitose die etwa 2 Meter menschlicher DNA zuerst eng verpackt und dann an die Zellpole transportiert, sodass sich die etwa 20 Mikrometer große Zelle durchschnüren kann. Die Kompaktierung des Chromatins - genannt Chromosomenkondensation - ist eines der am wenigsten verstandenden Prozesse der Zellteilung. Um die Chromosomenkondensation besser untersuchen zu können, ist ein Mikroskopie basiertes Chromosomenkondensationsmessverfahren in der Spalthefe *S. pombe* entwickelt worden, welches auf spezifischer Fluoreszenzmarkierung zweier Loci beruht. Mittels dieses Messverfahrens wurden aus einer Kollektion zufälliger, wärmeempfindlicher Mutanten drei Allele des zuvor kaum charakterisierten Gens *zas1* identifiziert, bei denen die Chromosomenkondensation beeinträchtigt ist (Petrova, 2012). In der vorliegenden Arbeit charakterisiere ich *zas1* und zeige, das seine Funktion von seinen Zinkfinger Domänen und einer kurzen, E2F-ähnlichen Peptidsequenz, welche zuvor noch nie in Einzellern beschrieben wurde, abhängt. Ich stelle fest, dass Zas1 die Transkription der Condensin-Untereinheit *Cnd1* reguliert, was den Kondensationsdefekt in *zas1* Mutanten erklärt. Damit wird zum ersten Mal eine Transkriptionsfaktor für eine Condensin-Untereinheit in *S. pombe* beschrieben. Im zweiten Teil der Arbeit verbessere ich das Chromosomenkondensationsmessverfahren, indem ich die rechnergestützte Bildverarbeitung und Datenanalyse weitestgehend automatisiere. Diese Optimierungen ermöglichen es, die Variabilität zwischen Experimenten zu messen. Gleichzeitig offenbart sich ein positiver Zusammenhang von Kondensationsrate mit der Distanz zwischen den Fluoreszenzmarkierungen. Diese Korrelation zeigt, dass die Kondensationsaktivität entlang des Chromosomenarms verteilt ist. Weitere Optimierung der Mikroskopkonfiguration und die Verbesserungen in der Datenverarbeitung erlauben es, die longitudinale Verkürzung der Chromosomen auf Einzelzellebene aufzulösen. Dies führt zur Beobachtung von longitudinalen Oszillationen und offenbart, dass die Kondensation linear verläuft. Schließlich etabliere ich eine verbesserte Version der Chromatin Markierung, indem ich nicht-rekombinierbare Tetracyclin Operator Wiederholungssequenzen für *S. pombe* adaptiere.

Für meine Eltern
und meine Großeltern.

Contents

Acknowledgements **199**

List of Acronyms

EDTA ethylenediaminetetraacetic acid xvi
EGFR epidermal growth factor receptor 2
ELM Eukaryotic Linear Motif database 40
EMBL European Molecular Biology Laboratory 43
EtOH Ethanol 114
ER endoplasmatic reticulum
FFT Fast Fourrier Transformation 20
FLIM fluorescence-lifetime imaging 13
FISH Fluorescence *in situ* hybridization 5
FOV field of view 21
FP Fluorescent Protein 13
FRET Förster resonance energy transfer 13
FROS fluorescent repressor operator system 14
FR Fluorescent repressor 30
FWHM full width at half maximum 136
MALS multi-angle light scattering 58
MW mass weight 58
GEF Guanosine Exchange Factor
HEAT Huntingtin, EF3, PP2A and TOR1 7
SAC spindle assembly checkpoint 4
GFP green fluorescent Protein 13
GUI Graphical User Interface 22
HA Haemagglutinin 34
nr-tetO non-recombining tet operator array 86
H2A histone 2 A
H2B histone 2 B 13
HU hydroxyurea 98
HRP horse radish peroxidase 127
HAT histone acetyltransferase 77
IMAC immobilized metal ion affinity chromatography 43
ITC isothermal titration calorimetry 95
IP immunoprecipitation 47
IPTG isopropyl β-D-1-thiogalactopyranoside 124
IgG immunoglobulin G
LacI Lac repressor protein 14
lacO lac operator DNA sequence 14
lncRNA long non coding RNA 25
MACS Model-based Analysis of ChIP-Seq Data 50

MAP Microtubule Associated Protein
MAPK mitogen-activated protein kinase 2
Mb megabases
mRNA messenger Ribonucleic Acid (RNA) 25
mTOR mechanistic target of rapamycin 2
NAA 1-Naphthaleneacetic acid 34
ncRNA non-coding RNA 50
NEB nuclear envelope breakdown 8
NGS Next Generation Sequencing 12
NLS Nuclear Localization Sequence 14
nt nucleotides
OD Optical Density 39
ORF Open Reading Frame 25
ori origin of replication 117
PCR Polymerase Chain Reaction ix
PMSF Phenylmethane Sulfonyl Fluoride 56
pFR fluorescent repressor expression plasmid
POI Protein Of Interest 47
pRb Retinoblastoma susceptibility protein 2
PVDF polyvinylidene fluoride
RE Regular Expression 63
RF Restriction free 117
RNA Ribonucleic Acid xv
ROI Region Of Interest 20
LB lysogeny broth
rRNA ribosomal RNA 132
RT room temperature 115
RNAi RNA interference 17
RT-qPCR reverse transcriptase quantitative PCR 98
SAC spindle assembly checkpoint 4
SAXS small angle X-ray scattering 11
RT-PCR reverse transcriptase PCR 40
ssDNA single stranded DNA 7
SDS-PAGE Sodium dodecyl sulfate (SDS) poly acrylamide gel electrophoresis 43
SDS Sodium dodecyl sulfate xv
SEC size exclusion chromatography 43
SMC structural maintenance of chromosomes 5
SPB spindle pole body 101

SPRI solid phase reversible immobilization 120
TAD topologically associated domain 17
TAE Tris-Acetate ethylenediaminetetraacetic acid (EDTA) 139
tetO tetracyclin operator DNA sequence 14
TetR tetracyclin repressor protein 14
TF transcription factor 2
tif tagged image file format 62
TIRF total internal reflection fluorescence 136
tRNA transfer RNA 25
TR transcribed region 51
ts thermosensitive 21
USER uracil-specific excision reagent 121
UV ultraviolet 12
UTR untranslated region 32
wt wild type 22
ZF zinc finger 25

Chapter 1

Introduction

1.1 Cells are the fundamental units of life

All living organisms from Bacteria and Archaea to plants and animals are built of cells, the fundamental units of life. All cells are surrounded by a lipid bilayer which isolates them from their environment and share many remarkable features and capabilities, including responsiveness to their environment and assimilation of matter.
One of their most remarkable capabilities is their own reproduction. Because all cells have originated from division of a parental cell this proliferative capability is a central prerequisite for evolution and for growth and development in multicellular organisms, including humans (Remak, 1854; Virchow, 1855). The basis for reproduction is the transmission of the cell's genetic information - encoded in its deoxyribonucleic Acid (DNA) (Avery et al., 1944) - to two daughter cells. Cells achieve this transmission of the genetic information an orchestrated series of events, called the cell cycle.

1.2 The cell cycle

Certain universal characteristics are common to all proliferating eukaryotic cells. Proliferating cells have to increase their cell mass by growth, while first replicating their genome, then correctly distributing each genome copy to each daughter cell to finally separate the physical connections. The cell follows this chronological order of events to ensure duplication. To achieve the correct order of events, cell cycle progression is controlled by a system of cyclin-cyclin dependent kinases (CDKs) complexes. CDKs activity and substrate specificity depends on the type of cyclin it interacts with. Degradation of the cyclins after each phase ensures unidirectionality of cell cycle progression. Due to this unidirectionality, cells have to complete a full round of the cell cycle once they committed to it. In addition to the cyclin-CDKs complexes, biochemical pathways called checkpoints control cell cycle progression by delaying initiation of the next event, if the previous one has not been completed.

1.2.1 Cell cycle commitment

Because cell cycle progression can not be reversed upon initiation, cells must tightly control their proliferation. For example, it is detrimental for a cell to enter the cell cycle when insufficient nutrients are available to synthesize the required components for replication and growth. In multicellular organisms this mechanism is central to suppress uncontrolled proliferation, known as cancer. Hence, cell cycle entry is blocked in the absence of mitogens and nutrients by a checkpoint called *Start* in yeast and *restriction point* in mammalian cells.
Extracellular signals (growth factors, nutrients) are sensed on the cell surface by receptors (e. g. epidermal growth factor receptor (EGFR), tyrosine kinase) and this information is integrated via signaling pathways (e. g. the mitogen-activated protein kinase (MAPK) pathway or the mechanistic target of rapamycin (mTOR) pathway). In mammalian cells, this signaling ultimately results in expression of the *myc* gene, which activates a G_1 CDK (Alberts et al., 2014, pp. 1103). The G_1 CDK phosphorylates the tumor suppressor Retinoblastoma susceptibility protein (pRb) (Rubin, 2013). In its un-phosphorylated state, pRb binds and thereby inhibits E2F transcription factors (TFs) and additionally recruits co-repressor proteins. The inhibitory pRb-E2F interaction is based on two contacts. First, E2F's C-terminal transactivation domain ($E2F^{TD}$), binds to the cleft of the central pocket domain of pRb. This strong interaction is mediated by a short linear motif (the pABgroove motif) in the $E2F^{TD}$ (Xiao et al., 2003). Second, pRb's C-terminal domain interacts with E2F's marked box domain. This interaction is weaker than the $E2F^{TD}$-pocket domain interaction. Upon phosphorylation by the CDK-cyclin complex, pRb dissociates from E2F TFs, initiating transcription of cell cycle progression genes, most importantly G_1/S cyclins (Alberts et al., 2014, pp. 1103).
In *S. cerevisiae* and *S. pombe*, a mechanistically similar mechanism exists, although the components are not homologous to those of mammalian cells. Structural homologs of pRb have not been described in neither *S. cerevisiae* nor *S. pombe*. It is clear though, that the pRb system was present in the last common ancestor of yeast and animals, because plants regulate their cell cycle via a pRb homolog. In *S. cerevisiae*, the functional analog to pRb - Whi5 - binds to the SBF complex (Swi4 and Swi6, in *S. pombe* Res1 and Cdc10). Whi5 dissociates from SBF upon phosphorylation, which activates the transcription of cyclins *cln1* and *cln2* and initiates DNA replication (Medina et al., 2016). Thereby, cell cycle is irreversibly started and the cell progresses to S-phase.

1.2.2 DNA is replicated during S-phase

After committing to the cell cycle, cells enter synthesis (S)-phase. During S-phase, the cell replicates its genomic DNA in a semi-conservative way (Meselson and Stahl, 1958). In eukaryotic cells, multiple origins initiate replication to be able to timely finish replication. This gives rise to two sister chromatids which are held together through topological entrapment by the cohesin complex (Haering et al., 2008). When replication is complete, the cell enters a second gap-phase (G_2 phase).

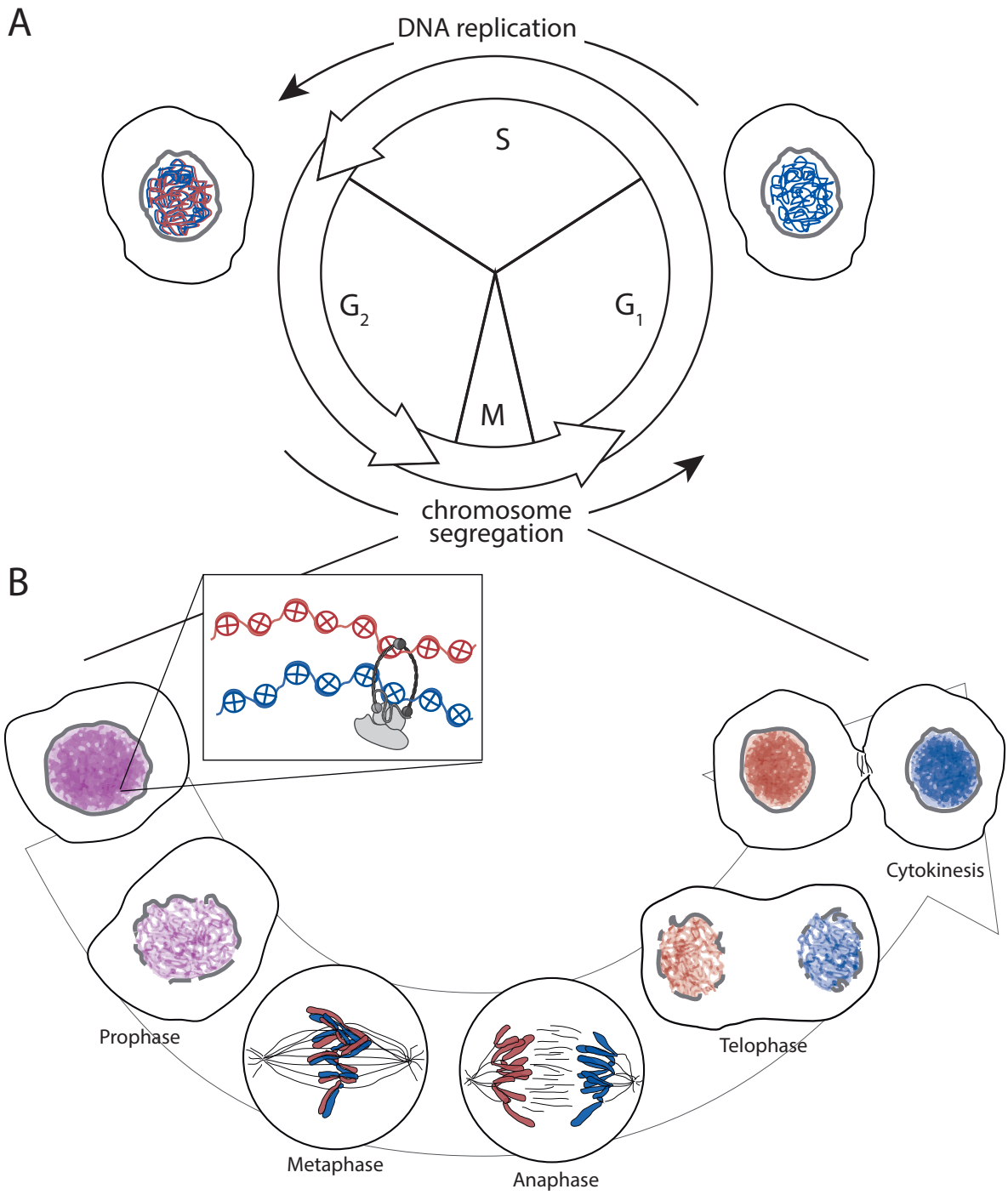

Figure 1.1: Schematic overview over the cell cycle. (A) Schematic overview over the cell cycle phases. After cell cycle commitment in G_1-phase, the genome is replicated in S-phase. The G_2 phase cell contains two copies of the genome, which are encoded on cohesed sister chromatids. (B) Sister chromatids are held together by the cohesin complex and segregated during mitosis. Detailed description in the main text.

1.2.3 Sister chromatids are segregated during mitosis

After replication is completed and the cell has reached a sufficient size, mitosis (M-phase) is initiated. Mitosis or nuclear division can be divided into Prophase, Prometaphase, Metaphse, Anaphase and Telophase.
During Prophase, chromatin starts to condense and mitotic chromosomes form. In mammalian cells, the nuclear envelope disassembles during Prometaphase, while chromosomes continue to condense. In many yeast species like *S. cerevisiae* and *S. pombe* the nuclear envelope stays intact during cell division. In Prometaphase, the microtubule skeleton rearranges to form the spindle apparatus, which helps to align the individualized, fully condensed chromosomes in the metaphase plate. Microtubules attach to the kinetochores at the chromosome's centromeres. As soon as all chromosomes are bioriented, the spindle assembly checkpoint (SAC) stops inhibition of the anaphase promoting complex/cyclosome (APC/C). Only when biorientation is complete, the SAC activates the ubiquitin ligase APC/C to commence Anaphase. Among many other important substrates, the APC/C degrades M cyclins to promote cell cycle progression and degrades securin, which induces cleavage of centromeric cohesin by activation of separase (Uhlmann et al., 1999, 2000). This results in simultaneous movement of the sister chromatids towards the spindle poles. During Anaphase A, chromatids are pulled apart by kinetochore/microtubule activity. In Anaphase B, the spindle elongates to further separate the sister chomatids. In Telophase, chromosomes decondense at the cell pole. In mammalian cells, the nuclear envelope reforms. Finally, during cytokinesis in yeasts and animal cells, a contracting actin ring destroys the physical connection between the sister cells.

1.3 Mitotic chromosome condensation

The structure of DNA confronts the cell with two fundamental problems for segregation of chromosomes: First, interphase chromatin is entangled, a feature inherent to replication (Wang, 2002). These entanglements have to be resolved to segregate the chromosomes without mechanical damage. Second, the DNA molecules are orders of magnitude longer than the distance between the cell poles. For example, the long arm of human chromosome I is 125×10^6 basepair (bp) long, which corresponds to a stretched length of about 41 mm, assuming a 3.3 Å rise per bp in the B conformation (Watson and Crick, 1953; Mandelkern et al., 1981). Yet, the pole-to-pole distance of the mitotic spindle in a human HeLa cell is about 15 µm (Cai et al., 2009). Therefore, DNA packaging mechanisms have evolved, which disentangle and compact chromatin during interphase and especially cell division.
Chromosome condensation is the process during prophase in which interphase chromatin is disentangled and reorganized into compact, discrete rod-shaped entities called mitotic chromosomes. Mitotic chromosomes are segregated by the spindle apparatus, and continue to compact after segregation to clear the cytokinesis furrow (Mora-Bermúdez et al., 2007; Petrova et al., 2013). Chromosome condensation is such a drastic rearrangement of chromatin that it has been revealed by the simple light microscopy techniques available more than a century ago (Flem-

ming, 1878). It has since been studied by cytogenetic analysis, Giemsa staining and Fluorescence *in situ* hybridization (FISH) experiments, which revealed that the order of genes on interphase chromosomes approximately follows the order of genes on mitotic chromosomes (Langer-Safer et al., 1982; Baumgartner et al., 1991). This view has been recently confirmed by HiC analysis (Naumova et al., 2013).
Yet, how the cell compacts its chromatin at the molecular level, and what underlying molecular architecture gives rise to the elongated nature of mitotic chromosomes, has largely remained unclear (Uhlmann, 2013).

1.3.1 Condensin and Topoisomerase II organize mitotic chromosomes

So far, two key factors have been identified to be necessary for mitotic chromosome formation: topoisomerase II and the five-subunit condensin complex.

Topoisomerase II

In addition to histones, topoisomerase IIα (topo II) was one of the first proteins identified as a major component of metaphase chromosomes (Gasser et al., 1986). Its localization to the central axis of mitotic chromosomes led to the development of the scaffold model (section 1.3.2). The catalytically active topo II dimer cleaves one DNA double strand and passes another double strand through the cleavage-induced gap. This reaction is catalyzed in an ATP-dependent manner (Wang, 2002). Topoisomerases of type II can catenate or decatenate DNA strands or change the linking number of circular DNA (Schoeffler and Berger, 2005). In the cell, topo II might disentangle sister chromatids, but could in principle also lead to knotting of the same chromatin strand. In *S. pombe*, *top2* deficient cells display the characteristic 'cell untimely torn' cut phenotype and are not able to fully compact their chromosomes (Petrova, 2012; Petrova et al., 2013). In a *X. laevis* extract / chicken erythrocyte nuclei *in vitro* system, topo II is required for chromosome condensation (Adachi et al., 1991).

Condensin

Structure of Condensin Condensin was initially isolated and identified to be required for chromosome condensation in cell-free *X. laevis* egg extracts (Hirano et al., 1997). Condensin is a protein complex comprised of five subunits, which can be divided into two sub-complexes, the structural maintenance of chromosomes (SMC) heterodimer and the trimeric non-SMC subcomplex.
The SMC heterodimer consists of SMC2 and SMC4, which are called Cut14 and Cut3 in *S. pombe*. SMCs are a structurally conserved protein family also found in two other eukaryotic chromosome organizing complexes (Strunnikov et al., 1993). SMC1 and SMC3 are part of the cohesin complex (Michaelis et al., 1997). A third SMC containing protein complex is the SMC5/6 complex (Fousteri and Lehmann, 2000). Prokaryotes also contain SMC complexes, namely Smc/ScpAB or MukBEF (Hirano, 2016).

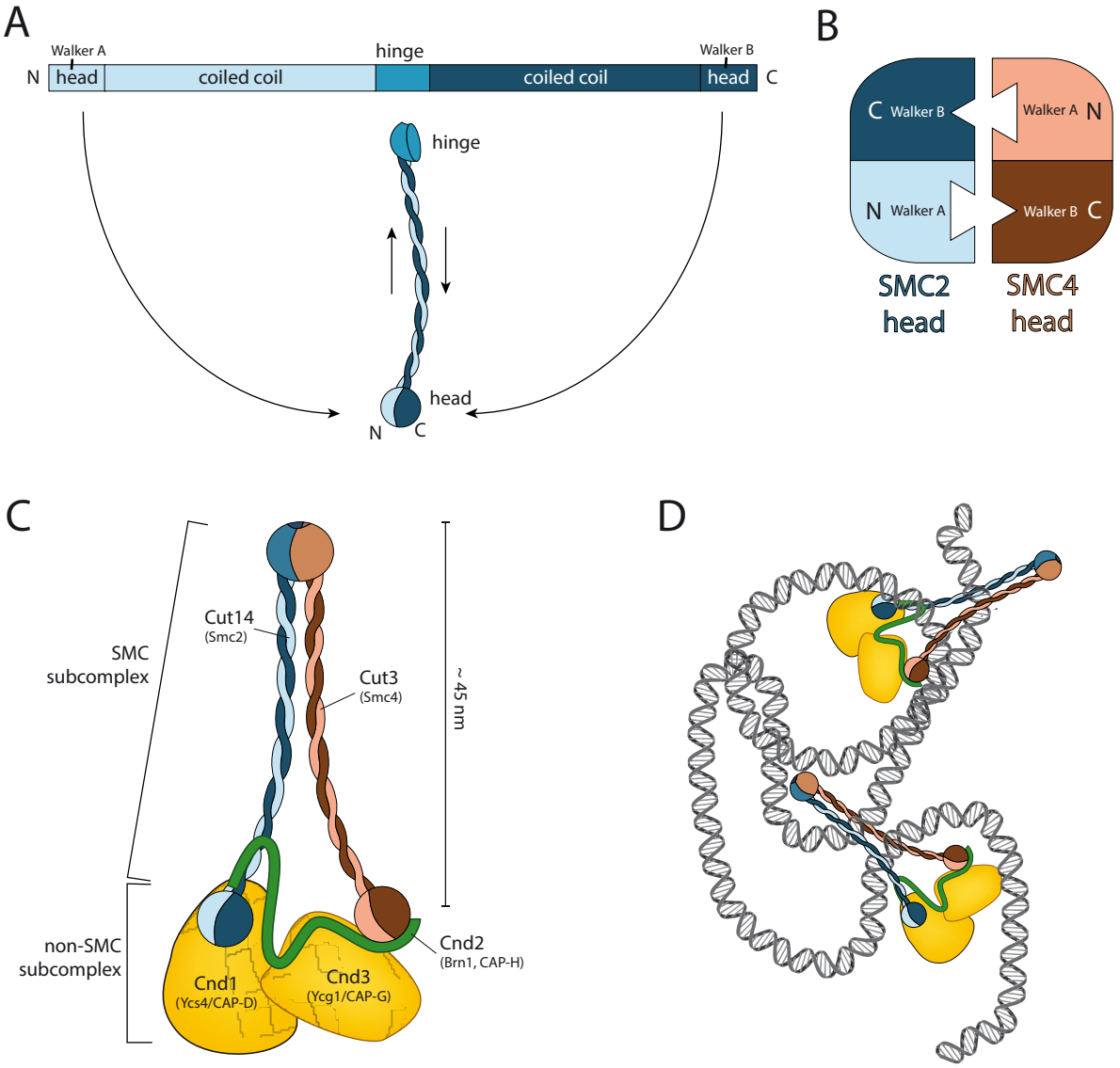

Figure 1.2: Molecular architecture of condensin. (A) Cartoon of a general SMC protein structure (B) Subunit arrangement of condensin, modified from (Haering and Gruber, 2016). *S. pombe* protein names are followed in brackets by *S. cerevisiae* and vertebrate protein ortholog names. (C) Topological entrapment of chromatin by condensin complexes.

All SMC proteins share a characteristic architecture. The center of the protein contains a so-called hinge domain. From this, peptide regions fold back onto each other to form an approximately 40 nm long, antiparallel coiled-coil (see fig. 1.2 A) (Melby et al., 1998; Haering et al., 2002). The length of the coiled-coil domains of SMC2 and SMC4 are conserved and highly flexible, at least in the absence of the trimeric complex (Eeftens et al., 2016). The antiparallel orientation of the coiled coils brings the N-terminal, adenosine triphosphate (ATP) binding site-containing domain (Walker A motif) and the C-terminal, Walker B motif-containing domain of one SMC molecule together (fig. 1.2 A), forming the so-called ATPase head domain. Yet, Walker A motif and Walker B motif from the same molecule do not form a functional ATPase. Only

dimerization with a second SMC juxtaposes the A and B Walker motifs from the individual monomers and forms two functional ATP binding cassette (ABC) ATPases (fig. 1.2 B).
The ATPase heads also serve as the interaction interface with the trimeric non-SMC subcomplex (fig. 1.2 C). The non-SMC subcomplex consists of a γ-kleisin subunit (called Cnd2 in *S. pombe*, Brn1 in *S. cerevisiae* and CAPH in vertebrates, Schleiffer et al. (2003)) and two Huntingtin, EF3, PP2A and TOR1 (HEAT) repeat proteins (Cnd1 and Cnd3 in *S. pombe*, Ycs4 and Ycg1 in *S. cerevisiae* and CAPD and CAPG in vertebrates). The N terminus of the kleisin interacts with Smc2 close to the head domain and the kleisin's C terminus interacts with the ATPase head of Smc4 (Onn et al., 2007). Both HEAT repeat proteins associate directly with the kleisin subunit. *S. cerevisiae* Ycg1 binds to a C-terminal region of Brn1, while Ycs4 has less well defined, binding site in the N-terminal part on Brn1. Both HEAT repeats subunits apparently make little or no contact with each other (Piazza et al., 2013).
Two isoforms of the non-SMC complex are present in multicellular animals (Ono et al., 2003). Both share the same SMC dimer, but contain different kleisin and HEAT repeat homologs. The non-SMCs of condensin I consist of chromosome associated protein (CAP)H, CAPD2 and CAPG, while condensin II consists of CAPH2, CAPD3 and CAPG2. Condensin I and II have different contributions to the formation of mitotic chromosomes (Hirota et al., 2004). In yeasts, all five condensin subunits are required for cell proliferation.

Activity of condensin Different DNA binding and modification activities have been reported for different subcomplexes from various organisms and *in vitro* systems, which at least in part contradict each other.
The *S. cerevisiae* and the *Chaetomium thermophilum* non-SMC complexes associate with micromolar affinity with free double stranded DNA (dsDNA) *in vitro*, but do not bind with high affinity to single stranded DNA (ssDNA) or nucleosomal DNA (Piazza et al., 2014). In contrast, the *S. pombe* non-SMC trimer appears to have only weak affinity to dsDNA *in vitro* (Sakai et al., 2003, Fig. 3C and D). Recent work has identified a conserved DNA binding site in *S. cerevisiae* Ycg1 (Kschonsak, unpublished results).
In contrast to the non-SMC subcomplex, the dimerized hinge of SMC2 and SMC4 binds to ssDNA with higher affinity than to dsDNA (Griese et al., 2010). The Cut3-Cut14 subcomplex overexpressed and isolated from *S. pombe* has ATP- independent ssDNA annealing activity (Sutani and Yanagida, 1997; Sakai et al., 2003). It has been claimed that this activity helps closing transcription bubbles during chromosome condensation (Sutani et al., 2015). The *X. laevis* condensin 13 S holocomplex binds to naked DNA *in vitro* and associates with higher affinity to cruciform DNA than to linear DNA (Kimura and Hirano, 1997).
Condensin's sister complex cohesin has been shown to be able to exhibit a special mode of DNA association. The SMCs and the kleisin form a tripartite ring in which sister chromatids are topologically entrapped (Haering et al., 2008). Based on this model, it has been shown that also condensin can topologically entrap artificial yeast minichromosomes *in vitro* (Frosi, unpublished results) and that this activity is required for correct chromosome segregation in *S.*

cerevisiae (Cuylen et al., 2011, 2013). A structural role for condensin in mitotic chromosomes as crosslinker of the chromatin fiber is therefore likely (fig. 1.2 D).
The ATPase activity of cohesin is required for its topological association with chromosomes (Arumugam et al., 2003). How topological entrapment is triggered for condensin has remained elusive. Although ATPase mutants of Smc2 and Smc4 are not viable, new data suggest that condensin's ATPase activity is not required for topological entrapment (Shaltiel, unpublished results). DNA can boost the weak ATPase activity of *S. cerevisiae* or *X. laevis* condensin holocomplex (Piazza et al., 2014; Kimura and Hirano, 1997).
When bound to dsDNA, condensin introduces bends or loops. This conclusion is based on the following two observations: First, in the presence of topoisomerase I (an enzyme that nicks dsDNA and re-ligates it after relaxation of supercoils), *X. laevis* condensin has been reported to change the linking number of circular DNA in an ATP-dependent manner (Kimura and Hirano, 1997). Second, the *S. cerevisiae* Smc2/4 dimers are sufficient to promote topo II-induced DNA knotting and coiling (Stray and Lindsley, 2003; Stray et al., 2005). This activity is not time-dependent, but condensin concentration-dependent, again indicating a structural role in conjunction with topological DNA binding for the formation of mitotic chromosomes.
It remains unclear whether the effects described above are due to a single underlying activity or whether the condensin complex exhibits multiple molecular activities. Most importantly, how these activities found *in vitro* are orchestrated *in vivo* to promote the formation of rod-shaped mitotic chromosomes has remained elusive.

Localization and activity of condensin *in vivo* In *S. pombe*, the bulk of condensin localizes to the cytoplasm during interphase and gets imported into the nucleus at the beginning of mitotis (Sutani et al., 1999) in an importin α (Cut15)-dependent manner (Matsusaka et al., 1998). It has been reported that a small number of condensin complexes, at least non-SMC subcomplexes, persist in the nucleoplasm during interphase, where it might be involved in DNA repair (Aono et al., 2002). In contrast, the *S. cerevisiae* condensin complex stays nuclear throughout the cell cycle (Strunnikov et al., 1995).
In most multicellular eukaryotes, the condensin I complex is cytoplasmic during interphase and localizes to chromosomes only after nuclear envelope breakdown (NEB). Condensin II localizes to the nucleus throughout the cell cycle (Ono et al., 2004). Its nuclear localization has led to the assumption, that it has interphase functions such as mediating long-range chromatin looping to control gene expression (Li et al., 2015). *D. melanogaster* condensin II subunit dCAP-D3 has been shown to interact with pRb via its LxCxE motif binding cleft (Longworth et al., 2008). Similar to topo II, condensin complexes localize to a central axis in metaphase chromosomes (Gasser et al., 1986; Maeshima and Laemmli, 2003; Ono et al., 2003). Whether this observation is an artifact, actively maintained, or whether condensin and topo II are passively localized to the core of mitotic chromosomes is still unclear.
The activity of the condensin complex must be regulated. During mitosis, condensin is phosphorylated by kinases Cdk1 (Sutani et al., 1999; Abe et al., 2011), Aurora-B (Nakazawa et al.,

2011; Tada et al., 2011) and Plk1 (Abe et al., 2011). How these modifications exactly regulate the activity of condensin has remained unclear. This suggests that the identities of all regulators of condensin have not been revealed so far.
In HeLa and chicken cells, residual chromosome condensation persists under knock-down conditions of condensin (Hirota et al., 2004; Hudson et al., 2003), indicating that not all molecular components of the chromosome condensation machinery have been identified.
In summary, how topo II and condensin accomplish the assembly of mitotic chromosomes, and whether they are the only factors involved, is poorly understood. Only few regulators of condensin have been identified and their contribution to the process of chromosome condensation remained elusive.

1.3.2 Models for the architecture of mitotic chromosomes

In eukaryotes, DNA winds around histones to form nucleosomes, which assemble into the beads-on-a-string like 11 nm fiber (Kornberg and Thomas, 1974; Olins and Olins, 1974). This lowest level of chromatin organization is is widely accepted to exist in interphase and mitotic cells. How condensin and topo II generate mitotic chromosomes from the 11 nm fiber has been controversial: Different models exist that describe the architecture of chromatin inside mitotic chromosomes. These models can be coarsely categorized into three classes, which are not necessarily mutually exclusive: (1) Hierarchical folding model, (2) scaffold radial loop model, (3) chromatin meshwork model and (4) mixed models. The main reason for the lack of definitive answers for this question is the absence of techniques that resolve the structures between 200 nm and the 11 nm fiber in a close to native state.

The hierarchical folding model

The oldest model for chromosome structure is the hierarchical folding model. After the observation of a 230 nm fiber by DuPraw (1966) in human liver metaphase chromosomes, the hierarchical folding model was proposed by Bak et al. (1977), based on their observation of a similar 400 nm 'unit fiber'. Bak et al. extrapolated between the 11 nm fiber and their 'unit fiber' observation and proposed that the nucleosomes of the 11 nm fiber arrange into a solenoid structure, giving rise to the 30 nm fiber. The 30 nm solenoid could then loop to into the 300-400 nm diameter 'unit fiber', which itself could fold fractally into the chromatid (fig. 1.3 A). This model and the existence of the unit fiber had been doubted early on (Klug, 1977) (see also section 1.3.2), because disintegration of mitotic chromosomes could only be observed after harsh chemical treatment. Despite these doubts, the hierarchical folding hypothesis is still represented in text books (Alberts et al., 2014). In this model, no axis is required to create the elongated nature of mitotic chromosomes.

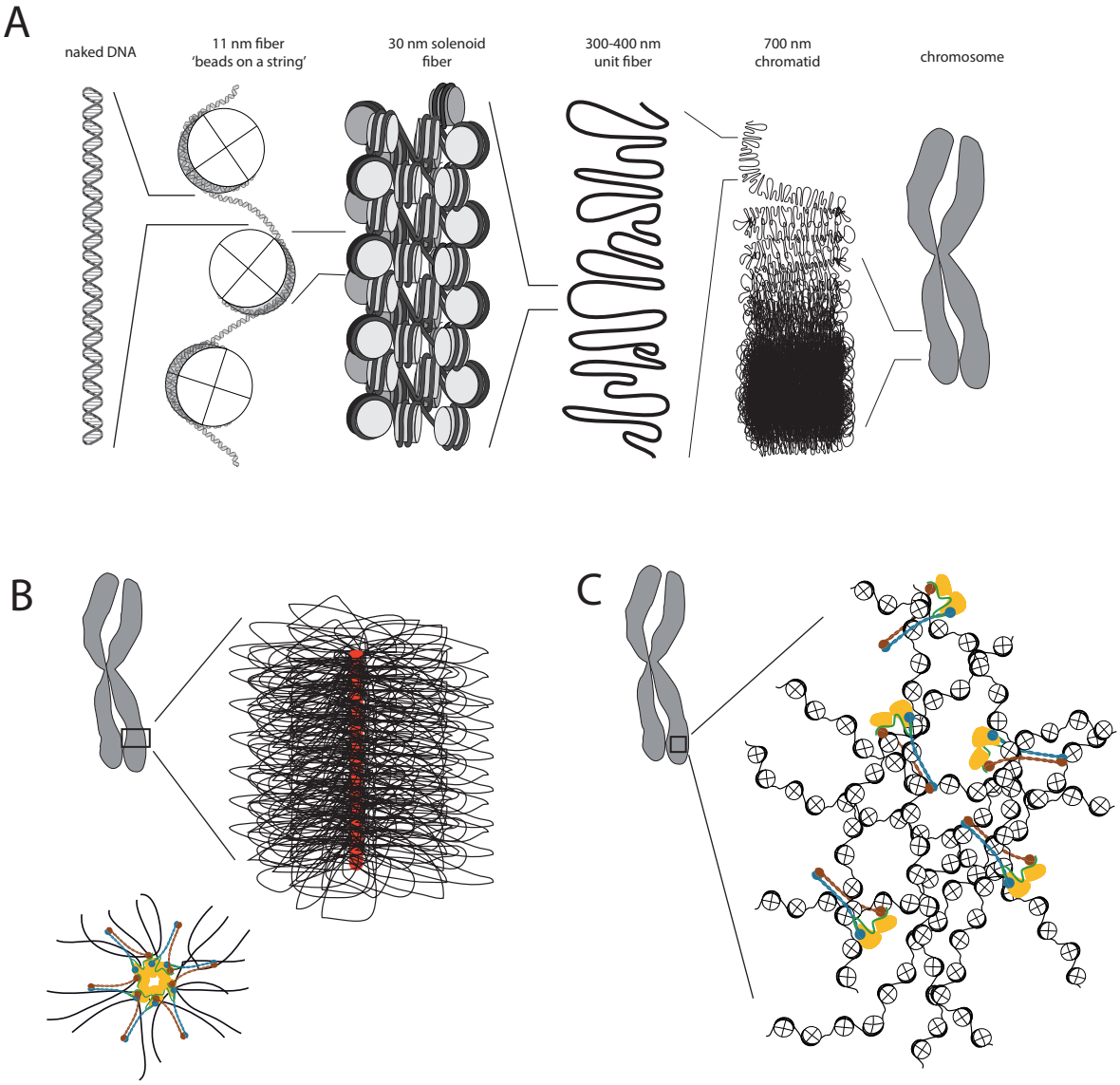

Figure 1.3: Models for the structure of mitotic chromosomes. Modified from Alberts et al. (2014); Petrova (2012); Kschonsak and Haering (2015); Piskadlo et al. (2016). (A) Hierarchical folding model. (B) Scaffold/ radial loop model. (C) Chromatin meshwork model.

The chromosome scaffold/radial loop model

Electron micrographs of histone-depleted metaphase chromosomes showed a structure that resembled a central, proteinacious core axis (Paulson and Laemmli, 1977). Both topo II and condensin localize to this protein axis, as shown by immunofluorescence (Gasser et al., 1986; Kimura and Hirano, 1997; Maeshima and Laemmli, 2003).
These observations led to the creation of the scaffold/radial loop model, in which loops of the 11 nm fiber are attached to a protein core scaffold. The protein core serves as a framework, which holds together the structure of the mitotic chromosome and is also responsible for its elongated shape (fig. 1.3 B). Although not necessary, it has been proposed, that scaffold and radial loop formation spread from the centromere (Maeshima and Laemmli, 2003).

Chromatin meshwork model

The mechanical properties of isolated mitotic chromosomes, measured in micro-mechanical manipulation experiments, suggest the absence of a central protein core (Poirier et al., 2000; Poirier and Marko, 2002). Protease treatment did not alter the mechanical properties of the extracted chromosomes, but DNA digestion affected the elastic properties. These experiments suggest that the DNA itself is responsible for the elastic properties of mitotic chromosomes, rather than a protein scaffold. In the chromatin meshwork model, 11 nm fibers interact randomly to create a meshwork. This can either be nucleosome interaction mediated (Nishino et al., 2012) or based on topological entrapment of chromatin fibers by condensin (Cuylen et al., 2011) (fig. 1.3 C).
Adding to this model, accumulating evidence suggests that no regular structure larger than the 11 nm fiber is present in mitotic chromosomes. Recent work did not find regular structures like the 30 nm fiber in mitotic chromosomes by small angle X-ray scattering (SAXS) or electron microscopy (Nishino et al., 2012).

Mixed models

Different hybrid models have been proposed that unify features of the above described classical models. For example, Kireeva et al. (2004) proposed a 'hierarchical folding, axial glue' model, in which the chromosome fiber folds hierarchically but is held together by a central protein axis.

1.3.3 Models for the formation of mitotic chromosomes

The above described models focus on the structure of the final condensed metaphase chromosomes, but only touch on the process of how these structures form. Some models imply a specific sequence of steps, e. g. in the hierarchical folding model, high order folds can only be formed after lower order folds are already present.
It has been proposed that condensation proceeds in distinct steps (Liang et al., 2015b; Kireeva et al., 2004), e. g. by reversible hierarchical folding, followed by irreversible chromosome axis formation (Hirano, 2005). Naumova et al. (2013) proposed a two-step model based on Hi-C data, in which linear compaction of chromatin is achieved by fromatin of chromatin loops,

which are laterally compacted in a second step.
One basic question, which has been subject to speculation but not approached by measurements, is whether the condensation activity is uniformly distributed along the arm throughout condensation (Kireeva et al., 2004) or spreads from a certain location, e. g. centromere (Maeshima and Laemmli, 2003) or the telomeres. Addressing this question has been challenging because sequence-specific staining like FISH or ultrastructural analysis by electron microscopy requires harsh fixation of cells. In combination with the resolution limit of about 200 nm for conventional light microscopy, the condensation process can only be observed at low resolution in live cells, at least for whole chromatin-specific staining methods.

1.4 Measuring chromosome condensation

In order to gain more insight in the formation and structure of mitotic chromosomes, researchers have developed different approaches to quantify the compaction of chromosomes during condensation. Quantitative assays are more sensitive and less prone to bias than qualitative judgement. Additionally, quantitative assays are able to detect even subtle differences. Another advantage of quantitative measurements is that they can lead to more exact models of a process by revealing dependencies that allow hypothesis generation by extrapolation.
Multiple methods have been established in different model organisms to quantify chromosome condensation. These methods can be divided into imaging-based and molecular biology-based approaches. An overview for the methods can be found in table 1.1.

1.4.1 Molecular biology-based chromosome condensation measurement methods

Currently, two molecular biology methods that can be used to quantify chromosome condensation have been established.
The recent developmet of proximity ligation methods has opened a new perspective on chromatin organization (Lieberman-Aiden et al., 2009). These methods allow identification of proximal DNA regions by Next Generation Sequencing (NGS). In HiC, the DNA and proteins in chromatin are chemically cross-linked and fragmented by restriction digest. DNA overhangs are filled with biotin-labelled nucleotides. After dilution, DNA fragments cross-linked within same complexes are ligated. Following enrichment by biotin-specific pulldown, ligated fragments are sequenced. The hybrid-fragment sequences are subsequently mapped to the reference genome. The frequency of how often parts of two sequence regions have been sequenced in one fragment reflects their contact probability and therefore their spatial proximity (Naumova et al., 2013).
The second method to probe chromosome condensation is based on histone-histone cross-linking Wilkins et al. (2014). In yeast, unnatural amino acids were incorporated into the tails of histones *in vivo*, and cross-linked upon ultraviolet (UV) irradiation. UV light-induced cross-linked histone-histone species were detected via western blotting. The abundance of histone-histone cross-linked species was used as a measure for the compaction of chromatin and therefore chro-

mosome condensation.
The common disadvantage of these molecular biology methods is that they are only compatible with ensemble experiments and often require lysis or fixation of the cells. Because cell populations are often heterogenous, these ensemble measurements may not represent states at the single cell level and can hide important correlations (Altschuler and Wu, 2010). Due to the prerequisite of cell lysis, time lapse experiments of the same cells is not possible.

1.4.2 Microscopy-based chromosome condensation measurement methods

Microscopy has several advantages over the molecular biology methods described above. First, it can deliver information at the single cell level. Second, imaging is a method that is minimally invasive and can therefore be applied to living cells. This enables the time-resolved observation of cellular processes at the single cell level.
Because chromosome condensation is a dynamic process, it is favorable to capture its kinetics over time. Therefore, live cell imaging is the method of choice to quantify chromosome condensation *in vivo*. Although the drastic chromatin rearrangement can be observed directly in differential interference contrast (DIC) transmission light microscopy, the advent of genetically encoded Fluorescent Proteins (FPs) has opened new labeling strategies and made specific staining in live cell imaging possible. Also, development of digital cameras and computational image analysis strategies makes microscopy more accessible to quantitative analysis.

Sequence-independent chromatin staining

Images of sequence-independent chromatin labeling (e. g. histone-FP or Hoechst 33342 staining) can be analyzed using image texture analysis, e. g. standard deviation of pixels' grey values (reviewed by Neurohr and Gerlich (2009)). In late prophase, when chromonemata become distinguishable, chromosome length and width can be measured. Confocal microscopes enable acquisition of 3D data that can be used for threshold-based segmentation to measure chromatin volume. This strategy has been successfully used to acquire time resolved live cell measurements of chromosome condensation in live rat kidney (NRK) cells (Mora-Bermúdez et al., 2007). Yet, this approach is limited to cells with large chromosomes. A disadvantage of whole chromatin labeling is the inability to resolve the initial time period of chromosome condensation, because chromatin appears as an amorphous mass inside the nucleus during interphase, in which individual chromosomes are not distinguishable. Recent approaches have used the semi-conservative nature of replication to selectively label one of the sister chromatids by nucleotide analogs and therefore reduce this 'overlabeling' (Nagasaka et al., 2016).
fluorescence-lifetime imaging (FLIM)-Förster resonance energy transfer (FRET) has been used to quantify chromosome condensation in live HeLa cells (Llères et al., 2009). Co-expression of histone 2 B (H2B)-green fluorescent Protein (GFP) and mCherry-H2B led to random incorporation of the histone-FP fusion proteins in nucleosomes. This labeled the complete chromatin. As chromosomes condensed, mean distance between nucleosomes decreases, increasing FRET

between incidental donor-acceptor pairs.

Locus-specific chromatin labeling

As condensation implies mostly axial shortening, the distance between two chromosome loci provides a quantitative measure for condensation. Fluorescent labeling of two loci allows detection of their relative position in the microscope and therefore calculation of their distance in space.

Fluorescence *in situ* hybridization (FISH) is a well-established method for fluorescent labeling of chromosome regions in fixed cells based on their sequence (Langer-Safer et al., 1982). Fluorescently labeled DNA fragment probes are prepared by PCR-mediated incorporation of fluorescent nucleotide-analogs or nick translation (Rigby et al., 1977). Cells are permeabilized and the fluorescent DNA fragment probes are hybridized to the genomic DNA *in situ*. The main limitation of FISH is that it is not compatible with live cell imaging, since cells have to be permeabilized to allow the fluorescent DNA probes to hybridize to the genomic DNA in the nucleus. In addition, the fixation process can in principle introduce artifacts. Nevertheless, this method is still used for measurements of loci distances on the population level (Iwasaki et al., 2015; Kim et al., 2016).

Straight et al. (1996) developed a strategy that combines locus-specific labeling with live cell imaging to be able to observe chromosome locus dynamics. A large array of lac operator DNA sequences (lacOs) (>100 repeats) is introduced at a locus of interest, e. g. by homologous recombination (fig. 1.4 A). Expression of FP-Lac repressor protein (LacI)-Nuclear Localization Sequence (NLS) fusion proteins, which bind the lacO sequences inside the living cell, labels the locus fluorescently (fig. 1.4 B). Subsequently, two more FROS have been established exploiting the tetracyclin repressor protein (TetR)-tetracyclin operator DNA sequence (tetO) system (Michaelis et al., 1997) and the λ repressor protein and λ operators (Lassadi et al., 2015). Next to these established systems, recent alternative loci labeling systems based on inactive Cas9-FP have been established, also in conjunction with expression of GFP-tagged nano bodies (SunTag) (Chen et al., 2013; Tanenbaum et al., 2014).

Vas et al. (2007) first used two fluorescent repressor operator system (FROS) labeled loci to measure chromosome condensation in live *S. cerevisiae* cells. The quantification of chromosome condensation was not based on loci distance but on the fraction of cells in which fluorescent FROS foci were distinguishable or overlapped. Petrova et al. (2013) improved this system in *S. pombe* by tracking the positions of the FROS foci over time and taking their distance as a measure of chromosome condensation. I use and improve this method in this work and hence discuss it in more detail in section 1.5.

A recent study describes that chromosome condensation affects the chromatin organization within FROS, such that fluorescent mCherry signal decreases due to quenching between mCherry molecules (Kruitwagen et al., 2015). In the study, decrease of fluorescence was used as a measure for chromosome condensation. It remains counterintuitive how an increase in FP concentration might decrease fluorescence emission by quenching. It is well established, that for quenching

to occur, a short range interaction < 2 Å between the fluorophore and quencher is required (Lakowicz, 2006, p. 278). In fluorescent proteins, the chromophore is contained within a protein barrel of about 3.4 nm diameter and 4.5 nm height (Shu et al., 2006) and hence not accessible to molecules that could cause quenching.

Method	Key variable(s)	Model organism(s)	Reference(s)
Microscopy-based methods			
Sequence-independent chromatin labeling	intensity, volume, width, length	live cultured cells	reviewed in Mora-Bermúdez and Ellenberg (2007); Neurohr and Gerlich (2009); Nagasaka et al. (2016)
Histone-GFP and -mCherry	FRET, fluorescence lifetime	live cultured human cells	Llères et al. (2009)
sequence specific chromatin labeling (FISH)	Euclidean distances	fixed yeast, fixed human cultured cells	Iwasaki et al. (2015)
FROS	Euclidean distances	live *S. pombe*, *S. cerevisiae*	Vas et al. (2007); Petrova et al. (2013)
FROS	FROS fluorescence intensity	live *S. cerevisiae*	Kruitwagen et al. (2015)
Molecular biology-based methods			
Histone site-specific cross-linking	Cross-linking efficiency	fixed *S. cerevisiae*	Wilkins et al. (2014)
5C and Hi-C	DNA proximity ligation probability	fixed cultured cells	Naumova et al. (2013)

Table 1.1: Overview of methods that can be used to quantify chromosome condensation. Detailed description can be found in the main text (section 1.4). See also Schiklenk et al. (2016).

1.5 A quantitative chromosome condensation assay in live *S. pombe* cells

In order to be able to study chromosome condensation, Petrova (2012) developed a FROS-based condensation assay in *S. pombe*.

1.5.1 *S. pombe* as a model organism to study chromosome condensation

The decision to use *S. pombe* as a model organism was based on the advantages that fission yeast combines (Schiklenk et al., 2016). *S. pombe* is as readily genetically manipulable as *S. cerevisiae*, but has some considerable advantages for the measurement of chromosome condensation. Fission yeast and baker's yeast have approximately equally sized genomes, but *S. pombe* has three long chromosomes (Wood et al., 2002), whereas *S. cerevisiae* has 16 short chromosomes (Goffeau et al., 1996). The long chromosome arms makes it possible to probe condensation over a wide range of marker spacings.
Compared to *S. cerevisiae*, the chromatin features of *S. pombe* are more similar to those of multicellular organisms, including RNA interference (RNAi)-induced heterochromatin formation (Zofall and Grewal, 2006), complex centromeres (Pidoux and Allshire, 2004) and organization of chromosome arms into topologically associated domains (TADs) (Mizuguchi et al., 2014).
Most importantly, mitotic chromosome condensation in mammalian cells and in fission yeast share common characteristics. For example, in both fission yeast and human cells, chromosome arms continue to condense when cells are arrested in a pre-anaphase stage (Petrova et al., 2013). In contrast, already compacted chromosomes decondense during nocodazole arrest in *S. cerevisiae* (Vas et al., 2007).
Unlike mammalian cells, both fission yeast and baker's yeast have only one condensin isoform. They are therefore simpler systems in which complementation by different isoforms is not possible, hence phenotypes are easier to analyze. In contrast to *S. cerevisiae*, *S. pombe* imports condensin into the nucleus upon entry into mitosis (see section 1.3.1), which has two considerable advantages. First, import of condensin (and therefore its concentration) and condensation dynamics can be correlated. Second, condensin import can serve as a marker for entry into mitosis. These advantages make fission yeast an ideal system for the study of chromosome condensation in a model organism amenable to genetic screens.

1.5.2 Microscopy-based chromosome condensation measurements in *S. pombe*

Despite the advantages of *S. pombe* described above, imaging-based measurements of chromosome condensation by whole chromatin staining are problematic. Compared to mammalian cells, fission yeast has a small overall cell size and small chromosomes, posing the objects much closer to the diffraction limit. In wild type mitoses, individual chromosomes are not discernible due to crowding in the nucleus (Hiraoka et al., 1984, p. 350). Additionally, condensed mitotic fission yeast chromosomes are about 0.8, 1.6 and 2.5 µm long and 0.4 µm wide on average

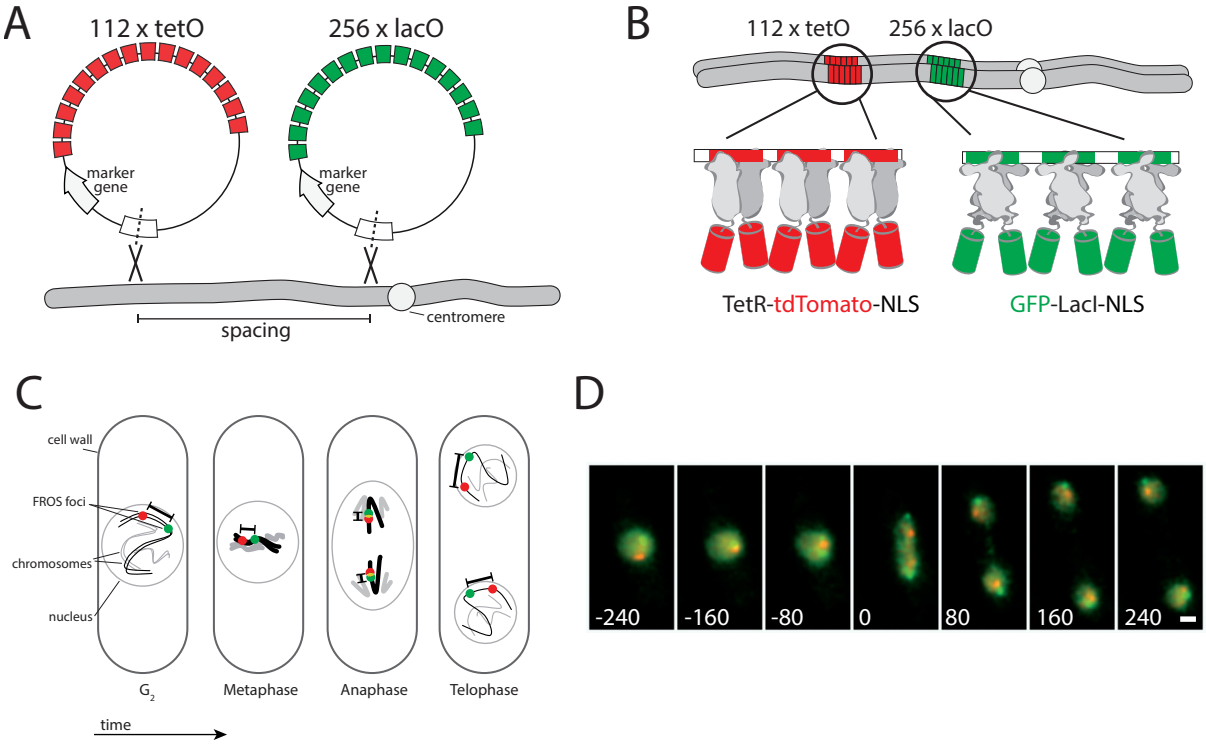

Figure 1.4: (A) tetO and lacO arrays and yeast marker genes are integrated at two loci along the long arm of chromosome one using plasmid integration (see section 4.5.6). The genomic distance in bp between the integration sites is called spacing throughout the thesis. (B) When expressed in a lacO and tetO containing strain, TetR-tdTomato-NLS and GFP-LacI-NLS fusion proteins bind to their operator sequences. The FROS thereby label the loci fluorescently in live cells. (C) Cartoon of behavior of FROS foci during mitosis in fission yeast cells. (D) Micrograph time lapse montage of a dividing fission yeast cell carrying the FROS. Unbound fluorescent repressor stains the nucleoplasm. Scale bar 1 µm, numbers indicate seconds in reference to anaphase onset. (A-D) Modified from Petrova et al. (2013).

(Umesono et al., 1983). Considering the diffraction limit of about 200 nm in conventional light microscopy (Abbe, 1873), accurate measurements of the chromatin volume cannot be expected from such an approach. Petrova's strategy to overcome this limitation was the spectrally distinct fluorescent labeling of two loci by FROSs, as described in section 1.4.2 (see also fig. 1.4 A and B). FROS are visible as diffraction limited foci in a wide field microscope (fig. 1.4 C and D). The euclidean distance between both FROS foci can be measured over time (fig. 1.4 C). Although each sister carries one lac and tet FROS each G_2, one fluorescent focus appears in the light microscope as resolution is not good enough to distinguish the tightly cohesed sister loci (fig. 1.4 C, G_2). As cells enter mitosis, chromosome condensation begins, leading to axial contraction of the chromosome arms and hence reduction in theFROS foci's euclidean distance (fig. 1.4 C, Metaphase). Upon anaphase onset, sister chromatid cohesion is lost, which results in splitting of sister FROS foci (fig. 1.4 C, Anaphase and D time point 0). The time point of FROS foci splitting can therefore be used as a temporal indicator for anaphase onset. Both FROS foci pairs move towards the cell poles as sister chromatids are segregated by the spindle. In telophase, chromosomes decondense and distance between FROS foci increases. To observe an increased number of cell divisions, Petrova et al. (2013) enriched cells in G_2 by lactose gradient

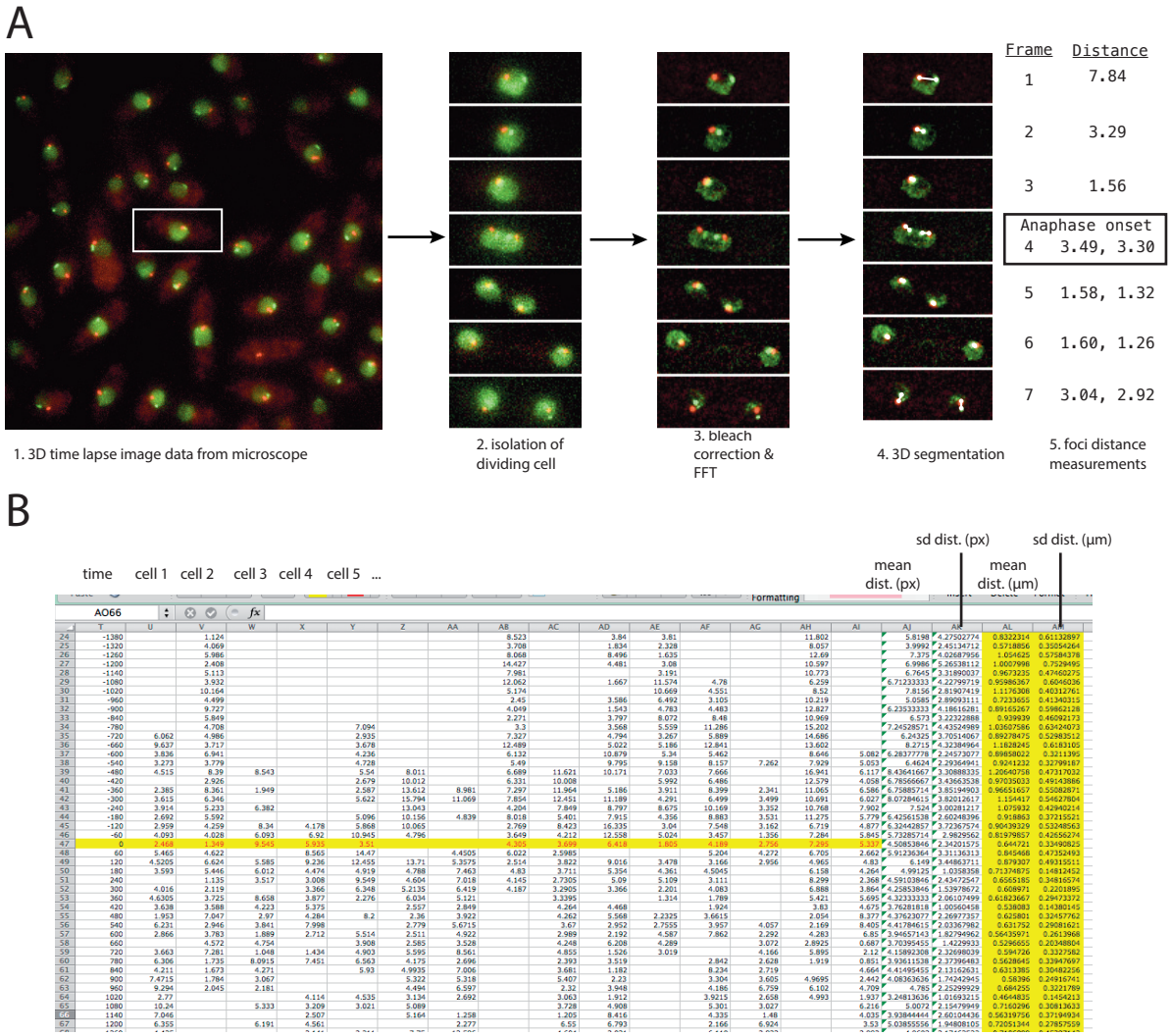

Figure 1.5: Overview of the CCA data analysis procedure in Petrova (2012); Petrova et al. (2013). (A) Data extraction procedure. (B) Example of data analysis procedure. Voxel distance values from (A 5.) were copied into Excel and vertically aligned to anaphase onset (yellow marked row) such that values of corresponding time points were shifted to the same row. values corresponding to frames in which segmentation was wrong were deleted manually. Average distances and standard deviation were calculated by row. Average and standard deviation values were multiplied by pixel size (0.12 µm per pixel) for conversion to metric scale.

density centrifugation (Hagan et al., 2016) one hour prior to time lapse imaging. These cells were spread to form a monolayer in a petri dish. Cell divisions were observed by acquisition of 3D stacks of the monolayer every 40 s for one hour (Petrova, 2012; Petrova et al., 2013).

Data extraction and analysis

Because part of this work improved the data extraction and analysis pipeline, I describe in detail the state of the data extraction and analysis process at the beginning of my PhD. To extract chromosome condensation values from the microscopy data, the position of each FROS focus had to be measured in each frame of the video. First, to avoid disambiguation between FROS

from different cells and optimize image processing parameters for each individual cell, Region Of Interests (ROIs) were excised manually in ImageJ using the 'rectangular selection' tool and duplicating the ROI (fig. 1.5 A). Each excised image file was saved and preprocessed by calling Kota Miura's plugin via ImageJ's application menu and the respective sub-menus. The plugin applied to the open image a histogram matching bleach correction algorithm (Burger and Burge, 2008) iterating over each frame's volume, before filtering large and small noise by applying the ImageJ Fast Fourrier Transformation (FFT) band filter to each frame. The preprocessed image was manually saved.

From the dual channel 3D time lapse data, a threshold-based segmentation algorithm determined the positions of FROS foci and calculated their distance, based on global nearest neighbor method. Details about this algorithm can be found in Petrova et al. (2013). The segmentation and distance calculation plugin was called again manually from ImageJ's general menu. After finishing computation, the plugin showed a results table containing FROS foci positions with respective distances and a z-projection image series of the input data to which the segmentation results were drawn. These segmentation result images were later used to assess the quality of segmentations in each frame. Distance and time columns were copied from the results table into a Microsoft Excel spreadsheet. Distances corresponding to frames in which segmentation was incorrect as judged based on the segmentation result images were deleted manually. The earliest frame which contained split fluorescent foci was defined as the time point of anaphase onset. This process resulted in distance time series that showed a clear decrease in FROS

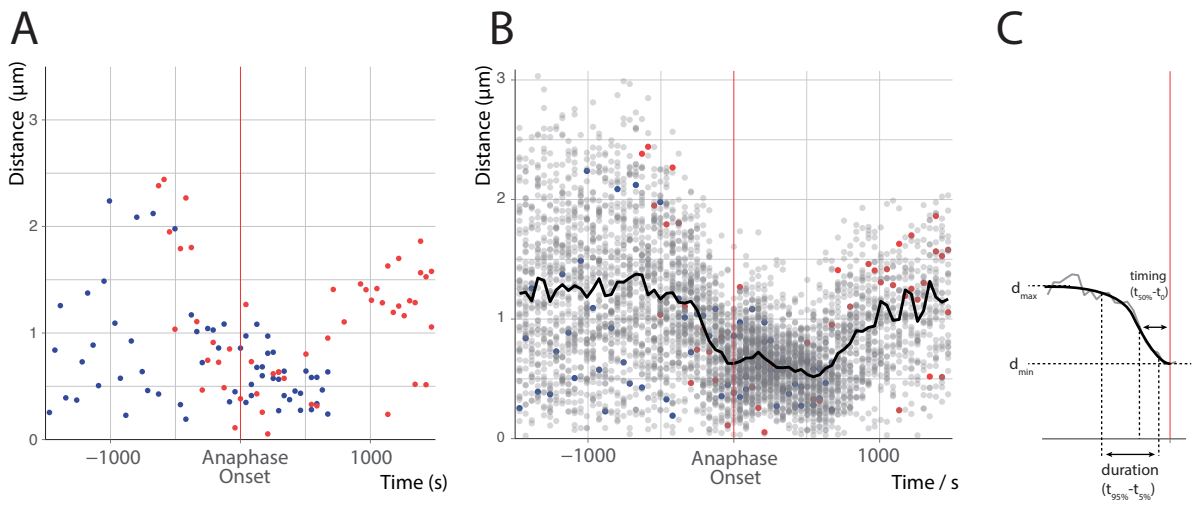

Figure 1.6: Alignment of time series to anaphase onset and per-time point averaging results in a quantitative description of chromosome condensation called condensation curve. (A) Distance-time plot of distance data from two different cells. (B) Averaging time series from multiple cells by each time point results in a condensation curve (black line) - a quantitative description of chromosome condensation. Individual data points are shown in light grey, the data points shown in (A) are plotted in the respective color. (C) Sigmoid fit to the distance averages enables extraction of condensation parameters timing, duration and compaction ratio (for definitions see main text). Modified from Petrova (2012).

foci distance during cell division. Nevertheless, data from single cells were not interpretable otherwise (fig. 1.6 A). Definition of anaphase onset based on the dot splitting criterium al-

lowed for temporal alignment between the distance time series from different cells. Averaging distance data from 20 or more cells (from multiple experiments) by each time point resulted in a quantitative description of chromosome condensation, which is called condensation curve throughout the thesis (fig. 1.6 B, black line). This quantitative, microscopy-based assay and its variations is called Chromosome Condensation Assay (CCA) throughout the thesis. Using the CCA, Petrova et al. (2013) showed that chromosomes compacted 2-fold, in accordance with measurements from mammalian cells (Mora-Bermúdez et al., 2007). Measurements were specific for chromosome condensation because FROS labels on different chromosome arms did not congress drastically and compaction was abolished upon inactivation of *cut14* and *top2* via thermosensitive (ts) mutants.
To extract condensation parameters from the condensation curve, a sigmoid function of the form $d = [c/(1 + e^{(a \times t + b)})] + d_{max}$ was fit to the last 20 distance averages before anaphase onset (fig. 1.6 C). In this equation, d corresponds to distance and t to time. The fit produced the parameters a (decay rate), b (proportional to the inflection point), c (difference between the asymptotes) and d_{max} (upper asymptote). For details about the fitting procedure, see the methods section of Petrova et al. (2013). The criteria compaction ratio (d_{max}/d_{min}), duration (time span between 5 % of compaction and 95 % of compaction) and timing (time span between 50 % of compaction and anaphase onset) were calculated based on the fit.

1.5.3 Limitations of the Chromosome Condensation Assay

Despite its usefulness, the CCA had limitations in data interpretation and could be improved in image acquisition, data extraction, data handling and data analysis aspects.
First, interpretation of data from individual cells was not possible. This made averaging data from multiple cells a central requirement. Average condensation curves from more than 15 to 20 cells become interpretable, but a strict criterium for how many data points are required to call a condensation curve significant was missing. In comparison to the large number of cells required to obtain an interpretable condensation curve, the data extraction procedure was inefficient. For example, the necessity to define rectangular ROIs limited the density of cells per field of view (FOV) at which data could be acquired. Whenever cell density was too high, isolation of cell regions by defining rectangular ROIs was not possible due to the random orientation of the elongated cells. A second factor limiting the cell density was positional drift during time lapse acquisition, resulting in translational movement of the FOV over time. In cell-dense FOVs, individual cells' ROIs drifted into each other. This resulted in FROS foci of multiple cells within one ROIs, too. In ROIs which contained FROS foci from multiple cells, segmentation misallocations were so frequent, that the data was unusable. Hence, time lapses were acquired only for fields of view with relatively low cell density. This limited the number of observable mitoses and hence only few time series per imaging experiment. These limitations resulted in too few distance-time series from a single imaging experiment to obtain a condensation curve. Therefore, time series from multiple experiments were averaged. Yet, whether pooling data series from different experiments enhanced variability or affected the condensation curve itself,

had not been tested. Most importantly, it was impossible to assess experiment-to-experiment variability. This made it difficult to define, whether a condensation curve was within the wild type (wt) variability or aberrant.
Second, averages do not necessarily reflect the behavior of single cells or correlate with the actual biological behavior. For example, averaging time series from many cells can neglect the presence of two or more subpopulations in condensation behavior. Subpopulation effects can skew the outcome and lead to biological misinterpretation (see fig. 3.1 and Altschuler and Wu (2010) for review).
Third, the central image processing and analysis algorithms for FROS position measurements had already been implemented by Kota Miura as Java plugins in ImageJ (Petrova et al., 2013). Due to lack of computational programming knowledge in the research group, data extraction was performed by calling the plugins from ImageJ's Graphical User Interface (GUI) and manually applying them to every single cell data set, which was repetitive and laborious. Determination of anaphase onset and assessment of segmentation results by switching between Excel's and ImageJ's GUIs was laborious, vexatious and prone to error. The temporal alignment of distance time series in Excel's GUI was error prone and was confusing when data from large numbers of cells was processed.
Fourth, a major advantage of yeast over other model systems is the readily available genetics. Yet, introducing alleles into strains with fluorescent repressor operator system by crossing was very inconvenient. The unstable nature of highly repetitive sequences in yeast caused by recombination led to loss or strong attenuation of FROS focus intensity during meiosis. Hence, FROS strains could not be crossed.
Fifth, fitting a sigmoid function to the data had disadvantages. First, it limited analysis to the pre-anaphase condensation process, although chromosomes compact during telophase. The decision to fit a sigmoid function to the data was not based on an underlying mathematical model but on observations of wt condensation curves. As no argument is described in Petrova (2012) and Petrova et al. (2013) why a sigmoid and not some other function was fit to the data, it has to be assumed that this choice was made arbitrarily. Condensation curves from some mutants did not follow a sigmoid regime, for some data sets, fits could not even be determined (Petrova et al., 2013, table 3). Hence, fitting the sigmoid function to mutants' condensation curves can be used to decide, whether a condensation curve is aberrant, but is not suited to extract of biologically meaningful parameters.

1.5.4 Identification of *zas1* as a chromosome condensation factor candidate

Boryana Petrova used the quantitative CCA as a means to screen for yet unknown chromosome condensation factors. She created a library of 1093 randomly mutagenized ts strains based on a strain with FROS labels at the centromere (*lys1* integration) and at 2.5 Mb on chromosome I (strain 2926). Each strain was imaged at the restrictive temperature and scored for segregation defects. Data from strains with defective chromosome segregation were imaged again to obtain condensation curves and fit criteria as described in (section 1.5.2). Strains of which condensation

parameters were significantly different from wt cells, were back-crossed to a wt *S. pombe* strain to isolate the alleles that conferred temperature sensitivity. The individual allele's underlying mutation was then identified by NGS (Petrova, 2012). Using this procedure, Petrova found three independent ts alleles of *zas1*, a poorly characterized gene that had not been implicated in chromosome condensation before.

1.6 Objective of this thesis

In this thesis, I want to determine whether *zas1* is indeed required for chromosome condensation and if so, characterize it. This implies elucidation the mechanistic connection between aberrant condensation curve and *zas1* mutations. Furthermore, I want to improve the throughput of the quantitative condensation assay and minimize existing shortcomings by optimization of the FROS and establishment of a computational data extraction and analysis pipeline. Finally, I want to use the pipeline to characterize axial chromosome condensation and decondensation at the population level and adapt the FROS-based chromosome condensation assay for measurements on the single cell level.

Chapter 2

Results

2.1 Characterization of Zas1

Using the quantitative chromosome condensation assay, Boryana Petrova identified multiple temperature sensitive mutants that showed defective chromosome condensation at the restrictive temperature (Petrova, 2012; Petrova et al., 2013). Among these mutants were eight condensin alleles, one *pol2* allele, one *fbh1* allele and three alleles of *zas1* named *W5*, *A1* and *AJ3*. *zas1* is a largely uncharacterized Open Reading Frame (ORF), which had previously not been associated with chromosome condensation.

2.1.1 The *zas1* gene

Zinc finger alternatively spliced 1 (*zas1*) is listed in pombase (`http://www.pombase.org`, Wood et al. (2012)) under systematic ID SPBC1198.04c. It is located on the long arm of chromosome II, at about 180 kb, flanked by a transfer RNA (tRNA) gene and SPBC1198.03c, a yet uncharacterized gene. A schematic diagram of the *zas1* locus is shown in fig. 2.1.
Two primary transcripts have been reported to originate from the *zas1* locus. The longer primary transcript (3266 nt) contains an ORF with 9 introns. Its second intron has been reported to be alternatively spliced (Okazaki and Niwa, 2000), making it one of four known primary transcripts in *S. pombe* with splice variants. The two alternative messenger RNAs (mRNAs) contain ORFs encoding proteins of 845 or 897 amino acids (aas), respectively. Both ORFs isoforms encode a canonical NLS (E9 – R17), followed by two C2H2 zinc finger (ZF) domains (R25 – K54, A55 – Q83). A third ZF domain lies within the alternatively spliced second intron. All aa numbers used in this work refer to the short isoform of Zas1. Automated computational annotation from the PFAM database (Finn et al., 2014) predicts a fungal specific transcription factor domain (PF04082) between aa 419 and 694. The second primary transcript of *zas1* is a long non coding RNA (lncRNA) (SPNCRNA.1321) of about 1320 nt length (Rhind et al., 2011). Its orientation is antisense to the longer primary transcript and its transcription starts at the ORF's stop codon (fig. 2.1).

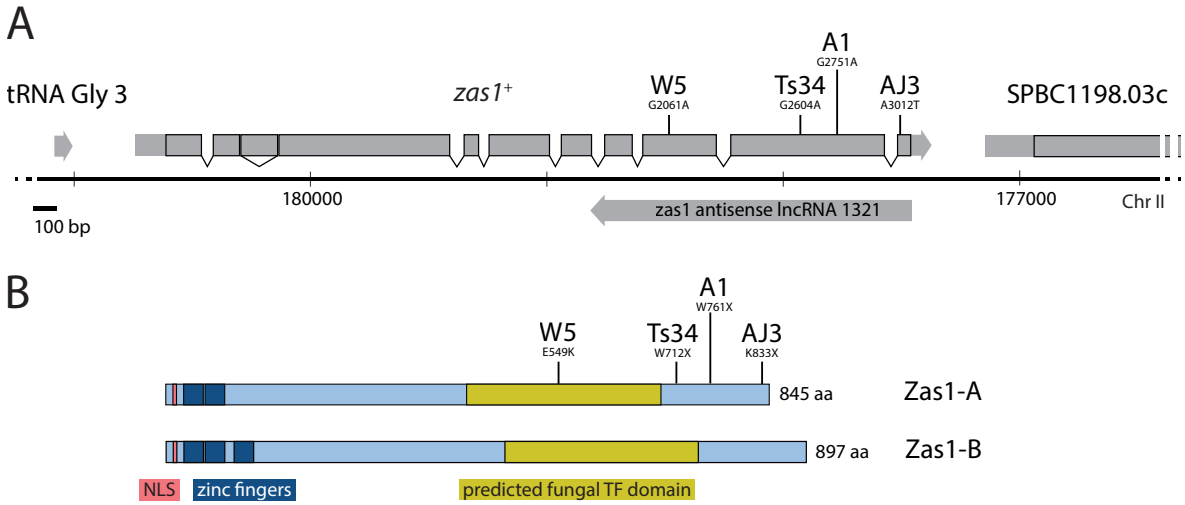

Figure 2.1: (A) Diagram of the *zas1* gene locus. Transcripts are pictured in grey, their protein coding regions are boxed. Introns are shown as v-shaped connectors. Positions of allele variants are indicated by vertical lines with respective names and variant bases. Numbers indicate the position of the base in relation to the ORFs start codon. (B) Predicted Zas1 protein isoforms and their domain organization in scale with (A) (3 nt correspond to one aa).

2.1.2 *zas1* mutants confer thermosensitive growth

All *zas1* ts mutants identified in the screen had been created by random UV or chemical mutagenesis (Petrova, 2012). Because these mutagenesis methods create strains with numerous mutations throughout the genome, it cannot be excluded that additional, unidentified mutations in the genetic background underlie the phenotypes observed in the screen. Effects from other mutations could be ruled out if the *zas1* mutations by themselves were able to confer temperature sensitivity and aberrant chromosome condensation. Using the loop-in loop-out strategy (section 4.5.7), I re-introduced the W5 (E549K), A1 (W761X) and AJ3 (K833X) mutations in a defined genetic background (strain 1283), containing the auxotrophic markers *ade6-M210*, *his7-366*, *leu1-32*, *lys1-131*, *ura4-D18* (strains 3673, 3693 and 4506). The auxotrophic strain was chosen to facilitate subsequent reintroduction into the original FROS strain by crossing (see section 2.1.3).

In addition to the mutations found by Petrova, Okazaki and Niwa (2000) had described a ts allele of *zas1* named Ts34. Similar to A1 and AJ3, Ts34 contains a nonsense mutation in the C-terminal region of Zas1's ORF (W712X). I introduced the W712X mutation into strain 1283 to test if it indeed conferred temperature sensitivity and how the ts strength compared between alleles (strain 3717).

Growth of the strains was assessed by a serial dilution spotting assay (section 4.5.1) on YE5S plates and incubation at 25 °C, 30 °C, 34 °C and 37 °C. All *zas1* mutants showed strongly decreased viability at 34 °C. Ts34, A1 and AJ3 fully inhibited growth at 37 °C, while a small fraction of W5 mutant cells were still able to proliferate (fig. 2.2). In addition to complete loss of viability at 34 °C or higher temperatures, all *zas1* mutant strains exhibited mild proliferation defects at permissive the temperatures of 25 °C and 30 °C. Therefore, I was able to confirm

the *zas1* mutations identified by Petrova (2012) as the cause of temperature sensitivity.

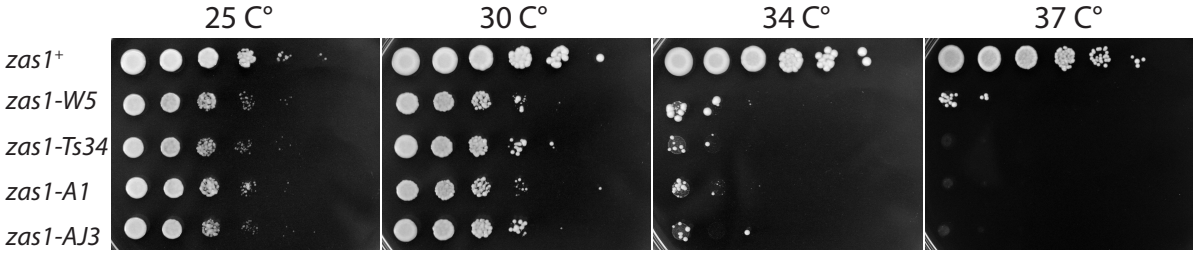

Figure 2.2: Growth of *zas1* ts mutants at permissive and restrictive temperatures. Indicated alleles were introduced into a h^-, *ade6-M210, his7-366, lys1-131, leu1-32, ura4-D18* strain (strain 1283). Equal cell numbers (based on OD) of exponentially growing yeast cultures were spotted in 10 fold serial dilutions on YE5S plates and incubated at 25 °C, 30 , 34 °C and 37 °C for 4 days (see section 4.5.1).

2.1.3 *zas1* mutants are defective in chromosome condensation

All *zas1* mutants show decreased proliferation at the repressive temperature. Although major condensation factors are essential for cell division, proliferation defects do not automatically imply impaired chromosome condensation. I therefore wanted to assess whether the *zas1* mutations cause condensation defects by measuring chromosome condensation using the quantitative chromosome condensation assay.

I crossed the four *zas1* mutants fig. 2.2 and the original FROS strain used for the screen (strain 2926, FROS at cen-arm, 1.2 Mb distance). I selected spores containing the *zas1* allele of interest and both FROS from tetrads where all markers had segregated 2:2. FROS foci intensity was reduced in all crossed strains compared to the original strain (2926), presumably due to deletion of repetitive operator sequences by meiosis induced recombination. Co-segregations of all four markers with the ts allele were rare due to genetic distance greater than 50 cM. I later addressed both of these problems to improve the condensation assay as described in sections 2.4.1 and 2.4.2.

zas1-W5, Ts34 and AJ3 mutants show defects in chromosome condensation kinetics

I imaged strains as detailed in section 4.6.2 and measured FROS distance over time. After data extraction and analysis (section 2.2) I obtained chromosome condensation measurements (hereafter called condensation curves) for each mutant from two independent imaging experiments (fig. 2.3), averaging measurements from 21 or more individual cells per strain (table 2.1). For each strain, a wt control curve was measured in parallel.

In all *zas1* ts mutant strains except *zas1-A1*, condensation curves diverged from control curves (fig. 2.3). Condensation curves of *zas1-W5*, *zas1-Ts34* and *zas1-AJ3* cells showed shallower slopes than *zas1*$^+$ cells (control), indicating a lower condensation rate. This can be interpreted as a defect in compaction kinetics. Notably, at anaphase onset FROS foci were separated by on average 0.8 µm to 0.9 µm in *Ts34* and *AJ3* cells, corresponding to wt distance. *W5* cells even seemed to hyper-condense their chromosomes at this stage to around 0.7 µm. This means

that the lower condensation rate co-occured with a longer period of condensation. In *zas1-Ts34* cells, it took about 600 s to 700 s between condensation initiation and anaphase onset, while in *zas1*$^+$ cells the corresponding time period took about 490 s (fig. 2.3, A second panel and table 2.4). This effect was more pronounced in *zas1-AJ3* cells, where chromosomes are significantly compacted 500 s before anaphase onset (fig. 2.3, A right panel).
The condensation defect of *zas1-Ts34* cells is of considerable interest, because this mutation had not been found in the screen and therefore its chromosome condensation behavior had not been observed previously. Hence, finding a condensation defect is a strong indication that *zas1* is a chromosome condensation factor. Additionally, this finding proofs that Petrova's FROS distance-based assay and screening strategy were successful in identifying previously unknown chromosome condensation factors.
Taken together, *zas1* mutant cells are less efficient in timely compacting their chromosomes, but not considerably impaired in the total extend of chromosome condensation per se. *zas1* is hence an excellent chromosome condensation factor candidate.

zas1 ts mutants show chromosome decondensation defects

Defects of a chromosome condensation factor or mitotic chromosome structure might similarly result in chromosome decondensation defects. As cells in *zas1* mutants were able to compact their chromosomes to more or less wt levels, I examined average decondensation behavior in the same imaging data.
A major limitation of using FROS foci distance to measure decondensation is the fact that distances can be skewed by chromosome segregation defects. For example, decondensation data from *zas1-Ts34* cells were not interpretable, due to frequent mis-segregation which were included in the distance averages (indicated by increased standard deviation). In contrast, segregation errors in *zas1* mutants *W5* and *A1* were less frequent (quantified in fig. 2.4). Analysis of *zas1-W5* and *zas1-A1* mutant strains revealed delayed chromosome decondensation. In wt cells, bulk chromosome decondensation occured between 600 and 850 s after anaphase onset (dotted vertical lines in fig. 2.3 B). In *W5* and *A1* cells, FROS foci were constantly closer during this time period compared to *zas1*$^+$ cells. Maximal chromosome compaction was attained at a later time point than in control (fig. 2.3 B).
Taken together, FROS distance measurements reveal that all *zas1* ts mutants have chromosome condensation defects, decondensation defects or both, indicating temporal mis-regulation of condensation or perturbed mitotic chromosome structure.

2.1.4 Zas1 has the characteristics of a chromosome condensation factor

The chromosome condensation and decondensation defects revealed by the CCA in *zas1* mutant cells are a strong indication that *zas1* is involved in chromosome condensation. Nevertheless, the FROS assay has limitations in its conclusiveness, like any method. For example, averaging data from the whole population can neglect the presence of two or more subpopulations in

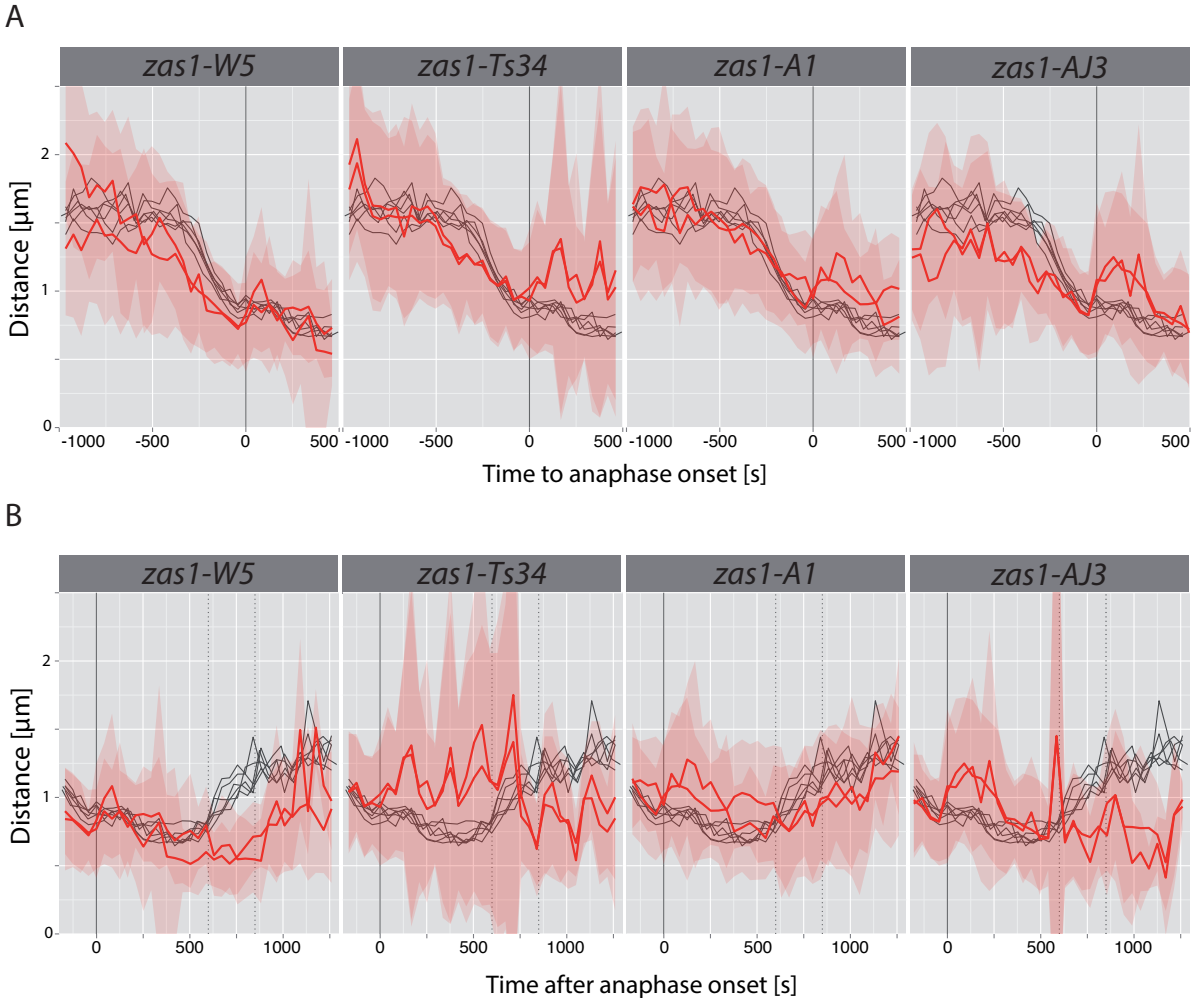

Figure 2.3: Condensation curves of *zas1* ts mutants. Strains with 1.2 Mb FROS spacing (2926) carrying either *zas1*$^+$ or one of the *zas1* ts alleles were imaged at the restrictive temperature (34 °C). FROS foci distances were measured over time in dividing cells, aligned to anaphase onset (time point 0), grouped by time point and averaged. Each line represents averages from one imaging experiment, grey lines indicate controls, red lines show *zas1* mutant measurements' averages. Red areas indicate respective standard deviation. Table 2.1 lists the number of analyzed cells for each experiment. (A) Chromosome condensation curves. Except for *zas1*-A1, chromosome condensation curves are shallower than control, indicating a defect in condensation kinetics. All mutants reach the same compaction at anaphase onset as control. (B) Chromosome decondensation curves of *zas1* ts mutants. Dotted lines at 600 s and 800 s after anaphase indicate time of bulk decondensation in *zas1*$^+$ cells. In *zas1* mutants, decondensation was either absent (Ts34, AJ3) or delayed (W5, A1). *zas1*-W5 and A1, chromosome decondensation is delayed compared to control.

Strain	*zas1* allele	Imaging Date	Number of mitoses analyzed
2926	wt	16/04/2013	29
2926	wt	25/04/2013	63
2926	wt	02/09/2013	58
2926	wt	27/10/2013	79
2926	wt	23/08/2013	40
2926	wt	27/11/2014	73
3766	W5	27/10/2013	33
3766	W5	07/06/2013	26
3809	Ts34	27/05/2013	24
3809	Ts34	27/05/2013	40
3399	A1	16/06/2013	51
3399	A1	30/08/2013	64
4106	AJ3	09/01/2015	21
4106	AJ3	10/01/2015	29
4094	Y289X	28/11/2014	112
4094	Y289X	20/01/2015	75

Table 2.1: Statistics for fig. 2.3 and fig. 2.9. All imaging experiments in this table were carried out at 34 °C. In all strains, FROS are located on Chromosome I arm at 2.49 Mb between SPAC19A8.02 and SPAC19A8.01c and near the centromere of Chromosome I at 3.74 Mb (*lys1*), about 1.2 Mb apart.

condensation behavior and lead to misinterpretation (see section 1.5.3). Therefore, I additionally decided to test if three main criteria common to known major condensation factors (like top2 and condensin subunits) apply to *zas1*: (1) segregation defects upon gene inactivation, (2) nuclear localization of the gene product and (3) essentiality of the gene for cell proliferation.

(1) *zas1* ts mutants show segregation defects at the restrictive temperature

When reviewing the FROS imaging data acquired at restrictive temperature (section 2.1.3), I observed a fraction of cells mis-segregating their chromosomes during mitosis. Measuring the frequency of mis-segregations and successful segregations in this data would clarify if mis-segregations are more abundant in *zas1* ts mutants compared to *zas1*$^+$ FROS strains and allow me to quantify the degrees of penetrance. Classification of mitoses into mis-segregation and accurate segregation was based on two criteria: (1) FROS did not segregate at all or not exactly one FROS of each color segregated into a daughter cell. (2) unequal background staining of nucleoplasm by unbound Fluorescent repressor (FR) indicating differentially sized daughter nuclei or incomplete nucleokinesis.

To be able to score efficiently, I integrated a manual annotation step in the computational dot measurement pipeline (section 2.2.8). During this step, the classification was performed blindly to minimize human bias using an ImageJ script that displays videos of wt and mutant cells randomly and without label. The user annotates if chromosome segregation was defective in

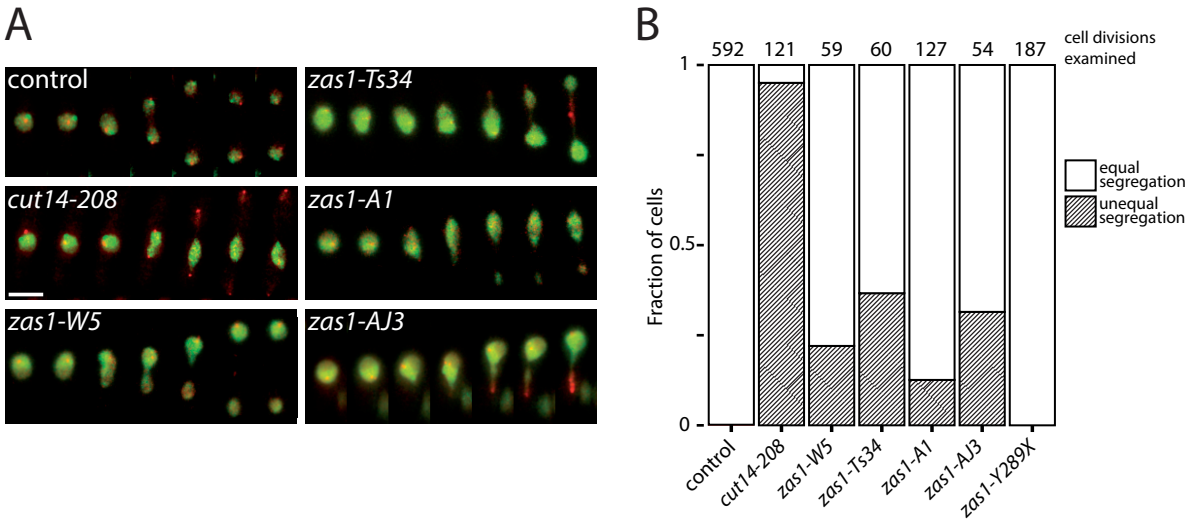

Figure 2.4: (A) wt nuclear divisions and mis-segregations. Examples of nuclear division observed during chromosome condensation assay. Red: lacI-GFP bound to centromere proximal FROS (*lys1*) and unbound staining the nucleoplasm. Green: tetR-tdTomato staining nucleoplasm background and FROS on Chromosome I at 2.49 Mb. Scale bar 5 µm. (B) Quantification of mis-segregation frequencies in control, *cut14*-208 and *zas1* strains.

her/his view (section 2.2.8).

In 592 wt cell divisions examined not a single was scored as unequal segregation. In the positive control strain, the SMC condensin subunit ts mutant *cut14-208*, more than 90 % of cells showed a mis-segregation phenotype (fig. 2.4 B) based on the above mentioned criteria. In most cases, mis-segregation followed the characteristic *cut* phenotype, in which the bulk of the chromatin mass remained in the cell center (fig. 2.4 A left column, middle panel). In contrast to *cut14-208*, segregation phenotypes varied between individual cells in all four *zas1* ts mutants. Nucleokinesis either resulted in two unequally sized daughter nuclei (fig. 2.4 A, *zas1-W5* example) or failed entirely (*zas1-AJ3* example). In other cases, centromeres remained in the cell center, while the bulk chromatin was distributed to the cell poles, but trailed along the spindle (fig. 2.4 A, *Ts34* and *A1* examples).

These or similar defects were observed in all *zas1* strains, yet the number of affected cells varied. *Ts34* and *AJ3* induced segregation defects in about one third of cell divisions, *W5* in one fifth. About every tenth division of *A1* cells resulted in mis-segregation. Frequencies of segregation phenotype did not correlate with the ts induced growth defects (fig. 2.2). For example, *W5* mutant cells grew best of all *zas1* ts strains.

(2) Zas1 localizes to the nucleus

In contrast to mammalian cells, the nuclear envelope remains intact during cell division in many yeast species (closed mitosis). Consequently, cytoplasmic proteins never access chromatin during the cell cycle, unless they are imported into the nucleus. Only proteins that are nuclear during at least one cell cycle stage can directly act on chromatin. This does not necessarily

apply to direct regulators of condensin that act in interphase or early mitosis, as fission yeast condensin localizes to the cytoplasm during interphase and is imported into the nucleus during prophase. Despite this caveat, regulators of condensin during mitosis or direct condensation factors are expected to localize to the nucleus.

To detect the spatiotemporal localization of Zas1, I tagged the endogenous ORF C-terminally with triple mCherry using PCR targeting (section 4.5.5) in a haploid strain. Staining with Hoechst 33342 (section 4.6.1) made nuclei visible. I observed unsynchronized live cells in a wide field microscope and acquired micrograph stacks. Z projections of the stacks are shown in fig. 2.5. Fluorescent signal was visible in the nucleus at mCherry excitation filter settings. The fluorescence did not appear evenly distributed within the nucleus but rather granular, indicating increased Zas1 concentration in certain nuclear regions.

This nuclear localization of Zas1 is in agreement with the predicted N-terminal NLS (fig. 2.1).

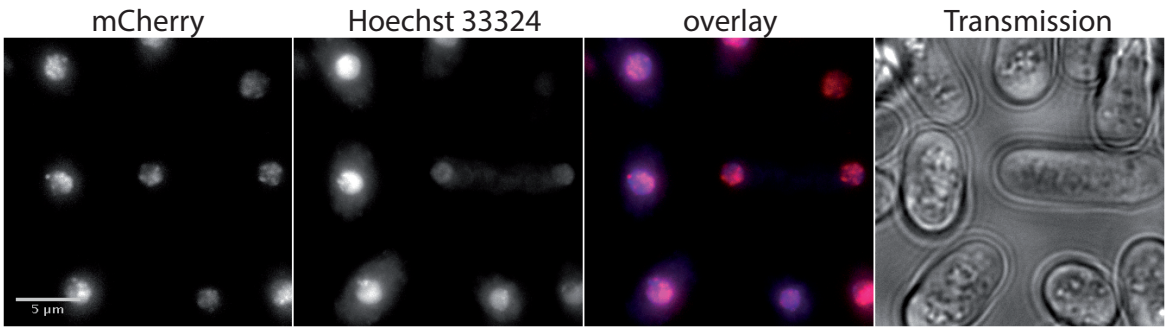

Figure 2.5: Zas1 localizes to the nucleus in interphase and mitosis. Zas1 was C-terminally tagged with 3 x mCherry using PCR targeting (strain 3782). Cells were grown to mid log phase and DNA was stained with Hoechst 33324 (section 4.6.1). Cells were observed under a wide field fluorescence microscope. A 10 slice focus stack (spacing 400) was acquired and images were overlaid by maximum projection.

(3) *zas1* is an essential gene

Since condensation is an absolute prerequisite for successful chromosome segregation, chromosome condensation factors must be essential for cell proliferation. *zas1* was previously identified to be required for viability in a high throughput screen covering the complete *S. pombe* genome (Kim et al., 2010). Careful analysis revealed that in this study, *zas1* as well as the adjacent glycine tRNA (SPBTRNAGLY.03) including its promoter and the 5' untranslated region (UTR) with the first 21 aa of adjacent ORF SPBC1198.03c had been deleted (fig. 2.6 A). Although neither tRNA nor SPBC1198.03c are essential (Hayles et al., 2013; Kim et al., 2010), genetically synthetic effects between all three genes can not be excluded.

To clarify whether *zas1* is indeed essential, I replaced the ORF of one *zas1* allele including start codon and stop codon by a *kanMX* cassette (section 4.5.7) in a diploid *ade6-M210/ade6-M216* strain by PCR targeting (section 4.5.5). Amplification of the locus by PCR followed by sequencing confirmed the deletion of one *zas1* allele in the diploid strain (strain 4005). Following sporulation, I isolated and dissected asci (see section 4.5.8). While all four spores formed colonies

in the untransformed strain, each tetrad from the *zas1*$^{+}$/*Δzas1::kanMX* strain contained two spores that were unable to proliferate (fig. 2.6 C). To test if the *kanMX* G418 resistance marker co-segregated with proliferating or non-proliferating spores, colonies were replica plated on a G418 containing agar plate (section 4.5.9).
No cells were able to grow on selective medium, indicating that loss of viability co-segregated with the resistance marker and therefore with deletion the of *zas1* ORF.
In conclusion, *zas1* is indeed an essential gene. Whether the *zas1* ORF or antisense lncRNA 1321 confer Zas1's essential function is investigated in the next paragraph.

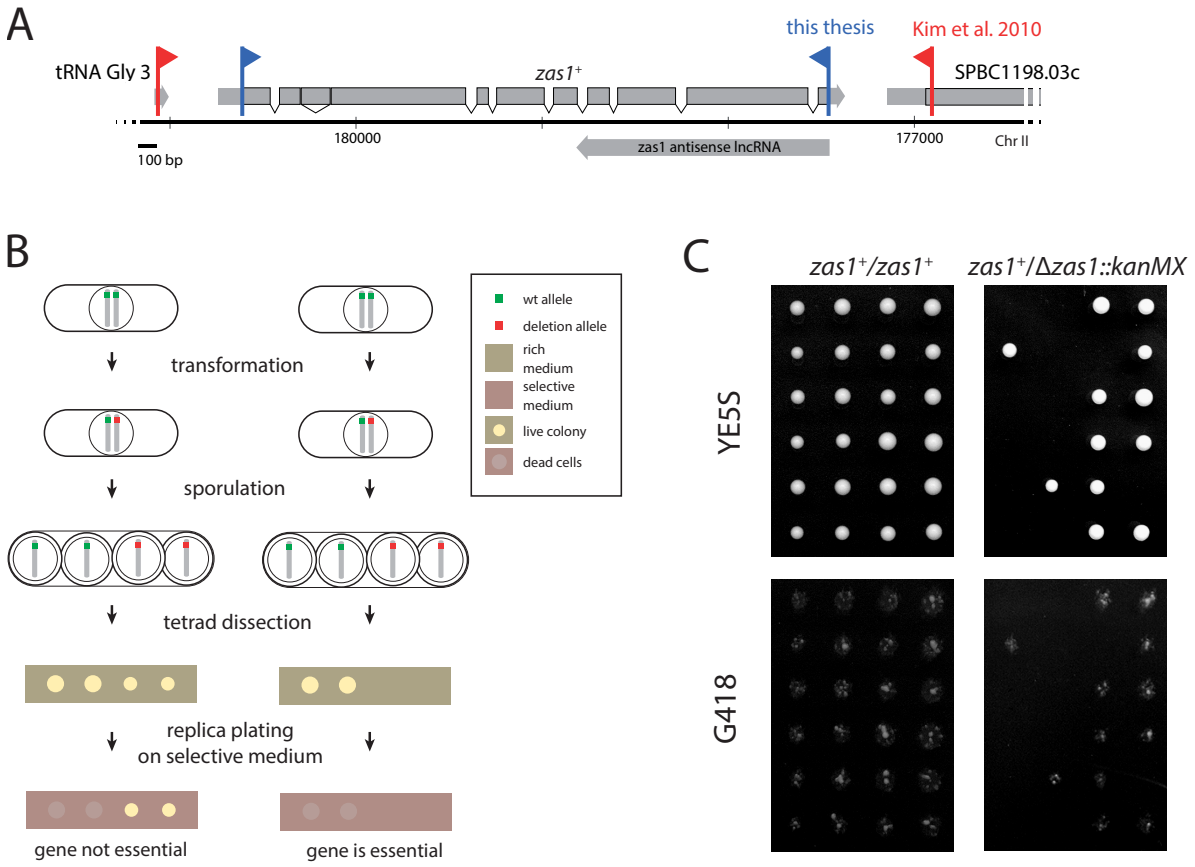

Figure 2.6: *zas1* is required for cell proliferation. (A) Red vertical lines: boundaries of the region deleted by kanMX cassette in Kim et al. (2010), Blue vertical lines: boundaries of deletion in my construct. Flags are pointing inward the deleted regions. (B) Diagram of the principle of tetrad dissection to test if an allele is functional of essential genes. (C) Left column: tetrad dissection of a diploid *ade6-M210/ade6-*M216 on YE5S and replica plating onto YE5S-G418. Right column: tetrad dissection of the *zas1*$^{+}$/*δzas1 kanMX*$^{+}$ strain and replica plating onto YE5S-G418.

2.1.5 *zas1*'s protein gene product is essential for viability

All ts-causing mutations are located in the C-terminal region of Zas1; the most C-terminal mutation truncates the ORF by only 13 aa. Remarkably, all four ts-causing mutations are also located within the antisense lncRNA 1321 transcript (see fig. 2.1). It is therefore possible that lncRNA 1321 is the transcript that mediated *zas1*'s essential function.

To address this hypothesis, I deleted the complete lncRNA in a diploid strain, truncating *zas1*'s ORF to the first 469 aa. Following the same strategy as before, I performed tetrad dissection of the heterozygous *zas1*$^{+}$/*zas1-V470X kanMX* strain. All four spores formed colonies and the *kanMX* marker segregated 2:2 fig. 2.8. PCR locus sequencing of one of the G418 resistant spores confirmed deletion of lncRNA 1321. This proves that lncRNA 1321 is a non-essential transcript of *zas1*. Because lncRNA 1321 is non essential, the Zas1 protein must be the essential gene product of *zas1*. Which regions of Zas1 are essential is investigated in section 2.1.7.

2.1.6 Auxin degron-induced Zas1 depletion does not affect growth

As shown above, the Zas1 protein is the essential gene product of *zas1* (sections 2.1.4 and 2.1.5). To dissect its mechanism of action, it would be of particular advantage to be able to conditionally deplete Zas1. Although ts mutants are very useful, the function of the protein is inactivated by an unknown mechanism at the restrictive temperature, complicating interpretation of experimental results. More importantly, all *zas1* ts mutants have a mild proliferation defect under permissive conditions (fig. 2.2). Accumulation of defects in these strains during permissive growth make it difficult to discriminate between direct and accumulated, indirect effects upon inactivation.
To avoid these drawbacks, I sought a system which can conditionally inactivate the protein. To be most useful, this system should meet the following two requirements: First, cells should show no defect under permissive conditions. Second, protein inactivation should be complete within one cell cycle (about 2.5 hours). This would make it compatible with the quantitative chromosome condensation assay and avoid accumulation of defects over generations. Because transcriptional regulation of protein levels is slow and has long lag times, promoter based repression systems like the *nmt1* promoter could not be considered. The auxin inducible degron system, on the other hand, had been reported to comply to all before mentioned criteria (Kanke et al., 2011; Nishimura et al., 2009).
In short, the protein of interest is tagged C-terminally with an IAA17 domain from *Arabidopsis thaliana*. Simultaneously, a skp1-TIR1 fusion protein is expressed in the strain, leading to formation of TIR1-containing SCF E3 ligase complexes. Upon addition of synthetic auxin 1-Naphthaleneacetic acid (NAA), TIR1 dimerizes with IAA17, inducing polyubiqutination of the IAA17 domain. The IAA17 domain and its fusion protein are then targeted for proteosomal degradation (fig. 2.7 A).

I tagged the endogenous *zas1* gene with an Haemagglutinin $(HA)_2$-IAA17 domain in the above described Skp1-TIR1 background, which did not affect cell proliferation in media containing no NAA. The resulting strain (strain 3921) was grown to mid log phase in liquid culture. The culture was split into two flasks, of which one culture was supplemented with 1.5 mM NAA. Equal amounts of cells were sampled from both cultures (section 4.5.10) after 20, 40, 60, 80, 100 and 120 min. I detected tagged protein via westernblot (section 4.4.7) against the HA tag (fig. 2.7 B). I observed an approximately two-fold reduction in Zas1-HA_2-IAA17 levels 80 min

to 100 min after addition of 1.5 mM NAA compared to culture without NAA addition. This NAA-dependent reduction of protein levels indicated that the degron is functional, but with lower efficiency than expected.

I used a spotting growth assay (section 4.5.1) to test if this reduction in protein levels was sufficient to inhibit Zas1 function and induce a growth phenotype. I spotted serial dilutions of log phase liquid cultures of skp1-TIR1, *zas1*$^{+}$ and skp1-TIR1, *zas1-HA*$_2$*-IAA17* cells on EMM2 plates with and without NAA. No difference in cell proliferation was detected (fig. 2.7 C). This shows that the reduction of Zas1 protein by the auxin inducible degron is not sufficient to cause a growth defect.

In conclusion, the auxin inducible degron system is able to reduce Zas1 protein levels by about 50 %. This reduction is not sufficient to induce a growth defect, indicating that Zas1 can function at reduced protein levels. Only few Zas1 molecules are probably required for its essential function(s). Because the expected growth phenotype could not be induced, the degron system was not found suitable for further experiments.

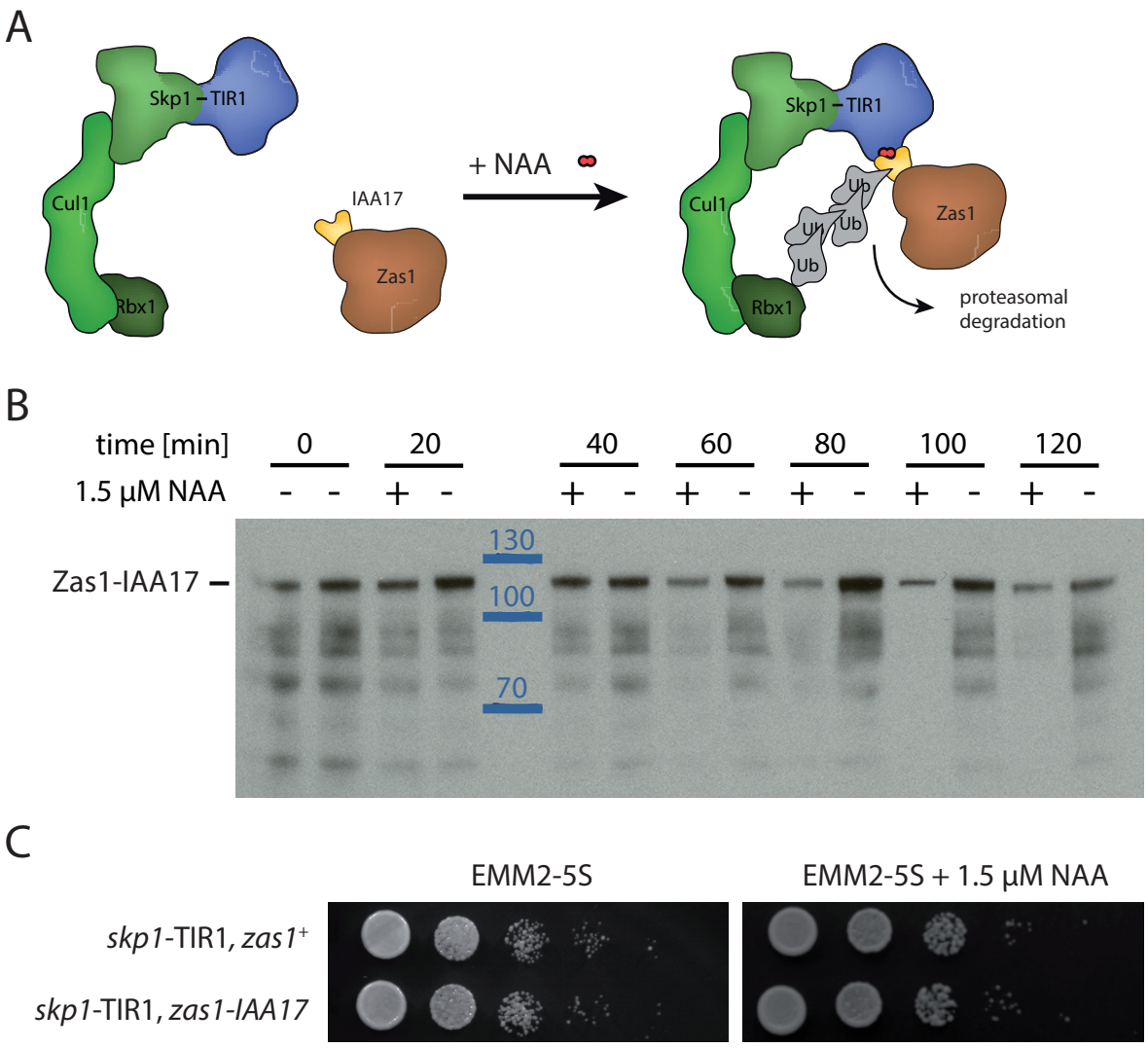

Figure 2.7: Application of an auxin inducible degron system to Zas1. (A) Schematic drawing of auxin degron mechanism. Expression of Skp1-TIR1 fusion protein (green-blue) forms a E3 ligase complex with Cul1 and Rbx1 (both green). The protein of interest (here Zas1, brown) is tagged C-terminally with the IAA17 domain (yellow). Upon addition of synthetic auxin NAA (red), IAA17 and TIR1 dimerize. The IAA17 domain is polyubiquinated (grey), leading to degradation of the Zas1-IAA17 fusion protein. (B) Time course after addition of NAA in the *ade6::Padh15-skp1-OsTIR1 natMX Padh15-skp1-AtTIR1-NLS$_2$::ade6$^+$*, *zas1-HA$_2$-IAA17 ura4*, *ura4-D18* strain. (C) Cell proliferation is not affected by protein reduction through the auxin inducible degron. Cycling cells were spotted onto EMM2+5S agar containing no NAA or 1.5 mM NAA. Plates were photographed 5 days after incubation at 25 °C.

2.1.7 Identification of essential regions in Zas1

zas1 encodes an essential protein (sections 2.1.4 and 2.1.5). This raises the question, precisely which parts of the protein confer essentiality. These regions are expected to contain the elements needed for *zas1*'s essential functions, and could therefore provide information about what these function(s) are and their mechanism. This information could also be useful for development of a more targeted conditional inactivation approach.
To identify the essential regions of Zas1, I created a range of partial deletions in the endogenous locus. Except for the NLS, ZFs and the vague fungal TF domain, specific protein domain information was missing for Zas1. Hence, approximately evenly spaced C-terminal truncations were designed (fig. 2.8 A) and introduced into diploid strains using PCR targeting with the forward primer containing a stop codon at the indicated aa position of the short splice isoform. Mutant viability and growth was then assessed employing the tetrad dissection method.

2.1.8 Truncations mitigate temperature sensitivity and reveal an essential short linear motif

Three of the four temperature sensitive mutants are nonsense mutations, truncating the C-terminal region of Zas1 by 133, 84 or 12 aa, respectively. This initially suggested the presence of a functionally important domain in this C-termial region of Zas1.
I created a truncation allele corresponding to the most N-terminal ts allele's (*Ts34*) nonsense mutation, *W712X* (strain 4006). After tetrad dissection, colonies formed by mutant spores grew slower than their *zas1* wt sister spores, confirming that ORF truncation at W712 induces a proliferation defect (fig. 2.2).
I expected that more N-terminal truncation would increase the growth defect or abolish proliferation entirely. To test this expectation, I repeated the experiment to create a shorter allele, *zas1-P590X*. *zas1-P590X* cells grew slower than *zas1*$^+$ but unexpectedly had an improved growth rate compared to *zas1-W712X*, judged by visual inspection (compare G418 resistant colonies in first and second column of fig. 2.8 B). This effect was similar for *zas1-V470X*, the allele which had been created earlier to test if lncRNA 1321 is involved in *zas1*'s essential function (section 2.1.5); *zas1*-V470X cells grew almost like wild type cells (fig. 2.8 B, third column), indicating that shorter truncations mitigate the ts growth defect. Despite the presence of ts mutations, Zas1's C-terminal third does not contain any elements involved in its essential function.
These results suggest that elements involved in the essential function of *zas1* are encoded in the N-terminal two thirds of its ORF. I created even shorter *zas1* alleles, *L360X* and *Y289X*. In both cases, the haploid strains expressing the short Zas1 constructs had only a mild growth defect (fig. 2.8 B fourth and fifth column).
To quantify the growth compared to *zas1*$^+$ and test for temperature sensitivity, I measured the haploid mutant strains' doubling time in YE5S liquid culture at 25 °C, 30 °C and 35 °C (fig. 2.8 C). Each strain was cultured to log phase and diluted in YE5S to about 0.1 to 0.2 OD/mL. I

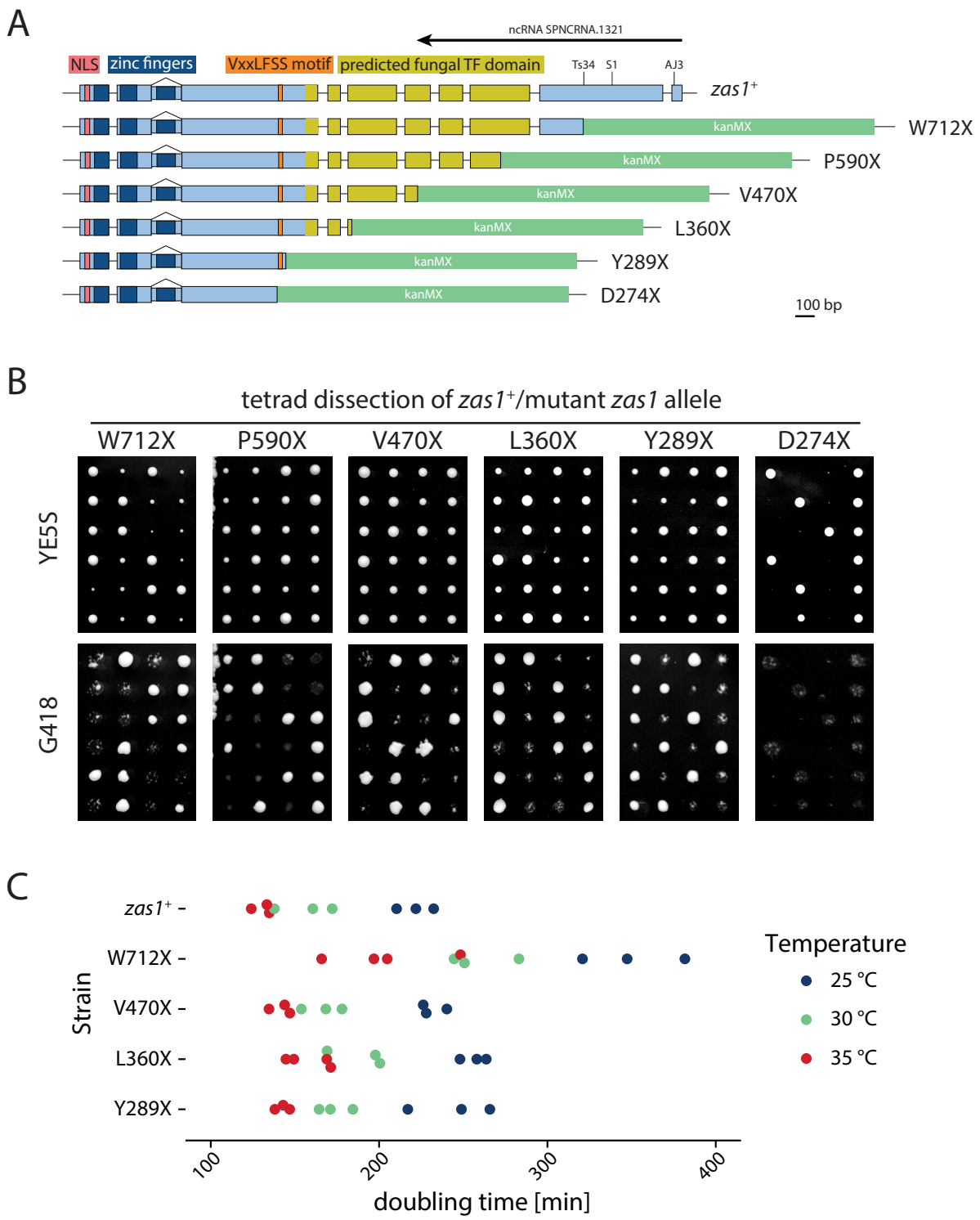

Figure 2.8: Zas1 truncations reveal a short linear motif. (A) Schematic representation of the *zas1* locus in truncation constructs corresponding to the mutant alleles in (B). (B) Tetrad dissections of heterozygous diploid strains carrying *zas1*$^{+}$ and the indicated *zas1* alleles as shown in (A). Strains: 4006, 4445, 4007, 4036, 4046, 4035 (C) Doubling times of Zas1 truncated haploid strains at 25 °C, 30 °C and 35 °C.

measured the Optical Density (OD) of this culture every 15 to 20 min. To calculate the doubling time, exponential function $OD_{start} * 2^{(time/doublingTime)}$ was fit to the OD measurements using R's `nls` function. Doubling times from three or more experiments are plotted in fig. 2.8 C.
At all temperatures tested, *zas1-Ts34* cells had a doubling time about twice as long as *zas1*$^+$ cells. The shorter alleles *V470X*, *L360X* and *Y289X* have only slightly longer doubling times compared to *zas1*$^+$, but still grow more than 1.5 times faster than *zas1-Ts34*. These results confirm the observations on agar plate.

zas1-Y289X cells show no chromosome condensation defect

Although alleles shorter than P590 did not display a strong growth defect, a defect in chromosome condensation could have been present, either too small to cause segregation defects or completely uncoupled from segregation defects. To test this possibility, I introduced the shortest allele with minimal growth defect (*Y289X*) into the FROS strain (2926) and measured chromosome condensation. From two imaging experiments, I obtained and analyzed distance measurements for 112 and 75 cells (table 2.1). Both condensation curves did not deviate from *zas1*$^+$ condensation observations and did not show the regime of ts mutants' condensation (fig. 2.9). Further truncation therefore not only mitigates the growth defect but also the chromosome condensation defect. In conclusion, Zas1 does not contain sequences required for chromosome condensation C-terminal of Y289, unless ts truncations induced hypermorphic *zas1* alleles which could not be excluded at this stage.

Truncation at D274 reveals a short, essential sequence

The wt-like growth and chromosome condensation dynamics of *zas1-Y289X* implies that the elements required for *zas1*'s essential function are situated within Zas1' first 288 aa. Remarkably, shortening Zas1 by 15 additional aa leads to a severe growth defect (fig. 2.8 B, last column).
In conclusion, this truncation data set shows that although all ts mutations are found in Zas1's C-terminal region, this sequence does not contain elements required for its essential function. In contrast, cells have only a very mild growth defect without Zas1' CTD (C-terminal of Y289), but are completely unable to proliferate when truncated after D274. This strongly suggests the presence of a functionally relevant sequence between D274 and Y289.

2.1.9 Zas1 contains an E2F-like pRb pocket AB groove ligand motif

Bioinformatics in this and the following paragraph were conceived by Toby Gibson, who initially predicted the motif and proposed a double cyclin fold for Zas1's C-terminal domain (CTD).
Truncation data suggested the presence of a functionally important sequence between D274 and Y289 (section 2.1.8).
Bioinformatic analysis revealed a conserved stretch of 5-8 aa within this region. The aa sequence of Zas1 (long isoform) was psi-BLAST searched (Johnson et al., 2008) and all hits were aligned using Clustal Omega (Sievers et al., 2011). An overview of the resulting alignment is shown in

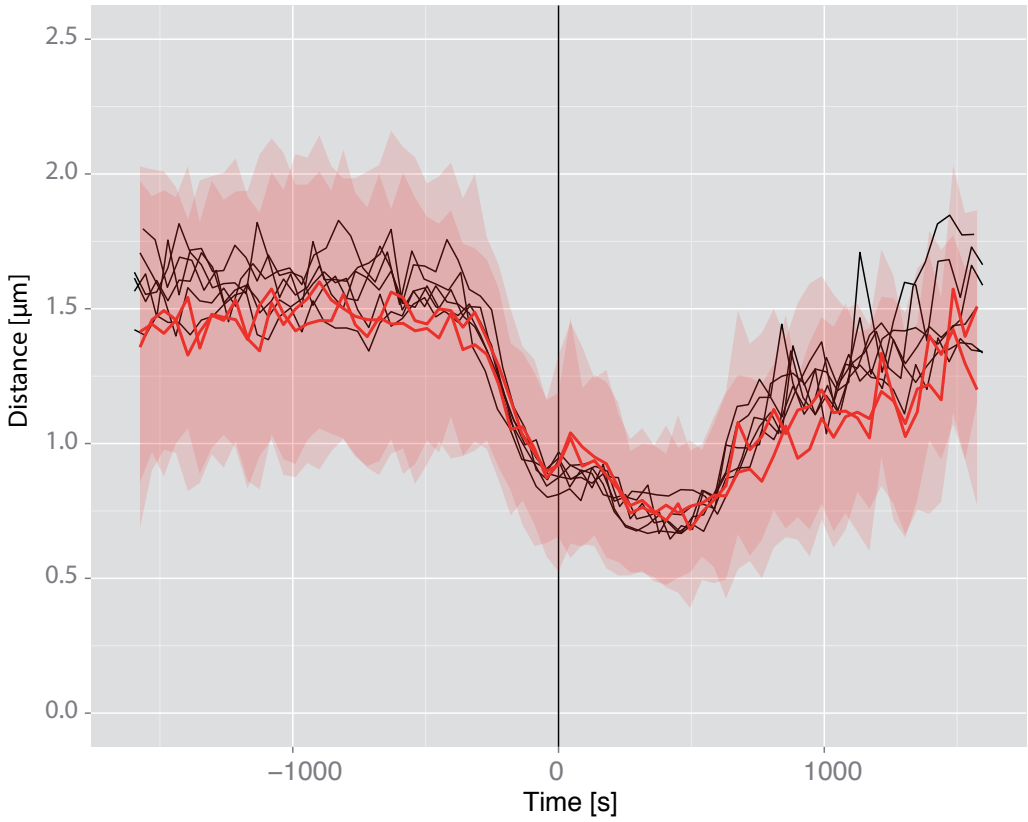

Figure 2.9: A strain with *zas1*-Y289X truncation (strain 4049) has no condensation defect. Black: control curves as in fig. 2.3. Red: Condensation curves of *zas1*-Y289X, averages of 112 and 75 cells, respectively.

fig. 2.10 A. Except for the ZF domains and the predicted fungal TF domain, a short stretch of 5 to 8 aa is conserved throughout almost all basic local alignment search tool (BLAST) hits (fig. 2.10 A 2). In Zas1, the respective conserved stretch ranges from V275 to S283 (VVRWLFSS) and is therefore contained within the region that had been identified as essential in the truncation experiments (section 2.1.7 and fig. 2.8).

If this sequence were indeed functionally important, then deletion of aa 276 to 282 should be sufficient to induce a strong proliferation defect. To test this hypothesis, I first created a complementary DNA (cDNA) allele of *zas1*'s short splice isoform via reverse transcriptase PCR (RT-PCR). The cDNA allele, introduced in the endogenous locus via PCR targeting, complemented the *zas1*$^{+}$ allele (B top an C second column). This indicates that the long, three ZF containing isoform is not required for vegetative growth.

To address the motif's functional importance, I deleted residues V276 to S282 from the cDNA allele and repeated the tetrad dissection experiment. Haploid cells in which the *zas1*$^{+}$ allele had been replaced by the *zas1-Δ276-282* allele showed a pronounced growth defect (fig. 2.10 C, third column). Strikingly, deletion of a 42 aa region N-terminally adjacent of the motif, where little conservation was detected, did not affect growth as drastically (fig. 2.10 C, fourth column).

The Eukaryotic Linear Motif database (ELM) (`elm.eu.org`, Dinkel et al. (2016)) contains

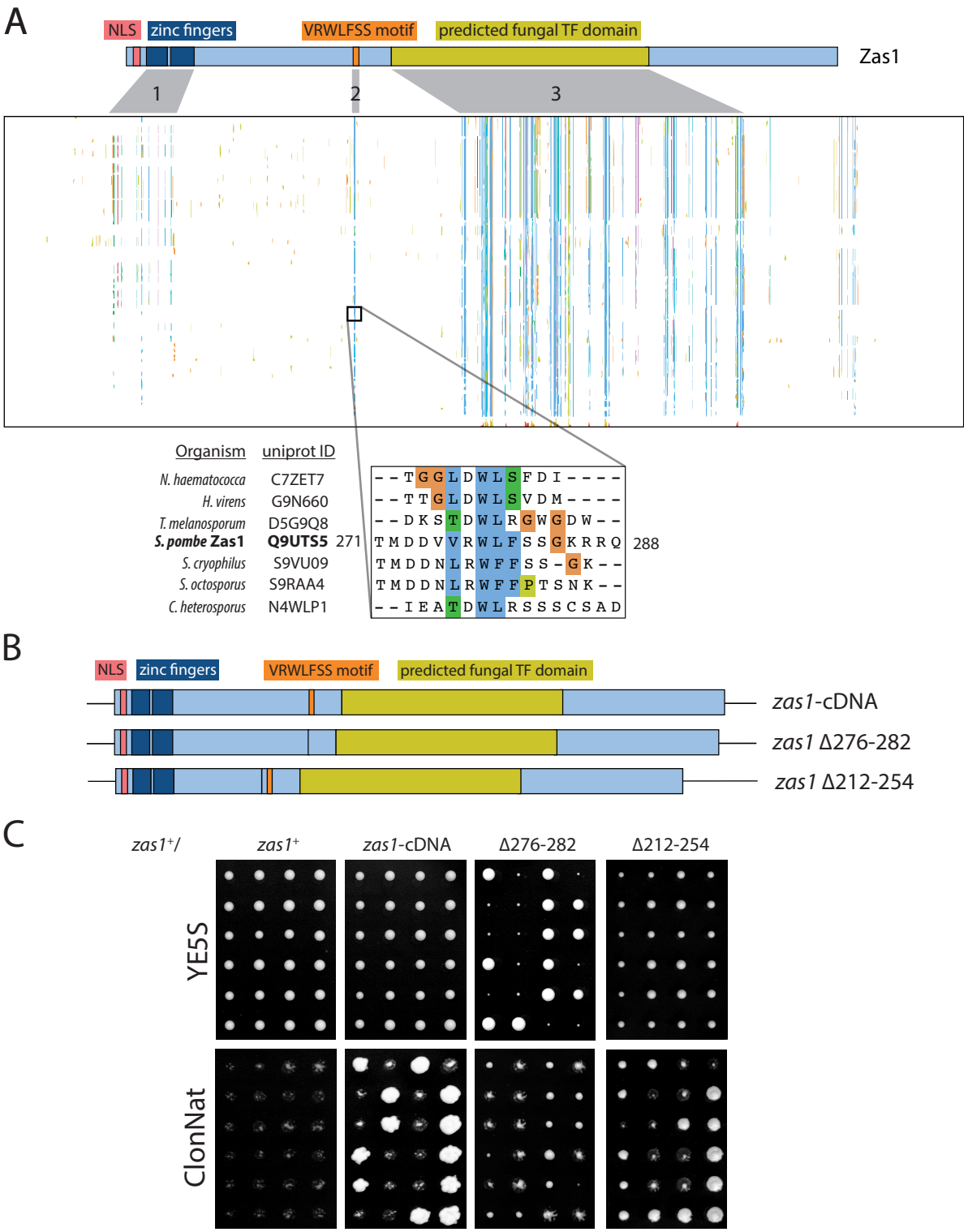

Figure 2.10: Zas1 contains an essential E2F pRb A B groove binding motif. (A) Overview of an alignment of a Zas1 psi-blast reveals three highly conserved regions in Zas1: The N-terminal zinc fingers (1), a C-terminal domain (3) and a VxWLF motif (2). Bottom: zoom-in on Zas1's motif. (B) Schematic representation of was alleles tested for functionality in (C). (C) Tetrad dissections of heterozygous diploid strains carrying one wt *zas1* allele and one mutant allele as indicated above. Strains 2457, 4083, 4093, 4387.

an entry that matches the conserved peptide sequence. The Rb pocket AB groove ligand motif (ELM accession number ELME000301) with the consensus sequence [LIMV]xx[LM][FY]D matches 276VxxLFS, except for the last residue serine. This short linear motif is found in metazoan E2F TFs, where it is involved in pRb-E2F interaction and mediates regulation of the start cell cycle checkpoint. According to its ELM database entry, this linear motif class had not been identified in unicellular organisms before.

The Zas1 motif deviated by a serine residue in the last motif position instead of aspartate. Phosphorylation could alter serine to bear a negative charge and thereby regulate binding to the motif. Contrary to this assumption, substitution of serine 281 with alanine (S281A) did not affect cell proliferation. Zas1's paralog Klf1 contains an aspartate residue followed by an asparagine at the corresponding position (fig. 2.11 A). Altering serines 281 and 282 accordingly

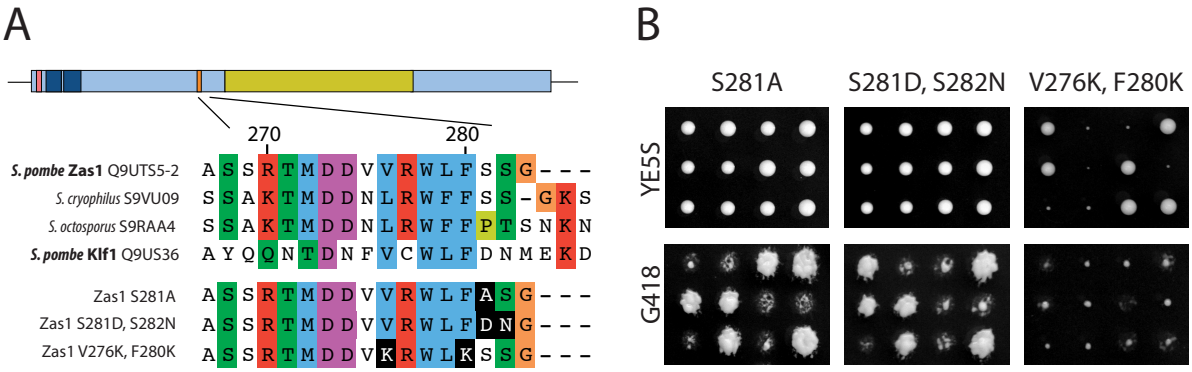

Figure 2.11: Viability of Zas1 motif point mutants. (A) Alignment of *S. pombe* Zas1 motif with *S. cryophilus*, *S. octosporus* and *S. pombe* Klf1. Below position of mutated residues (white font on black background) in the motif. (B) Tetrad dissections of heterozygous diploids carrying one *zas1*$^+$ allele and one cDNA allele with the mutation indicated. While mutation of S281 or S282 to alanine or aspartate and asparagine has no significant effect on proliferation ((B), left and center column), mutation of V276 and F280 to lysine strongly impairs proliferation. Strains 4386, 4389, 4415.

(S821D, S282N) likewise did not alter growth. Both targeted mutagenesis results argue against an involvement of serines 281 and 282 in Zas1's essential function(s).

In contrast to the serine mutations, a V276K F280K double mutation recapitulated the motif deletion phenotype (fig. 2.11). A second match is a cyclin recognition site (277-280) RWLF (consensus [RK]xLx(0,1)[FYLIVMP]). Both linear motifs have in common that they are ligands of cyclin fold domains.

2.1.10 Zas1' AB grove binding motif region is accessible to other proteins

In metazoan E2F TFs, the motif binds to the groove formed by two of pRb's cyclin folds. If Zas1's motif were involved in protein-protein interactions like in E2F transcription factors, the peptide region had to be accessible to other proteins and therefore exposed on the protein surface. To probe surface accessibility, I chose a limited proteolysis approach. Limited proteolysis can reveal accessible regions and unstructured loops in the native protein by incubation with a protease. Most accessible regions are hydrolised first, while folded domains form metastable

products. N and C termini of the fragments correspond to exposed regions and can be mapped using mass spectrometry.

I inserted the Zas1 cDNA into the insect cell expression vector pFastBac HTb (plasmid 3) in frame with an N-terminal His_6-TEV-tag. His_6-Zas1 was recombinantly expressed in *Spodoptera frugiperda* cells (section 4.3) and purified using immobilized metal ion affinity chromatography (IMAC) (section 4.4.1) followed by His_6 tag cleavage and dialysis (section 4.4.2). To increase purity, Zas1 was further separated from contaminants by size exclusion chromatography (SEC). Purified Zas1 was incubated with the proteases trypsin (fig. 2.12 A) or subtilisin (fig. 2.12 B) and the reaction was stopped after defined time points by addition of SDS Lämmli loading buffer (section 4.9.2) and instantaneous heating to 95 °C. Proteolysis fragments were separated on SDS poly acrylamide gel electrophoresis (SDS-PAGE) (fig. 2.12). Bands corresponding to stable fragments were isolated from the gel and N and C termini were sequenced by mass spectrometry in the European Molecular Biology Laboratory (EMBL) proteomics core facility.

Positions of the fragments' termini were mapped to the Zas1 primary sequence along theoret-

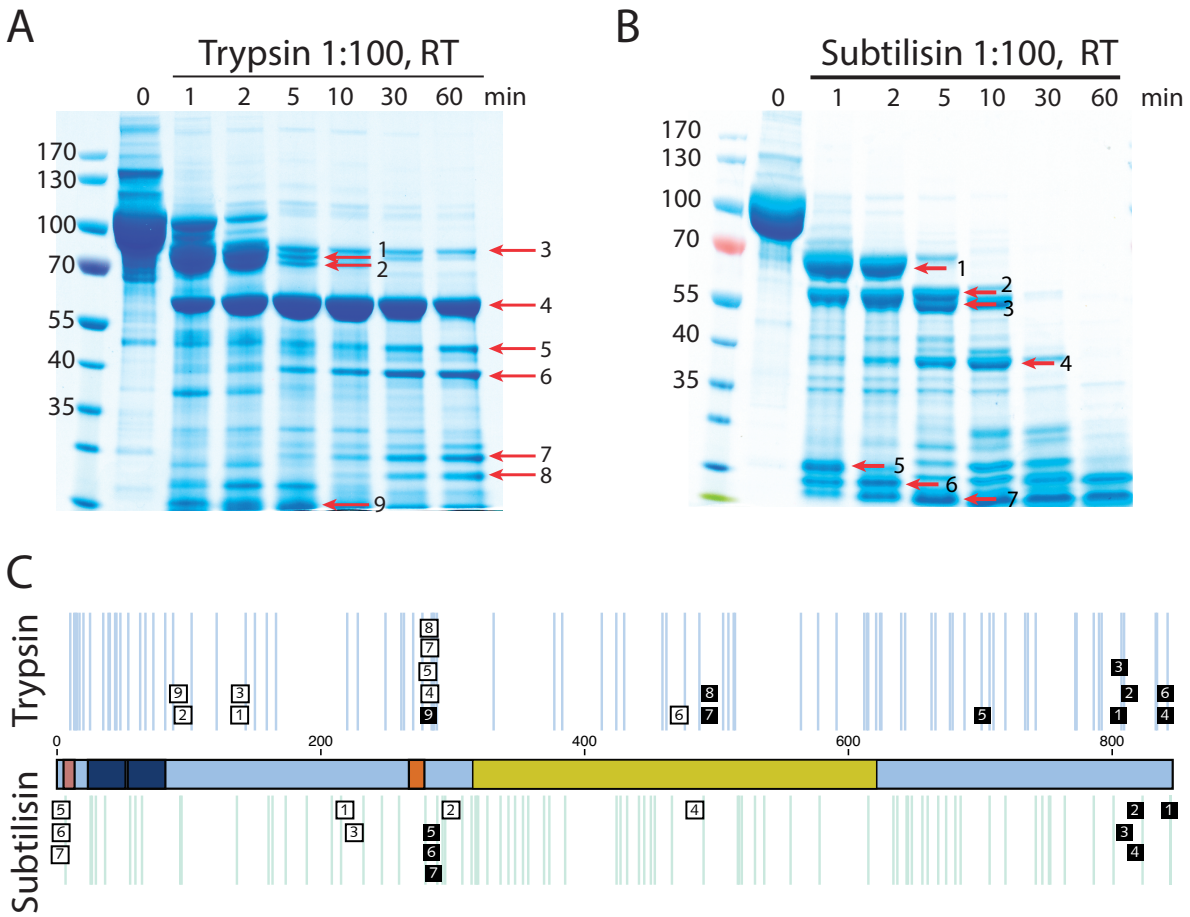

Figure 2.12: Limited proteolysis reveals exposed regions of Zas1. (A) and (B) Coomassie stained SDS-PAGE of recombinant Zas1 and limited proteolysis fragments after indicated time.The experiment was carried out using Trypsin (A), and subtilisin (B). (C) Plot of mapped fragments along the protein sequence of Zas1. Boxes indicate the position of mapped peptides' termini. top trypsin fragments, bottom subtilisin fragments. Horizontal lines show possible cleavage sites for trypsin (light blue) and subtilisin (light green). White boxes indicate N termini, black boxes indicate C termini.

ical cleavage sites (fig. 2.12 C). 9 out of 16 cleavage products had boundaries within 30 aa of the motif. Some of the fragments appear as early as 1 min to 5 min after protease addition, indicating that the corresponding regions were surface-exposed. I therefore concluded that the motif is in a region of Zas1 that is surface accessible to other proteins. The C-terminal region folds into a protease-resistant, stable domain, corresponding to trypsin fragment 4 and subtilisin fragments 2 and 3. Toby Gibson hypothesized based on sequence analysis that this region of Zas1 folds into a pRb-like tandem cyclin fold domain (see also section 2.1.15). Overall, these findings support the hypothesis that the motif is involved in protein-protein interactions and make it unlikely that its deletion merely causes protein folding defects.

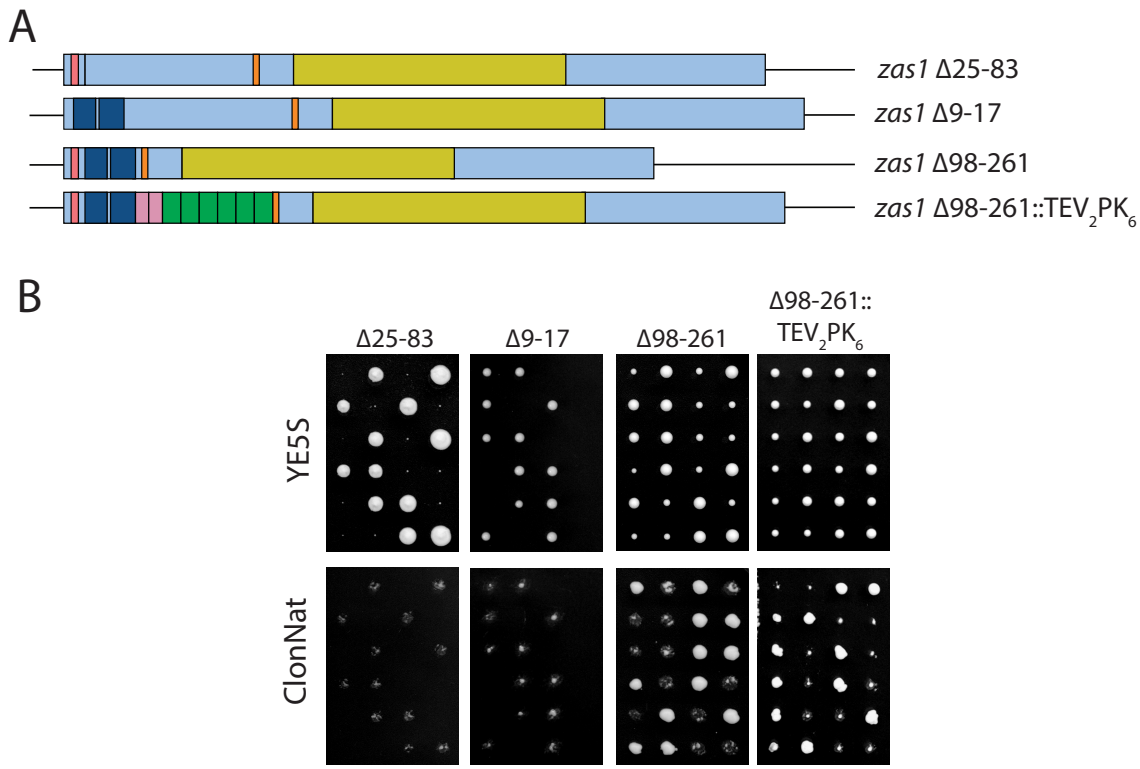

Figure 2.13: NLS and ZFs are essential, the region between ZF and motif has a spacer function. (A) Diagram of the N-terminal internal deletion constructs tested. (B) Tetrad dissections of diploid strains after replacement of one *zas*$^{+}$ allele with the respective allele depicted in (A). Strains 4093, 4470, 4390, 4486.

2.1.11 Zas1's NLS and ZFs are essential, but not the region connecting ZFs and motif

The results described in the previous paragraphs revealed an essential short motif at V275 and the dispensability for growth of all aa C-terminal of the motif. To finalize identification of all essential regions in Zas1, I systematically deleted domains N-terminal to the motif.

ZFs and NLS are essential

In their publication, Okazaki and Niwa (2000) describe canonical C2H2 zinc fingers in Zas1, but whether this domain is necessary for Zas1's essential functions remained unanswered. I showed in section 2.1.9 that the third ZF is not required for vegetative growth. Yet, if the first two ZFs are required for Zas1's essential function had not been tested. Likewise, the canonical NLS is in accord with the nuclear localization of the protein (section 2.1.4). However, a second, cryptic NLS could be redundant with the canonical NLS.

I created deletion alleles of ZFs (aa 25-83) and NLS (aa 9-17) based on the previously created cDNA allele (see section 2.1.9 and fig. 2.10). Again, I tested these alleles' ability to accomplish Zas1's essential function by replacing the endogenous wt allele with the mutant alleles in a

diploid strain and preforming tetrad dissection. Deletion of both ZFs leads to viable, but very slowly proliferating haploid cells (fig. 2.13 B, first column). This experiment therefore identifies the ZFs as a second essential domain in addition to the motif. This suggests that recruitment to the ZFs's target DNA binding sites is a part of Zas1's essential function. The role of the third, alternatively spliced ZF is to be determined.
Deletion of the NLS leads to inviable cells. This suggests that the canonical NLS is the only sequence regulating Zas1 nuclear import.

The sequence connecting ZFs and motif has a spacer function

Zas1's NLS, the first two ZFs and the AB groove binding motif are essential for *S. pombe* proliferation (section 2.1.9 and previous paragraph). However, the sequence between ZFs and motif has remained untested for its contribution to Zas1 function. Thus, I deleted aa 98-261 in the cDNA and tested this *zas1-Δ98-261* allele's ability to complement the deletion as previously described. Haploid *zas1-Δ98-261* cells displayed a mild proliferation defect (fig. 2.13 B, third column).
I considered two plausible explanations as cause of the mild growth defect. First, a functionally important sequence could be present between ZFs and motif. Alternatively, close proximity could induce sterical hindrance between ZF domains and the motif's ligands. To test both hypotheses, I replaced aa 98-261 by a non-related sequence of approximately equal length, TEV_2PK_6. Haploid cells had a minor growth defect that was less severe than that of *zas1-Δ98-261* (fig. 2.13 B, fourth column). In conclusion, aa 98-261 do not contain functional sequences but rather serve as a spacer sequence.

2.1.12 Genome wide identification of Zas1 binding sites by ChIP seq

To improve our understanding of *zas1* function, it is indispensable to identify its binding sites in the genome (section 3.2.8). Because Zas1 localizes to foci in *S. pombe* nuclei section 2.1.4, I reasoned that it might bind to specific sequences in the genome.
A powerful method to determine binding sequences of chromatin-associated proteins genome-wide with high precision is chromatin immunoprecipitation followed by next generation sequencing (ChIP seq). In short, proteins are formaldehyde cross-linked to DNA *in vivo*. Cells are lysed, the chromatin is sheared and Protein Of Interest (POI)–DNA cross linked fragments are enriched by immunoprecipitation (IP). Enriched DNA fragments are purified and used for NGS library preparation, followed by high throughput sequencing.
To enable IP of Zas1, I fused the *zas1* ORF to a C-terminal PK_6 epitope tag at its endogenous locus using PCR targeting (section 4.5.5). An anti-PK antibody (AB) (V5, see table 4.13) detected a single, specific band of expected size in a western blot (fig. 2.14 A). Using the Zas1-PK_6 strain and an untagged strain as control, I performed the ChIP protocol (section 4.1.17). I measured isolated DNA amounts from PK_6-tagged and untagged strains using Qubit DNA quantification (section 4.1.2). In three biological replicates, about 5 times more DNA immunoprecipitated in tagged samples compared to untagged samples (fig. 2.14 B). This supports the notion that Zas1 is chromatin bound.
Two ChIPed and input DNA sample sets were used to create NGS libraries with the help of the EMBL Genomics Core Facility (section 4.1.18). Libraries were sequenced on a Illumina HiSeq 5000 NGS system by the EMBL Genomics Core Facility in single end, 50 nt read length mode. Genome Biology Computational Support (Charles Girardot and Jelle Scholtalbers) helped in the analysis of the sequencing data using the Galaxy platform (Afgan et al., 2016) implementation at EMBL. Base calling certainty was high throughout the 50 sequencing cycles in samples from both replicates, as indicated by average quality scores (fig. 2.14 C). Reads were mapped to the recent *S. pombe* genome version (verison 29) (Wood et al., 2002; McDowall et al., 2015) using Bowtie2 (version 1.4) (Langmead and Salzberg, 2012). To which chromosomes each read aligned is broken down in fig. 2.14 D. Notably, in Zas1-PK_6 tagged experiments, the amounts of mitochondrial DNA in the ChIPed samples is considerably lower compared to input. This indicates specific pulldown of Zas1-bound DNA. Reads that did not align to the *S. pombe* genome were discarded, duplicate reads were kept.

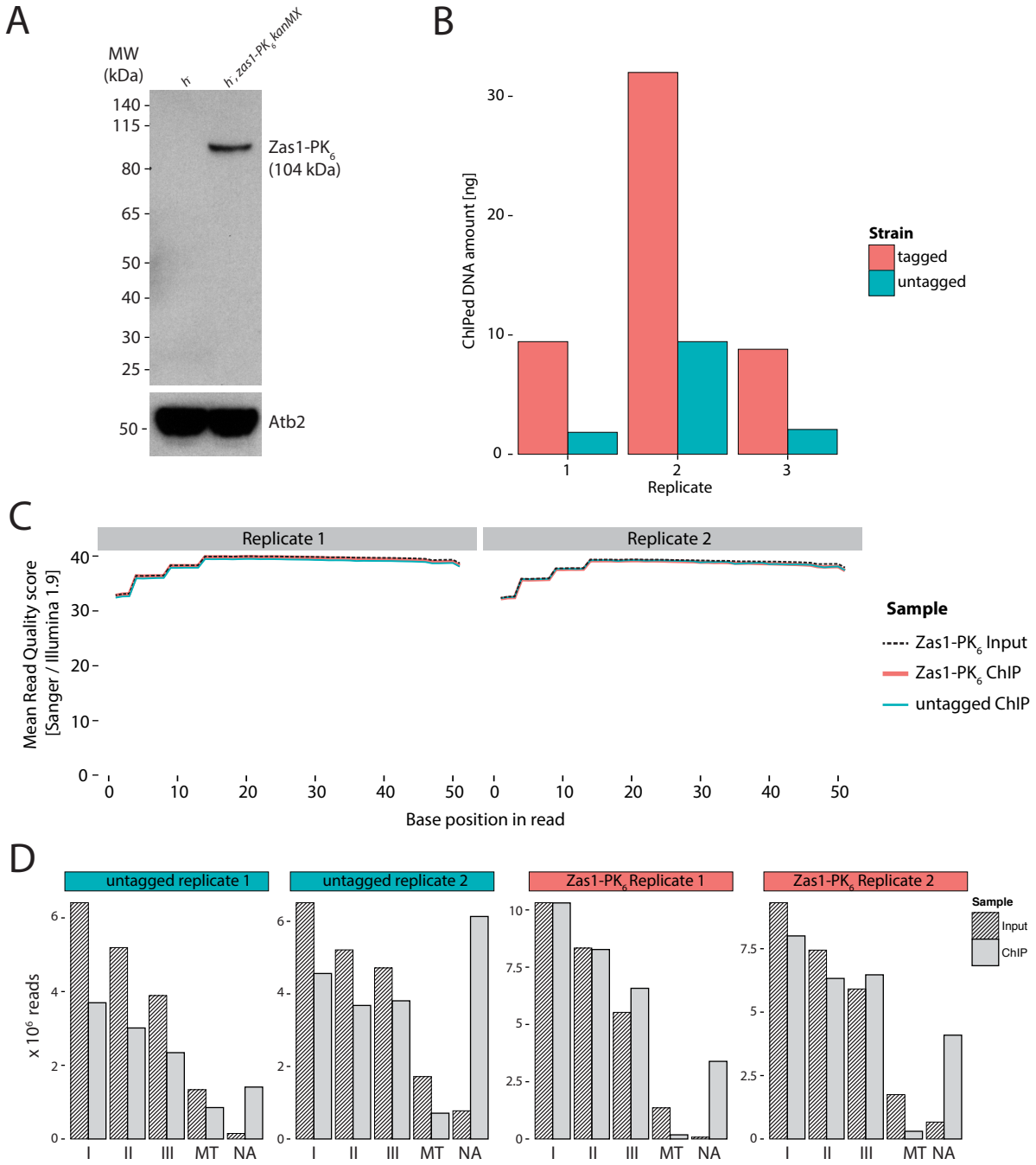

Figure 2.14: (A) Zas1 can be C-terminally PK_6 tagged (strain 4120) and the antibody detects a specific band in western blot. (B) DNA amounts isolated from tagged and untagged strains in ChIP experiments. Replicates 1 and 2 were processed for sequencing. (C) Average sequencing base call quality after each cycle. (D) Number of reads per chromosome. I, II, II: Reads aligned to the respective chromosome. MT: mitochondrial genome. NA: reads that did not align to the *S. pombe* genome.

Zas1 binds to the *cnd1* promoter region

I used alignment files to create .bigwig alignment maps, which I visualized in IGV (version 2.3.68) (Thorvaldsdóttir et al., 2013). I visually inspected gene regions of known condensation factors for read enrichment. While condensin subunit gene regions *cnd2*, *cnd3*, *cut3*, *cut14* as well as *top2* did not show an enrichment of reads, the *cnd1* promoter region was significantly enriched in reads compared to input and untagged controls (fig. 2.15).

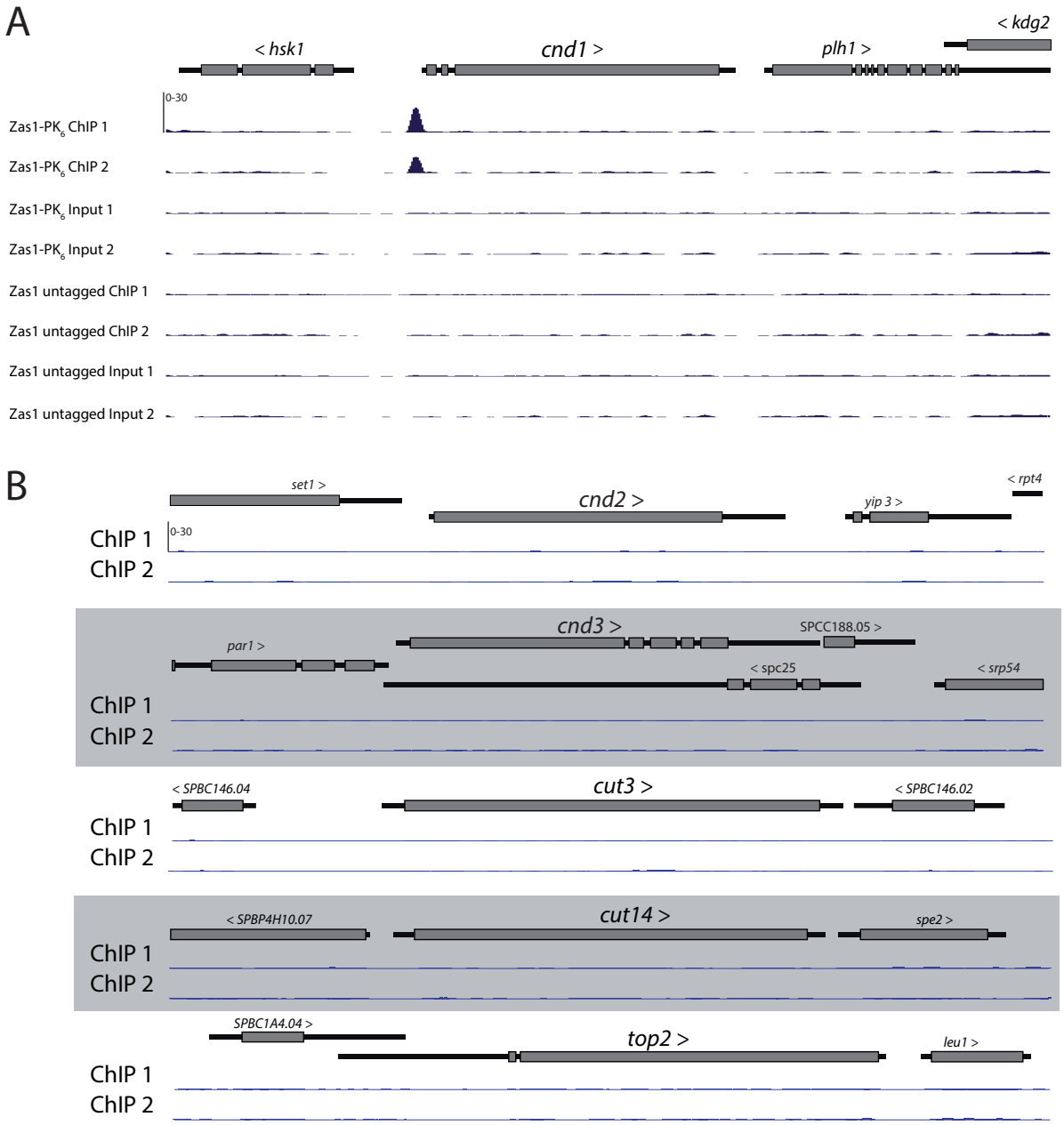

Figure 2.15: ChIP seq reveals Zas1 localization to the *cnd1* promoter but not to other chromosome condensation genes. (A) Read alignment maps at *cnd1* locus.

Identification of prominent Zas1 binding sites

To identify the most prominent Zas1 binding sites in an unbiased manner, peaks were called using Model-based Analysis of ChIP-Seq Data (MACS) (Zhang et al., 2008; Feng et al., 2011) on both replicates, using the input sequencing data for background correction. Reproducibility of peaks was assessed using the IDR algorithm implemented on the EMBL Galaxy platform (Landt et al., 2012). Binding sites with more than 6-fold enrichment over λ_{local} are listed in table 2.2, along with corresponding gene regions, the genes' functions and whether the genes are essential for viability.
18 of the 20 most prominent binding sites coincide with promoter regions (peak summit closer than 700 bp 3' of transcription start site). This implies that Zas1 could function as a transcription factor. The chromatin immunoprecipitation (ChIP) experiment also revealed binding sites in TR or promoters of many non-coding RNAs (ncRNAs). Two of the three most enriched binding sites, lie within the promoters of genes *SPBC887.16* and *SPBC713.14C*, genes containing sort, dubious ORF. For neither of these genes information about homologous genes or whether they are required for viability was available in pombase. *SPBC713.14C* codes for 73 aa and 108 aa, respectively; the *SPBC887.16*'s ORF is 109 aa long. Could these short, dubious peptides be involved in chromosome condensation? To obtain initial information, I used tetrad dissection analysis to assess whether their ORFs are essential. I found both *SPBC713.14C* and *SPBC887.16* not to be required for vegetative growth (fig. 4.4).

Table 2.2: Top binding sites of Zas1. Chr: Chromosome. E: enrichment over λ_{local}. TR: transcribed region. MAP: Microtubule Associated Protein. GEF: Guanosine Exchange Factor. ER: endoplasmatic reticulum. [1]see fig. 4.4. Information about ORF essentiality from Kim et al. (2010).

Chr	postion	E	Gene region, gene function	essential
II	3574612	8.76754	SPBC887.16 promoter and TR, dubious ORF	no[1]
II	4255750	8.76745	SPBC1652.02 promoter, ER aa transporter	no
II	891339	8.76128	SPBC713.14C promoter, dubious ORF	no[1]
II	3702847	8.75815	*puc1* promoter, G_1 type cyclin	no
I	3158038	8.75502	SPNCRNA.217 promoter	NA
			peg1 promoter, MAP	yes
I	4360643	8.66738	*ayr1* 3'UTR	no
			SPNCRNA.244 promoter	NA
I	2689543	8.66425	SPAC644.09 promoter, alanine racematase	no
I	304248	8.49209	SPAC18B11.09c terminator, serine acetyltransferase	no

continued on next page.

Chr	position	E	Gene region, gene function	essential
			SPAC18B11.08c promoter, conserved fungal protein	no
I	2031004	8.40758	*tom22* promoter, mitochondrial import complex	yes
II	3058533	8.12587	*rbd1* promoter, mitochondrial protease	no
			brf1 3'UTR, TFIIIB	yes
			vrp1 5'UTR, verprolin	no
I	4705992	8.05702	*pmo25* promoter and 5'UTR, mo25 family protein	yes
I	5298604	8.03119	*pyp3* promoter, cdc2 tyrosine phosphatase	no
II	3200034	7.92242	*cnd1* promoter, condensin HEAT repeat subunit	yes
I	1294160	7.87057	SPAC1565.03 promoter, pombe specific protein	no
			SPAC1565.03 asRNA 3' region	NA
I	2406091	7.81133	SPAC1B9.03c promoter, rRNA assembly	yes
I	2313567	7.77217	*teb1* promoter, telomere binding protein	yes
II	4391299	7.63925	*pob1* promoter, Boi family protein	yes
II	2585225	7.61036	SPNCRNA.1531 transcribed region (TR)	NA
			SPNCRNA.1532 TR	NA
			SPNCRNA.402 TR	NA
I	934205	7.56181	SPNCRNA.160 TR	NA
I	2326509	7.189	SPAC6C3.03c coding region, uncharacterized	no
			SPAC6C3.03c TR, antisense RNA (asRNA)	NA
I	3222213	7.17745	*pre5* promoter, proteasome subunit	yes
I	2095388	7.09019	SPNCRNA.794 TR	NA
			obr1 promoter, ubiquitinated protein	no
			obr1 3'TR, asRNA	NA
II	1080123	7.05072	SPNCRNA.337 promoter	NA
			SPNCRNA.1409 TR	NA
II	3980077	6.88679	SPNCRNA.111 TR, double peak	NA
I	1150514	6.71651	SPAC56F8.15 terminator, uncharacterized	NA
			mug115 3'UTR, meiotically upregulated	no

continued on next page.

Chr	position	E	Gene region, gene function	essential
II	2113410	6.70391	*rga7* promoter and 5'UTR, Rho GEF	no
I	1951716	6.69672	SPNCRNA.777 TR	NA
			pcs2 terminator, phytochelatin synthetase	no
I	3395387	6.65786	False Positive: Peak in untagged	
I	2876728	6.46334	*mug153* 3'UTR (meiotically upregulated)	no
			SPACUNK4.16c promoter, α,α-trehalose-PO_4-synthase	no
II	625870	6.40818	False Positive: Peak in untagged	
I	1149045	6.40289	SPAC56F8.15 promoter, uncharacterized	NA
			mug115 3'UTR	no
II	2585883	6.32078	SPBC2G5.05 promoter, transketolase	yes
I	4787913	6.25283	SPNCRNA.253 promoter and 3'TR	NA
I	1600311	6.23842	SPAC23H4.05c terminator, uncharacterized	NA
I	4457041	6.23842	SPNCRNA.989 TR	NA
I	1358354	6.20981	SPNCRNA.86 promoter	NA
			SPNCRNA.736 TR	NA
			SPNCRNA.737 TR	NA
II	3155412	6.18145	SPNCRNA.1583 TR	NA
			SPNCRNA.415 terminator	NA
			SPBC609.01 promoter, ribonuclease	yes
II	4465536	6.17894	SPNCRNA.1696 TR	NA
			SPNCRNA.532 terminator	NA
I	783907	6.16642	SPAC4G8.12c 3'UTR, α-1,2-mannosyltransferase	yes
I	5315538	6.01618	*ofd2* 3'UTR, H2A dioxygenase	no
			rpl22 TR and terminator, ribosomal protein	no

Top binding sites of Zas1

2.1.13 Cnd1 levels, but not Cnd2 levels, are reduced in *zas1-K833X*

The ChIP seq data revealed that the promoter region of *cnd1* is a prominent binding site of Zas1 (section 2.1.12 and table 2.2). This suggests that Zas1 might regulate transcription of *cnd1*. This hypothesis would explain the chromosome condensation defects and chromosome mis-segregations observed in *zas1* ts mutants (section 2.1.3 and fig. 2.4). A prediction of this model is that Cnd1 protein levels are altered in *zas1* ts mutants. To test this prediction, I compared Cnd1 protein levels qualitatively between *zas1*$^+$ and *zas1* ts strains by western blotting.

Cnd1 levels are reduced in *zas1-K833X* cells

Because no Cnd1 antibody was available, I tagged the endogenous *cnd1* ORF C-terminally with a PK_6 epitope tag by PCR targeting (section 4.5.5) in a diploid strain. Epitope tags can impair protein function. Since Cnd1 is essential for proliferation, I judged Cnd1 functionality based on colony size compared to *cnd1*$^+$ after tetrad dissection. I did not find a difference in colony size between *cnd1-PK*$_6$ cells and *cnd1*$^+$ cells (fig. 2.16 A, left column). I therefore concluded that Cnd1-PK_6 is functional. The V5 antibody (table 4.13) specifically recognized a band of the expected size (138.5 kDa) on a western blot of whole cell extracts from tagged cells (sections 4.4.7 and 4.5.10). I introduced a heterozygous *zas1-AJ3* like truncation (K833X) of Zas1 at its endogenous locus by PCR targeting into the *cnd1*$^+$*/cnd1-PK*$_6$ strain. Sporulation and tetrad dissection revealed a 2:2 segregation of a pronounced growth defect linked to the *zas-K833X* truncation. I chose colonies from two independent tetrads in which *cnd1-PK*$_6$ had segregated with one *zas1*$^+$ allele and one *zas1-K833X* allele (encircled colonies in fig. 2.16 B, left). I cultured these strains to log phase in liquid medium and prepared protein extracts from 5×10^7 cells. I used equal amounts of extract for western blotting, as shown by a tubulin loading control (fig. 2.16 B, lower western blot panel). In both *zas1-K833X* strains, the V5 antibody detected less Cnd1-PK_6 compared to *zas1*$^+$ strains. I concluded that functional Zas1 is required to maintain wt Cnd1 protein levels. There results link the *zas1* ts phenotype to chromosome condensation defects.

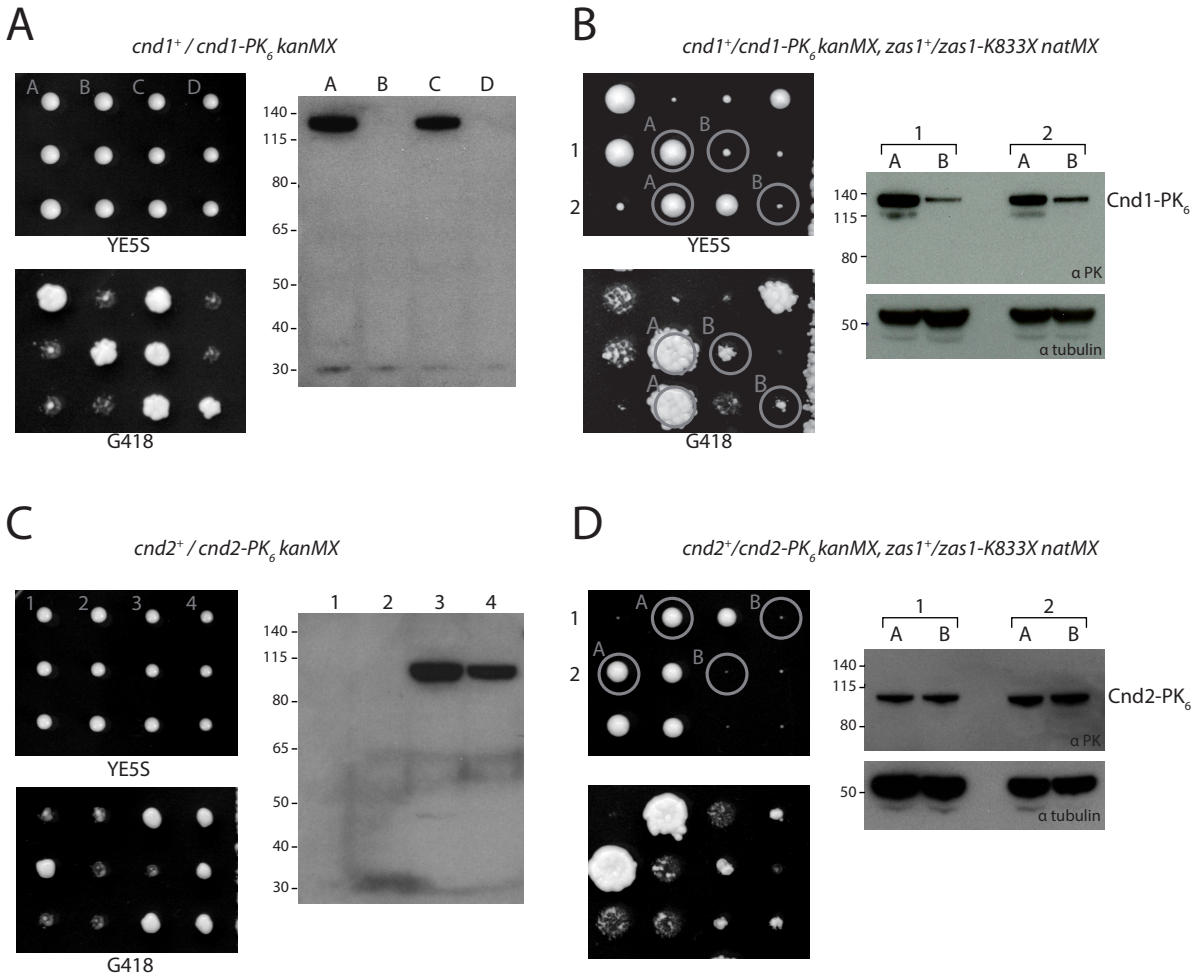

Figure 2.16: Cnd1-PK$_6$ levels are reduced in *zas1-K833X* cells. (A) Left: C-terminal epitope tagging of Cnd1 (strain 4503) does not affect cells' ability to proliferate, indicating that Cnd1-PK$_6$ is functional. Right: Western blot showing 2:2 segregation of tagged (A, C) and untagged (B, D) Cnd1 genes. (B) One *zas1* allele in the strain from (A) was truncated to *zas1-833X* (strain 4543). The resulting strain was tetrad dissected and *zas1-833X* cells showed a growth defect and Cnd1-PK6 levels are reduced in *zas1-K833X* cells compared to *zas1*$^+$ cells. (C) PK$_6$-tagging *cnd2* (strain 4303) did not affect cell growth (left). Cnd2-*PK$_6$* could be detected by western blotting (right). (D) A heterozygous *zas1-833X* truncation was introduced into the *cnd2/cnd2-PK$_6$* background (strain 4610). *zas1-833X* had a pronounced growth defect (left). Cnd2-PK$_6$ levels did not differ between *zas1*$^+$ and *zas1-833X* background (right). Western blots in (A) (B, top blot), (C) and (D, top blot): 1° AB α V5 1:10000, 2° AB α mouse-HRP 1:10000. Western in (B, bottom) and (D, bottom): 1° AB α TAT1 1:500, 2° AB α mouse-HRP 1:10000.

Cnd2 protein levels are not affected by *zas1* ts mutation

I next tested if protein level reduction in *zas1* ts cells is specific to Cnd1 or whether other subunits of the condensin complex – including subunits where Zas1 had not been found at the genes' promoters – were also affected by Zas1 inactivation. I repeated the experiments described above for *cnd2*. C-terminal PK_6 tagging of Cnd2 in its endogenous gene locus did not influence cell growth (fig. 2.16 C, left). The V5 antibody detected a single protein of the expected size for Cnd2-PK_6 (90.4 kDa) (fig. 2.16 C, right). Again, introduction of the Zas1-*K833X* truncation induced a pronounced growth defect (fig. 2.16 D). In contrast to Cnd1, Cnd2-PK_6 levels were similar in *zas1*$^+$ and *zas1-K833X* strains. This implies that Zas1 does not regulate Cnd2 expression levels. A further implication is that reduction of the Cnd1 concentration does not affect Cnd2 concentration.

2.1.14 The *cnd3* promoter complements *cnd1*'s promoter but does not affect *zas1-833X* induced growth defect

Because Cnd1 is an essential protein, I assumed that the reduction of Cnd1 protein levels is the cause of the growth defects of *zas* ts mutant strains (fig. 2.2). To test this assumption, I decoupled transcriptional regulation of *cnd1* from Zas1 by replacing the *cnd1* promoter with the promoter of *cnd3*. *cnd3* encodes a protein of similar size and structure to Cnd1, and Zas1 does not bind the promoter of *cnd3* (fig. 2.15 B). The essential gene *hsk1* is located 3' of *cnd1*' promoter in antisense orientation (fig. 2.17 A). To avoid affecting transcription levels of Hsk1 by altering the possibly bidirectional promoter sequence, I displaced the *cnd1* promoter by integration of a *kanMX* marker cassette instead of deleting this region. This promoter displacement made cells inviable, suggesting that without proximal promoter region, no or only insufficient transcription occured at the *cnd1* locus. I introduced the *kanMX* cassette together with the *cnd3* promoter and 3' UTR into a heterozygous *zas1*$^+$/*zas1-K833X natMX* strain and performed tetrad dissection.
Growth of cells in which *cnd1* promoter had been replaced by the *cnd3* promoter was undistinguishable from growth of *cnd1*$^+$ cells (fig. 2.17 B center column, second tetrad, third and fourth colony). Cells carrying the *zas1-K833X* allele showed a strong proliferation defect. Whether *cnd1*$^+$ or *cnd1* under *cnd3* promoter co-segregated with the *zas1-K833X* allele or with *zas1*$^+$, growth was affected to the same degree. I concluded from this data that the *zas1* ts growth defect is not due to reduced *cnd1* transcription levels. I assessed, if this conclusion held true for a *zas1* mutant with a less severe growth defect. I repeated the experiment described above with a second *zas1* allele, *Δ98-261*, that had induced a mild growth defect (see fig. 2.13). Again, I did not observe any difference in growth between *zas1* mutant cells with *cnd1*$^+$ allele or *cnd3* promoter-driven *cnd1*.

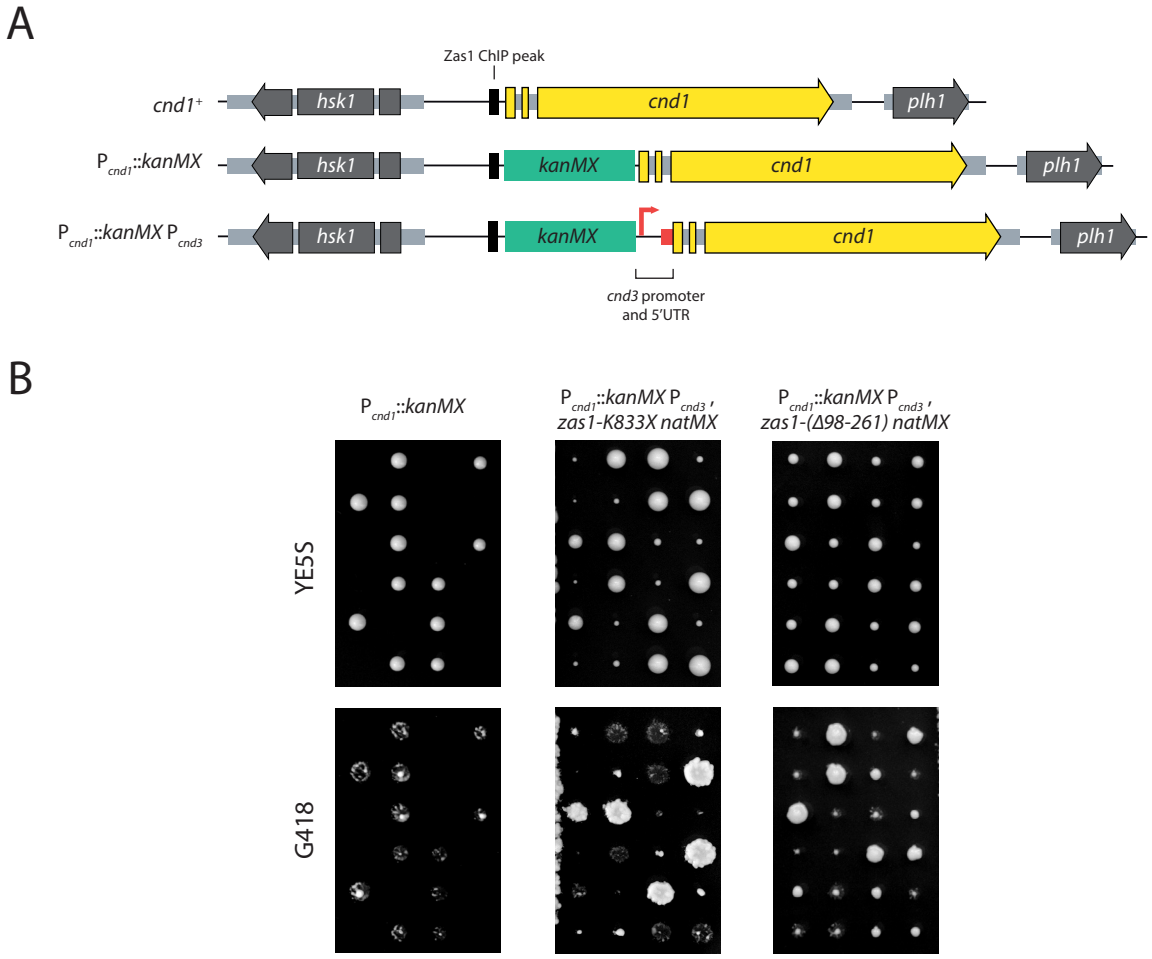

Figure 2.17: Zas1 ts induced growth defect is not due to reduced Cnd levels. (A) Schematic overview of the *cnd1* locus in *cnd1* promoter displacement and replacement strains (B) Tetrad dissections of diploid strains heterozygous for *cnd1* promoter displacement (left column), or *cnd1* promoter replacement by *cnd3* promoter in heterozygous *zas1* ts strains (center and left column). Cells containing the *cnd1* to *cnd3* promoter replacement form colonies on G418 (bottom row).

2.1.15 A peptide fragment close to the motif binds Zas1's C-terminal domain *in vitro*

I was interested to find out, which factors bind to Zas1's other essential region, the pRb A B groove binding motif. Could the motif interact with one of Zas1's other domains, e. g. the ZFs or the CTD? To address this question in an unbiased way, I combined limited proteolysis and analytical size exclusion chromatography (SEC). I incubated recombinant Zas1 with subtilisin as previously described (section 2.1.10 and fig. 2.12). In contrast to the previous limited proteolysis experiment, I terminated the hydrolysis reaction after 2 min by addition of 2 mM Phenylmethane Sulfonyl Fluoride (PMSF), a potent, covalent serine protease inhibitor (section 4.4.9). I set up a control reaction which I did not treat with subtilisin. I separated the fragments by size on an analytical SEC Ettan liquid chromatography system. Because the protein was kept in native conditions, fragment complexes of interacting domains should stay intact. Because fragment complexes are larger than the individual fragments, interacting frag-

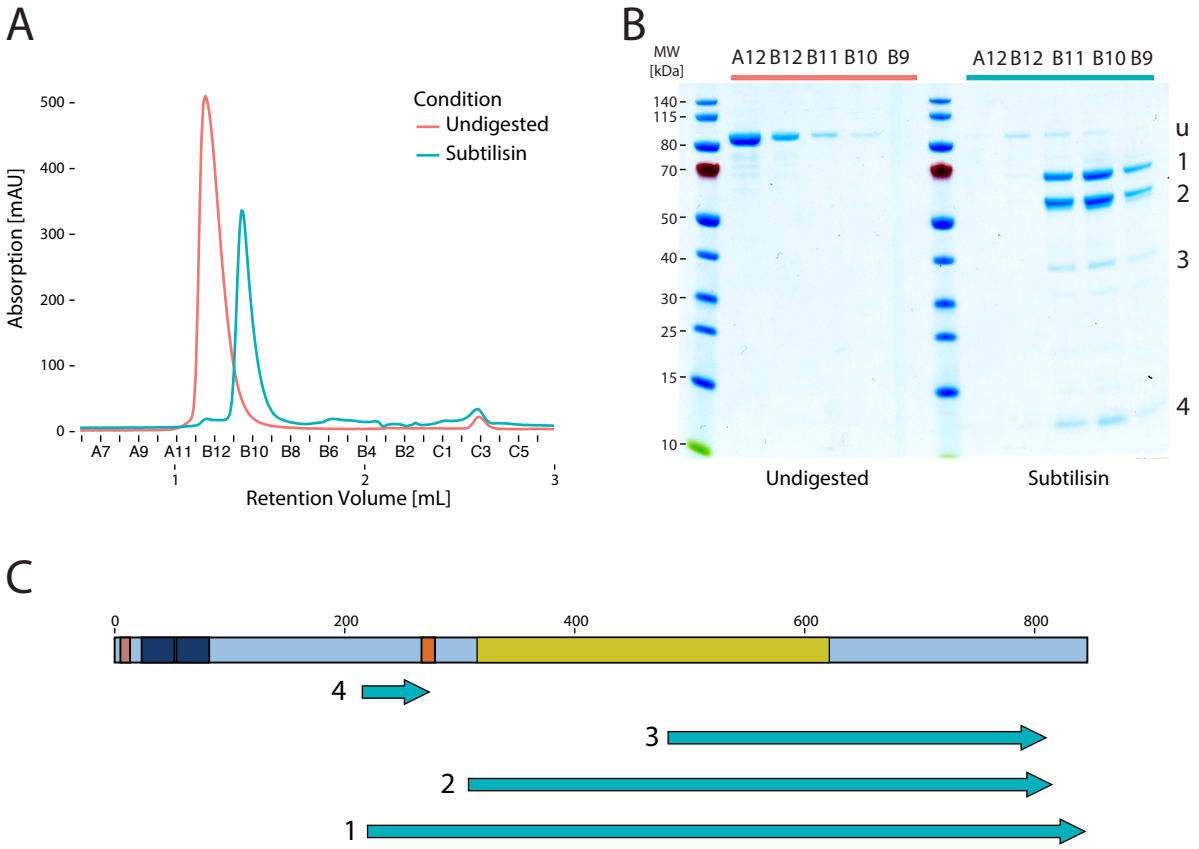

Figure 2.18: Limited proteolysis followed by SEC reveals interaction of Zas1's C-terminal domain with a peptide fragment containing the motif. (A) UV_{280nm} absorption plotted against elution volume after analytical SEC of intact Zas1 and subtilisin limited proteolysis products. (B) Coomassie stained SDS-PAGE gel. u: undigested, 1–4: Fragments mapped in C. (C) Map of fragments along the Zas1 primary structure.

ments elute at an earlier retention volume on the SEC than expected.

The undigested sample eluted at 1.16 mL. The LC UV detector detected the majority the subtilisin-digested protein at 1.35 mL retention volume, indicating reduced a protein size compared to untreated Zas1. I analyzed peak elution fractions from both experiments by SDS-PAGE and Coomassie staining (fig. 2.18 and sections 4.4.4 and 4.4.5). The major elution peak of the digested sample contained trace amounts of undigested Zas1, two fragments of around 60 kDa (fragments 1 and 2) and one short fragment between 10 and 15 kDa (fig. 2.18, B). Additionally, I observed minor quantities of a 40 kDa-fragment (fragment 3). The early elution volume of the 10 to 15 kDa-fragment indicated that this fragment interacted with the larger fragments during the SEC run. To reveal the molecular identity of the short fragment, its N and C termini were identified by the EMBL Proteomics Core Facility as described in section 2.1.10. I mapped the termini to the Zas1 primary sequence (fig. 2.18, C). For the smallest fragment (fragment 4), the most N-terminal peptide detected in the mass spectrometer started at K220, the most C-terminal fragment ended at W277. Both long fragments (1 and 2) contained the C-terminal region of Zas1. The longest fragment (1) partially included the motif and about 50

more N-terminal aa. Fragment 2 consisted of the C-terminal region only, starting from S309. The third, less abundant fragment consisted of the C-terminal half of Zas1. In conclusion, this data indicates that a short fragment from about K220 to about W277 is able to bind to the C-terminal domain of Zas1.

2.1.16 Zas1 forms homo-dimers *in vitro*

With 1.6 mL, the intact Zas1's elution peak appeared at a lower retention volume than expected for a 96.8 kDa protein (section 2.1.15 and fig. 2.18). One Zas1 molecule has a monomeric mass weight (MW) of 96.78 kDa. Usually, globular proteins the size of Zas1 have a larger retention volume, suggesting that Zas1 molecules form multimers *in vitro*. Additionally, a stretch of about 50 aa binds to Zas1' CTD *in vitro*. This interaction could either be intramolecular, involve two Zas1 molecules or induce even higher number oligomerization. Information about the oligomeric state of Zas1 would be informative to exclude some of these hypotheses. A reliable method to measure the MW of macromolecular complexes in solution is SEC with subsequent multi-angle light scattering (MALS) (SEC-MALS). Protein complexes in solution are separated by size on an analytical SEC and fractions are directly passed through a MALS spectrometer. Macromolecule-containing solutions scatter monochromatic light depending on the MW of the contained complex. Measurement of the intensity of the scattered light in dependence of the scattering angle provides information about the average MW of the complexes. I provided purified Zas1 protein to Vladimir Rybin (EMBL Biophysical support), who performed the SEC-MALS experiments and analyzed the data. In two independent experiments, he determined a MW of 198.03 kDa and 199.98 kDa as the average Zas1 MW of the peak fraction (fig. 2.19 A and B). Because both measurements correspond to twice the calculated monomeric MW of Zas1, I concluded that Zas1 forms dimers *in vitro*.

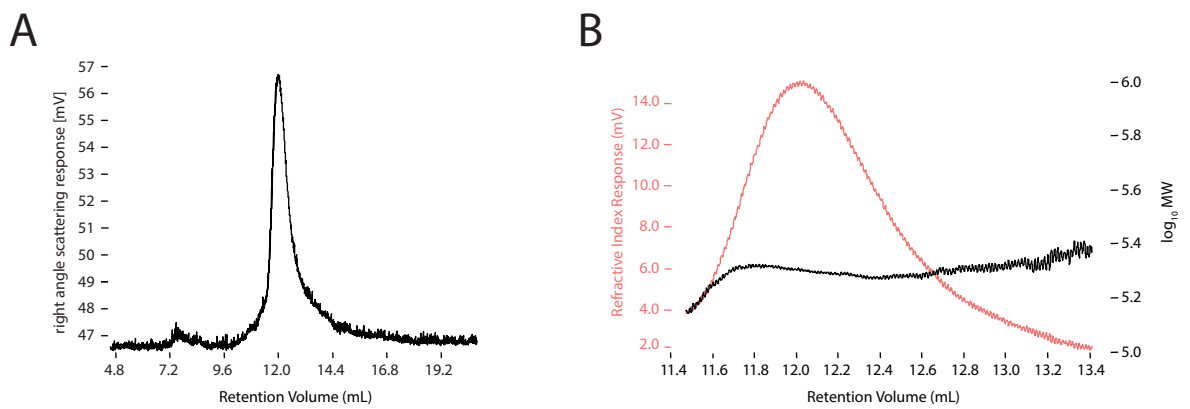

Figure 2.19: SEC-MALS shows that Zas1 molecules dimerize *in vitro* (A) Right angle scattering response as a function of SEC retention volume (B) Refractive index and refractive index adjusted MW calculation for scattering of the respective retention volume.

2.1.17 Abundant, cytosolic proteins co-immunoprecipitate with Zas1

To reveal potential regulators of Zas1 and ligands of the pRb A B groove binding motif, I took a co-Immunoprecipitation (co-IP) approach. Yeast cells expressing a PK_6 tagged version of Zas1 (strain 4120, see fig. 2.14) were lysed using cryomilling (section 4.5.12). I immunopurified Zas1-PK_6 by incubation with V5 antibody (table 4.13). From 4 L of culture, I isolated Coomassie-stainable amounts of Zas1 (section 4.4.3). Apart from the Zas1 full-length band and IgG heavy chain and light chain bands, I could detect 3 prominent additional bands at 70-80 kDa and 40 kDa, respectively (fig. 2.20). Mass spectrometric identification revealed that the two larger bands contained N-terminal truncations of Zas1. The smaller, 40 kDa-band contained GAPDH (Tdh1) and ADH (Adh1), two abundant, cytoplasmic enzymes. Because of the nuclear localization of Zas1, I concluded that both were false positives.

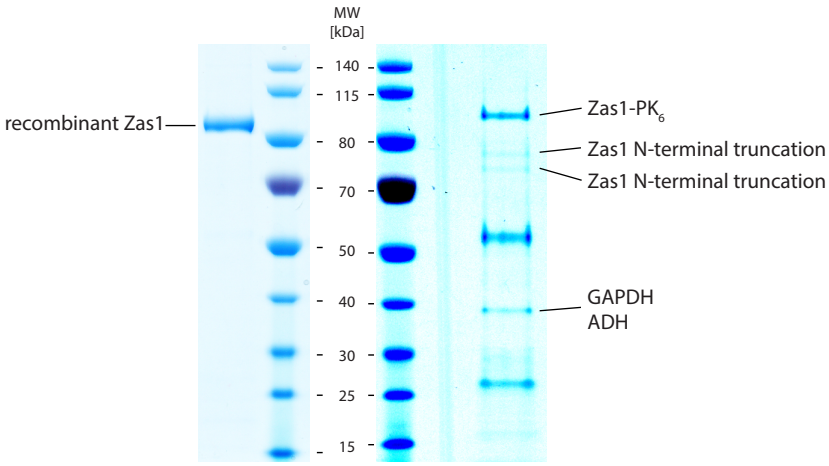

Figure 2.20: Zas1 co-IP. Left: SDS-PAGE migration of recombinantly purified Zas1 as reference. Right: SDS-PAGE of Zas1-PK_6 co-IP

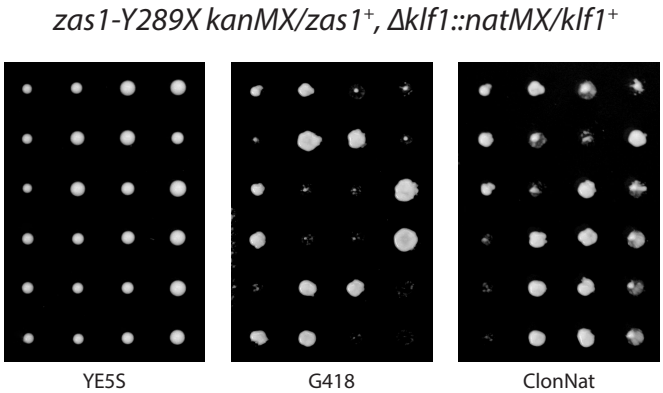

Figure 2.21: *klf1* and Zas1's CTD do not interact genetically. Strain 4572. See main text.

2.1.18 *klf1* and Zas1's CTD do not interact genetically

Zas1's CTD is not essential (section 2.1.8). I hypothesized that a parallel pathway complements the CTD's function. A good candidate for a parallel pathway component is *klf1*, *zas1*'s only non-essential paralog in *S. pombe*. Shimanuki et al. (2013) described that Zas1 and Klf1 form a heterodimer *in vivo* during G_0 phase. To clarify whether *klf1* and Zas11 CTD interact genetically, I deleted *klf1* in the diploid *zas1-Y289X kanMX/zas1*$^+$ strain (see section 2.1.8, resulting strain 4572) and tetrad dissected the resulting strain. If *klf1* complemented *zas1-Y289X*, deletion of *klf1* in a *zas1-Y289X* background should affect cell proliferation. After tetrad dissection, both single *Δklf1* mutants and double *Δklf1*, *zas1-Y289X* mutant spores formed equally sized colonies (fig. 2.21). These results confirm that *klf1* is not essential under the conditions tested here. They also demonstrate that *klf1* does not genetically interact with Zas1's CTD, rejecting the hypothesis that *klf1* acts in a parallel pathway to *zas1*.

2.1.19 Reduced Puc1 protein levels in *zas1-K833X* cells

The promoter of *puc1* was the forth most enriched region in Zas1 ChIP seq (table 2.2). *puc1* encodes a non-essential ORF with a primary sequence similar to cyclins and Puc1 had been found to complement G_1/S cyclins in *S. cerevisiae* (Forsburg and Nurse, 1991). Forsburg and Nurse (1994) found that Puc1 plays a role in mitotic exit. I asked, if Zas1 might regulate *puc1* transcription. Hence, I PK_6 tagged *puc1* at its C terminus in a diploid strain. Following the strategy in section 2.1.13, I truncated Zas1 at K833. I tetrad dissected the resulting strain heterozygous for *puc1-PK*$_6$ and *zas1-K833X*. *zas1-K833X* cells had a pronounced growth defect; growth was not influenced by presence of the PK_6 tagged *puc1* allele (fig. 2.22). I extracted equal amounts of protein from cycling *zas1*$^+$ or *zas1-K833X* cells and subsequently detected Puc1-PK_6 protein levels by western blot (fig. 2.22 B). Less Puc1-PK_6 protein was detected in *zas1-K833X* cells than in *zas1*$^+$ cells. In combination with the knowledge about Zas1's association with the *puc1* promoter I concluded that Zas1 positively regulates *puc1* expression.

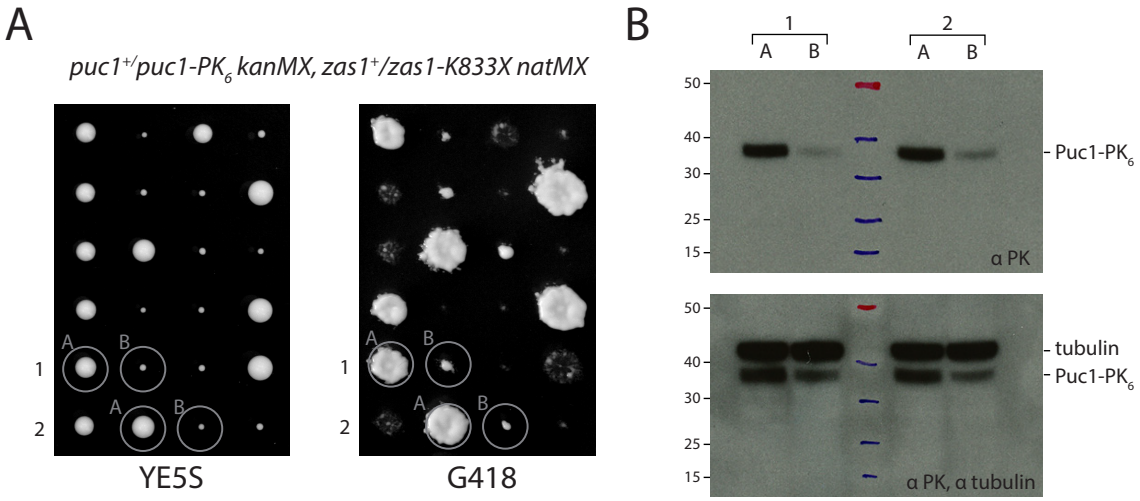

Figure 2.22: Puc1 protein levels are reduced in *zas1-K833X* cells. (A) Tetrad dissection of a diploid *puc1*$^{+}$/*puc1-PK*$_6$ *kanMX*, *zas1*$^{+}$/*zas1-833X natMX* strain (4674). (B) Indicated colonies in (A) were grown over night in liquid YE5S, diluted to the OD 0.4 – 0.5 the next day and grown 1.5 h. Protein from 5 ODs of each culture were extracted as described in section 4.5.10. Lysates were separated by Bis-Tris 4-14% SDS-PAGE in MES buffer (section 4.9.2) and blotted onto PVDF membrane. The membrane was incubated in mouse α V5 AB 1:10000, washed and incubated in α mouse-HRP 1:10000. After detection (top panel), the membrane was rinsed, incubated first in mouse α TAT1 AB 1:1000, and then again in α mouse-HRP 1:10000 (bottom panel).

2.2 A computational pipeline for FROS foci distance-based chromosome condensation measurements

2.2.1 Implementation

I implemented a FROS foci location extraction pipeline for condensation assay data as 6 Jython plugins for the ImageJ distribution Fiji (Schindelin et al., 2012). The main reason for choosing ImageJ as a platform was the availability of the core image processing and analysis algorithms for FROS tracking as ImageJ plugins (Petrova et al., 2013). Fiji is a suitable program to develop image analysis software because it is freely available (open source), runs on many operating systems due to Java's platform independence and facilitates distribution. It provides a framework for organization of microscopy images and metadata (e. g. ImagePlus class). Many implementations of image processing algorithms are included in Fiji, creating convenience for addition of image processing and analysis steps.
Where applicable, I used ImageJ's GUI or implemented GUIs with the Java Swing toolkit (`https://docs.oracle.com/javase/8/docs/technotes/guides/swing/index.html`). Therefore, no programming experience is required to operate the data extraction pipeline, increasing accessibility for unexperienced users. I implemented all plugins in Jython 2.7.0 (Foundation). Their source code is listed in section 4.15.

2.2.2 Structure and handling of the data extraction pipeline

I divided the data extraction process into six steps: (1) Metadata integration and drift correction, (2) isolation of dividing cells, (3) image preprocessing, (4) segmentation, (5) quality control and (6) tracking. I created Fiji plugins for each step. I listed an overview of all plugins in table 2.3.
Two of the steps (isolation of dividing cells and quality control) require user interaction. Sequential application of the plugins to image stacks would result in repeated interruption of the program due to user input promt. Therefore, one plugin is applied to a bulk of image stacks at a time before continuing with the next processing step. This implementation fosters modularity of the pipeline due to defined in- and output between steps. The modularity can facilitate replacement of individual steps (e. g. segmentation algorithm) by improved algorithms without changing other components. Further, bulk application enables blind user analysis during the quality control step (section 2.2.8). Each plugin stores its output in a folder that serves as input for the next step. All output folders are contained inside the same directory, from now on called 'experiment folder', creating a folder structure for each imaging experiment. An overview of the structure in order of appearance is shown in fig. 2.23 A. All calculation results are saved as comma separated value (csv) format. Csv files are compatible with many data analysis programs, most importantly Excel and R. Images are stored as tagged image file format (tif) files.

2.2.3 Preparations

For each imaging experiment, an experiment folder (section 2.2.2) must be created to use with the pipeline. All data analysis files associated with this experiment will automatically be created in this folder. The folder should be named in the format date (YYMMDD) - yeast strain collection number - temperature, e. g. 160201-2779-25C for an experiment performed on first February 2016 in which yeast strain 2779 was imaged at 25 °C (fig. 2.23 A 1). It is highly recommended to comply with this naming scheme, since the information will later be extracted by Regular Expressions (REs) in the metadata and drift correction plugin (section 2.2.4). Within the experiment folder, a folder named `raw/` must be created. The imaging data from the microscope must be copied into this `raw/` folder (fig. 2.23 A 2).
3D timelapse multichannel imaging data is usually formatted by microscopy platforms in one image file (tagged image file format or big tif file format (btf)) per field of view (fig. 2.23 A 3). Each image stack containing all images of one field of view will be referred to as 'position'. The pipeline input is only compatible with the format in which one image stack file contains data from one position. In case images have been saved as individual files, they need to be converted into to the format described. The image order within the image stack file must be xyczt.

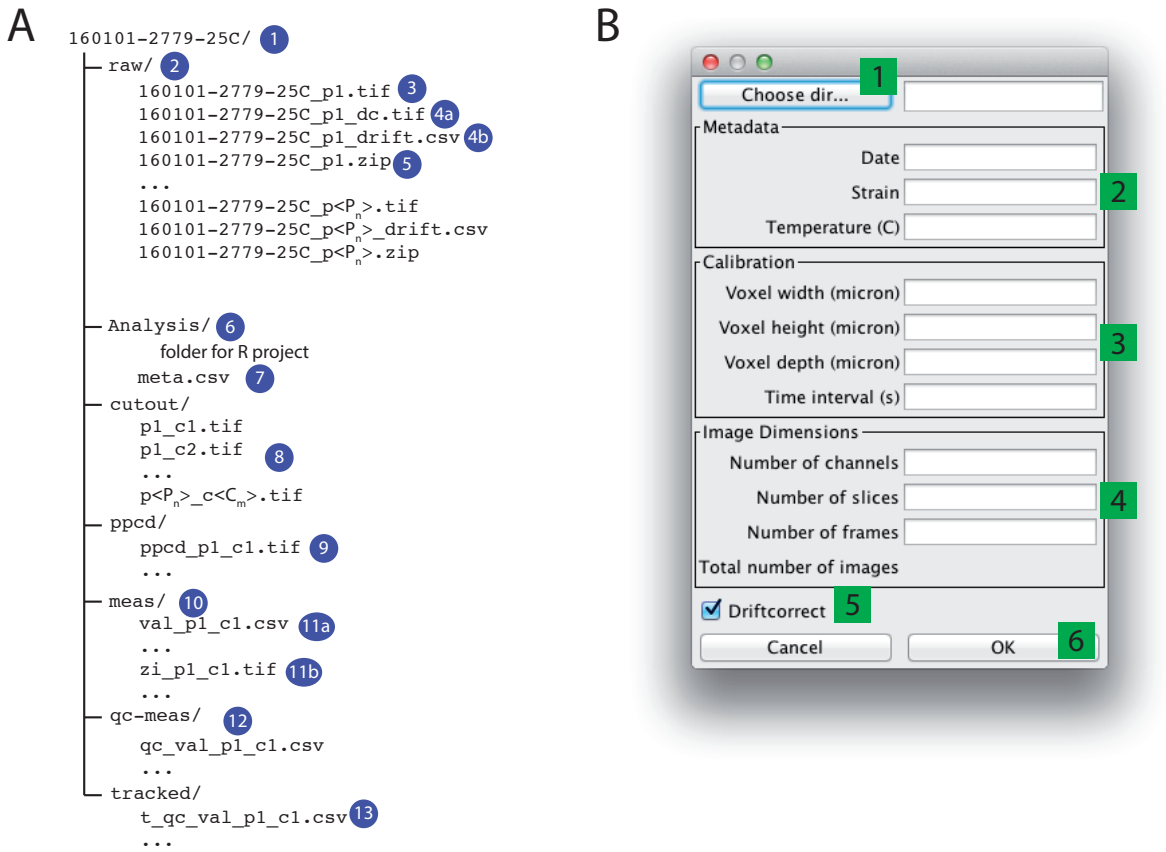

Figure 2.23: Pipeline folder structure and GUI of the MetadataDrift plugin. (A) Experiment folder tree structure; 1: experiment folder. Detailed descriptions in the main text.

2.2.4 Step 1: Metadata and xy dirft correction

Modern commercially available microscope systems save acquisition meta information like voxel dimensions, acquisition intervals and exposure times in their output image. This crucial information can be extracted from the images and directly used to convert distances from pixel/voxel-based measures to micrometers without further user input. This automation eliminates manual steps and therefore minimizes human errors in unit conversion. Metadata formats can vary from microscope to microscope, making parsing unreliable. The purpose of the MetadataDrift plugin is to complete and possibly correct metadata and to perform correction of xy drift on each position's image stack.

Metadata extraction

Starting this plugin opens a dialog frame, which is shown in fig. 2.23 B. The top left button `Choose dir ...` (fig. 2.23 B 1) will open a dialog from which the experiment folder has to be chosen. The script assumes that the experiment folder contains a raw folder and is named as described above section 2.2.3. In a first step, it will attempt to extract experiment date (160201), strain number (2779) and temperature from the experiment folder's name via the RE `^(?P<date>\d{6})[-_ ](?P<strain>\d{4})[-_ ](?P<temp>\d{2}).*` (section 4.15.1, line 247-252).
In a second step, the plugin will try to extract metadata from the first image file in the `raw/` folder using the Bio-Formats library (Linkert et al., 2010). The extracted information includes voxel dimensions, time period between consecutive frames and number of channels, number of focal planes (slices) and number of time points acquired (frames). All retrieved values are required for calculation of the FROS distances. It is essential that they are complete and precise. The extracted metadata information is displayed in the respective text fields (fig. 2.23 B, 2-4). Values can be edited and added in the text fields. The values in the text fields will be saved as metadata to each position image file and are extracted from the images later. Additionally, the script creates an `Analysis/` subfolder in the experiment folder (fig. 2.23 A 6) in which it stores all metadata in a `metadata.csv` file (fig. 2.23 A 7).

Drift correction

A common problem in multi-position time lapse microscopy is drift over time (section 1.5.3). Drift is a systematic error that affects the whole position's FOV, and can be corrected for using rigid body registration.
Activation of the checkbox `Driftcorrect` will apply the following drift correction algorithm to each of the positions. First, the plugin isolates the center slice of the first channel from each frame, assuming that it contains in-focus information over the course of the video. The TurboReg plugin (Thévenaz et al., 1998) is used to calculate frame to frame drift offset by registration of consecutive frames. The reason for registering subsequent frames is that frame-to-

frame differences are minimal compared to first frame to last frame differences. Offset calculation results are saved in csv format under the image stack's filename with addition of the suffix `_drift.csv` (fig. 2.23 A 4b). Next, cumulative x and y offsets of each frame in respect to the first frame are calculated by summing up drift of all preceding frames. Subsequently, each frames' stacks (including all z-slices and both channels) is translated by the respective cumulative x and y offsets. The stack is cropped to the largest common xy area. The image stack is saved as tif file under the initial stack's filename with the addition of `_dc` (fig. 2.23 A 4a).

2.2.5 Step 2: Isolation of dividing cells with the CellExciser plugin

With the CellExciser plugin, regions of dividing cells can be manually defined, automatically isolated and indexed. Executing the plugin opens a dialog that asks to provide a path to a position image stack file. The image stack opens and the CellExciser control window is displayed. Regions of interest containing dividing cells (fig. 2.24 A 2) are now to be defined manually using the freehand selection tool (fig. 2.24 A 1). Once a ROI is defined, clicking the `Add to ROI list` button (fig. 2.24 A 4) will execute two actions.
First, a new image file is created from a duplication of the freehand selection ROI. This duplication image is named based on its index which consists of its position index followed by an underscore and a running number cell index (e. g. p1_c1.tif). The position index is determined based on its rank in the list of .tif files within the raw folder. It is shown in the top text field (fig. 2.24 A 3) and can be manually corrected by editing the text. Position and cell indices are preserved over the data extraction and data analysis pipeline. If not present, the plugin creates a subdirectory named `cutout/` in the experiment folder (fig. 2.23 A 8) and saves the duplicated image as .tif file.
Second, the freehand selection is added to the ROI-list. ROIs in the list are displayed in yellow (fig. 2.24 A 2) with their respective cell index, which also corresponds to the index in the ROI list. The program is compatible with overlapping ROIs.
The ROI list can be deleted by clicking the `Clear ROI list` button (fig. 2.24 A 5). When clicking the `Save ROI list` button (fig. 2.24 A 5), it is saved in the `raw` folder as a file with the position file name with the extension .zip.
In case a ROI list with matching filenames of position and ROI list is present, the CellExciser plugin will open and display this ROI list on the position imaging data. Clicking the `Quit script` button (fig. 2.24 A 7) prompts the user to save the ROI list and subsequently closes all images and the control window.
Once all dividing cells have been isolated for each position, the user can proceed to the next step in the pipeline - preprocessing the isolated imaging data.

2.2.6 Step 3: Preprocessing the imaging data

The BatchPreprocessor plugin prepares the imaging data for volume segmentation. The loss of signal over time caused by photobleaching can negatively affect the segmentation results in

late time lapse frames. Therefore, a photobleaching correction algorithm (Burger and Burge, 2008) is applied in a first step. This algorithm (implemented by Kota Miura, CMCI) and matches the cumulative histogram of each frame's volume to the cumulative histogram of the first frame's volume. Because photobleaching affects each channel to a different degree, the correction algorithm is applied to each channel separately.
Accurate segmentation requires the smoothing of images to suppress noise (Burger and Burge, 2008). In a second step, images are smoothed and small and large objects are filtered using ImageJ's FFT band width filter. Filter parameters can be changed in Fiji menu Plugins > EMBLtools > Bory > PreProcess > Set FFT parameters.
Running the plugin asks the user to provide the path to the `cutout/` directory. The plugin iterates through all .tif files in the folder whose file names match the `p` $< P_n >$`_c` $< C_n >$ format (where P_n and C_n are integers and correspond to the respective position and cell index). It applies both photobleach correction and FFT to each channel in each file separately. Finally, the plugin saves the preprocessed image stacks in a new folder `ppcd/` with the prefix `ppcd_` (preprocessed) followed by the position and cell indices in the `cutout/` folder filenames (fig. 2.23 A 9).

2.2.7 Step 4: 3D segmentation-based FROS location measurements

After preprocessing, image stacks are segmented in the batchMeasurement plugin to determine FROS foci positions in each channel and frame. The batchMeasurement plugin is a batch processing wrapper of the original ImageJ plugin (3DAutothreshold) written by Kota Miura as described in Petrova et al. (2013). Its algorithm determines the FROS location by calculating the foci's centroids after threshold-based segmentation. Starting the plugin opens a dialog, asking the user for the path to a `ppcd/` directory. Preprocessed image stacks are sequentially opened and processed by 3DAutothreshold.
Per analyzed cell, two output files are created: a `val_` (values) csv file (fig. 2.23 A 11a) and a z-projected image stack containing visualization of segmentation results. All output files are stored in the experiment folder `meas/` subdirectory (fig. 2.23 A 10). The `val_` csv table contains foci's x, y and z location in respect to the origin the of excised region in µm for both channels and each frame. If no FROS focus was detected, NA replaces all values in the respective row.
The 3DAutothreshold plugin creates a z-projected image for each frame in which the location of the segmented object is indicated by a red or yellow circle, respectively. The z-projected image stacks are saved as tif file with a `zi_` prefix followed by position and cell index (fig. 2.23, A 11b).

2.2.8 Step 5: Manual anaphase onset determination and review of segmentation results

At anaphase onset, FROS foci are often too close to be recognized as split by the segmentation algorithm. The precise determination of the first frame in which FROS foci split is essential for

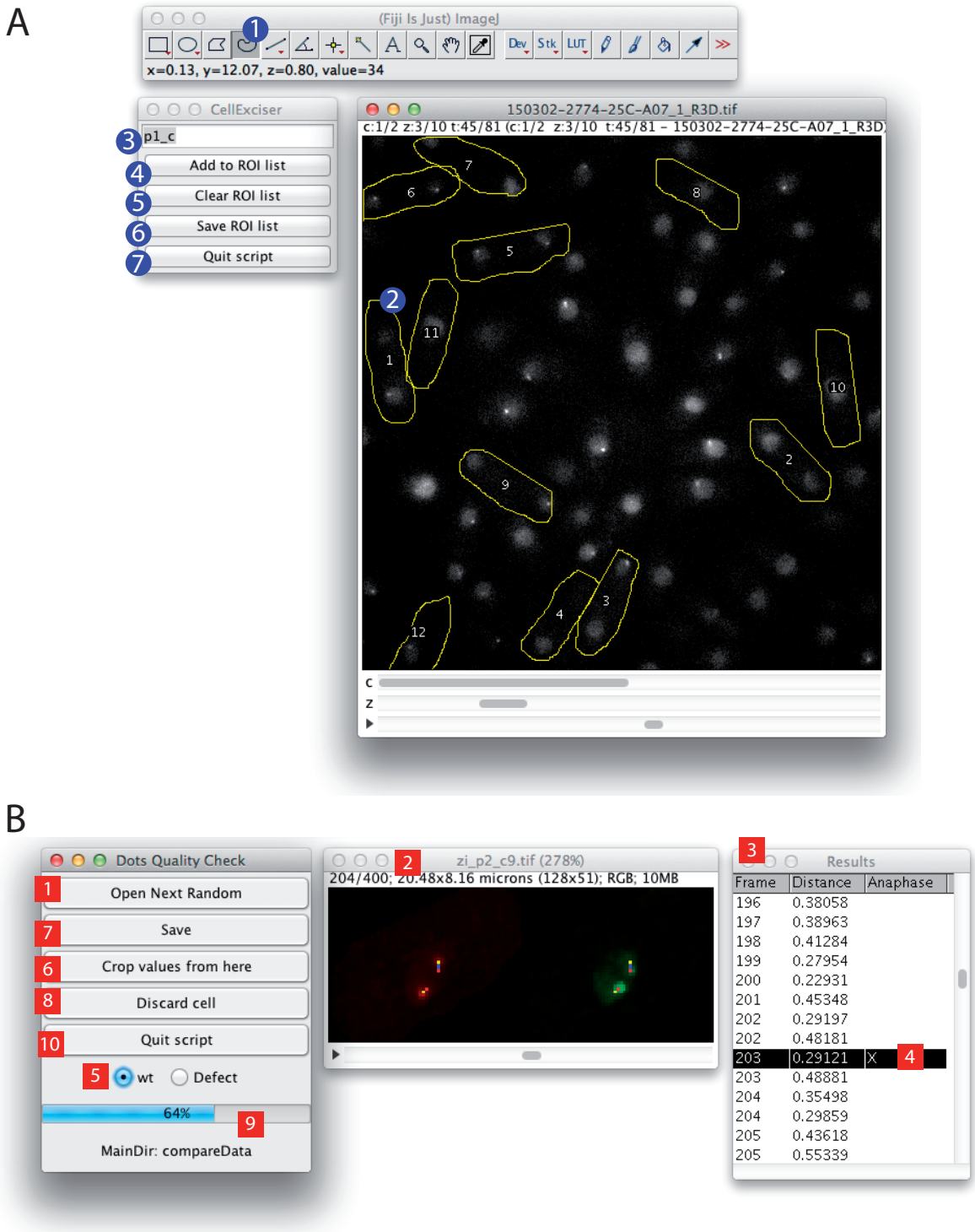

Figure 2.24: GUI and handling of pipeline plugins CellExciser (A) and QualityControl (B). Description in section 2.2.5 and section 2.2.8.

accurate temporal alignment during data analysis. Therefore, the frame in which FROS foci split has to be determined by the user. In addition, the 3D segmentation algorithm has been found to be error prone despite optimization of parameters (Petrova, 2012). To ensure only correct segmentation results are processed, they need to be reviewed by human eye and wrong segmentations have to be deleted.

The purpose of the QualityControl plugin is to optimize and increase the convenience of the human segmentation reviewing process. Human assessment harbors the danger to introduce bias into the data. To minimize this bias, data assessment is performed blindly by comparing at least two data sets. Two or more experiment folders, both of which have been processed up to step 4 (section 2.2.7), and therefore contain BatchMeasurement output files in the `meas/` folders, are required for blind reviewing. Both folders have to be moved into a higher-level folder. When starting the QualityControl plugin, the `Dots Quality Check` window appears (fig. 2.24, B, left), which serves as overview and control window. Upon clicking the `Open Next Random` button (fig. 2.24 B, 1), a directory selection dialog opens, from which the folder containing two or more experiment folders should be chosen.

The plugin creates a list of all segmentation result files contained in experiment folders within the top-level folder. From this list, data of one cell is randomly selected and the z projected image is displayed (fig. 2.24, B 2) alongside the results table containing the associated distances for each FROS pair (fig. 2.24, B 3). When the results table window is in focus, the data can be navigated using the keyboard's left and right arrow keys. The image will display the frame of the selected row. Thereby, the user can review the video frame by frame and assess segmentation results. Incorrect segmentation results can be deleted by pressing the `q` key. Pressing `Crop values from here` (fig. 2.24, B 6) will delete all values below the selected row. The frame of initial sister FROS splitting (anaphase onset) can be marked by pressing the `O` key. An `X` will appear in the row to which anaphase onset is set (fig. 2.24, B 4). Once all frames have been reviewed, cell division has to be scored as 'wild type' or 'defective' by activating either `wt` or `Defect` radio button (fig. 2.24 B 5). After both anaphase onset and phenotype are annotated, the `Save` button is enabled (fig. 2.24, B 7). Clicking the `Save` button saves the results table as csv with the filename prefix `qc_val_` followed by position and cell indices in the `qc-meas` folder (fig. 2.23 A 12) of the respective experiment. Subsequently, the next cell can be reviewed by clicking the `Open Next Random` button again.

In case most segmentation results of a cell are incorrect, e. g. if the cell is out of focus, all distance measurements of that cell can be deleted by clicking the `Discard cell` button (fig. 2.24, B 8).

A progress bar indicates what percentage of cells has been processed (fig. 2.24, B 9).

2.2.9 Step 6: Tracking

The purpose of the Trackfinder plugin is to link FROS foci movement from frame to frame, especially after nuclear division. This will enable analysis of the daughter cells' chromosome decondensation behavior and monitoring condensation during meiosis. The Trackfinder plugin

is not fully functional and still experimental. Using an algorithm that minimizes the sum of distances between foci of subsequent frames in one channel (global nearest neighbor) assigns to each FROS instance a track ID, which links to the global nearest neighbor in the next frame. When starting the plugin, the user is asked to provide the path to a `qc_meas` folder (fig. 2.23) via a dialog. The plugin applies the tracking algorithm file by file, saving its output in a `tracked` experiment folder subdirectory (fig. 2.23 A 13).

2.2.10 Chromosome condensation data analysis in R

The data extraction pipeline allows the user to obtain large amounts of chromosome condensation data that cannot be readily analyzed in GUI-based software like Excel. R is a popular programming language designed for statistical data analysis (R Core Team, 2015). I wrote the CurveAnalysis.R script (section 4.15.8) to automate data analysis and plotting routines for chromosome condensation measurements. The R script has to be run from the `Analysis` folder to work without adjusting the wokring directory path. In a first step, data from tracked files is united in one table (data frame), `df` (section 4.15.8 l 41–71). The scripts asks for user input to complete metadata (section 4.15.8 l 52 – 62). It saves the unified data as a csv file (section 4.15.8 l 72) to make it available for further analysis. Using the dplyr package (Wickham and Francois, 2015) mean, standard deviation and number of observations are calculated for each time point (section 4.15.8 l 78 – 86), and the results are saved (l 88). The number of cells is calculated (l 75). Raw data and averaged data are visualized using the ggplot2 library (Wickham, 2009) (l 90 – 104).

Plugin name	Source	Input	Process	Output
MetadataDrift	4.15.1	microscopy data as one image stack file per field of view	Completion of metadata, calculation and correction for xy drift	metadata table, drift corrected video, drift measurements table
CellExciser	4.15.3	path to xy drift corrected video	semi-automatic definition of ROIs containing dividing cells	folder `cutout/` containing a .tif file for each ROI, .zip file containing ROI information of respective position
BatchPreProcessor	4.15.4	path to `cutout/` folder containing image stacks of single, dividing cells	Histogram matching bleach correction and FFT smoothing as described in Petrova et al. (2013) on each channel	folder `ppcd/` containing preprocessed single cell images
BatchMeasurement	4.15.5	path to `ppcd/` folder containing preprocessed single cell images	channel-wise threshold based volume segmentation (Petrova et al., 2013)	.csv table containing positions for each frame, z-projected image image with indication of segmentation result
QualityControl	4.15.6	path to a folder containing measurement results as z-projected image and .csv table	Blind, manual definition of anaphase onset, assessment of segmentation results	.csv table of position measurements without manually deleted values and time corrected for anaphase onset.
Trackfinder	4.15.7	path to folder containing quality controlled FROS location measurements	crude global nearest neighbor tracking of each dot (still experimental)	.csv tables containing all measurement values and track ID

Table 2.3: Overview of plugins implementing the steps of the optimized data extraction pipeline

2.3 Application of the data extraction pipeline

In section 2.2, I have described a computational pipeline for data extraction and analysis for FROS distance measurement data. Computational improvement of the Chromosome Condensation Assay (CCA) data extraction workflow enabled me to address questions that were otherwise unaddressable or very laborious to explore.

2.3.1 The pipeline increases data extraction efficiency more than 2-fold

Automation, introduction of shape ROIs and drift correction (section 2.2) enabled imaging a denser monolayer of cells than before. Did this change in data acquisition and extraction strategy indeed considerably increase the number of analyzed mitoses per experiment? From all imaging data sets produced with the new data extraction pipeline, I counted the number of analyzed mitoses per imaging experiment. This included data from figs. 2.3 and 2.9. For comparison, I took the numbers of analyzed mitoses per condensation curve data set from Petrova et al. (2013). Note that in Petrova et al., measurements from more than one experiment were combined in condensation curve data sets. Unfortunately, I could not trace from how many imaging experiments the data had been obtained. Therefore, these figures represent an overestimation of the number of analyzed cells per experiment. Numbers of analyzed mitoses from each imaging experiment are plotted in fig. 2.25. Using the new pipeline, I obtained on average data from 40 mitoses per imaging experiment. In one case, I could extract data of more than 100 mitoses from a single imaging experiment. Datasets in Petrova et al. (2013), contained on average data from half as many mitoses. Therefore, I conclude that my computational data extraction pipeline is more than twice as efficient as the previous data extraction process.

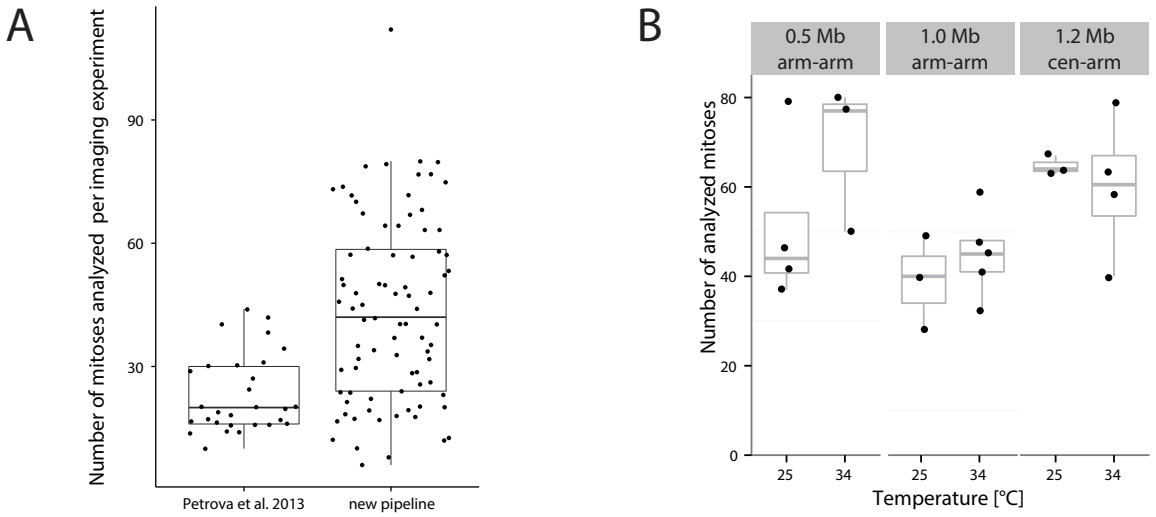

Figure 2.25: The data extraction pipeline increases the number of analyzed mitoses per imaging experiment about 2-fold. (A) Number of analyzed mitoses per condensation curve in Petrova et al. (2013) and number of analyzed mitoses per imaging experiment in this thesis using the data extraction pipeline (section 2.2). (B) Number of analyzed mitoses in fig. 2.26 broken down by strain and temperature.

2.3.2 Experiment-to-experiment variability and reproducibility of condensation curves

The conclusiveness of an assay depends on how precise and reproducibly it can measure the process it probes. Reproducibility can usually be examined by repeating measurements under identical conditions and by quantifying by how much measurements vary. A quantitative assessment of how reproducible condensation curves were between identical experiments had been missing for the previous CCA, due to technical limitations. The major technical limitation was the data extraction procedure, which, in the majority of cases, was not efficient enough to produce a sufficient amount of data from a single imaging experiment. The markedly increased number of mitoses that could be analyzed from a single imaging experiment with the new pipeline allowed me to probe the reproducibility of condensation curves and their experiment-to-experiment variability. Primarily, I asked the question whether the variance between replicates was larger than that between different FROS positions or temperatures. I imaged three strains with FROS loci at 0.5 Mb, 1 Mb or 1.2 Mb distance at 34 °C or 25 °C (fig. 2.26 A). For each condition, I conducted three or more imaging experiments. I processed the image data using the optimized data extraction pipeline, extracting not only FROS distances from prophase and metaphase but also from anaphase, telophase and the subsequent G_1 phase. I grouped the data by imaging experiment and calculated condensation curves by averaging measurements from same experiment for each time point as described in section 2.2.10.

Condensation curve features are reproducible

Plots of the time point averaged distances are shown in fig. 2.26 B. Condensation curves were in good agreement with observations from Petrova (2012). All curves shared an equivalent sequence of features. G_2 distance was constant over time on average until about 750 to 500 s before anaphase onset. Chromosome condensation start followed a sigmoid-like FROS convergence to about half the G_2 distance. Directly after anaphase onset, FROS separated to a minor degree, followed by a further compaction to the point of closest FROS proximity during late anaphase. Afterwards, FROS distance increased in a non-linear decondensation phase. Measurements at 25 °C temperature were more variable than measurements at 34 °C in all three FROS loci strains. I asked whether a lower number of analyzed mitoses in the measurements at 25 °C could be the reason for this increased variability. However, only in the 0.5 Mb strain, calculations for the measurements at 25 °C were based on data from fewer mitoses (fig. 2.25 B).
Condensation curves were more similar between replicates than curves from different conditions. I therefore concluded, that condensation curves are reproducible from experiment to experiment for the numbers of mitoses in these data sets.

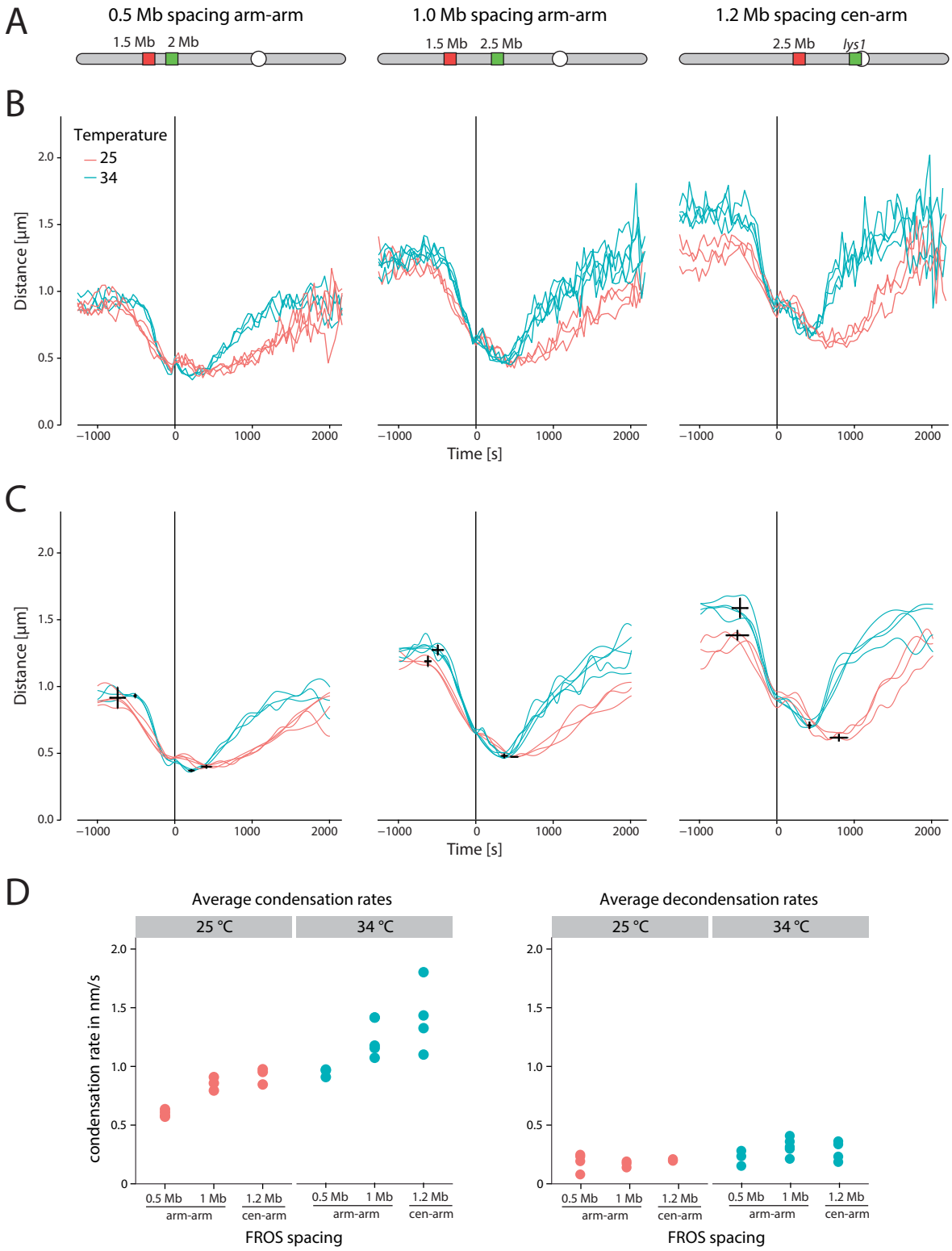

Figure 2.26: Variance of condensation assay results. (A) Schematic representation of FROS loci on chromosome I in the strains. Corresponding strain numbers in the collection are 0.5 Mb distance arm-arm: 2774, 1.0 Mb distance arm-arm: 2779, 1.2 Mb distance cen-arm: 2926. (B) FROS distance measurements averaged by each time point. Each line represents data from one imaging experiment. (C) Spline fits to the data in (B). Crosshairs indicate beginning of condensation and point of highest compaction (see table 2.4). Extracted parameters are found in table 2.4. (D) Average condensation rates (left) and decondensation rates (right), as stated in table 2.4.

2.3.3 Average G_2 phase FROS distance depends on chromosomal locations

I noted a difference in G_2 phase FROS foci distances between 25 °C and 34 °C in measurements from the cen-arm FROS loci strain but not in the arm-arm FROS loci strains. To quantify mean euclidean G_2 interphase distances, I averaged all distance measurements before time point -750 s for each experiment. I observed that at 0.5 Mb and 1.0 Mb label loci spacing, euclidean G_2 interphase distance only varied by 30 nm and 10 nm between 34 °C and 25 °C, respectively (see table 2.4). In contrast, in the measurements based on cen-arm 1.2 Mb FROS loci separation, euclidean G_2 interphase distance varied about 300 nm between 25 °C and 34 °C (about ten times more).

2.3.4 Spline fits allow quantification of condensation curve features

I next desired to accurately measure values and variance of major features of the condensation curves. Previously, this had been achieved by fitting a sigmoid function to the data. I observed that a sigmoid fit was not appropriate in some cases - especially when measurements came from condensation mutants. Most importantly, previous fitting did not address features past anaphase onset such as time point of highest compaction and decondensation rate. I therefore implemented spline fits, which allowed me to extract all previous parameters, in addition to post-anaphase features. Spline fits could in principle also be applied to non-sigmoid curves.
To extract curve features from the fits, I defined them as follows:

Start of condensation ($\mathbf{t_{start}}$) Last time point before 135 s prior to anaphase onset, where the slope of the condensation curve is smaller than $-0.2\,\mathrm{nm\,s^{-1}}$.

Condensation velocity ($\mathbf{v_{cond}}$) Mean slope of the fit between t_{start} and anaphase onset.

Anaphase onset distance ($\mathbf{d_{t0}}$) Fit distance at anaphase onset (time point 0).

Timing ($\mathbf{t_{50}}$) Last time point before anaphase onset at which half compaction is reached.

Full compaction distance ($\mathbf{d_{min}}$) Minimal distance value of the fit.

Time point of highest compaction ($\mathbf{t_{dmin}}$) Time point of d_{min}.

decondensation velocity ($\mathbf{v_{decon}}$) Maximal fit slope between 0 and 2000 s after anaphase onset.

Source code definitions can be found in section 4.15.9, lines 83 ff. For each experimental data set, I created a spline fit using the `smooth.spline` function in R (stats package). Distance averages were weighted by the number of measurements the respective average was calculated from. Plots of the resulting fits are depicted in fig. 2.26 C. I extracted the beforementioned curve features from each experiment fit (table 2.4). In case of average values, the script calculated fit distance values for each second (see section 4.15.9). The average values with standard deviations are listed in table 2.4.

FROS spacing	T (°C)	d_{G2} (µm)	t_{start}(s)	v_{cond} (nm s^{-1})	t_{50} (s)	d_{t0} (µm)	d_{min} (µm)	t_{dmin} (s)	v_{decond} (nm s^{-1})
arm-arm 0.5 Mb	25	0.941 ± 0.043	-740 ± 95	-0.599 ± 0.029	-423 ± 17	0.482 ± 0.016	0.399 ± 0.015	406 ± 64	0.186 ± 0.076
arm-arm 0.5 Mb	34	0.909 ± 0.025	-513 ± 9	-0.950 ± 0.035	-293 ± 7	0.484 ± 0.026	0.370 ± 0.011	212 ± 33	0.220 ± 0.065
arm-arm 1.0 Mb	25	1.213 ± 0.046	-627 ± 36	-0.854 ± 0.058	-273 ± 53	0.612 ± 0.016	0.473 ± 0.004	489 ± 47	0.166 ± 0.026
arm-arm 1.0 Mb	34	1.200 ± 0.036	-499 ± 68	-1.248 ± 0.159	-197 ± 12	0.640 ± 0.020	0.480 ± 0.018	358 ± 37	0.315 ± 0.073
cen-arm 1.2 Mb	25	1.315 ± 0.147	-524 ± 139	-0.925 ± 0.069	-203 ± 81	0.875 ± 0.068	0.616 ± 0.029	786 ± 111	0.199 ± 0.007
cen-arm 1.2 Mb	34	1.613 ± 0.032	-490 ± 97	-1.416 ± 0.293	-227 ± 11	0.915 ± 0.047	0.710 ± 0.027	406 ± 19	0.276 ± 0.083

Table 2.4: Summary of condensation curve feature values and their experiment-to-experiment variability. Values were calculated for individual experiments and subsequently averaged. Each value is followed by the respective standard deviation. Additional information and feature definitions in the main text. The R source code used for calculations can be found in section 4.15.9.

2.3.5 Temperature and FROS spacing influence chromosome condensation and decondensation kinetics

On average, chromosomes compacted axially at a rate of approximately 1 $\mathrm{nm\,s^{-1}}$. In comparison, the average decondensation was 5 to 3 times slower ($0.2\,\mathrm{nm\,s^{-1}}$ to $0.3\,\mathrm{nm\,s^{-1}}$) (fig. 2.26 and table 2.4). This suggests, that condensation and decondensation are distinct processes. They are discussed in more detail in section 3.4.1.

Condensation and decondensation rates increase with temperature

Being able to extract prophase compaction speed from unbiased fits, I asked how condensation rates depended on temperature. In all three FROS loci configurations, condensation was 1.5 to 2 times faster at 34 °C than at 25 °C. Similarly, decondensation rates were faster at 34 °C compared to 25 °C in all three strains, although the effect was not as pronounced as during condensation.

CCA-measured condensation rate increases with FROS loci distance

Next, I analyzed whether the condensation rates measured in the CCA depended on the FROS spacing. Information about this dependency could reveal principles underlying the condensation process (section 3.4.3). At both temperatures, chromosome condensation rate increased with FROS spacing (table 2.4 v_{cond} column and fig. 2.26 D). This suggests that condensation acts on many active centers along the chromosome length, such that the condensation activity increases with FROS spacing (see section 3.4.3). In contrast to the increase in condensation rate with FROS spacing, the time point of largest compaction occurred later in strains where FROS loci were further apart. This could indicate a change in the regulation of chromosome condensation after anaphase onset.
For decondensation rates, I did not observe an increase with FROS spacing, again suggesting that condensation and decondensation are distinct processes (table 2.4, v_{decond} column).

Degree of maximal compaction

The volume of most non-living materials (e. g. gasses) depends on temperature. If this were true for mitotic chromosomes, then the full compaction distance d_{min} should increase with temperature. At 0.5 Mb FROS spacing, d_{min} was greater at 25 °C than at 34 °C. In contrast, at 1.0 Mb and 1.2 Mb FROS spacing, full compaction distances were greater at 34 °C than at 25 °C. From this data, models of non-living matter do not hold true for mitotic chromosomes *in vivo*, arguing for a complicated structure of mitotic chromosomes.

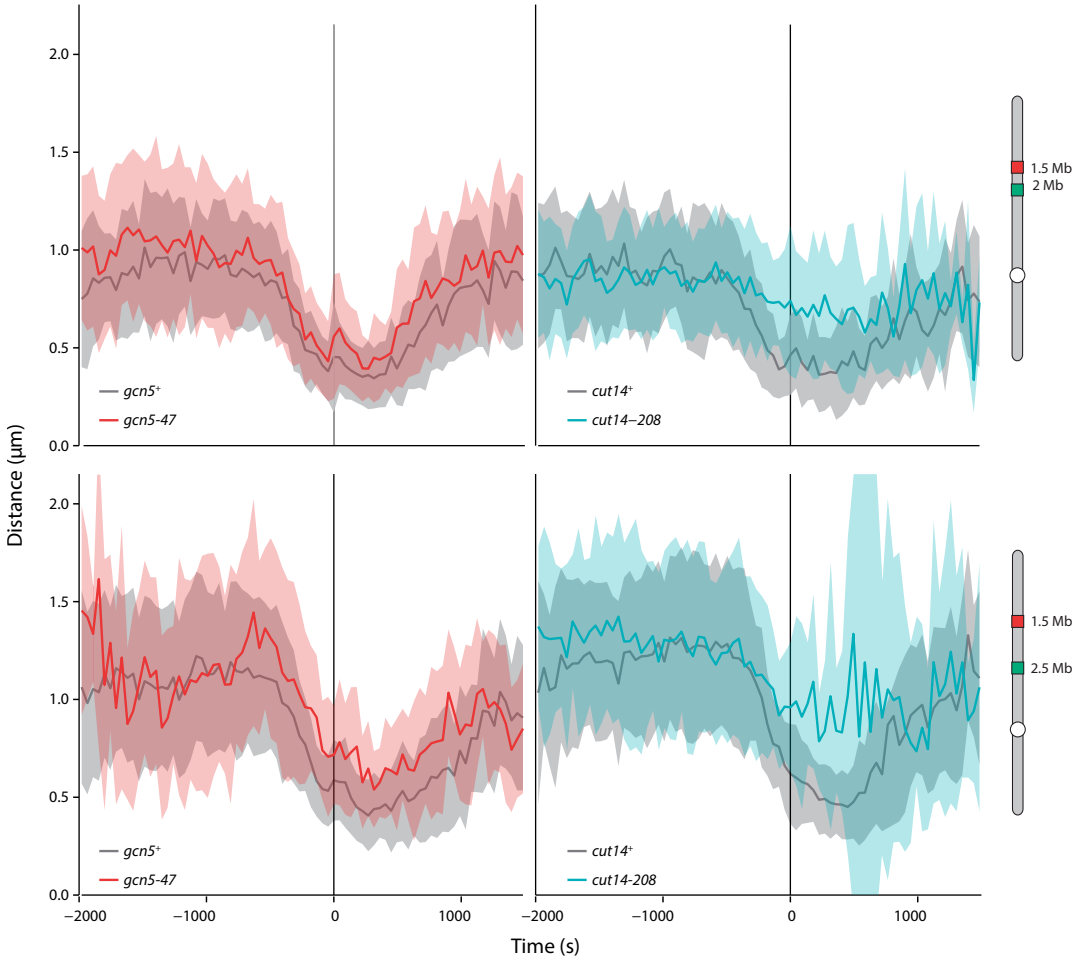

Figure 2.27: *gcn5-47* cells are defective in chromosome condensation. Solid line: Average distance at respective time point. Shaded areas indicate to standard deviation. Adapted from Toselli-Mollereau et al. (2016).

2.3.6 Mitotic chromosome structure is affected in *gcn5-47*

Results from this section were partially contributed by Carlo Klein. Details about his contributions can be found in his master thesis (Klein, 2015). The results presented here are part of the publication Toselli-Mollereau et al. (2016).

Pascal Bernard's group identified *gcn5-47*, an allele of *gcn5* which lowers the restrictive temperature of condensin ts allele*cut3-477*. Gcn5 is a histone acetyltransferase (HAT), which acetylates histone tails at active promoters (Yamada et al., 2004). *gcn5-47* is a nonsense mutation that deletes Gcn5's bromodomain, a domain which recognizes acetylated lysines. Acetylated histones are evicted from chromatin, making DNA accessible to condensin, which binds naked DNA with higher affinity than nucleosomes (Piazza et al., 2014). To test, whether *gcn5-47* cells are defective in chromosome condensation, we used the CCA to compare the population average condensation behavior of *gcn5-47* and *gcn5*$^+$ cells. The group of Pascal Bernard introduced *gcn5-47* into FROS strains by crossing. The strains were created for FROS a spacing of 0.5 Mb and 1.0 Mb on chromosome I (tetO sequences at 1.5 Mb and lacO sequences at 2.0 Mb and

Strain	FROS separation	genotype	N experiments	total N cells
4215	0.5 Mb	*cut14*$^+$	1	44
4217	0.5 Mb	*cut14-208*	2	63
4219	0.5 Mb	*gcn5*$^+$	1	50
4221	0.5 Mb	*gcn5-47*	2	65
2779	1.0 Mb	*cut14*$^+$	1	59
2930	1.0 Mb	*cut14-208*	1	32
4020	1.0 Mb	*gcn5*$^+$	2	105
4021	1.0 Mb	*gcn5-47*	2	52

Table 2.5: Statistics for *gcn5* condensation curves shown in fig. 2.27

2.5 Mb respectively).

For all measurements of *gcn5*$^+$ and *gcn5-47* cells, we obtained data from 50 or more mitoses. For comparison, we repeated the same experimental setup with *cut14-208*, a ts allele of a condensin subunit with known condensation defects (Saka et al., 1994; Petrova et al., 2013). All statistics are listed in table 2.5. Distance measurements were averaged for each strain, the corresponding condensation curves are shown in fig. 2.27.

In both *gcn5-47* strains, FROS distances were consistently larger during mitosis than in *gcn5*$^+$ cells. This effect was visible in both strains, but more pronounced at 1.0 Mb label spacing than at 0.5 Mb. Furthermore, FROS distances were larger during late G_2 phase, in the 0.5 Mb strain. This effect was not present for 1 Mb FROS spacing.

From our CCA data, we concluded that Gcn5 function is required for chromosome condensation, but the effect of Gcn5 inactivation is less dramatic than the effect of Cut14 inactivation.

2.3.7 Single cell chromosome condensation measurements reveals linear kinetics of axial shortening

Part of the methods development for this section was supported by Carlo Klein. He has described his contributions and additional data in his master thesis (Klein, 2015).
In section 2.3, I showed how averaging FROS foci distance time series from a population of cells can result in a quantitative description of chromosome condensation (condensation curve). This method has been proven successful to screen for condensation factors (Petrova et al., 2013) and validation of *zas1* and *gcn5* as regulators of mitotic chromosome condensation (section 2.3.6). Nevertheless, evidence that the averaging-based condensation curves reflect the biological axial compaction process during chromosome condensation in individual cells is lacking. Rather, the assay itself provides evidence for cell-to-cell heterogeneity of the condensation process, indicating that averaging the time series might be inappropriate (Altschuler and Wu, 2010). At the average mitosis entry time point (t_{start}), only a minor fraction of cells' FROS are at a distance corresponding to full extension of the chromatin structure, the maximum of the distance distribution (discussed in depth in section 3.4.2). In the majority of cells, FROS foci are closer. I

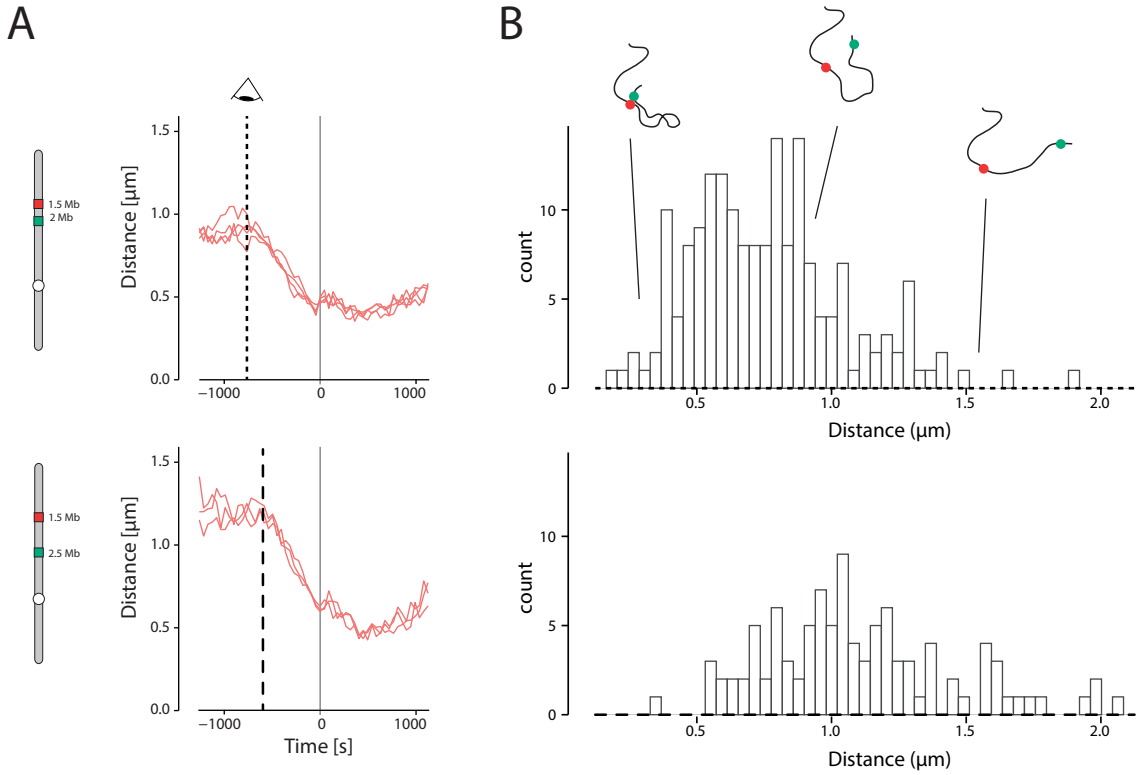

Figure 2.28: Chromatin between FROS loci is stretched in only a minor fraction of cells before entry into mitosis. (B) shows the FROS distance distributions over the population at t_{start} (dashed lines in A) (in table 2.4) for strain 0.5 Mb and 1.0 Mb FROS separation.

identified two hypothetical reasons for this observation: First, cells are heterogeneous in the duration of prophase and metaphase, caused by a SAC delay. Because the time series are aligned to anaphase onset, this distribution could reflect subpopulations of cells with either interphase,

condensing or fully condensed chromatin (cell cycle progression heterogeneity). In this case, one would rather expect a bimodal distribution of distances - provided that condensation is fast. Second, the chromatin fiber is folded within the nucleus (Lieberman-Aiden et al., 2009; Mizuguchi et al., 2014) and this fold varies between cells (heterogeneity in chromatin fiber conformation). The folding implies that FROS cannot be at an euclidean distance corresponding to the contour length.

In the previous data analysis procedure, information about cell-to-cell heterogeneity in chromatin fiber conformation and cell cycle progression had been masked during data analysis due to integration of measurements from many cells by temporal alignment and averaging. Hence, I asked the question whether it were feasible to use the CCA setup to measure chromosome condensation in single cells. Because loci movements are continuous, I expected that a sufficient increase in temporal resolution would reveal interpretable axial shortening of the chromatin fiber on a single cell level. CCA information on the single cell level would be valuable to clarify three questions:

First, are cell cycle progression heterogeneity and chromatin conformation heterogeneity the cause for the FROS distance distribution before condensation? Second, in cells where FROS distance is close to full extension before condensation, does axial compaction follow a sigmoid regime? Third, a comparable experimental setup has been approached by molecular dynamics simulations to explain chromosome condensation (Cheng et al., 2015). Are the experimental condensation results obtained from single cells consistent with this model?

Before approaching these questions, I tested whether increasing temporal resolution in the assay was feasible. I identified three major limitations for increasing the temporal resolution: Phototoxicity and photobleaching, speed of the microscope hardware (stage movements and channel switching) and processing large amounts of imaging data.

I used a wide field microscope setup (Olympus Cell^{R} TIRF system provided by EMBL's Advanced Light Microscopy Facility (ALMF)), which featured an electronically switchable laser excitation and a multi band dichroic mirror for fast excitation wavelength selection. The microscope setup also had a faster stage and Z drive than the system used for previous experiments. The Cell^{R} TIRF system's more sensitive 16 bit camera enabled me to lower excitation light intensity, reducing bleaching and photodamage. I optimized exposure time (80 ms) and excitation laser intensity to 15 %, corresponding to 280 for both 488 nm and 561 nm lasers. To further reduce excitation light intensity, albeit speeding up stack acquisition, I decreased the of number of focal planes per FOV to eight (previously 10) and increased focal plane spacing to 500 nm (previously 400 nm). Taken together, this configuration prevented photodamage and limited bleaching in long, fast time lapses (Klein, 2015). Data processing limitations had been overcome by using the more efficient extraction procedure (sections 2.2 and 2.3.1). Using the improved microscopy setup, I obtained 3D videos with a frame interval of 15 s from cells with FROS spacing of 1.0 Mb (strain 2779). About 40 cells divided during this single imaging experiment. FROS distance measurements from 28 cells could be extracted and were plotted against time for each individual cell (fig. 2.29).

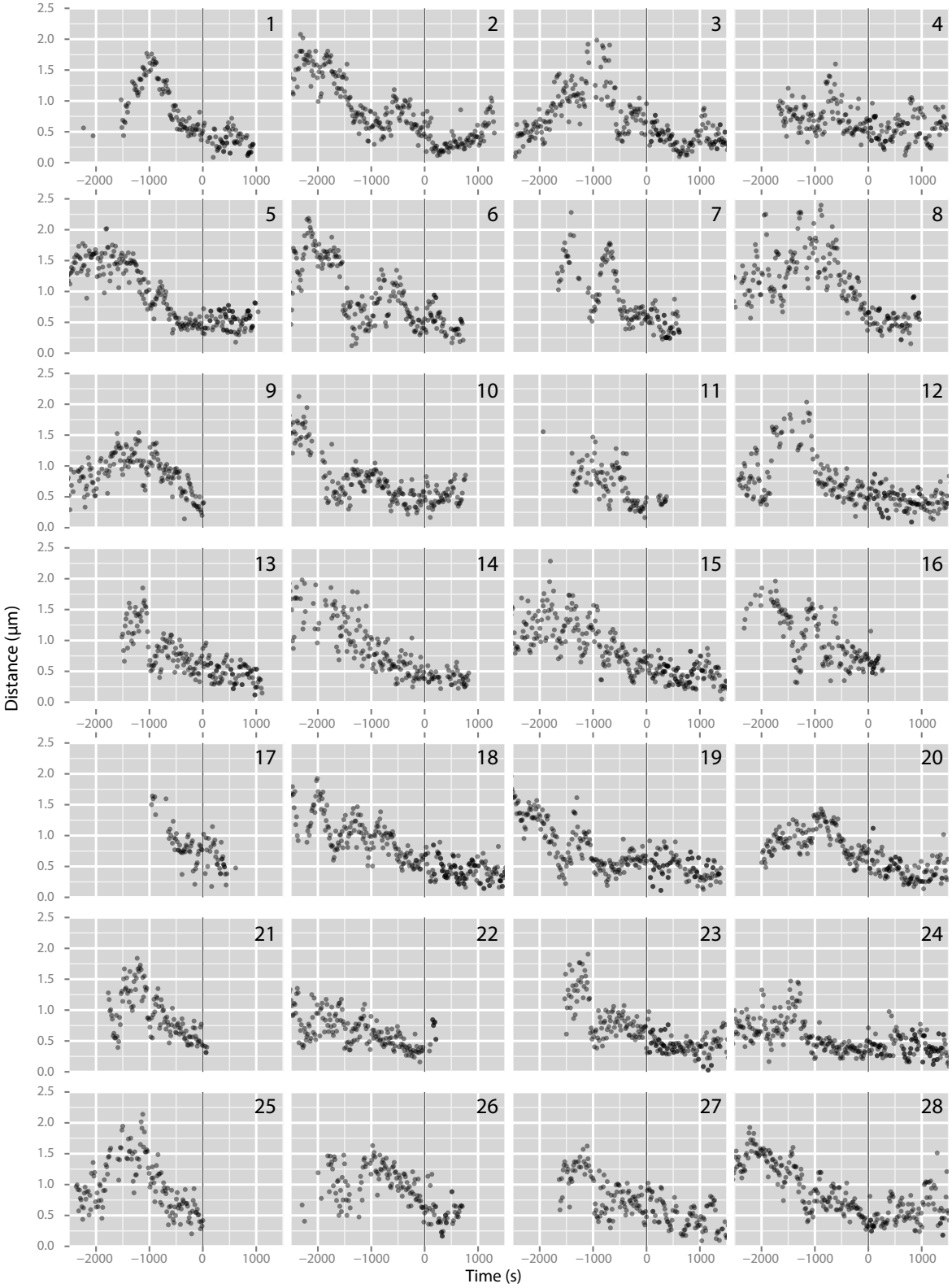

Figure 2.29: Axial compaction in single cells during chromosome condensation. Each panel shows FROS distance time series from a single cell, measured every 15 s. FROS spacing of 1.0 Mb in all cells (strain 2779)

Remarkably, distance-time traces were highly diverse between cells. In all time series, FROS distance decreased before anaphase onset and remained low throughout anaphase. This indicated that chromosome condensation can indeed be measured on the single cell level with the CCA.

In the majority of axial compaction events, kinetics did not follow a sigmoid regime comparable to average condensation curves. Rather, compaction rate appeared constant over time. An second distinct difference to the average curves was the absence of a stable interphase distance before condensation. In many cells, FROS distance increased before the condensation phase (e. g. cells 1, 3, 4, 7, 12, 21, 25 in fig. 2.29).

In several cells, FROS distance oscillated with period lengths around minutes (e. g. in cells 15 and 18, less pronounced in 6, 7, 8, 19). Carlo Klein found in his master thesis that these oscillations occur not only in late G_2 phase but are present throughout interphase and that they do not depend on cytoplasmic microtubules (Klein, 2015). I had hypothesized that SAC activation could lead to an anaphase onset delay while chromosomes are condensed. A delay of progression to anaphase with condensed chromosomes was apparent in cells 5, 10, 12, 13, 21 and 24. This observation can be interpreted as SAC-dependent anaphase delay.

I repeated the single cell imaging experiment with a strain of 0.5 Mb FROS spacing and increased the acquisition rate to 13 s. I obtained data from 32 cells (fig. 2.30). Again, O observed linear distance–time dependence during condensation (cells 7, 16, 21, 24, 25, 27), SAC activation delay (e. g. cells 1, 14, 16, 25, 32) and distance oscillations (e. g. cells 1, 9, 30). The single cell condensation data showed that both cell cycle progression and chromatin conformation were highly heterogeneous. In addition, unexpected oscillations and FROS dispersal ahead of condensation contribute to the wide distribution of FROS distances before condensation. Unlike the average condensation curves, axial compaction did not follow a sigmoid regime in most cells. Compaction seemed rather linear over time. I therefore concluded that the CCA can be used to monitor chromosome condensation on the single cell level. Despite their usefulness for screening and validation of condensation factors, average condensation curves do not reflect condensation behavior of individual cells.

2.4 Improvement of the tet fluorescent repressor operator system

2.4.1 A plasmid suite for expression of fluorescent TetR and LacI fusion proteins from one locus

Despite the deeper biological insight that can be obtained, single cell condensation curves are laborious to create and therefore not suitable for routine measurements or high throughput applications. The main limitations are the manual or semiautomatic steps in the data extraction pipeline. Especially laborious and time consuming is the reviewing of segmentation results, which are often incorrect due to insufficient signal to background ratio of the FROS foci. In the

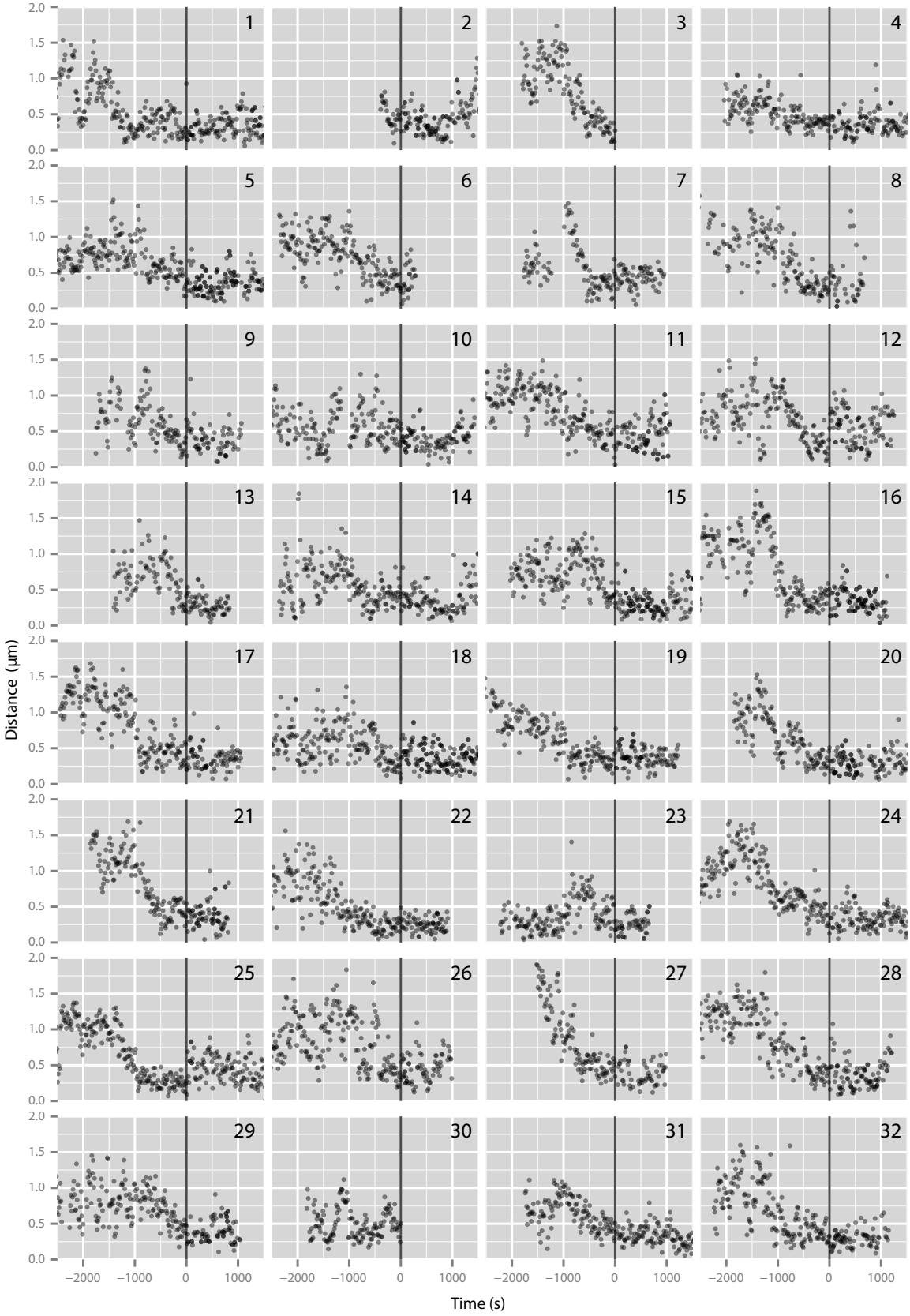

Figure 2.30: CCA at the single cell level at 0.5 Mb FROS spacing. Again, linear condensation behavior can be observed.

data set described above, about one fourth of the cells could not be analyzed due to low FROS intensity to background signal ratio.
I desired to enhance FROS focus intensity to test if segmentation accuracy could be improved to a degree at which manual curation of the segmentation results becomes obsolete. I sought to optimize fluorescent repressor levels by testing different promoters to increase the fraction of bound fluorescent repressor and lower background levels. In addition, I wanted to be able to test brighter and more photostable FP variants with the FROS systems. Finally, I asked if it were feasible to investigate performance of FP variants of different colors to add a third FROS or fluorescent protein-tagged condensin subunits. A LacI-GFP integration plasmid for *S. pombe* was not available in the lab and the tetR-tdTomato plasmid was not suitable for easy replacement of the promoter or the tdTomato ORF. I therefore designed an integration plasmid system (pFR) based on the pUC19 backbone (Yanisch-Perron et al., 1985), which allows expression of both GFP-LacI and TetR-tdTomato from the same locus. Both fusion proteins can therefore be integrated using only one marker. Unique restriction sites between each gene element facilitate exchange of fluorescent protein variants and their promoters. Insertion of target genome integration homology sequences is facilitated by the presence of a unique FseI recognition site, which is rare in the *S. pombe* genome. Omitting unnecessary sequences minimized plasmid size and broadened the range of restriction enzymes that could be used for linearization of the plasmid prior to genome integration. Maps of the plasmids are shown in fig. 2.31.

Maria Saez Garcia, Carlo Klein and I created the pFR plasmids (table 2.6) by PCR and restriction cloning (sections 4.1.12 and 4.1.16). I inserted the pFR TetR-tdTomato ura4 at the *srk1* locus and confirmed expression of TetR-tdTomato by fluorescence microscopy (strain 4617). *srk1* is close to the auxotrophic marker gene *ade6*. Additional integrations at the *ade6* locus would therefore co-segregate with the pFR integration during crossing.

Collection number	Plasmid	created by
2815	pFR P_{dis1} EGFP-LacI ura4 srk1	Klein
2980	pFR P_{adh1} TetR-tdTomato ura4 srk1	Schiklenk
2872	pFR P_{adh1} TetR-tdTomato ura4 P_{dis1} EGFP-LacI srk1	Schiklenk

Table 2.6: List of fluorescent repressor expression plasmids. Maps are shown in fig. 2.31.

2.4.2 Implementation of stable tetO arrays for the quantitative chromosome condensation assay

I next tested whether the pFR-expressed TetR-tdTomato are able to bind to operator sequences and form a fluorescent focus. I took this as an opportunity to optimize the tetO sequence arrays. These had been problematic especially in crossing situations. Boryana Petrova and Christian Haering had hypothesized that deletion of the repetitive sequences by intrachromosomal recom-

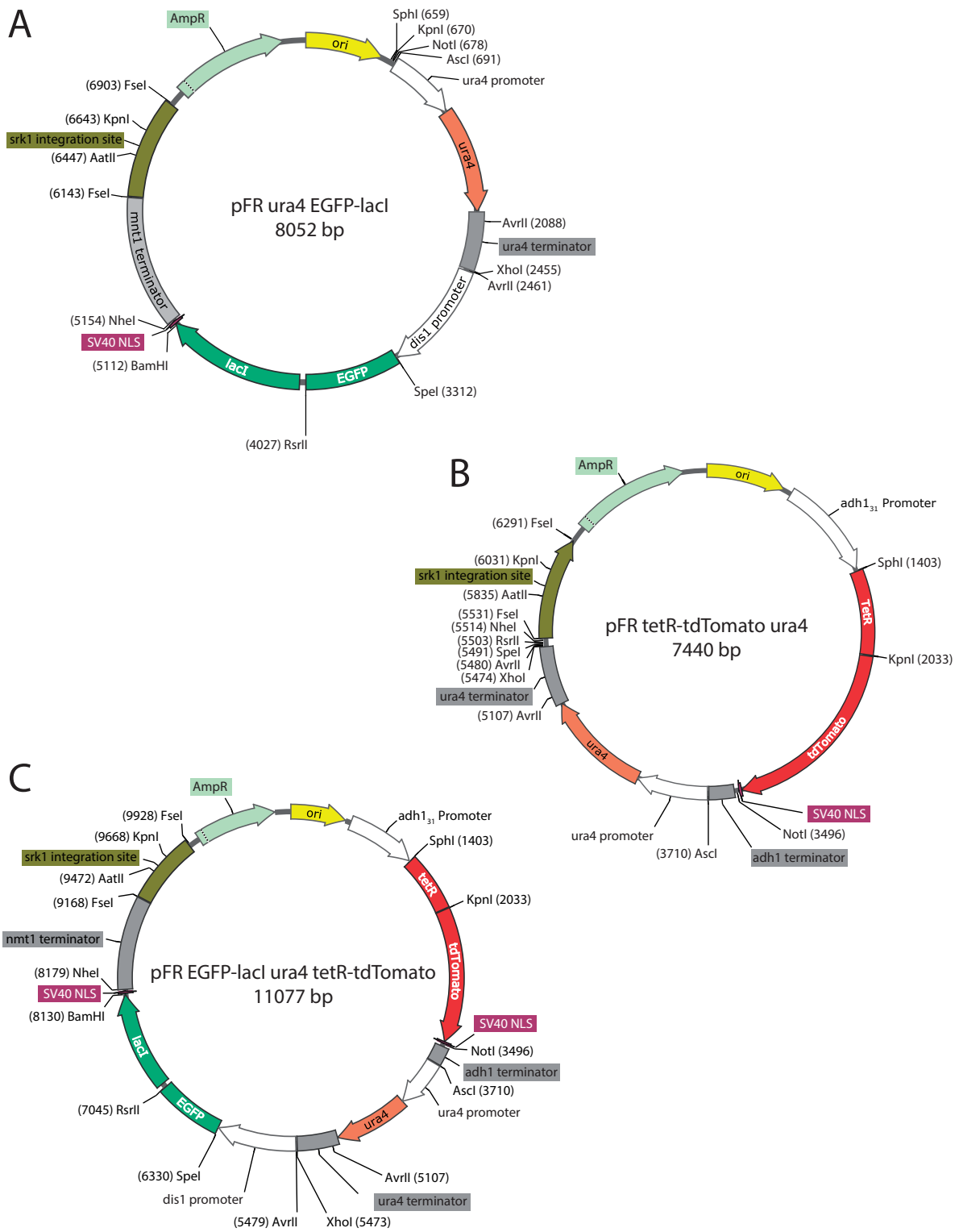

Figure 2.31: Integration plasmids for expression of tetR-tdTomato and GFP-lacI. (A) Map of pFR ura4 EGFP-lacI. (B) Map of pFR tetR-tdTomato ura4 (C) Combination of A and B, resulting in pFR tetR-tdTomato ura4 EGFP-lacI (2872).

bination occurs during meiosis (personal communication).
Lau et al. (2003) had reported tetO arrays that were less prone to recombination in *E. coli* (non-recombining tet operator array (nr-tetO)). To achieve this increased stability, Lau et al. slightly degenerated tetO sequences and spaced adjacent repeats by ten random base pairs. In contrast to the established tetO arrays, the marker gene was located between two operator repeat arms. Inter-arm recombination therefore would delete the marker gene, which further limits recombination under selection conditions.
I investigated, whether these modifications increased stability of tetO repeats in *S. pombe*. To be able to integrate the pLau44 construct into the *S. pombe* genome, I first replaced its *E. coli* marker gene flanked by the repeats with an *hphMX* cassette (Hentges et al., 2005), creating pTetO (plasmid 2779, see fig. 2.32 A, right). In a second step, I inserted a homology region for genome integration at *sec73* on Chr I, 2.49 Mb via restriction cloning (pTetO-*sec73*, plasmid number 2880). I transformed pTetO-*sec73* into a pFR TetR-tdTomato *ura4* EGFP-LacI containing strain (strain 4477), which led to the appearance of a bright fluorescent focus in each cell of this strain (strain 4507) in the red, but not in the green channel.
I next compared stability of the nr-tetO array sequences to the established system during meiosis. I crossed a strain auxotrophic for relevant markers (strain 3968) to the strains with either the nr-tetO or the established tetO arrays and performed tetrad dissection. I selected three clones in which the relevant markers had segregated 2:2 and acquired z-stacks of the cells' td-Tomato fluorescence in a wide field microscope.
I wrote a Jython script for Fiji to estimate FROS focus intensity compared to intensity of unbound tetR-tdTomato in the nucleoplasm (background). In short, the maximum grey value of gaussian filtered nuclear regions was used to estimate the average nucleoplasm signal. The brightest voxel value within the nuclear region was used as an estimate of FROS brightness. I manually segmented nuclear regions of cells in G_2 phase (elongated, single, mono-nucleated) to which I applied the algorithm. The script calculated the ratios between FROS brightness estimate and nucleoplasm estimate, which are shown in fig. 2.32 B. In cells without tetO, the brightest voxel was $1.2 - 1.3$ times brighter than the background estimate, reflecting fluctuations of protein concentration in the nucleus. In the starting strains, the tetO foci were about 2 times brighter than the nuclear background and the nr-tetO were on average 2.8 times brighter than nucleoplasm. After crossing, FROS intensities were reduced in the established tetO arrays. In one of three clones many cells FROS brightness estimate was indistinguishable from cells without tetO arrays. nr-tetO foci intensities were reduced after crossing, but not affected such that the ratio was reduced to a ratio of cells without tetO. I therefore concluded that nr-tetO have an improved signal to background ratio compared to the previously established system and are stable over meiosis.

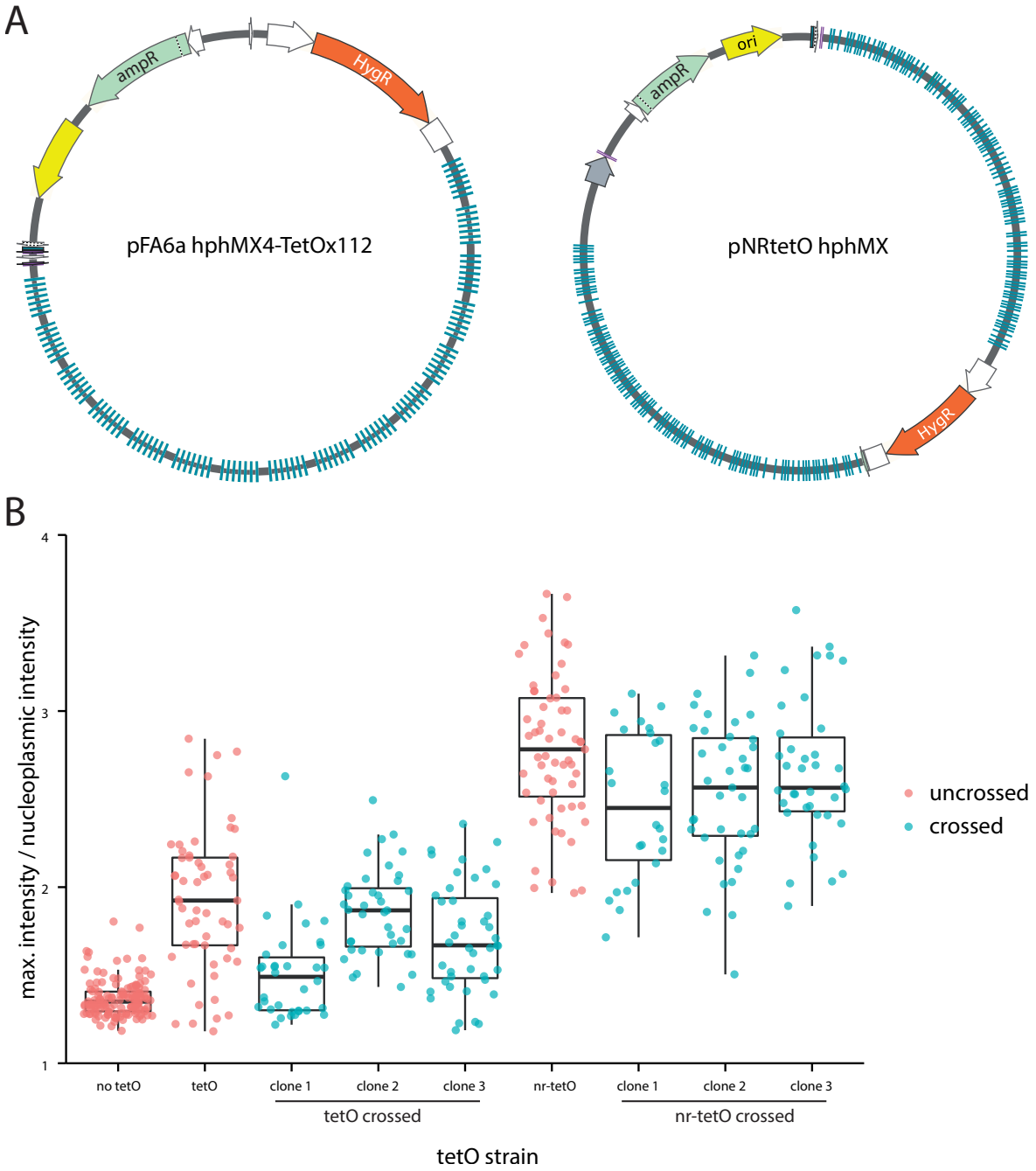

Figure 2.32: (A) Plasmid maps of tetO vectors, left: established tetO array plasmid with *hphMX* cassette adjacent to tetO repeats. Right: pTetO (nr-tetO), a modification of pLau44 (Lau et al., 2003), where the *E. coli* marker was exchanged to *hphMX*. (B) Ratio in G_2 cells of indicated strains.

Chapter 3

Discussion

3.1 Summary of the results

Although condensin is known to play a role crucial for chromosome condensation, knowledge about its regulation is still limited.
In the first part of this work, I have confirmed the function of Zas1 as a condensation factor. The essential function of Zas1 critically depends on a conserved short linear motif and its zinc finger domains. The sequence of the short motif is related to the E2F pRb AB groove binding motif, which is part of the 'start' cell cycle checkpoint in multicellular eukaryotes and had not been previously identified in unicellular organisms. Zas1's second essential domain are the ZF domains, which indicate that the protein binds DNA. I identified Zas1's chromosome binding sites by ChIP seq and found that the protein binds to the promoter region of the condensin subunit gene *cnd1*. I discovered that in a *zas1* ts mutant, Cnd1 protein levels are reduced, explaining the condensation defects of the mutant. Regulation of *cnd1* transcription is the plausible mechanism by which Zas1 regulates chromosome condensation. Zas1 is the first transcription factor identified of for a condensin subunit. Therefore, my work is important for the understanding of condensin transcriptional regulation in the context of the cell cycle. The surprising structural similarities between Zas1 and E2F/pRb shed light on the evolution of these central cell cycle regulators.
In the second part of my work, I have improved the FROS-based quantitative chromosome condensation assay. By building a computational pipeline for semi-automated data extraction and analysis, I was able to increase the assays's throughput more than 2-fold. I used this increased throughput to examine chromosome condensation kinetics under different conditions and found that condensation kinetics are temperature-dependent. Strikingly, the condensation kinetics measured by the assay depended on the spacing between the labelled chromosome loci. This suggests a model in which condensation activity acts evenly over the chromosome. In addition, I investigated axial chromatid compaction in single cells, which revealed that condensation kinetics are highly variable between cells, but follow a linear rather than a sigmoid regime. To be able to further improve the CCA, I have developed constructs for FROS signal enhancement.

In addition, I have established non-recombining tet operator arrays in *S. pombe* and shown that these have an improved signal-to-background ratio compared to the previously established system. These tools will be helpful in future screens for regulators of chromosome condensation and decondensation. They will facilitate characterization of condensin mutants and allow complex interpretation of condensation curves in a biologically meaningful way. Finally, they can be used to dissect the dynamics of the chromosome condensation process in detail to improve our understanding of cell division.

3.2 Characterization of *zas1*

3.2.1 *zas1* encodes a chromosome condensation regulator

Petrova identified *zas1* as a candidate condensation factor gene by screening for mis-segregation and abnormal condensation curves. When reintroduced in a defined genetic background, all three mutations isolated in the original screen induced temperature sensitivity, confirming Petrova's observations. For two of theses alleles (*W5* and *AJ3*), altered condensation curves were measured in the chromosome condensation assay, while the condensation curve of *A1* appeared *zas1*$^+$ like. The reason why the condensation phenotype for allele *A1* could not be confirmed might be the low penetrance of the phenotype, since only about 12 % of cells showed segregation defects. Although *A1* does not show a chromosome condensation defect, chromosome decondensation is abnormal, arguing for a defect in mitotic chromosome structure also in this mutant.

Okazaki and Niwa described the phenotype of *zas1-Ts34* as defective in nuclear division at the restrictive temperature, but did not provide data to support this claim. Consistent with this report, reintroduction of *Ts34* into a defined genetic background induced temperature sensitivity. When measured in the condensation assay, the condensation behavior of *Ts34* cells resembled *W5* and *AJ3* curves. All aberrant condensation curves displayed a shallower slope than *zas1*$^+$ curves. The consistence between different ts mutants argues for a common underlying cause. More importantly, observing a condensation defect in an allele of *zas1* that had not been identified in the screen strongly supports the conclusion that the gene is the underlying factor required for chromosome condensation.

The quantitative chromosome condensation assay is the best technique currently available to study chromosome condensation dynamics in yeast. Non-time resolved condensation measurement methods are not likely to detect the kinetics defect. Nevertheless, because information from multiple condensation events is averaged during data analysis, two interpretations are possible for the shallow condensation curves of *zas1* ts mutants. First, shallow curves could be interpreted either as defect in condensation kinetics in the bulk of the cells. Second, temporal variability between cells in APC/C activation would lead to high anaphase onset delay timing variability. Because the time series are aligned to anaphase onset, single cell curves would be shifted on the time axis (fig. 3.1). When averaging distances, the time shift would lead to a shallow curve similar to what one would expect from defects in condensation kinetics. To clarify

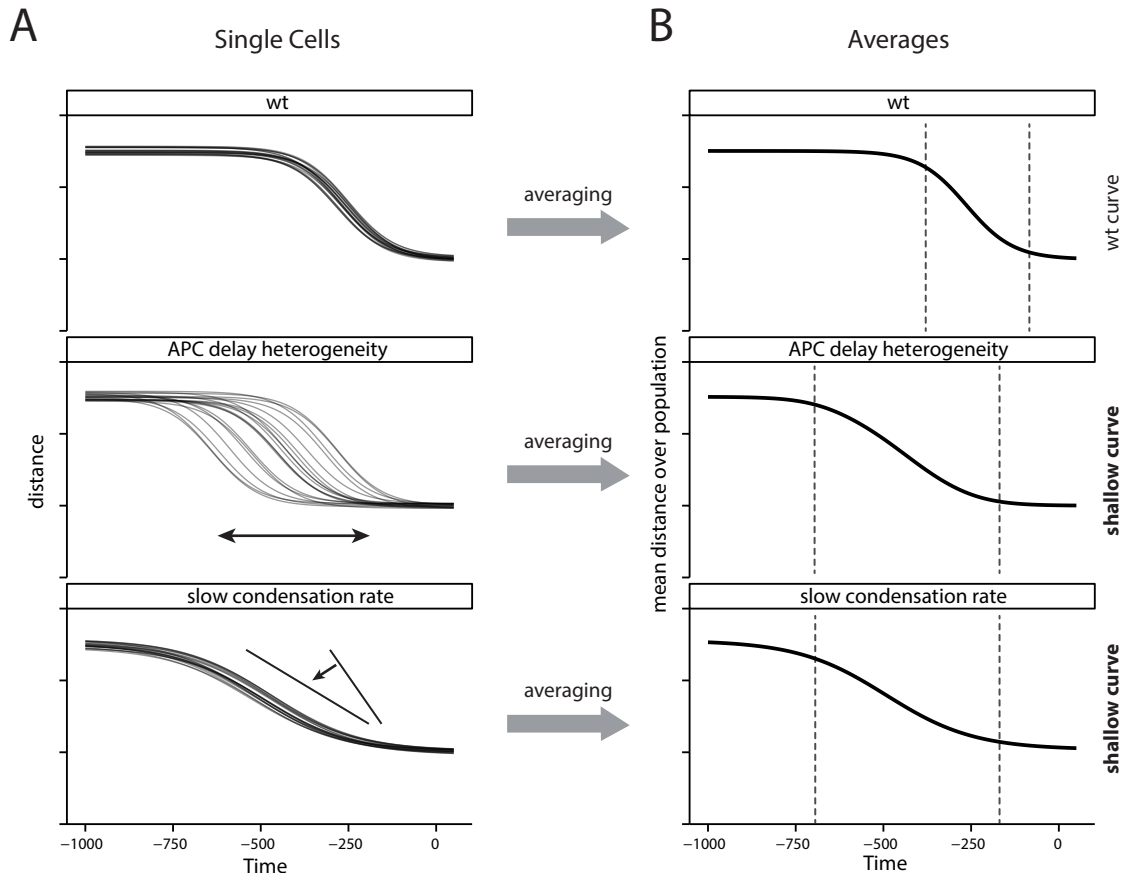

Figure 3.1: Both temporal heterogeneity in APC/C activation and slow condensation kinetics can result in shallower average condensation curves like observed in *zas1* ts mutants. (A) Simulation of sigmoid condensing cell populations, either synchronously (top), with heterogenous delay in anaphase onset (curves from top shifted on time axis, middle), or lower condensation rate (bottom). Each line represents dataset from a single cell. (B) Time point grouped averages of (A) for wt, APC delay and low condensation rate. Note that average curves of APC delay and low condensation rate are virtually indistinguishable. Source code for the models is listed in section 4.15.10. wt: wild type

which of the alternative explanations is true, chromosome condensation kinetics of *zas1* mutants should be examined at the single cell level.

I found that Zas1 shares important characteristics with the known condensation factors condensin and topoisomerase II, like chromosome mis-segregation, essentiality and nuclear localization of the protein. *zas1* ts mutants showed chromosome mis-segregation at the restrictive temperature, confirming the results of Okazaki and Niwa (2000). However, chromosome mis-segregation does not necessarily imply condensation defects, as defects in other pathways result in mis-segregation as well, e. g. cohesion or SAC. Therefore, mis-segregations by themselves are not sufficient to indicate a role of *zas1* in condensation. Yet, in the context of the condensation curves, it argues for the idea that *zas1* contributes to chromosome condensation. Although mis-segregation was detectable in all ts strains, penetrance of the phenotype was low. Only 12–30 % of mitoses resulted in mis-segregation (fig. 2.4). In contrast, all ts mutations affected growth drastically. This discrepancy between the mild segregation phenotype and the strong

impact on cell proliferation suggests that *zas1* has other essential functions in addition to the regulation of chromosome condensation. An efficient and rapid conditional depletion system would be useful to investigate whether Zas1 functions in cell cycle stages other than M-phase.

Zas1 localizes to the nucleus, where it accumulates in distinct foci (fig. 2.5). The nuclear localization corroborates the bioinformatic prediction of the N-terminal NLS and data from an ORFeome-wide protein localization analysis study (Matsuyama et al., 2006). The accumulation at distinct spots had previously not been reported, refining the previous findings. The spotted localization suggests a non-structural role rather than a function in mitotic chromosome structure, in which case staining of whole chromosomes would be expected. The idea of Zas1 fulfilling a non-structural role in condensation is also consistent with its low protein expression levels. Marguerat et al. (2012) reported Zas1 to be expressed at approximately 500 molecules per cell. Along this line, the auxin-induced depletion system could even attenuate protein levels further, to about half the wild type concentration, without affecting cell growth (fig. 2.7). This argumentation matches Zas1's role as transcription factor. Taken together, nuclear localization, essentiality for proliferation and mis-segregation and are strong evidence that *zas1* is a chromosome condensation factor.
Other ZF-containing proteins have been implicated in chromosome condensation. For example, AKAP95 has been shown to be responsible for condensin recruitment to chromosomes *in vitro* (Eide et al., 2002). Kim et al. (2016) described that ZF containing TFs Ams2 and Ace2 recruit condensin to chromosomes in *S. pombe*.

3.2.2 Identification of *zas1*'s essential elements

I next addressed the question how *zas1* regulates chromosome condensation. Because *zas1* is essential (fig. 2.6), I systematically tested partial deletion alleles for their ability to complement *zas1* deletion, to gain information about the functionally important elements of *zas1*.
I found that although all mutations conferring temperature sensitivity were located in the region of the antisense lncRNA and Zas1 CTD, neither lncRNA nor CTD were required for cell proliferation. ncRNAs can have regulatory roles or can be transcriptional noise. The antisense lncRNA could also be part of a regulatory mechanism mediated by *S. pombe*'s RNAi machinery. An alternative experiment to investigate lncRNA function could be to alter its nucleotide sequence by replacing codons without affecting the aa sequence of the ORF.
The C-terminal truncations corresponding to the nonsense mutation alleles phenocopied the respective point mutations (figs. 2.8 and 2.16). Surprisingly, cells with drastic truncation alleles (*Y289X*, *L360X* and *V470X*) grew faster than ts-inducing truncations (*Ts34* and *W712X*). It is counter-intuitive that short ORF alleles do not show the same or a more severe growth phenotype that longer ORF truncation alleles. A possible explanation for this apparent contradiction is that *zas1*'s CTD requires approximately the last 250 aa to fold stably. Truncation within the last 250 aa could destabilize the fold, leading to entire unfolding of the CTD domain. Presence of this large unfolded peptide region would lead to degradation of the whole protein via the proteolytic pathway, thereby depleting the essential regions in the N-terminal part of Zas1. By

deleting the complete CTD, no unfolding is induced and the protein is not degraded.
A different hypothesis to explain this apparent contradiction is that short truncations induce hyperactivity of the protein, which is reduced to normal upon further deletion. A hyperactive allele is expected to be dominant in diploid cells. I did not notice growth defects of heterozygous diploids, arguing against this gain-of-function hypothesis. Structural information for the CTD, e. g. from X-ray crystallographic data, would be beneficial to address these hypotheses.

3.2.3 Discovery of an essential pRb AB groove binding-like motif in Zas1

Further truncation of *zas1*'s ORF revealed that a short stretch of about 6-7 aa N-terminal of the CTD (VRWLFS) is essential for cell proliferation and therefore for Zas1 function (figs. 2.8 and 2.10). This stretch is conserved between Zas1 orthologs and in its paralog Klf1. I confirmed the result of this truncation experiment by deletion or mutation of only these residues of the motif, which resulted in a strong proliferation phenotype. Deleting a stretch of 42 aa just N-terminal of the motif did not significantly affect cell growth, emphasizing the importance of the motif region (fig. 2.10). The essential stretch matches the consensus of a pRb-binding motif in E2F TFs. In higher eukaryotes, this motif is involved in regulation of the 'start' cell cycle checkpoint (Alberts et al., 2014). It mediates the interaction between pRb and E2F TFs in conjunction with a LxCxE motif. Upon pRb phosphorylation, these inhibitory interactions are broken, and pRb dissociates from E2F, thereby regulating cell cycle entry. According to the Eukaryotic Linear Motif database (ELM), this is the first description of a motif belonging to the AB groove binding class in unicellular organisms. A reason why this motif had previously not been identified by Okazaki and Niwa (2000) could be that the conserved sequence is very short. Linear motifs usually act synergistically. That a single motif has a strong impact on cell functionality as found here is unusual (Toby Gibson, personal communication).

3.2.4 Orthologs of Zas1 in other organisms

Zas1 is conserved in *S. cryophilus* and *S. octosporus*, but has no obvious ortholog in *S. japonicus*. Of the four genome *Schizosaccharomyces* species whose genomes have been sequenced, *S. japonicus* is the only one with open mitosis (nuclear envelope breakdown during cell division). Could *zas1* function be specific to closed mitosis?

pombase lists SDD4 (YPR022C) as a possible *S. cerevisiae* ortholog of *zas1*, although this has been disputed by Okazaki and Niwa (2000). To clarify, whether SDD4 and Zas1 are functional homologs, one could test if SDD4 regulates the transcription of Cnd1 homolog Ycs4. A high throughput screen identified genetic interaction between SDD4 and CLN1, a G_1-S cyclin like *puc1* (see below) (Bandyopadhyay et al., 2010).

A simple BLAST search did not identify orthologs of Zas1 in higher eukaryotes, probably

because Zas1's VRWLFS motif is too short to reveal homology. In multicellular organisms, pRb binds to AB groove binding motifs in E2F TFs to inhibit proliferation. The strong sequence similarity between pRb AB groove binding motifs in E2F TFs and Zas1's VRWLFS motif suggests the presence of a structurally similar ligand in fission yeast, a *S. pombe* ortholog of pRb. This could be Zas1's CTD, as discussed in section 3.2.5. A functional similarity between Zas1 and the pRb/E2F complex is the structure of a target gene. When not inhibited by pRb, E2F transcription factors initiate transcription of cyclins E and A to promote S-phase entry. Zas1's fourth prominent binding site is the promoter of *puc1* (table 2.2) and Puc1 levels are reduced in *zas1-K833X* (section 2.1.19). *puc1* encodes a cyclin, which is not essential in *S. pombe*, but is able to complement CLN1, CLN2 and CLN3 depletion in *S. cerevisiae* cells, overcoming alpha-factor arrest (Forsburg and Nurse, 1991). Forsburg and Nurse (1994) described that Puc1 has a role in exit from the mitotic cell cycle.
Structural pRb orthologs have not been found in *S. cerevisiae* or *S. pombe* until now. As both, plants and animals, share pRb as regulator of cell cycle start, it is likely that their common unicellular ancestor had a similar mechanism. Therefore, it is astonishing that yeasts do not have a structural pRb homolog. Instead, cell cycle regulation is mediated by its functional homologs SFB/WHI5 proteins (Medina et al., 2016). Identifying the binding partners of Zas1's VRWLFS motif could be a very promising approach to reveal structural yeast pRb homologs (see also sections 2.1.15 and 3.2.5). This would be very important to understand the evolution of a central cell cycle switch in multicellular organisms, including humans.
The essential VRWLFS sequence not only matches the pRb AB groove ligand motif, but also a cyclin recognition site (both ligands are cyclin folds). Recognition by a cyclin or a cyclin-CDK complex might play a role in Zas1 regulation, especially because two putative CDK phosphorylation consensus sites are located six and ten residues N-terminal of the VRWLFS motif. It is conceivable, that a cyclin could recruit a CDK and thereby mediate phosphorylation of these residues. A candidate for this cyclin could be Puc1, as Zas1 binds to the *puc1* promoter and hence, might regulate its transcription via a feedback loop. In *S. cerevisiae*, a genetic interaction between SDD4 and CLN1 had been reported. Viability of a Zas1 CTD and *puc1* co-deletion strain could be examined via tetrad dissection. In addition, mutually exclusive binding between a cyclin and a pRb homolog could be envisioned, implementing a molecular switch.

3.2.5 Identification of Zas1's VRWLFS motif interaction partners

Co-IP did not identify Zas1 interaction partners

Identification of ligands of Zas1's VRWLFS motif is essential to understand Zas1 function. I have tried to identify Zas1 interaction partners by co-IP (section 2.1.17 and fig. 2.20). The reasons why no interaction partners could be identified in this experiment can be manifold. First, the low expression levels of Zas1 make co-IP a challenging experiment (section 3.2.1). Second, the C-terminal PK_6 tag might not be accessible when in complex with binding partners. To address this hypothesis, N-terminal or internally PK_6 tagged proteins should be immunoprecipitated.

Third, interactions might be very transient or complexes might not be stable in IP buffers. An idea worth exploring is that, under the conditions tested, Zas1 might not interact stably with its ligands and that stable interactions might be induced during stationary phase or under stress conditions. In mammalian cells, pRb and E2F TFs interact in non-cycling cells. If the Zas1 VRWLFS motif were indeed a component of a 'start'-like cell cycle checkpoint, and if this checkpoint were structurally conserved, one would expect an interaction between the motif and its ligand in non-cycling cells, too. Therefore, the co-IP experiment should be repeated from non-cycling, stationary phase cells. This experiment would also provide an opportunity to confirm the Zas1 - Klf1 interaction reported by Shimanuki et al. (2013).

A peptide in the motif region binds to Zas1's CTD

In an *in vitro* experiment, I was able to show that a peptide fragment containing the N-terminal half of the VRWLFS motif interacts with the CTD (section 2.1.15 and fig. 2.18). An alternative explanation for this observation could be that the protease subtilisin was not completely inactivated and cut the protein only during or after the SEC run. This is not likely though, because I added a nearly 100-fold molar excess of the protease inhibitor PMSF over subtilisin. Furthermore, SEC should spatially separate the small, 27 kDa subtilisin molecules from the larger 60 kDa fragments early during the chromatography run.
Mass spectrometry mapping results are low in resolution, because not every peptide can be detected in the mass spectrometer. It is therefore possible that the VRWLFS motif itself interacts with the C-terminal domain. Binding of the VRWLFS motif would suggest that Zas1 CTD consists of cyclin folds and supports Toby Gibson's prediction that the CTD has an pRb-like structure. Recombinant expression and purification of the CTD protein should be established to address this hypothesis. First, the recombinant protein would be useful to quantify binding of different Zas1 peptides in isothermal titration calorimetry (ITC) or fluorescence polarization experiments. Systematic peptide variants could be used to map the exact sequence required for binding. Second, an X-ray crystal structure of the CTD, ideally bound to its peptide ligand could provide strong evidence for the presence of cyclin folds and structural pRb homology.

3.2.6 Zas1 forms dimers *in vitro*

I described in section 2.1.16, that Zas1 can form dimers *in vitro*. This leads to the question of which of Zas1's domains are required for dimerization. Repeating the SEC-MALS experiment with different mutant versions of the protein could identify these domains. If the VRWLFS motif were involved in dimerization, an alternative way to investigate its role could be competition experiments with VRWLFS peptides during SEC. Most importantly, the questions in how far Zas1 homodimerization plays a role *in vivo* and whether dimerization is required for protein function need to be examined. *In vivo* homodimerization could be competed by other proteins, especially by interaction with Zas1's paralog Klf1 (Shimanuki et al., 2013). Differential homo-/heterodimerization in each cell cycle phase could alter the complexes' target DNA binding

sequences and thereby regulate gene expression. Other zinc finger TF have been shown to dimerize, some even mediated by specialized ZF domains, e. g. *Drosophila* Sry-delta (Payre et al., 1997). A means to test homo- or heterodimerization is to epitope-tag two different Zas1 copies with different tags, e. g. PK_6 and HA in a diploid. Interaction can be assessed by IP via one tag and western blot detection of the second tag. The same strategy can be applied to test heterodimerization between Zas1 and Klf1.

3.2.7 Zas1's ZFs are essential for its function

I identified the ZFs domains as a second essential region of Zas1 (section 2.1.11 and fig. 2.13). ZF domain deletions were almost inviable. This suggests that recognizing specific DNA binding sites is central to the function of Zas1.
Okazaki and Niwa (2000) described alternative splicing of the third ZF domain and named the gene accordingly. Alternative splicing is rare in *S. pombe*. As of August 2016, four transcripts are listed as alternatively spliced in pombase (*prp10*, *trt1*, *SPAC1A6.03c* and *zas1*). Unlike Okazaki and Niwa (2000), I was not able to detect *zas1*'s long splice isoform by RT-PCR, despite using alternative exon-specific specific primers (data not shown). Yet, the RT-PCR reaction might have been inhibited for unknown reasons. Furthermore, alternative splicing might occur only under certain conditions, like cell starvation or entry into a meiotic cell cycle program.
A second indication that only the short ZF isoform exists in cells is that only a single band was appeared in a western blot of C-terminally PK_6 tagged Zas1 (fig. 2.14 A). Still, it is possible that the long, three ZF isoform is too rare be detected or that both isoforms were not separated by SDS-PAGE. For the conditions used in this thesis, the two ZFs cDNA variant perfectly complemented deletion (fig. 2.10). Hence, in contrast to the first two ZFs, the third ZF is not essential for growth. The role of the third ZF could be experimentally addressed by degenerating splice sites for the second ZF to enforce expression of the long isoform.

3.2.8 A working model for Zas1: The VRWLFS motif recruits binding partners to ZF target sequences

Finally, I attempt to combine the information discussed in the previous paragraphs into a working model for *zas1* function in cell proliferation and chromosome condensation. *zas1* encodes a protein that contains three essential elements: NLS, the first two ZFs and the VRWLFS short linear motif. What are the functions of these elements?
It is fair to assume that the NLS's exclusive function is to mediate nuclear import of Zas1. ZFs and VRWLFS motif are both short and unlikely to act in isolation on proliferation and chromosome condensation. Also, a structural role of Zas1 as a chromosome scaffold protein can be excluded because the protein expression levels are very low (section 3.2.1) and the protein localizes only to certain chromatin regions.
It is reasonable to assume that Zas1 serves as a platform, to recruit VRWLFS motif bind-

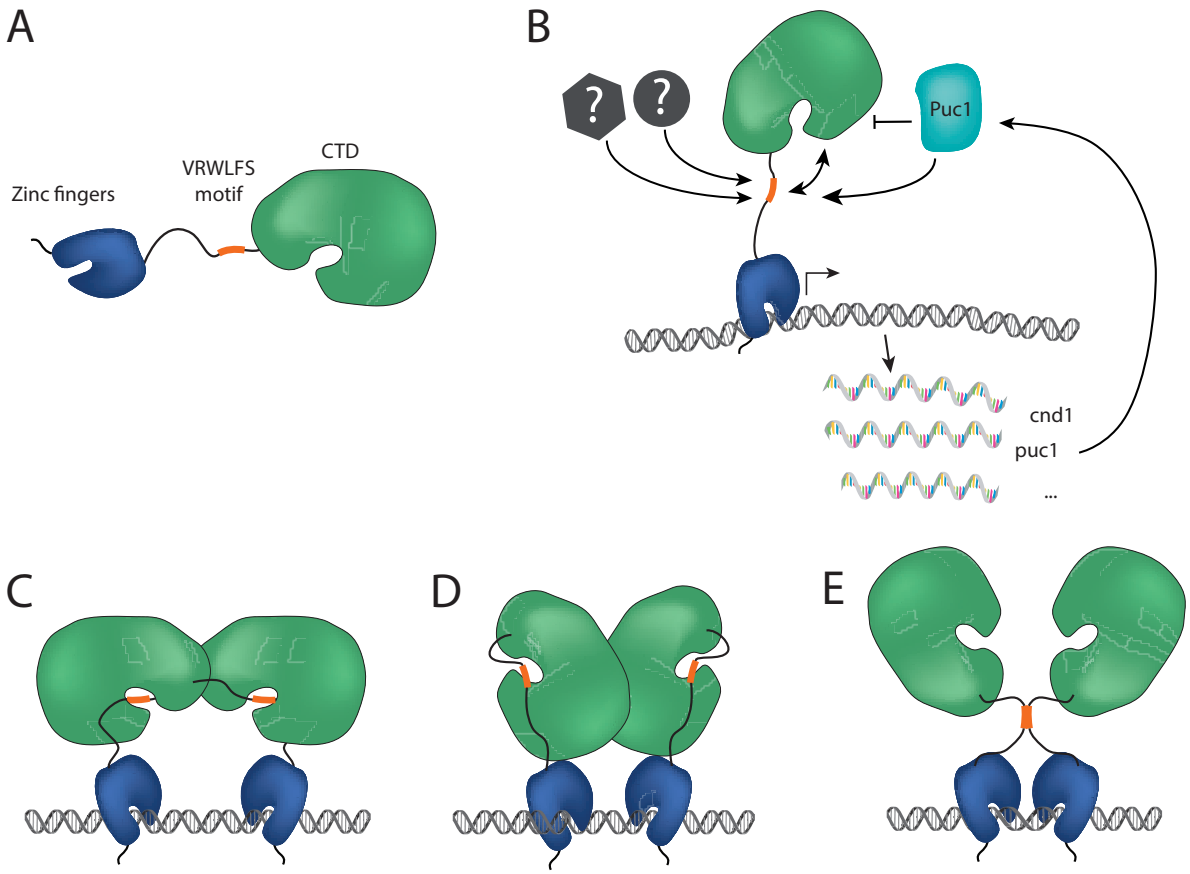

Figure 3.2: Structural and functional models for Zas1. (A) Structural model of Zas1 monomer, ZF and CTD fold into domains, while the VRWLFS motif is in an unstructured region and accessible for binding partners. (B) Functional model for Zas1. Zas1 regulates the transcription of *cnd1*, *puc1* and other genes. Puc1 could regulate Zas1 by binding to the VRWLFS motif, creating a feedback loop. VRWLFS motif binding is competed for by Zas1's CTD and other unknown factors to regulate transcription activity. (C-E) Different models for dimerization of Zas1.

ing partners to ZF chromatin binding sites. By this mechanism, Zas1 could integrate signals and amplify them by activating transcription of target genes, e. g. *cnd1* and *puc1* (fig. 3.2). Transcriptional activity could then be modulated by the interaction between the CTD and the unstructured linker. Such a domain organization of Zas1 is supported by the structure predictions and the limited proteolysis results. The NLS is followed by the two zinc finger domains, which mediate binding to chromatin. C-terminal of the zinc fingers is a unstructured linker region, which contains the VRWFLS motif. The unstructured linker connects with the large, folded CTD, which might have sub-domains that could not be resolved in the limited proteolysis experiments (fig. 3.2 A). On the quarternary structure level, different combinations are conceivable and supported by the data. Future research has to be done to rule out or verify one of these models. If Zas1 formed homodimers *in vivo*, it is likely that dimerization is mediated by the CTD – VRWLFS motif region interaction (figs. 2.18 and 3.2). It is also conceivable that CTDs might dimerize independent of the VRWLFS motif – CTD interaction (fig. 3.2 D). In both these cases, dimerization would not be possible in CTD deletion strains and would there-

fore not beessential for Zas1's function. Binding of the CTD to the motif region could sterically hinder other motif ligands from binding and thereby regulate Zas1 activity e. g. transcriptional activation. Two VRWLFS motifs are not likely to induce homodimerization due to their small size (fig. 3.2 E). It is also possible that Zas1 forms different multimers depending on the cell cycle phase.

3.2.9 Zas1 as a TF for *cnd1*

I showed that Zas1 binds to the promoter of the condensin subunit gene *cnd1* and that Cnd1 levels are reduced in Zas1-*K833X* mutants. This data strongly suggests that Zas1 is a TF that positively regulates expression of *cnd1*. As a next step, *cnd1* mRNA levels should be compared between wild type and Zas1 mutant strains, e. g. by reverse transcriptase quantitative PCR (RT-qPCR).

Hight throughput data indicates that *cnd1* mRNA levels change over the course of the cell cycle (Peng et al., 2005). Hence, an alternative explanation for the observation of reduced Cnd1 levels in *zas1* ts cells could be that *zas1* mutations enrich cells in a cell cycle stage at which *cnd1* transcription is low.

Another hypothesis is that Zas1 mediates *cnd1*'s cyclic transcription. Both these hypotheses should be tested in cell cycle synchronization experiments. Cells could be synchronized by *nda3-KM311*, *cdc25-22*, M-factor or hydroxyurea (HU) arrest. Protein and RNA levels of *cnd1* gene products and a known cycling protein (e. g. cyclins) could be monitored at different time points after release from the cell cycle block.

Further experiments should investigate the connection between reduced Cnd1 levels and the aberrant condensation curve in *zas1* ts mutants. Cells in which the *cnd1* promoter was replaced by the *cnd3* promoter (P_{cnd3} *cnd1*) did not show a growth defect. An antibody against Cnd1 will be helpful to compare protein levels between *cnd1*$^+$ and P_{cnd3} *cnd1* cells. If Cnd1 levels are approximately equal in both strains, condensation in P_{cnd3} *cnd1* cells carrying either *zas1*$^+$ or *zas1* ts alleles should be compared.

If condensation and segregation defects persist in a *zas1* ts P_{cnd3} *cnd1* strain, impairment of other factors than Cnd1 level are responsible for the condensation defects. These factors could are likely to be other Zas1-regulated genes. A good candidate is *brf1*, *S. pombe*'s TFIIIB. A different component of an RNA polymerase III transcription factor, *sfc3*, has been implicated in condensation of chromosome arms in *S. pombe* (Tada et al., 2011).

If *cnd1* promoter replacement rescues the condensation phenotype of *zas1* ts strains, the Cnd1 protein level reduction is the only cause of the condensation defect. In this case, conclusions about Cnd1's contribution to chromosome condensation can be drawn based on the condensation curves. Either, Cnd1 is only required to speed up chromosome condensation, but not for compaction per se. Alternatively, only very few Cnd1 molecules are required for full compaction, and reduction in condensin molecule number scales with condensation kinetics. An efficient protein degron system would be useful to test these hypotheses by comparing *zas1* ts-induced Cnd1 level reductions with degron-induced Cnd1 level reductions.

cnd1 promoter replacement did not rescue the growth defects of *zas1* ts mutants. This has two implications. First, Zas1 must have essential functions beyond regulation of *cnd1*. These are likely to be other essential genes, for example *peg1*, *tom22*, *pmo25* and others (see table 2.2). Often, transcription factors change expression levels of their target genes in response to signal transduction cascades. Identification of all directly regulated genes of *zas1* will be key to find out commonalities between these regulated genes. This could give hints to which cellular processes might regulate Zas1. Hence, transcriptomes should be compared between *zas1* mutants and *zas1*$^+$ cells. These questions are currently being addressed by Jin Wang. Second, it should be tested, if the condensation-influencing feature of *zas1* and its essentiality can be separated. This would show that condensation factors do not always have to be essential, proving the previous expectation in section 2.1.4 wrong. Hence, it would make sense to screen non-essential genes for involvement in chromosome condensation. One screening approach would be to examine deletion of each non-essential ORFs with known nuclear protein localization for condensation defects with the CCA. This could be done by crossing a FROS strain with the respective strains of the ORFeome-wide deletion collection (Kim et al., 2010). To enable efficient screening with the CCA, I created a computational data extraction and analysis pipeline, which is discussed in the next section.

3.3 A data analysis pipeline for FROS-based condensation measurements

In section 2.2, I have presented a series of Fiji plugins that facilitate and automate data extraction for the FROS based quantitative Chromosome Condensation Assay (CCA). Using this pipeline, I was able to significantly increase the number of analyzable cells per imaging experiment from which data. This markedly improved reproducibility and reliability of the CCA. In addition, it allowed me to assess experiment-to-experiment variability and to increase temporal resolution to gain insight of chromosome condensation on the single cell level. These improvements will be useful for analysis of the wild type chromosome condensation process as well as for characterization of condensation factor mutants. Furthermore, the improved data handling will facilitate screening for other condensation factors like regulators of condensin.
Next to increasing throughput, I implemented mechanisms that limit human error and thereby enhance the accuracy of the data compared to the previous process. I replaced manual data handling steps by automated scripts. These included semi-automation of ROI definition process, temporal alignment in an Excel spreadsheet and meta data reading from microscopy images (e. g. pixel size). The blind assessment of segmentation results and determination of anaphase onset limits human bias. The application of this pipeline is not restricted to data for chromosome condensation measurements. In principle, it can be used for tracking of interphase live cell chromatin loci in *S. pombe* and *S. cerevisiae* or other immobile cell types that can be imaged in a monolayer. For example, results from proximity ligation experiments (HiC etc.) can be tested and refined by tracking loci during interphase.

Parts of this pipeline can be modified to measure condensin nuclear import timing. This information would be of interest for interpretation of single cell data. For this customization the current implementation as scripts is disadvantageous. Because most of the source code already utilizes classes, it is desirable to implement the programs in a more modular way. This will reduce redundant code, make the pipeline easier to maintain and more usable for custom applications. A package structure will also facilitate distribution. Another limitation of the pipeline is the central segmentation algorithm for the FROS foci which currently has some major shortcomings. For example, the centroid of the segmented voxels is not weighted by voxel intensity. Sub-voxel resolution can be improved by adjusting for each intensities. Also, background subtraction is not implemented and can improve segmentation accuracy. The infrequent but vexatious `IndexOutOfBounds` and `Object not found` exceptions caused by the chicken implementation should be addressed (Zongker, 2006). Available 3D particle segmentation algorithms should be compared in their performance with the existing algorithm on CCA data (Chenouard et al., 2014). Performance could be enhanced by assessing whether a fluorescent focus is present in the respective frame based on the data in fig. 2.32 before the time consuming 3D segmentation is started. This will also prevent segmentation of weak and out-of-focus FROS signal.

Another strategy to improve segmentation is to utilize temporal information. Currently, the segmentation algorithm does not take information from previous frames into account. Although FROS movement can be assumed as random, the change in FROS position is continuos and its velocity is limited. If position and maximum velocity of a FROS focus are known for one frame, a prediction for the position at which the focus should be observed in the next frame can be made. Because the FROS locus can not move outside the nucleus, the intersection between the nuclear volume and a sphere with radius $r = v_{\max} \cdot \Delta t$ centered around a FROS position determines the volume to which the focus can locate in the next frame. The radius of the sphere decreases with temporal resolution of the video due to its dependence on Δt. Application of such a prediction algorithm for segmentation has advantages and disadvantages. A disadvantage is that a wrong segmentation favors incorrect tracking, self-reinforcing wrong analysis. Therefore, correction mechanisms should be installed, e. g. try to find the focus in the predicted volume before evaluating the full volume. An advantage of such integration of temporal information is that once found correctly, correct segmentation is favored. An increase in analysis speed is also expected, as computation time scales with volume. This is of particular use, because analysis of long, high frequency videos is computationally intense. The trajectory information about the FROS will be very useful to characterize decondensation on the single cell level. Last, fluorescent foci from other cells entering the FOV during the time course are less prone to be falsely segmented in favor of the cell's of interest's FROS foci. This will be especially helpful for data in which dividing cells had been detected automatically. Increasing segmentation reliability will facilitate complete automation of the data extraction procedure, the long-term objective of this work and of the proposed improvements. Next to improvement in segmentation reliability and quality, two more steps are required for complete automation of the data extraction pipeline.

First, detection of dividing cells and segmentation of their volume has to be implemented, e. g. by segmentation of the nucleoplasm based on unbound fluorescent repressor signal. Second, the time point of FROS segregation has to be detected computationally to determine anaphase onset. When fully automated, the computational pipeline will eliminate human bias and allow investigation of high cell numbers accelerating screens of large mutant collections.

3.4 Advanced characterization of chromosome condensation dynamics

3.4.1 Condensation and decondensation in population averages CCA measurements

I applied the computational pipeline to determine average chromosome condensation curves at the population level at 25 °C and 34 °C for three different FROS positions and spacings 0.5 Mb, 1.0 Mb and 1.2 Mb (fig. 2.26). For each condition, I measured more than 3 replicate experiments to create condensation curves and quantify the inherent experiment-to-experiment variability, which had previously been unknown. Variance increased with both FROS spacing and temperature.

This data is useful to determine whether condensation curves from two strains are significantly different or within the experiment-to-experiment variance of wild type condensation behavior. It will be particularly valuable to interpret screening results. Some condensation curve features, e. g. the small increase of distance after anaphase onset, were replicable, suggesting they are the result of underlying biological processes. Because all data described in section 2.3.2 and discussed here was acquired on the same microscope setup (API DeltaVision RT), the data should be tested for reproducibility with other microscopes. Also, to assess errors introduced by chromatic aberrations, a FROS strain should be constructed and measured in which both lacO and tetO arrays are integrated next to each other.

Dependence of the condensation curves on temperature

In strains carrying both labels on one chromosome arm (arm–arm, 2774 and 2779), G_2 distances did not change with temperature. In contrast, in the strain with one centromere label and one arm label (cen–arm, 2926) G_2 interphase distance increased with temperature (in agreement with Petrova et al. (2013, fig. S3 D and E)). This dependence suggests that the condensation measurements in the cen–arm strain are superimposed by a second, unknown process, at least during G_2. Because of its variable G_2 distance, the cen–arm strain (2926) is hence not ideal to use as a chromosome condensation readout. Future measurements of chromosome condensation factors should be based on a strain with both FROS labels on one chromosome arm, e. g. with 1.0 Mb spacing.

The following hypotheses could explain the distance–temperature dependence. During G_2, *S. pombe* centromeres are attached to the spindle pole body (SPB), which in turn is moving by

the pushing movements of cytoplasmic microtubules (Tran et al., 2001; King et al., 2008). It is conceivable that the distance between centromere and arm-locus depends on theses centromere movements. The stiffness of chromatin between between centromere and chromosome arm might change with temperature, thereby changing the degree of correlation between arm FROS and centromere FROS movements. Also, microtubule growth and catastrophe is temperature dependent (Fygenson et al., 1994). Altered microtubule dynamics might change the velocity of SPB movements. It should be tested whether the dependence between G_2 distance and temperature holds true for FROS labels on other chromosomes.

Both condensation and decondensation rates increased with temperature in all strains. Many biological processes (e. g. growth rate of yeast cells) increase in rate with temperature up to an optimum. Because only two temperatures were probed, the temperature optimum for the condensation process cannot be inferred. It is nevertheless likely that 34 °C is close to the maximal condensation rate since 35 °C is approximately the optimal growth temperature for *S. pombe* (Petersen and Russell, 2016). Measurements at other temperatures could reveal the dependence between temperature and chromosome condensation rates and also whether this dependence is linear. In particular, condensation measured at lower temperatures (e. g. 20 °C) should be established. Due to a slower compaction rate, observing condensation at low temperature can be a means to achieve more data points for each condensation event without changing the acquisition frequency. This quasi-increase in temporal resolution might be useful to resolve subtleties of the condensation process. More importantly, boosting the number of measurements should increase accuracy of the compaction rate estimation, especially at the single cell level (sections 2.3.7 and 3.4.2). This highlights another advantage of yeast as a model system over mammalian cells, which are restricted in temperature tolerance to about 37 °C.

The volume of most non-living materials depends on temperature. If this dependency applied to mitotic chromosomes, a temperature-dependent isotropic change in volume should correlate positively with the full compaction distance (d_{min} in table 2.4, definition in section 2.3.4).

The minimal distance varied with temperature at all three FROS spacings, but not as expected. For 0.5 Mb FROS spacing, d_{min} was higher at 34 °C than at 25 °C, while for both other FROS spacings, d_{min} increased with temperature. The d_{min} measurements for 0.5 Mb FROS spacing are close to the diffraction limit and might contain a high fraction of noise. Measurements of condensation at different temperatures will therefore also be helpful to clarify, whether a physical effect underlies the heat-induced contraction of mitotic chromosomes at 0.5 Mb. In case of a physical effect, a correlation between temperature and d_{min} should be observed. Alternatively, a local effect could be responsible for the decrease of d_{min} with temperature in 0.5 Mb FROS spacing. In a first step, comparing condensation curves of the same FROS spacing but for various loci should clarify, whether compaction is homogeneous throughout the chromosomes or whether some regions compact more than others.

Positive dependence between FROS spacing and condensation rate

Measured chromosome condensation rate increased with FROS spacing (section 2.3.5). This observation is in accordance with data presented in Petrova et al. (2013). Although condensation rates had not been analyzed in this publication, estimates can be deduced from fig. 2. Different hypotheses can explain the observation that condensation rates appear faster at larger FROS spacings. Although integration of FROS arrays could, in principle, influence genes involved in chromosome condensation, this possibility is unlikely. Nevertheless, this can be tested, if correlation between condensation rate and FROS spacing persists for same spacings on different chromosomes. Even though anaphase onset timing is probably underestimated for the strain with larger spacing between centromere and centromere-proximal FROS, this should not affect the condensation rate.

The most likely hypothesis to explain the FROS spacing and condensation rate dependence is that the global chromosome condensation rate is constant, irrespective of FROS spacing, but only appears slow for close FROS spacing. Interphase chromatin can be seen as the substrate for the condensation reaction catalyzed by condensin and topoisomerase II. In this sense, condensed chromatin would be the reaction's product and euclidean distance between FROS labels would scale with substrate concentration. The lower rates could be explained as less substrate - meaning fewer condensin binding sites - between close FROS than between distant FROS. Fewer condensin binding sites would mean fewer substrate and accordingly less activity. This model has important premisses and implications, which I elaborate on in section 3.4.3.

To confirm the dependence between spacing and condensation rate, rates for more FROS positions and distances should be quantified. When measuring condensation for different FROS spacings, confinement of the chromatin fiber by the nuclear envelope has to be considered. At more than 1.0 Mb spacing, nuclear diameter limits the distance between the two FROS (see Petrova et al. (2013), fig. 2 C). This implies that at spacings greater than 1.0 Mb, the chromatin structure is probably in a folded conformation before the onset of condensation. This fact will enhance the underestimation effect for average-based measurements of the condensation rate (see also fig. 2.28). Systematic quantification of condensation rates for different FROS spacings below 1.0 Mb should uncover the relation between condensation rates and genomic spacing. Another advantage of the relatively short 0.5–1.0 Mb spacings is that same spacings can be measured at different positions on all chromosomes. In the long run, implementation of a third chromosome locus label (e. g. λ phage repressor operator system, Lassadi et al. (2015)) will be helpful to test whether different chromosome regions share the same condensation features.

Comparison of average compaction rates with other DNA processing enzymes

In section 2.3.5, I determined, from whole population average measurements, chromosome condensation rates of about 1 $\mathrm{nm\,s^{-1}}$. For decondensation, the rate was even lower. Both activities appear rather slow compared to other enzymes with longitudinal DNA processing activity. For example, T4 DNA polymerase processes about 750 nt/min (McCarthy et al., 1976), which cor-

responds to about 60 $nm\,s^{-1}$. At low force load *in vitro*, the bacteriophage Φ29 portal motor can condense up to 100 bp/s (Smith et al., 2001), corresponding to approximately 34 $nm\,s^{-1}$. Two arguments support the notion that the measured population average values are underestimates. First, assuming random conformation of the chromatin fiber between FROS foci (section 2.3.7), only a small fraction of FROS distances will be close to contour length in a population of cells. Hence, in the majority of cells distance will not change as drastically during condensation as expected from condensation of an extended fiber. These cells therefore only contribute little to the slope of the average condensation curve, but rather skew the mean towards a lower condensation rate. Second, averaging data with unavoidable variance in temporal alignment will lower the condensation rate, as described in fig. 3.1. More precise condensation rate measurements could be made based on condensation data from single cells (section 3.4.2).

Quantification of chromosome decondensation *in vivo*

Chromosome decondensation, the resolution of mitotic chromosome structure into transcriptionally active, organized interphase chromatin, can be informative about the architecture of mitotic chromosomes. Yet, compared to condensation, the decondensation process is understudied. *X. laevis* egg extract-based *in vitro* systems have been established previously to quantify chromosome decondensation (Magalska et al., 2014). This system has been successfully applied to show ATP-dependence of decondensation and the involvement of RuvB-like helicases. Notably, Rvb1 and Rvb2 associate with condensin in fission yeast in a non-DNA dependent manner (Piazza et al., 2013, p. 105).
In section 2.3.4, I showed that the FROS-based CCA setup can also be used to quantify mitotic chromosome decondensation *in vivo* on the population level. I measured decondensation rates of around 0.2 $nm\,s^{-1}$. By these measurements, decondensation is about 5 times slower than condensation. One interpretation for the large difference in condensation and decondensation rates is that both processes are based on very different molecular mechanisms. Yet, the decondensation analysis strategy has to be improved, including the definition of the decondensation rate. For example, averaging the rate over the 0 s to 2000 s time period after anaphase onset, was set arbitrarily (see section 2.3.4). The rate underestimation problem due to imprecise temporal alignment, as previously described for condensation, also applies for decondensation (fig. 3.1). This means cells could decondense their chromosomes fast, but at very different time points after anaphase onset. To bypass all above mentioned limitations, chromosome decondensation rate measurements should be established at the single cell level. Implementation of foci tracking after anaphase onset will be key to distinguish between decondensation processes of the daughter cells.

3.4.2 Chromosome condensation measurements at the single cell level

Population average condensation curves have been useful to judge whether a mutant has condensation defects and to screen for condensation mutants. Nevertheless, the average of a population

might not reflect the biological process of condensation. To reveal the distance-time traces the CCA produces for a single cell, I observed chromosome condensation at a high temporal resolution. This made single cell data sets interpretable (section 2.3.7) and resulted in the first measurement of compaction between two loci during mitosis for live, single cells. The improved assay hence enables the analysis of cell-to-cell variability of chromosome condensation measurements.

All cells analyzed in the single-cell CCA compacted their chromosomes and loci were at approximately the equal distances in the condensed chromosome. This observation is in agreement with other sequence-specific stainings like FISH. Classical Giemsa staining of mitotic chromosomes show reproducible banding patterns.

In contrast, how chromosomes condensed was highly heterogeneous. In many cells, FROS distances briefly increased before they started to decrease. This had not been apparent from previous measurements in FROS-based condensation assays (Petrova et al., 2013; Vas et al., 2007). This observation might be interpreted as a structural rearrangement of chromatin in 'preparation' for condensation, which includes resolution of long-range interactions. For some cells, the data showed multiple waves of regular distance increase and decrease (oscillations) between FROS. Mechanical stress-induced expansion and compaction cycles have been observed in condensing chromosomes of human and indian muntjac cells (Liang et al., 2015a). Whether the same mechanism underlies Liang et al.'s and these observations remains to be determined.

Unexpectedly, in data sets where the condensation period was apparent, change of distance over time appeared constant, suggesting linear condensation kinetics. This is in disagreement to the sigmoid distance-time dependence observed in curves from average measurements. Understanding the kinetics of the condensation reaction *in vivo* can give important hints about the mechanism of the condensation machinery and will be helpful to interpret *in vitro* results. Yet, although condensation and SAC delay phases could often be inferred in the single cell data, an objective measurement of prophase start time point is missing. This could be established by determination of condensin import timing.

The discrepancies between single cell and measurement averages and shows that the single cell condensation assay is able to unravel an additional level of information for chromatin dynamics during cell division.

FROS-based chromosome condensation measurements have been simulated (Cheng et al., 2015). Neither linear dependence between distance and time nor decondensation-condensation cycles have been predicted in Cheng et al.'s model. Hence, this model is insufficient to describe chromosome condensation for fission yeast, demonstrating that our understanding of chromosome condensation is still limited.

A strategy to extract condensation kinetics from single cell measurements

It is clear that the interphase chromatin is highly folded, even before condensation, due to confinement by the nuclear envelope, a crowded environment and TADs. This has been described (Lieberman-Aiden et al., 2009; Mizuguchi et al., 2014; Phillips et al., 2009), but can also be

deduced from the FROS distance distribution. The distance distribution in G_2 for 1 Mb FROS spacing had a maximum distance of about 2.0 µm (fig. 2.28), which can hence be assumed as the longest extension of chromatin. The 11 nm fiber has a linear packaging density of about 0.125 nm/bp, the 30 nm fiber about 0.01 nm/bp (Phillips et al., 2009, pp. 293). According to these estimates, the contour length of 1 Mb as 11 nm fiber conformation is 125 µm and as 30 nm fiber is about 10 µm. Even in the 30 nm fiber conformation packaging, the contour length is approximately five times longer than the observed maximal distance. This proves the existence of a highly folded state of chromatin. The heterogeneity in chromatin folding just before condensation is likely the cause of the variety of compaction patterns observed. Yet, in cells in which the FROS distance is in the upper quintile of the G_2 distance distribution, the chromatin between FROS can be assumed to be in an extended conformation (with intact TADs) because FROS distance is not confined by the 3 µm diameter of the nucleus. Data sets from cells in which the FROS distance is greater than the upper quintile of the interphase distribution prior to condensation should be selected. From these, the condensation rate can be estimated by manual definition of the time span of condensation. The condensation rate can be estimated in these by the slope of a linear function fit. Comparing maximum condensation between different FROS spacings will be important to test whether the spacing-rate correlation holds true. This data can also be used to test whether condensation is indeed linear, by fitting linear, sigmoid or other functions and evaluating whether residuals are Gaussian-distributed. To get significant results, a further increase in temporal resolution might be necessary. This could be achieved by optimizing the microscopy setup even further. For example, a beam splitter in front of the camera could redirect both color channels to separate regions on the camera chip. This would enable simultaneous acquisition of both color channels and hence double the maximal acquisition frequency.

3.4.3 A model for formation of mitotic chromosomes

Analysis of average condensation curves led to the conclusion that the condensation rate is FROS-spacing dependent. This means that the more distant two loci are, the faster they converge during condensation. Single cell measurements suggest that the compaction is linear over time, indicating a constant condensation rate during the condensation process.
Different models are conceivable for the formation of mitotic chromosomes. Condensation could spread along the chromosome arm, either from the centromere or from the telomere (fig. 3.3 A and B). Alternatively, it is conceivable, that condensation initiates from 'seed'-loci that are randomly distributed along the chromosome arm (fig. 3.3 C) and proceeds from all 'seeds' simultaneously by spreading outwards. Assuming a constant condensation rate, these models make distinguishable predictions for the distance-time dependence of two different loci spacings arrangements, as shown in fig. 2.26. If condensation activity spread from the centromere towards the telomere, the short spacing were initially not affected by condensation, while the long spacing compacted (fig. 3.3 A). Only as the condensation activity moved further along the chromosome arm, short spacing loci converged (fig. 3.3 A, right). In the second model, the condensation

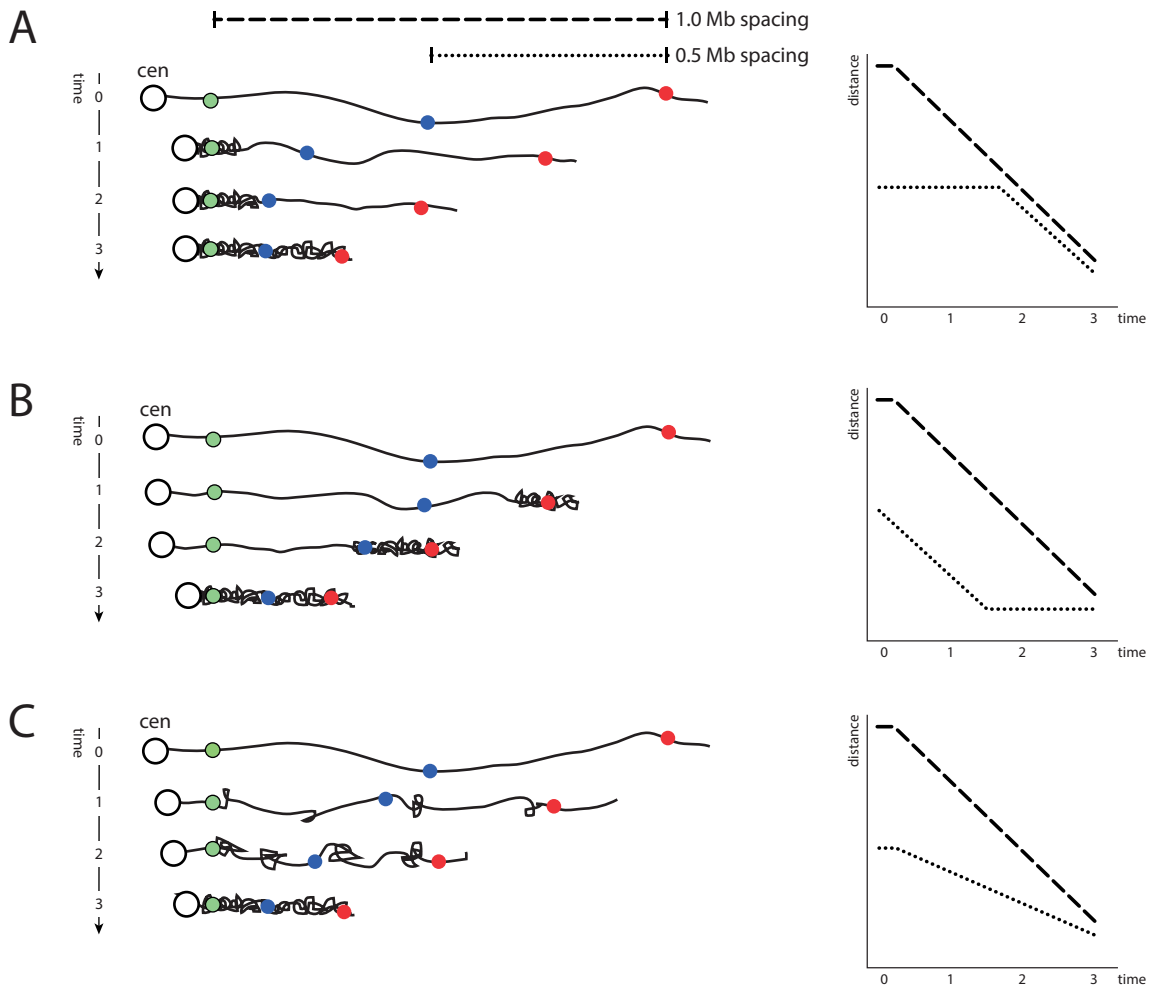

Figure 3.3: Different models of chromosome condensation and theoretical changes in FROS distance over time. (A) Condensation activity moving from centromere to telomere. (B) Condensation activity spreading from telomeres to centromeres. (C) Parallel model. Condensation activity is distributed along the chromosome arm during the whole condensation process.

activity moves from the telomere towards the centromere. In this case, both loci spacings compact at equal rate until the shorter spacing is fully compacted. The shorter spacing stays compact until compaction of the long spacing is complete (fig. 3.3 B, right). In both these models, the condensation rate is equal for both loci spacings. They only differ in the timing of the compaction period.

In contrast, in the third model the condensation activity is distributed along the chromosome arm during the whole condensation process. Because of the distribution, close loci converge at a lower rate than distant loci. This is in agreement with the observation of FROS spacing-dependent condensation rates. Hence, this model is favored over the other two models based on the data.

The distributed activity model implies the existence of condensation 'seeds' (i. e. condensation

activity islands), raising the question what the nature of an initial condensation 'seeds' is. It is conceivable that these are simply random association sites of condensin with chromatin. Their position could be random or determined by chromatin structures like TAD boundaries or certain DNA sequences. I speculate that these seeds later form the chromosome axis composed of condensin and topoisomerase II in metaphase chromosomes. In *zas1* mutants, Cnd1 levels are reduced, and therefore the number of functional condensin complexes is lower. The reduced number of chromatin associating condensin complexes could correspond to a reduced number of condensation 'seeds'. This serves as a possible explanation for the lower compaction rate observed in *zas1* ts mutants (fig. 2.3).
Further studies should try to evaluate this condensation 'seed' model and attempt to characterize mean distances between the seeds, condensation activity per seed and ultimately their molecular identity.

3.5 pFRs and non-recombining operator arrays

Currently, the main limitation of the FROS-based condensation assay are segmentation errors. If one of the fluorescent foci is not recognized or segmented incorrectly, no distance can be measured. I therefore improved the signal-to-background ratio of the tet FROS by implementing nr-tetO arrays and integration plasmids for expression of fluorescent repressors (sections 2.4.1 and 2.4.2). It is apparent from the signal-to-background ratio distribution in established tetO arrays that, in a fraction of cells, the signal-to-background ratio is comparable to the signal-to-background ratio in cells without any tetO array (fig. 2.32). This observation indicates that the classical tetO arrays are unstable and recombine spontaneously in vegetatively growing cultures. During tetrad dissection, cells are singled out, corresponding to a sampling from the signal-to-background ratio distribution. Meiotic recombination during crossing might add to this effect.
In contrast, nr-tetO have a high, stable signal-to-background ratio even after crossing and are hence more suitable for segmentation. This is highly beneficial for high throughput applications such as automated screening for condensation mutants. Also for low throughput and single cell measurements, this new system has significant advantages: next to improved segmentation, lower light dosage is required to obtain comparable intensity values. It enables short exposure time, which speeds up image acquisition for higher temporal resolution and limits photobleaching and phototoxic effects. At established exposure levels, localization at sub-pixel resolution might also be more precise, because higher signals result in a lower fraction of camera noise.

3.5.1 A concept for measuring chromosome condensation for lethal mutations

The second advantage of the nr-tetO is their stability during meiosis, which makes new experiments conceivable.
One of the major limitations in chromosome condensation research is that integrity of the central

players condensin and topoisomerase II is required for cell division, and therefore cell proliferation. This makes it challenging to dissect the functions of the condensation machinery by studying mutants *in vivo*. Yet, these factors are not necessarily required for interphase viability. Combining tetrad analysis with imaging might result in a technique that could overcome this dilemma. A diploid strain homozygous for tetO and lacO arrays could be created, which is heterozygous for e. g. a condensin subunit deletion. If the fluorescent lacI and tetR genes are integrated in close proximity to this deletion, co-segregation of deletion and fluorescent signal can be assumed. Cells in which lacO, tetO and pFR integration loci have co-segregated should be easy to identify in the microscope by presence of fluorescent foci. Growth of the spores can be tracked in the microscope to observe the first mitosis after sporulation. FROS distance measurements could then be used to measure condensation in the mutant cells. The level of functional protein stemming from the intact allele needs be monitored, e. g. by blue fluorescent protein (BFP) fusion to ensure it is degraded by normal protein turnover before entry into the first cell division after meiosis. Still, this strategy might be an alternative to a degron system, which has not convincingly worked in *S. pombe* until now (section 2.1.6).

Chapter 4

Materials and Methods

4.1 Analysis, purification and manipulation of nucleic acids

4.1.1 Measurement of nucleic acid concentration by NanoDrop

The NanoDrop is a specialized spectrophotometer for rapid absorbance measurements of a liquid sample in a range of wavelengths from 200 - 500 nm. DNA has an absorption maximum at 260 nm and an extinction coefficient of about 50 µg per 1 OD_{600} (Mülhardt, 2009, p. 43). By measuring absorption at known length of light passage, the concentration of DNA can be calculated using Lambert-Beer law. Purity of DNA can be assessed by measuring light absorption at 280 nm, the wavelength at which proteins absorb. Nucleotides, RNA and ssDNA contribute to absorbance and can not be distinguished from dsDNA in these measurements.
The NanoDrop 2000 Spectrophotometer (Peqlab) was initialized by pipetting 2 µL H_2O onto the measurement pedestals, closing the lever and starting measurement. A negative control of 2 µL H_2O or TE was measured to correct for solvent absorbance. After blank measurement, absorbance of 2-3 µL sample were measured. Pedestals were cleaned with a Kimtech Science precision wipe tissue (Kimberly-Clark, KC 7552) between measurements. Values lower than 1 ng/µL were considered noise.

4.1.2 Measurement of dsDNA concentration using Qubit

The Qubit (Thermo Fisher Q33216) is a fluorometer for precise measurement of dsDNA concentrations. The solution of interest is mixed with a dye which becomes fluorescent upon specific binding to dsDNA. dsDNA binding dye and two standard solutions with known DNA concentration were equilibrated to room temperature for 20 min. Dye mix was prepared by adding 199 µL buffer to 1 µL dye and vortexing. In thin-walled, low fluorescent 500 µL tubes, 10 µL of each standard were diluted in 190 µL dye mix. For the samples, 1 µL was diluted in 199 µL dye mix. All dilutions were vortexed and incubated for 3 min at room temperature. The Qubit fluorometer was calibrated by first measuring both standard solutions. Finally, dsDNA concentration was determined by measuring fluorescence of the samples.

4.1.3 Agarose gel electrophoresis

For analytical and preparative DNA electrophoresis, 0.8 % agarose was prepared by dissolving 2.5 g Agarose (Sigma Aldrich, A9539-500G) in 300 mL 1 × TAE buffer (section 4.9.1) by heating the mixture in a microwave to its boiling point. 50 mL of the solution were mixed with in a 100 mL beaker with 2.5 µL SYBR safe DNA gel stain (Invitrogen, S33102) or 1.5 µL

Midori Green Advance stain (Bulldog Bio, MG04). The mixture was poured into a gel chamber (Peqlab) containing a comb and left for solidification at room temperature or placed in a fridge. After the gel was solid, the gel chamber was filled with 1 × TAE buffer. Alternatively, gels could be stored over night in the fridge wrapped with cling wrap. DNA samples were prepared for loading by mixing with 6 × loading dye (section 4.9.1). From PCRs, 5 µL product were used, analytical restriction digests were loaded completely (10 µL). In one lane, 5 µL 1 kB ladder (NEB, N2323, see section 4.9.1) were loaded as a standard for DNA fragment size. Gels were generally run at 220 V for 10 to 20 min depending on the size of the DNA fragment of interest or until the fragment of interest was resolved.

4.1.4 Analytical restriction digest

Analytical restriction digests were used to check for plasmids for correct sequence, e. g. after plasmid manipulation (e. g. restriction cloning, PCR-based manipulations), transformation into *E. coli* and miniprep (section 4.1.9). The amount of water was adjusted according to the amount of plasmid. Usually 200-800 ng plasmid were digested using this protocol. The reaction components were mixed in 200 µL tubes as in table and incubated at 37 °C for 20 min or longer and subsequently analyzed by agarose gel electrophoresis (section 4.1.3). Reaction buffer was chosen based on the restriction enzymes at `www.neb.com`.

Component	Volume	
10 × reaction buffer	1	µL
DNA	300	ng
Restriction enzyme	0.5	µL
H_2O	a 10	µL

Table 4.1: Mix for analytical restriction digest reaction

4.1.5 Sanger DNA sequencing

Sanger sequencing of plasmid regions or PCR products were performed by GATC. Per sequencing primer, up to 1 kb reads were expected. 20 µL of template at a concentrations of 30 - 100 ng/µL were sent in 1.5 mL reaction tubes along with 20 µL primer solution at 10 pmol/µL (2 µL primer stock solution plus 18 µL H_2O). Sequencing reactions were defined and orders were placed online at `https://www.mygatc.com/`. Chromatogram sequencing results were downloaded as .ab1 files and analyzed in SnapGene software.

4.1.6 Colony PCR

Colony PCR was used to screen large numbers of *E. coli* or *S. pombe* colonies for the desired construct after plasmid or genome manipulation. For reaction mixes, Qiagen TopTaq kit (200205) was used as described in the manufacturer's manual. Because colony PCR frequently gave false positive bands, a negative control (*E. coli* or *S. pombe* colony material without the manipulation). As little as possible material was taken from each colony. Colony PCR mix is described in table 4.2, a typical thermocycler program is described in table 4.3. Annealing temperature was adjusted based on the primer sequence (calculated by SnapGene software), elongation time was adjusted to 1 min per kb. Primers were chosen such that the expected

product was between 500 bp and 2.5 kb long. Reaction products were analyzed by agarose gel electrophoresis (section 4.1.3).

Component	Volume (µL)
H_2O	6.4
10 × TopTaq Buffer	2
dNTP mix 2 mM (Thermo Fisher, R0241)	1.4
10 × Coral dye	2
5 × Q Solution	4
Primer fw 5 mM	1
Primer rev 5 mM	1
Colony material	pipet tip
TopTaq Polymerase	0.2

Table 4.2: Components of a colony-PCR mix

Step	Temperature (°C)	Time (min)	
Initial denaturation	94	4:00	
Denaturation	94	0:30	35 cycles
Annealing	adjusted to primer	0:20	35 cycles
Elongation	72	1:00 per kB	35 cycles
Final Elongation	72	2:00	
Cooling	4	∞	

Table 4.3: Colony-PCR thermocycler program

4.1.7 DNA purification from reaction mixes

To purify DNA from PCR reactions or preparative restriction digests, the Qiagen PCR purification kit (28104) was used according to the manufacturer's instruction with the following modifications. The reaction-PB buffer mixture was applied to a spin column and centrifuged at 19750 × g for 10 s. The flow through was discarded and the column was washed with 750 µL buffer PE, at 19750 × g for 10 s. Again, the flow through was discarded and the column was dried by centrifugation at 20000 × g for 30 s. 22 µL H_2O were added to the silica membrane and after incubation for 1 min at room temperature, DNA was eluted by centrifugation. DNA concentration in the eluate was determined using a Nanodrop (section 4.1.1).

4.1.8 Purification of DNA fragments by gel elution

Gel elution was performed with the Qiagen QIAquick gel extraction Kit (28704) following the manufacturer's instructions.

4.1.9 Plasmid purification from *E. coli* (miniprep)

For small scale plasmid preparation from *E. coli*, the QIAGEN Miniprep Kit (12123) was used following the manual's instructions with the following modifications. 2 mL of over night culture were spun down at 21000 × *g* for 5 s. For low copy plasmids, supernatant was discarded and another 2 mL of over night culture were added and spun down. Centrifugation of denatured proteins in neutralized lysate was performed for 3:30 min at 21000 × *g*. Subsequent centrifugation steps were performed for 30 s at 17500 × *g*. DNA was eluted in 22 µL H_2O. For miniprep buffer components see 4.9.7. Depending on size and origin on the plasmid to purify, the yield was in the range 0.1-1 µg/µL as measured by Nanodrop (section 4.1.1). In principle, the silica membrane columns can be reused (Siddappa et al., 2007).

4.1.10 Preparation of genomic DNA from *S. pombe*

S. pombe cells were grown over night in 5 mL of the appropriate growth medium. 4 mL of the culture were spun down at 2200 × *g* and resuspended in 400 µL SCE buffer (section 4.11.12) complemented with 10 µL 10 mg/mL Zymolase T-100 solution (SEIKAGAKU, 120493), 8 µL 10 mg/mL RNase A (ROCHE, 10109169) and 3.2 µL 2- mercaptoethanol. After incubation for 30 min at 37 °C, completion of digestion was checked by microscopy of cells diluted in 1:1 in 10 % SDS. 400 µL SDS lysis buffer (section 4.11.12) were added and the suspension was incubated at 65 °C for 5 min. 400 µL 5 M KAc were added and the suspension was centrifuged for 10 min at 20000 × *g*. The supernatant was transferred to a new 2 mL reaction tube and centrifuged for 3 min at 20000 × *g*, to pellet residual precipitated material. 525 µL of supernatant were added to 1.2 mL abs. Ethanol (EtOH) and spun again for 10 min at 20000 × *g*. After washing with 1 mL 70 % EtOH, the pellet was air-dried for 10 min and then solved in 50 µL H_2O at room temperature for 10-30 min.

4.1.11 Phenol/Chloroform extraction of RNA from *S. pombe*

diethylpyrocarbonate (DEPC) water was prepared by adding 0.1 % DEPC to H_2O and incubating for at least 1 h at 37 °C and subsequent autoclaving or heating to 100 °C for at least 15 min to inactivate DEPC. A 25mL culture of *S. pombe* cells were grown to OD_{600} 0.2 – 0.3 and cells were harvested by centrifugation for 2 min at 2200 × *g*. The supernatant was discarded and the pellet was snap frozen in liquid N_2. Cells could be stored at -80 °C if desired. The pellet was thawed on ice for about 5 min and resuspended in 1.5 mL ice-chilled DEPC-treated H_2O. The suspension was transferred to a 2 mL reaction tube and centrifuged for 30 s at 2200 × *g* to wash the cells. The cell pellet was resuspended in 750 µL TE buffer (section 4.11.11) and 750 µL phenol/chloroform/isoamylalcohol mixture (ROTH A156.2) were added and vortexed immediately to rapidly deactivate as many proteins (including RNases) as possible. To keep incubation time short in this critical step, not more than 6 samples were processed at a time. The emulsion was incubated at 65 °C under a fume hood for 1 h. Each tube was vortexed for 10 s every 10 min. During incubation time, 1.5 mL of 100% EtOH with 50 µL 3 M NaAc (pH 5.3) were prepared in one 2 mL reaction tube for each sample.
The phenol/chloroform/isoamylalcohol/water emulsions were placed on ice for 1 min and vortexed for 20 s before centrifugation for 15 min at 21000 × *g* at 4 °C to separate phenol and water phases. 700 µL of the water phase (top) were added to 700 µL phenol/chloroform/isoamylalcohol mixture, mixed thoroughly by inverting (no vortexing) and centrifuged for 5 min at 14000 × *g* and 4 °C. This step was repeated. 500 µL of water phase were added to the EtOH/NaAc solution. The mixture was vortexes for 10 s and subsequently nucleic acids were precipitated by incubating the sample at -80 °C for 30 min or -20 °C over night. Precipitated nucleic acids

were pelleted for 10 min at 21000 × *g* at room temperature (RT). Supernatant was discarded and 500 µL of 70 % EtOH (made with DEPC water) were added. The sample was mixed by pipetting and spun for 1 min without changing tube orientation in the centrifuge. Supernatant was removed and the sample was briefly centrifuged, followed by removal of residual liquid using a P200 pipette. The pellet was air dried for 5 min at RT on the bench with open reaction tube lid. 100 µL DEPC water were added to the pellet and incubated at 65 °C for 1 min. The pellet was dissolved by gently pipetting up and down (about 30 times) until no particles were left. The concentration was measured by Nanodrop (section 4.1.1) with expectancy value of about 2 µg/µL. Most of the RNA was ribosomal.

4.1.12 PCR with proofreading polymerases

PCR is a method for *in vitro* synthesis, manipulation and analysis of DNA (Mullis and Faloona, 1987). PCR with proofreading polymerases was performed for amplification of DNA for cloning, sequencing or PCR targeting (section 4.5.5) purposes. Proofreading polymerases have a significantly higher fidelity (lower mutation rate) than non-proofreading polymerases like *Thermus aquaticus* DNA polymerase. Two different proofreading polymerases were used in this work.

Phusion polymerase

A major limitation of most proofreading polymerases like Pfu1 is their low processivity. Phusion polymerase (Thermo Fisher F531L) is a commercially available fusion protein between Pfu DNA polymerase and the SSo7d domain. The SSo7d is a DNA binding domain that strongly enhances the processivity of the polymerase.

X7 polymerase

X7 polymerase (available from the Protein expression and purification facility at EMBL) is a combination of a Pfu V93Q mutant and a highly processive Pfu-SSo7d fusion polymerase (Phusion). Pfu-SS07d is commercially available as Phusion polymerase. The Pfu V93Q mutant is able to incorporate dUTP primers with high efficiency, making it suitable for uracil based cloning (Nørholm, 2010). An alternative reaction buffer for X7 polymerase is listed in section 4.9.

Component	Volume (µL)
H_2O	29.8
Phusion Buffer HF 5x	10
dNTPs (2 mM)	5
Forward primer (5 mM)	2
Reverse primer (5 mM)	2
Plasmid DNA 10 ng/µL	1
Phusion	0.2

Table 4.4: PCR mix for plasmid template reactions

When using plasmid DNA as template, reaction mixes were prepared as described in table 4.4. When using genomic DNA as template, reaction mixes were prepared as described in table 4.5. The dNTP mix used throughout the thesis is from Thermo Fisher (R0241).

Component	Volume (µL)
H_2O	27.8
Phusion Buffer HF 5x	10
dNTPs 2 mM	5
Primer fw 5 mM	3
Primer rev 5 mM	3
genomic DNA 100 ng/µL	1
Phusion	0.2

Table 4.5: Mix for PCR with genomic templates

Reactions were incubated in a PTC-200 DNA Engine Thermocycler (BioRad). The thermocycler program was adjusted in annealing temperature and elongation time depending on primers and length of the amplicon for each reaction. Due to the presence of the dsDNA binding domain, primer annealing efficiency was increased, making higher annealing temperatures feasible. When using Phusion or X7, annealing temperatures were calculated using the NEB Tm calculator (`http://tmcalculator.neb.com/`). The general thermocycler program is listed in table 4.6. PCR products were analyzed by agarose gel electrophoresis (section 4.1.3).

Step	Temperature (°C)	Time (min)	
Initial denaturation	98	2:00	
Denaturation	98	0:30	35 cycles
Annealing	primer	0:20	35 cycles
Elongation	72	0:30 per kB	35 cycles
Final Elongation	72	2:00	
Cooling	4	∞	

Table 4.6: General thermocycler program

4.1.13 cDNA synthesis

cDNA was synthesized using Maxima reverse transcriptase (Thermo Scientific, EP0741), an engineered M-MuLV reverse transcriptase variant according to the manufacturer's instructions. Total RNA was prepared from a *S. pombe* 972 h^- strain (database strain *28*) as described in section 4.1.11. 1 µL of 2.5 µg/µL total RNA extract solution were mixed with 4.5 µL H_2O, 5 µL 2 mM dNTP mix and 2 µL 10 mM reverse primer. The mixture was centrifuged briefly and incubated at 65 °C for 5 min to denature potential secondary structures in the RNA template. RT-buffer, RNase inhibitor and reverse transcriptase were added and the reaction was incubated for 30 min at 50 °C. The reaction was terminated for 5 min at 85 °C. 1 µL of RT reaction was used as template in a subsequent Phusion PCR amplification reaction (section 4.1.12). table 4.7 lists an overview for the RT-PCR of Zas1.

Component	Volume (µL)
H_2O	4.5
total RNA (2.5 µg / µL)	1
dNTPs 2 mM	5
Primer 16 rev 10 mM	2
Mix, centrifuge and incubate at 65 °C for 5 min	
5 x RT-Buffer	4
RNase Inhibitor	0.5
Maxima RT	1

Table 4.7: Components of RT-PCR reaction with Maxima reverse transcriptase kit)

4.1.14 Site directed mutagenesis PCR on plasmid templates

Mutagenesis PCR is a fast and efficient method for insertions, deletions and mutations of 1-6 nt. The sequence to be mutagenized was cloned into a circular plasmid (e. g. by restrictionCloning) containing an *E. coli* origin of replication (ori) and an *E. coli* resistance marker gene, e. g. amp^r encoding β-lactamase. Primers were designed to bind to the region of mutagenesis and contained the mutations of interest. 10-15 nt annealed 5' of the mutation and 20-25 nt annealed 3' of the mutation. Primers were designed for both forward and reverse complement. 2-5 ng of plasmid were used as template for a PCR with both mutagenesis primers. If a band of expected size was visible in agarose gel electrophoresis (section 4.1.3), 5-10 µL PCR mix were directly used for chemical transformation into *E. coli* (section 4.2.2). Four to six colonies were selected and used to inoculate 3 mL cultures. The next day, plasmids were prepared from these cultures (section 4.1.9) and sent for sequencing. In most cases one or more plasmids carried the desired mutation.

4.1.15 RF cloning

Restriction free (RF) cloning was performed as described in van den Ent and Löwe (2006), with Phusion or X7 polymerase (section 4.1.12). 0.2-1 µL were transformed into *E. coli* by electroporation (section 4.2.4).

4.1.16 Restriction-ligation cloning

Preparative restriction digest

For cloning, 2 µg of plasmid were digested and usually yielded around 70-80 ng/µL in 20 µL after purification with the QIAquick reaction cleanup kit (section 4.1.7). To isolate backbone from insert, gel elution was performed (section 4.1.8), which yielded significantly less DNA. To prepare linearized plasmid for transformation of *S. pombe*, up to 5 µg plasmid were digested. Reactions were incubated longer than 3 h or over night. Reaction buffer and incubation temperature were chosen based on the restriction enzymes at `www.neb.com`. The components for each reaction are listed in table 4.8.

Component	Volume	
10 × reaction buffer	5	µL
DNA	> 2	µg
Restriction enzyme	1	µL
H_2O ad	50	µL

Table 4.8: Reaction mix from preparative restriction digests.

DNA 5' end dephosphorylation

For some cloning purposes it was desirable to dephosphorylate the 5' ends of plasmid backbone fragments (ori and antibiotic resistance) after restriction digest to reduce background colonies from plasmid recirculation during ligation. 10 × Antarctic Phosphatase Buffer was added to the restriction digest to 1 × dilution and 1 µL Antarctic phosphatase (NEB, M0289) were added per 50 µL reaction. The mixture was incubated at 37 °C for 20 min and subsequently heat inactivated at 65 °C for 10 min. Incubating the dephosphorylation reaction over night at 37 °C reduced the number of colonies dramatically.

Production of inserts from PCR products

For the creation of most plasmid constructs, inserts were PCR amplified to create compatible restriction site ends. Primers were designed to amplify the desired insert sequence. 5' ends of the primers contained 5 nt dubious sequence followed by the restriction site. After PCR amplification (section 4.1.12), product size was verified by agarose gel electrophoresis (section 4.1.3). If the PCR product had been amplified from a plasmid, the PCR mix was incubated with DpnI at 37 °C for >1 h. To produce compatible ends, the PCR products were incubated with the respective restriction enzyme(s). Restriction enzymes which are active in Phusion buffer[1], were directly added to the PCR product. To digest with restriction enzymes not active in Phusion buffer, PCR product was purified (section 4.1.7) and then digested in under the optimal buffer conditions (section 4.1.16). Before further processing, DNA was purified (section 4.1.7).

DNA ligation

Insert and plasmid backbone were prepared as described in sections 4.1.7 to 4.1.9 and 4.1.16 or the previous paragraph. A backbone to insert molar ration of 1:3 was calculated online using `http://www.insilico.uni-duesseldorf.de/Lig_Input.html` for 50 ng of plasmid backbone. The reaction components were mixed on ice as listed in table 4.9 and incubated for >3 h in the refrigerator (16 °C). To circularize linear plasmids, no insert as added. Ligation products were transformed into *E. coli* (sections 4.2.2 and 4.2.4) to individualize, amplify and select the desired plasmids.

4.1.17 Chromatin Immunoprecipitation

The ChIP protocol is based on Sutani et al. (2015) with modifications.

[1] As listed on the NEB website: `https://www.neb.com/tools-and-resources/usage-guidelines/activity-of-restriction-enzymes-in-pcr-buffers`

Component	Amount	
10 × T4 reaction buffer	52	µL
Backbone DNA	50	ng
Insert DNA as calculated		
H_2O ad	20	µL
T4 DNA ligase	0.2	

Table 4.9: Components for T4 DNA ligation.

Crosslinking 200 mL tagged and untagged strain were cultured at 30 °C until an to OD_{600} 1.0 was reached. 22 mL (1/10th volume) of freshly prepared formaldehyde fixation solution (see section 4.9.8) were added and the culture was incubated for 10 min in a 26 °C shaking water bath. The reaction was stopped by addition of 22 mL 2.5 M glycine solution. The mixture was chilled on ice in the cold room for 30 min with occasional shaking. Cell suspension was transferred to five 50 mL tubes and pelleted at 1000 × *g* and 4 °C for 3 min. One pellet was resuspended in 1 mL ice cold ChIP buffer 1 (section 4.9.8) and the suspension was used to resuspend an additional pellet until all cells were combined. This suspension was transferred to a 2 mL tube. Cells were pelleted at 2200 × *g* for 2 min and washed with 1 mL ice cold ChIP buffer 1. This step was repeated with 1 mL ice cold buffer 1 containing 2 × cOmplete protease inhibitor (Sigma-Aldrich 11836170001 Roche) and 1 mM PMSF. Supernatant was discarded and the pellet was frozen in liquid N_2. Tubes were stored at -80 °C.

Cell disruption and chromatin shearing For each sample, 1.5 mL ChIP buffer 1 containing 2 × cOmplete and 1 mM PMSF (both added shortly before usage) were prepared and chilled on ice. Each pellet was resuspended in 250 µL ice cold ChIP buffer 1 with PMSF and cOmplete. The suspension was transferred to a 2 mL screw cap tube compatible with the tube adapter for MP FastPrep (see section 4.5.11). Cells were disrupted for five 60 s cycles at 6.5 m/s interrupted by 3 min cooling periods on ice. Samples were checked for efficient lysis in a transmission light microscope to ensure more than 80 % lysis. Lysate was collected as described in section 4.5.11. Pellet was resuspended in the supernatant and the suspension was transferred to a fresh 1.5 mL tube and kept on ice.
130 µL suspension were transferred to a microTUBE AFA tube (Covaris, 520045) and the microTUBE was placed in the sample holder (Covaris, 500114), which was inserted into a Covaris S220 sonicator. If water bath temperature was between 4 °C and 8 °C, chromatin was sheared by sonication at intensity 4, duty factor 10 % and 200 cycles per burst for 100 s. Sonicated suspension was transferred to a new tube and kept on ice. If sample volume exceeded 130 µL, the sonication procedure was repeated in the same microTUBE in 130 µL aliquots until the complete sample was processed. Sonicated sample was centrifuged for 15 min at 14000 × *g* and 4 °C to pellet cell wall fragments and debris. Supernatant was transferred to a fresh 1.5 mL tube.

Immunoprecipitation Protein concentration was measured in samples by adding 1 µL of sample to 1 mL Bradford reagent and diluting this mixture 1:1 with Bradford reagent. Usual protein concentration values were 20-40 mg/mL. All samples were diluted to 20 mg/mL or the lowest sample concentration. 10 µL of each sample were combined with Laemmli buffer (sec-

tion 4.9.2). For each condition, 25 µL were sampled and stored at -20 °C (Input sample). Equal sample volumes (e. g. 600 µL) were transferred to a fresh 1.5 mL tube and 1 µL V5 antibody solution (1 µg/µL, see table 4.13) were added to each sample. Tubes were placed in a rotary wheel in the cold room and incubated rotating at low speed for 1 h. 10 µL Dynabeads Protein G (ThermoFisher, 10003D) were added and the sample was kept rotating at low speed for 1 h. Sample tube was placed on a magnet so that beads accumulated. The supernatant (flow through sample) was transferred to a new tube. After aspiration the flow through, Dynabeads were immediately resuspended in 200 µL ice cold ChIP buffer 2 (section 4.9.8) to avoid drying. 25 µL of flow through sample were frozen at -20 °C to later monitor DNA fragmentation efficiency and fragment size. 10 µL were sampled and added to 23 µL Laemmli buffer to check protein levels by western blotting. Dynabead suspension was incubated for 5 min at low rotation, the tube was placed on a magnet for 1 min and supernatant was aspirated. 10 µL of supernatant were combined with Laemmli buffer. The wash was repeated with 1 mL ice cold buffer 2. After discarding the supernatant, beads were resuspended in 200 µL of ice cold ChIP buffer 3 (section 4.9.8) and incubated 5 min for washing. The wash was repeated with 1 mL ice cold ChIP buffer 3. Finally, beads were washed in 1 mL ice cold TE with a transfer to a new tube. Supernatant was aspirated completely and the Dynabeads were resuspended in 75 µL TES (section 4.9.8).

DNA recovery IP sample, input sample and flow through samples were filled up to a volume of 110 µL with TES and 3 µL RNase A solution (10 mg/mL, Roche) were added. Samples were incubated for 15 min at 37 °C to digest RNA. 3 µL Proteinase K solution (20 mg/mL) were added to each sample and incubated at 37 °C for an additional 30 min. SDS solution was added to a final concentration of 0.25 % and samples were incubated in a 65 °C oven over night. DNA was isolated using phenol-chloroform extraction. 0.1 sample volumes of 3 M Na-acetate (pH 7.0) and one sample volume phenol/chloroform/isoamlyalcohol (Roth) were added and an emulsion was created by vortexing for 30 s. The emulsion was incubated at 65 °C for 10 min. Phases were separated by centrifugation at 21000 × g for 5 min. The water phase was transferred to a fresh tube. If present, precipitated protein was pelleted at 21000 × g for 5 min. The supernatant was transferred to a fresh tube and mussel glycogen (Roche, 10901393001) was added to a final concentration of 0.125 µg/µL as co-precipitant. Mussel glycogen strongly increased the recovery of DNA. 2 sample volumes of 100 % EtOH were added and the sample was stored at -20 °C longer than 30 min to precipitate the DNA. The sample was centrifuged for 15 min at 4 °C and 21000 × g. The supernatant was aspirated and 1 mL 70 % EtOH were added to the tube to wash the DNA. The tube was centrifuged for 15 min at 4 °C and 21000 × g. The supernatant was aspirated and the sample was air-dried or dried in a vacuum centrifuge (Eppendorf Concentrator 5301). DNA pellets were resuspended in the desired volumes of H_2O (e. g. 6 for ChIP sample). DNA concentrations were determined by Qubit (section 4.1.2). DNA yield was in the 1-10 ng range.

4.1.18 Next generation sequencing Illumina library preparation from ChIP DNA

Library preparation was performed using the NEBNext ChIP-Seq Library preparation kit (NEB E6240L). The manufacturer's instructions were followed.

DNA purification steps Each library preparation step was usually followed by DNA purification step. For this, either reaction cleanup columns (Macherey Nagel 740609.10) or solid phase reversible immobilization (SPRI) beads (Beckmann Coulter A63880, DeAngelis

et al. (1995)) were used according to manufacturer's instructions. Mixes for tagged and untagged ChIP and input samples were calculated and mixed in a 96 well thermocycler plate row (Biorad HSP9601). With each processing step, samples were transferred to the next plate row.

End repair Sonicated DNA ends were repaired by mixing 5µL NEBNext End Repair Reaction buffer with the DNA sample and 1 µL NEBNext End Repair Enzyme Mix. The volume was adjusted to 50 with H_2O. The sample was mixed by pipetting and incubated in a thermocycler at 20 °C for 30 min. DNA was purified as described above and eluted in 44 µL.

deoxyadenosine (dA)-tailing Pure repaired end DNA was mixed with 5 µL 10 × NEBNext dA-tailing Reaction Buffer and 1 µL 3' to 5' end exonuclease deficient Klenow fragment. The mixture was incubated in a thermocycler for 30 min at 37 °C. DNA was purified as before and eluted in 19 µL H_2O.

Adaptor ligation Hairpin adaptor DNA oligos (containing uracil in the hairpin sequence) were ligated to the A-tailed DNA. The 19 µL DNA sample was mixed with 6 µL 5 × Quick Ligation Reaction Buffer, 1 µL 1.5 mM NEBNext hairpin adaptor and 4 µL T4 DNA ligase. The reaction was incubated for 15 min at 20 °C. To open the hairpin, 3 µL uracil-specific excision reagent (USER) enzyme mix were added and the reactions were mixed by pipetting and incubated for 15 min at 37 °C. DNA was purified and adapters were depleted by using the correct bead-mixture/sample ratio during SPRI bead purification. Efficient adaptor depletion is central to avoid adaptor amplification in the next PCR step. DNA was eluted in 23 .

Introduction of index sequences and amplification of adaptor ligated DNA by PCR 23 µL adaptor ligated sample DNA were mixed with 25 µL NEBNext High-Fidelity 2 × PCR Master Mix, 1 µL 25 mM universal PCR primer and 1 µL 25 mM respective index primers (NEBNext Multiplex Oligos Set 1 NEB, E7335L). Thermocycler program was run as described in table 4.10. PCR product was purified as described above and eluted in 20 µL H_2O.

Step	Temperature (°C)	Time (min)	
Initial denaturation	98	0:30	
Denaturation	98	0:10	35 cycles
Annealing	65	0:30	
Elongation	72	0:30	
Final Extension	72	5:00	
Cooling	4	∞	

Table 4.10: ChIP seq library amplification thermocycler program

Depletion of primer dimers selection of DNA fragment size by gel elution To deplete primer dimers and select for the desired fragment size of 200 bp, the PCR-amplified library was gel-eluted from an agarose e-gel system (Thermo Fisher G6500, G6512) according to the manufacturer's instructions.

NGS sequencing The library was single end sequenced on an Illumina HiSeq2500 machine ('Ken') for 50 cycles by the EMBL Genomics Core facility.

4.2 *E. coli* methods

4.2.1 Preparation of chemical competent *E. coli*

Before cell handling, a shaking incubator was booked and pre-cooled to 18 °C. 250 mL centrifuge bottles and a 2.8 L Erlenmeyer flask were autoclaved. 200 mL transformation buffer per liter *E. coli* culture were prepared as described in section 4.10.1. PIPES buffer looses buffering capacity over time, hence transformation buffer pH was verified before usage. The *E. coli* strain of interest (e. g. $DH5_\alpha$, see table 4.14) were streaked for single colonies on an LB agar plate (section 4.10.4) containing appropriate antibiotics and incubated at 37 °C over night (e. g. XL1 blue: tetracycline, Rosetta pLys: Chloramphenicol). The next day, 5 mL starting culture were inoculated from a single colony and grown at 37 °C over night.10 mL of 1 M $MgCl_2$ solution were added to 1 L LB medium (section 4.10.2) appropriate containing antibiotics and transferred to a 2.8 L Erlenmeyer flask. This medium was inoculated with 3-4 mL starting culture. *E. coli* were cultured at 18 °C and 200 rpm to an OD_{600} of 0.2-0.4. The doubling time of $DH5_\alpha$ cells under these conditions is about 5-6 h.
Before pelleting the cells, rotor JLA16.25 or (Beckmann), the centrifuge and centrifuge bottles were chilled to 4 °C, as well as 200 mL transformation buffer per L culture. Liquid N_2 was filled in a Dewar flask (KGW Isotherm 26 B).
All steps were performed in the cold room and on ice from here on. The culture was transferred to centrifuge bottles and cells were pelleted at 4500 × *g* for 10 min at 4 °C. The supernatant was decanted and the cell pellet was resuspended in 160 mL cold transformation buffer per L culture. The suspension was transferred to 50 mL tubes in 40 mL aliquots and cells were pelleted again at 4500 × *g* for 10 min at 4 °C. The pellet was resuspended in 10 mL transformation buffer per tube and pooled in one 50 mL tube. 3 mL of room temperature dimethyl sulfoxide (DMSO) were added and the suspension was mixed well. The suspension was aliquoted á 200 µL in 1.5 mL tubes and immediately snap-frozen in liquid N_2. Cells were stored at -80 °C up to one year. Competency was checked by transforming different plasmid concentrations. Transformation efficiency should reach 100 colonies of $DH5_\alpha$ at 10 pg pUC plasmid and about 100 colonies of BL21 at 1 µg of pUC plasmid. In addition, untransformed cells were streaked out on ampicillin, kanamycin and chloramphenicol LB agar plates to exclude background resistance.

4.2.2 Transformation of chemical competent *E. coli*

Competent cells were taken from the −80 °C freezer and thawed on ice for about 10 min. DNA was added, in case of ligation the whole reaction volume was added, in case of retransformations 10 ng of plasmid were sufficient. Cells were mixed carefully to disperse DNA and incubated another 10 min on ice. Cells were heat shocked for 2 min at 42 °C and the suspension was immediately returned to ice for 2 min. 1 mL of LB medium was added and the cells were incubated at 37 °C for 30 min and 500 rpm. In case of transformation of a ligation reaction (section 4.1.16), cells were pelleted for 1 min at 6000 × *g*. 1 mL of supernatant was aspirated and the cells were resuspended in the remaining 200 µL. 2 µL, 20 µL and 188 µL, were spread on agar plates containing appropriate selection antibiotics using glass beads section 4.2.5. In case of retransformations, 2 µL of the cell suspension were spread on a selective agar plate.

4.2.3 Preparation of electrocompetent *E. coli*

The strain of interest (e. g. DH5α, Rosetta pLys) was streaked out from -80 °C glycerol stock on a LB agar plate containing appropriate antibiotics. After over night incubation at 37 °C

30 mL pre-culture was inoculated from a single colony and incubated over night. 2 L LB were pre-warmed to 37 °C.
The next day, two 1 L main cultures of LB were inoculated with 15 mL pre-culture and grown at 37 °C, 120 rpm until OD_{600} 0.5 to 0.8 was reached. This step took about 2 hours for DH5 α, depending on pre-culture density. All of the following steps were carried out in the cold room. Cultures were transferred to 500 mL centrifuge bottles and incubated on ice for 20 min. Cells were pelleted for 10 min at 4800 × *g* and 4 °C. Each pellet was washed with 150 mL H_2O. Resuspension was facilitated using a blue inoculation loop. Cells were pelleted again for 10 min at 4800 × *g* and 4 °C. Pellets were resuspended in 100 mL and suspensions of two pellets were combined. Cells were pelleted as before. Each pellet was washed with 15 1 mL0% glycerol and transferred to a 50 mL tube. Cells were pelleted at 4800 × *g* for 12 minat 4 °C. Finally, each pellet was resuspended in 3 mL 10 % glycerol and all suspensions were pooled. Empty tubes were rinsed with 1 mL 10% glycerol. 50 µL aliquots were made and frozen in liquid N_2. Cells were stored at -80 °C.

4.2.4 Electroporation of *E. coli*

50 µL electrocompetent *E. coli* were thawed on ice and 1 pg of plasmid or 1-1.5 µL of ligation reaction were added to the suspension. Electroporation cuvettes were cooled on ice, SOC medium was pre-warmed to 37 °C. The cell suspension DNA mixture was transferred to the electroporation cuvette and the cuvette was beat on the table to eliminate bubbles in the mixture. To prevent short circuit the cuvettes electrodes were dried from the outside by paper tissue and placed in the electroporator (Biorad). Electroporation was performed at 400 Ω, 25 µF and 2.5 kV (maximum). A time constant between 7 and 10 indicated successful electroporation. Cells in the cuvette were immediately resuspended by adding 1 mL 37 °C warm LB medium and placed in a thermo block for 20-30 min and shaken at 700 rpm. Finally, 2 µL, 20 µL and 200 µL were plated on respective selection agar plates with glass beads (section 4.2.5). In case of short circuit, salt concentration was too high. Electroporation was more efficient than chemical transformation.

4.2.5 Regeneration of glass beads used for plating

Plating glass beads (Merck Millipore 71013) were used to spread *E. coli* and *S. pombe* cells on agar plates. After spreading, beads were collected in a beaker containing 70 % EtOH. Beads were reusable and could be regenerated as follows. Beads were soaked in 1 M NaOH for 20 min. Subsequently beads were rinsed with tap water, drained and rinsed with ddH_2O. A 800 mL-beaker was filled with the glass beads and water and sonicated in in a water bath sonicator for 10 min. In the water bath, water bath level was equal or higher than water level in beaker. Beads were washed with once abs. EtOH and spread on a tissue to dry. Finally, beads were aliquoted in 250 mL Schott flasks using a funnel and autoclaved.

4.2.6 Recombinant protein expression in *E. coli*

T7 promoter based protein expression

Rosetta pLys or Arctic Express (table 4.14) were transformed with 500 ng expression plasmid containing the ORF of interest. Both chemical transformation (section 4.2.2) and electroporation (section 4.2.4) could be used. All cells were plated on appropriate selection medium. The

next day, all colonies were resuspended in 5 mL LB medium containing the appropriate antibiotics. A 100 mL culture was inoculated with these 5 mL and grown at 37 °C till OD_{600} 0.5. 1 L of pre-warmed 2 ×YT (section 4.10.3) was inoculated with the 100 mL culture and grown to OD_{600} 0.4 at 37 °C. The culture was shifted to induction temperature for 30 min before inducing expression by addition of isopropyl β-D-1-thiogalactopyranoside (IPTG) to a final concentration of 0.2 mM. Typical expression times are 37 °C for 1-3 h, 30 °C for 2-4 h or 18 °C over night. Cells were centrifuged and pellet was resuspended in lysis buffer, depending on tag and purification strategy, chicken chicken chicken (Zongker, 2006) and snap-frozen in liquid N_2.

4.3 Protein expression in Sf21 cells

4.3.1 Sf21 cells culture maintenance

Sf21 cell cultures were maintained as described in Piazza (2013).

4.3.2 Baculovirus creation

Construct creation

Zas1 cDNA sequence was cloned into pFastBac HTb (plasmid 3) in frame with the N-terminal His_6-TEV tag via BamHI and NotI (plasmid 2341).

Transposition into Bacmid

10 ng of pFastBac plasmid were mixed with 50 µL electro-competent DH10MultiBac^{Turbo} EmBacY *E. coli* cells and incubated on ice for 15 min. The cells were transformed using electroporation (4.2.4). Subsequently, cells were incubated at 37 °C over night in LB shaking culture. The next day, cells were plated on ampicillin (100 µg/mL), gentamycin (7 µg/mL), IPTG (40 µg/mL), kanamycin (50 µg/mL) and X-Gal (100 µg/mL) plates. Recombined clones were selected.

Bacmid purification

Bacmid was purified as described in Bieniossek et al. (2008). A single clone containing composite bacmid was inoculated into 5 mL LB medium containing kanamycin and grown over night at 37 °C. Cells were pelleted for 5 min at 8000 × *g* and the supernatant was aspirated. Bacmid DNA was isolated by, generic alkaline lysis protocols (as described in section 4.1.9). 800 µL of alkaline lysis supernatant were added to 800 µL isopropanol to precipitate DNA. The sample was centrifuged for 15 min at 4 °C. The pellet was washed two times with 70 % EtOH. Composite bacmid was resuspended in 35 µL H_2O. The last step was performed in a sterile hood. At the point of isopropanol precipitation, the composite bacmid could be stored indefinitely at -20°C. Successful transposition was checked by PCR using primers IP60 (`5' GTTTTCCCAGTCACGA`) and IP61 (`5' CAGGAAACAGCTATGAC`), which amplified the integrated region.

Generation of baculovirus

Baculovirus was created as described in Piazza (2013, pp. 113).

4.4 Methods for purification and analysis of proteins

4.4.1 His_6-Zas1 NiNTA Protein purification from insect cells

Cell lysis. Frozen insect cell pellet was resuspended in 35 mL lysis buffer (50 mM Tris pH 7.5, 500 mM NaCl, 5 mM 2- mercaptoethanol, 25 mM imidazole, 2 × cOmplete protease inhibitor and 1 mM PMSF) in a 50 mL tube. 2- mercaptoethanol was used because DTT strongly chelates Ni^{2+} ions. The suspension was sonicated for 3 cycles for 45 s on ice using a Branson Sonifier 250 (output approx. 5) with 45 s cooling intervals to disrupt cells and shear genomic DNA. The lysate was transferred to a round bottom tube and spun for 30 min in rotor JA 25.50 at 20000 × g and 4 °C. During centrifugation, 0.3 mL Ni-Sepharose 6 FastFlow (GE 11-0008-87 AE) per 100 mL cell culture were transferred to a 50 mL tube and washed with 50 mL H_2O.

Binding. From here on, all centrifugation steps were carried out at 1200 × g for 3 min and at 4 °C. 100 µL lysate supernatant were taken as input sample, the residual supernatant was added to the Ni-Sepharose and incubated for 1 h on a rotation wheel in the cold room to allow binding of His-tagged protein to the immobilized Ni^{2+} ions. Ni-Sepharose beads were collected by centrifugation. A sample of supernatant was saved as flow through fraction sample for later SDS-PAGE analysis, the rest was discarded.

Washing. The Ni-Sepharose bead pellet was resuspended in 10 mL lysis buffer, transferred to a 15 mL tube and washed for 10 min on shaking wheel in the cold room. Washing was repeated at least 3 more times with lysis buffer, taking a sample from each wash fraction.

Elution. Elution was performed by adding 3 mL elution buffer (lysis buffer with 250 mM imidazole, pH 8.2) to the pelleted beads and shaking 10 min in the cold room. Elution was monitored by mixing 5 µL sample with 5 µL Bradford reagent (Bio-Rad 500-0006). Elution steps were repeated until no protein could be detected in the fractions by Bradford reagent.

4.4.2 Dialysis

For buffer exchange, dialysis was used. 2 L of buffer to dialyze against (e. g. 50 mM Tris-HCl pH 8.25, 375 mM NaCl, 1 mM DTT in case of Zas1 purification) were prepared in the cold room. Cellulose based SnakeSkin Dialysis tubing with 10 kDa mass weight cutoff (MWCO) (88243, Thermo) was wetted and filled with the dialysis sample (2 mL per cm tubing). Optionally, tag cleaving protease (TEV or 3C Protease) were added. The sample was incubated over night in the cold room with stirring.

4.4.3 Zas1 immunoprecipitation

4 L culture were grown to OD_{600} 1.0 at 30 °C and lysed by cyromilling in IP lysis buffer with protease inhibitors (section 4.9.6) as described in section 4.5.12. In the cold room, lysate powder was split into four 50 mL tubes and thawed by adding 7 mL IP lysis buffer with protease inhibitors to each tube. Samples were placed on ice and sonicated with a Branson Sonicator 3 × 45 s at output 50, with 1 min cooling break between runs. Cell wall debris was pelleted by centrifugation for 20 min at 800 × g at 4 °C. In the cold room, the supernatant was transferred to a new 50 mL tube using a serological pipet. 10 µg V5 antibody (table 4.13) were added to the lysate and the sample was incubated for 30 min on the rotation wheel in the cold room for antibody binding. 100 µL Dynabeads G (Thermo Fisher 10004D) were equilibrated with 100 µL lysis buffer and subsequently added to the IP sample. The sample was incubated for

40 min on the rotation wheel in the cold room. The samples were aliquoted in 2 mL tubes and placed in a magnet for 2 min. Supernatant was aspirated and beads were resuspended in 1 mL lysis buffer in total by using the resuspension from one tube to resuspend beads in the next one. The bead suspension was washed five times for 5 min with lysis buffer by incubating on the magnet for 1 min, aspirating the supernatant and resuspending the beads. In the last washing step, the sample was transferred to a new 1.5 mL tube. IP was eluted by adding 20 µL Laemmli buffer (section 4.9.2) to the Dynabeads and heating to 95 °C for 5 min. Samples were taken after each step and mixed with Laemmli buffer for analysis on SDS PAGE or western blot.

4.4.4 SDS-PAGE for protein analysis

Protein in samples prepared with Laemmli buffer (section 4.9.2) or modified loading buffer (section 4.9.2) were separated by size using polyacrylamide gels using the XCell SureLock mini-cell electrophoresis system (Thermo Fisher, EI0001). Bis-tris buffered 4-12 % gradient acrylamide gels (Thermo Fisher NP0321BOX, NP0322BOX, NP0323BOX) were loaded into the mini-cell electrophoresis system according to the manual's instructions. The gel chamber was filled with either MOPS running buffer (section 4.9.2, proteins >80 kDa), or MES running buffer (section 4.9.2, proteins <80 kDa), depending on the size of the protein of interest. Gel wells were rinsed using a P1000 pipette. Depending on well number and size, up to 20 µL sample could be loaded. The electrophoresis was performed at 175 V for 65 min. Gels were analyzed by Coomassie staining (section 4.4.5), silver staining (section 4.4.6) or western blotting (section 4.4.7).

4.4.5 Protein Coomassie staining

To stain proteins after SDS-PAGE, with Coomassie, the gel was taken from the plastic cassette and equilibrated in destain solution for 2-5 min (section 4.9.5). The gel was transferred to Comassie staining solution (section 4.9.5) and incubated for at least 30 min on a horizontal shaker. Coomassie solution was decanted and could be reused. The gel was briefly rinsed with water and subsequently incubated in destain solution (section 4.9.5) for 30 min. Destain solution was refreshed until protein bands appeared. This protocol was compatible with mass spectrometry. For more rapid staining, the gel can be heated in the microwave before staining, but this introduces cross links and makes the gel unsuitable for analysis by mass spectrometry.

4.4.6 Protein silver staining

Silver staining is a very sensitive method for protein staining based on Silver precipitation with a detection limit of about 0.1 ng protein per band (Lelong et al., 2009). After protein separation (section 4.4.4), the gel was incubated fixation solution (section 4.9.3) for 60 min. The gel was transferred to 100 mL 50% EtOH for 10 min and subsequently transferred to 100 mL 30% EtOH for another 10 min to wash out SDS from the gel. To enhance sensitivity, the gel was washed with 0.1 mg/mL sodium thiosulfate solution for 1 min, followed by three H_2O washing steps. The gel was impregnated with silver by incubating in silver staining solution (section 4.9.3) for 20 min. After two rinsing steps in H_2O (each 20 s), the gel was incubated in developing solution until the desired staining was achieved. The reaction was immediately stopped by transferring the gel to 5 % Acetic acid solution. The gel was washed twice for 10 min with H_2O.

4.4.7 Westernblot

Preparations PVDF membrane (Bio-Rad, 162-0177) was cut to fit the SDS-PAGE (section 4.4.4) gel size and activated by incubation in methanol for 2 min, rinsing twice with H_2O

and equilibration in transfer buffer (section 4.9.4) for longer than 10 min on a horizontal shaker. The gel, membrane and four whatman papers (Biorad) per blot were soaked in transfer buffer (section 4.9.4) for longer than 10 min.

Blot assembly Blots were assembled either in the TE 79 PWR (Amersham, 11-0013-41) or the Trans-Blot Turbo Transfer system (Bio-Rad 1704155) blotting machines. The membrane was stacked on top of two whatman papers and placed in the blotting machine. The gel was placed on top of this stack while avoiding the formation of air bubbles between membrane and gel. Two whatman papers were stacked on top. A small amount (2-4 mL) transfer buffer was added and air bubbles were eliminated from the stack by gentle rolling with a 5 mL pipette. The blotting machine was closed. In case of blotting in TE 79 PWR, the proteins were transferred at 4 mA per gel for 2 h (depending on protein size). In case of blotting in Trans-Blot Turbo Transfer system, the proteins were transferred at 1 /25 V for 30 min.

Ponceau S staining To test, whether transfer of proteins had been efficient, the proteins on the membrane could be stained after transfer. Ponceau S solution (0.1 % Ponceau S (Sigma, P3504), 5 % glacial acetic acid (Merck,1.00063.2511) in H_2O (WEK)) was incubated with the membrane for 2 min on a horizontal shaker and subsequently washed twice with WEK-water. The staining was documented by scanning to a computer. Despite some reports, interference of Ponceau with antibody binding (e. g. higher background) were not observed.

Detection After protein transfer, the membrane was blocked for longer than 20 min in blocking solution (section 4.9.4) while shaking. The primary (1°) antibody, targeting the epitope of interest, was diluted (see table 4.13) in 10 mL blocking solution in a 50 mL tube. After blocking, the membrane was transferred to the 50 mL tube containing the 1° antibody dilution solution. The tube was incubated for 1 h or over night on a roll shaker in the cold room. Afterwards, the membrane was transferred to washing solution (section 4.9.4). 1°antibody dilution solutions were stored at -20 °C and reused up to 4 times. The membrane was rinsed twice and washed two times with wash solution for 5 min and three times for 10 min on a horizontal shaker. The secondary (2°) antibody (horse radish peroxidase (HRP) conjugated and targeting the 1°antibody) was diluted 1:10000 in 10 mL blocking solution in a 50 mL tube. The membrane was transferred into the 50 mL tube containing the 2° antibody dilution and incubated for 1 hon a roll shaker in the cold room. Membrane was again washed by first rinsing with wash solution and two 5 min washing steps followed by three 10 min washing steps.
Antibody was detected by enhanced chemiluminescence (ECL). 70 µL of each ECL reaction solution (Advansta K-12045-D20) were mixed in a 1.5 mL tube and incubated with the membrane for 30 s. The membrane was placed into clear wrap inside a autoradiography cassette (Amsersham Hypercassette). Chemiluminescence signal was detected by exposing Amersham Hyperfilm ECL (GE Healthcare 28906835) for 1 min or such that bands were clearly visible but not overexposed.

4.4.8 Limited proteolysis

Limited proteolysis is a method to experimentally identify domain boundaries, loops and disordered N or C termini in proteins. The native protein of interest or protein complex is treated lightly with a proteolytic enzyme. Folded domains are more resistant to proteolytic cleavage than disordered loops, given that they contain the same frequency of target residues. Suitable proteases are trypsin (EC 3.4.21.4) and subtilisin (EC 3.4.21.62). Chymotrypsin is not recommended due to lack of specificity. The presence of denaturing agents like SDS or urea usually

increases protease activity (Roche manual for Trypsin), so a fast inactivation is required upon addition of Laemmli buffer.
5 µL Laemmli Buffer (section 4.9.2) were prepared per time point and 100 mM PMSF were added for rapid inactivation of the protease. 120 µL of 1 mg/mL protein of interest were prepared. 15 µL control sample were taken before trypsin or subtilisin was added in a ratio 1:100 and 1:1000 protein to protease (w/w). 2 µg/µL trypsin (Roche, 11 418 025 001) stock solution was prepared in 1% acetic acid, and 1 µL and 0.1 µL were added respectively. 15 µL samples were taken after 1, 2, 5, 10, 30 and 60 min and each quenched immediately by addition of 5 µL Laemmli Buffer-PMSF and boiling for more than 6 min.
Cleavage products were analyzed on a SDS-PAGE (section 4.4.4) followed by coomassie staining (section 4.4.5). Boundaries of breakdown intermediates were determined by an acidic lysis protocol of the Proteomics Core Facility at EMBL.

4.4.9 Stopped limited proteolysis

50 µL of 3.5 µg/µL purified Zas1 protein solution were thawed on ice and spun at 21000 × g for 10 min to pellet precipitation. 1.75 µL of 1 µg/µL subtilisin stock solution were prepared. Stock solution was added and the reaction was mixed. The mixture was incubated at 24 °C for 2 min and stopped by addition of 1 µL 100 mM PMSF solution (final concentration 2 mM) and mixing by pipetting gently. Fragments were separated on an Ettan liquid chromatography system (GE Healthcare), which had been equilibrated with 5 mM Tris-HCl pH 8.1 (at 4 °C), 400 mM NaCl and 2 mM dithiothreitol (DTT) using a Superdex 200 increase 3.2/300 column (GE Healthcare, 28990946). Fractions containing a 280 nm absorption peak were analyzed on SDS-PAGE (section 4.4.4) and Coomassie staining (section 4.4.5).

4.5 Fission yeast methods

4.5.1 Spotting growth assay

Yeast strains were grown to mid log phase (OD_{600} 0.4-0.7) in liquid medium e. g. YE5S (section 4.11.2) or EMM2 (section 4.11.1). 3×10^6 cells (0.3 ODs) were resuspended in 100 µL H_2O. The suspension was transferred to a 96-well plate, which contained 90 µL H_2O in 7 wells for each sample. Cells were diluted 10-fold by mixing 10 µL with 90 µL H_2O. Dilutions were repeated in serial steps until eight 10-fold serial dilution suspensions were created. 2 µL of each dilution were spotted on appropriate agar plates using a multichannel pipette. Plates were incubated at desired temperatures until single colonies appeared.

4.5.2 Growth curves

Liquid medium was inoculated with *S. pombe* cells and grown over night such that the culture had not reached stationary phase the next morning. Cells were diluted to OD_{600} 0.1 into 50 mL fresh medium which had been pre-warmed to the respective temperature. OD_{600} was monitored every 30 min until cells had reached end of log-phase using a Ultrospec 2100 Pro spectrophotometer (Amersham Bio). Time points and OD values were entered in an Excel spread sheet and exported as csv file. The doubling time was calculated using R's nls function to fit a function of the form $OD = OD_0 \times 2^{(t/T_{\text{doubling}})}$ with OD_0 being the OD at start of log phase, and T_{doubling} being the doubling time.

4.5.3 Freezing *S. pombe* strains for long-term storage

A patch of *S. pombe* cells was grown on 1/8 th of a YE5S agar plate for 2-3 days. 150 µL glycerol were filled in a 1 mL CryoTube vial (Thermo, 366656) and mixed with 850 µL YE5S. Cells were scraped off the plate using a 1 µL inoculating loop (Sigma Nunc I7773) and resuspended in the glycerol/YE5S mixture. The tube was labeled and stored at -80 °C.

4.5.4 *S. pombe* lithium acetate transformation and strain selection

For each transformation, *S. pombe* cells were grown in 50 mL YE5S (section 4.11.2) or appropriate medium to OD_{600} 0.4-0.8 and collected by centrifugation at 2200 × *g* for 2 min in a 50 mL tube. The supernatant was discarded and cells were twice washed in 50 mL H_2O followed by a washing step in 50 mL 0.1 LiAc/TE buffer (section 4.11.11). Cells were resuspended in 200 µL 0.1 LiAc/TE, transferred to a 2 mL tube and incubated for 1 h at room temperature. 10 mg/mL ssDNA solution was heated to 95 °C and cooled abruptly on ice. 2 µL were added to the cells per 100 µL cell suspension. 1 µg or more PCR product or digested plasmid were added and cells were incubated for 1 h at room temperature. For each 100 µL cell suspension 260 µL 40 % PEG 3350 in 0.1 LiAc and 1 × TE buffer were prepared and the PEG-LiAc-TE solution was mixed well with the cell suspension. The mixture was incubated for at least 2 h but preferentially longer, or even over night. DMSO was added to 1 % v/v and cells were incubated at 42 °C for 15–20 min. All haploid strains were washed in 1 mL H_2O and incubated in 2 mL MSL-N medium (section 4.11.4) for recovery over night at the appropriate temperature and 190 rpm. The following day, cells were spun down and resuspended in 300 µL H_2O and 2 × 150 µL were plated on appropriate selection media using glass beads (section 4.2.5). Diploid strains were directly plated on YE5S, incubated at 30 °C over night and replica plated (section 4.5.9) to selection medium the following day.
As soon as colonies appeared, they were tested for correct 5' integration by colony PCR (section 4.1.6). Clones that produced a PCR product of expected size were streaked out for single colonies on selective agar. As soon as colonies formed, they were tested by another colony PCR targeting the 3' of the integration. Up to eight positive colonies were patched on rich medium. In case of diploid cells patched strains were frozen after 2-3 days to avoid sporulation due to starvation (section 4.5.3). From each clone, genomic DNA was extracted (section 4.1.10) and used as a template to amplify the integration region with primers outside the modified region (section 4.1.12). In case of expected PCR product size as judged by agarose gel electrophoresis (section 4.1.3), the PCR product was purified (section 4.1.7) and Sanger sequenced using appropriate primers (section 4.1.5). Strains with correct integration were stored in the laboratory's strain collection.

4.5.5 PCR based gene targeting for tagging, disruptions or deletions

PCR based gene targeting is a rapid and flexible method to delete or introduce genomic sequences (e. g. epitope or FP tags) in *S. pombe* with single nt fidelity. For DNA amplification during PCR, primers are necessary to hybridize about 20 nt on their 3' end. DNA polymerases extend from 5' end to 3' end, so non-base pairing sequences can be appended to the primer's 5' end and will be incorporated in the PCR product (Mullis and Faloona, 1987; Scharf et al., 1986). Primers can therefore be used to obtain DNA fragments with arbitrary sequence ends. Because *S. pombe*'s genome sequence is available (Wood et al., 2002), primer sequences can be designed to contain homologous genome sequences at their 5' end. dsDNA fragments introduced in *S. pombe* cells were integrated into the genome by homologous recombination based on their end sequences with two crossovers (Bähler et al., 1998; Wach et al., 1994). 60 bp homologous region

were in principle sufficient (Bähler et al., 1998) to achieve integration with acceptable efficiency at the locus of interest. Nevertheless, longer homology sequences of about 150 bp facilitated integration at the correct locus and reduced random integration.
Nested primers were designed to create homology ends that delete genome regions or tag an ORF of interest (section 4.5.5 A and B). The primer were used to amplify plasmid template containing the tag of interest followed by marker cassette (section 4.5.7) or a marker cassette only in 2-3 PCR reactions (section 4.1.12, Bähler et al. (1998); Wach et al. (1994)). 5 µL of PCR product was used to verify the product's size on agarose gel electrophoresis (section 4.1.3), the remaining PCR product volume was pooled and purified (section 4.1.7) and eluted in 20 µL H_2O. The PCR product was introduced into the *S. pombe* genome by transformation (section 4.5.4).

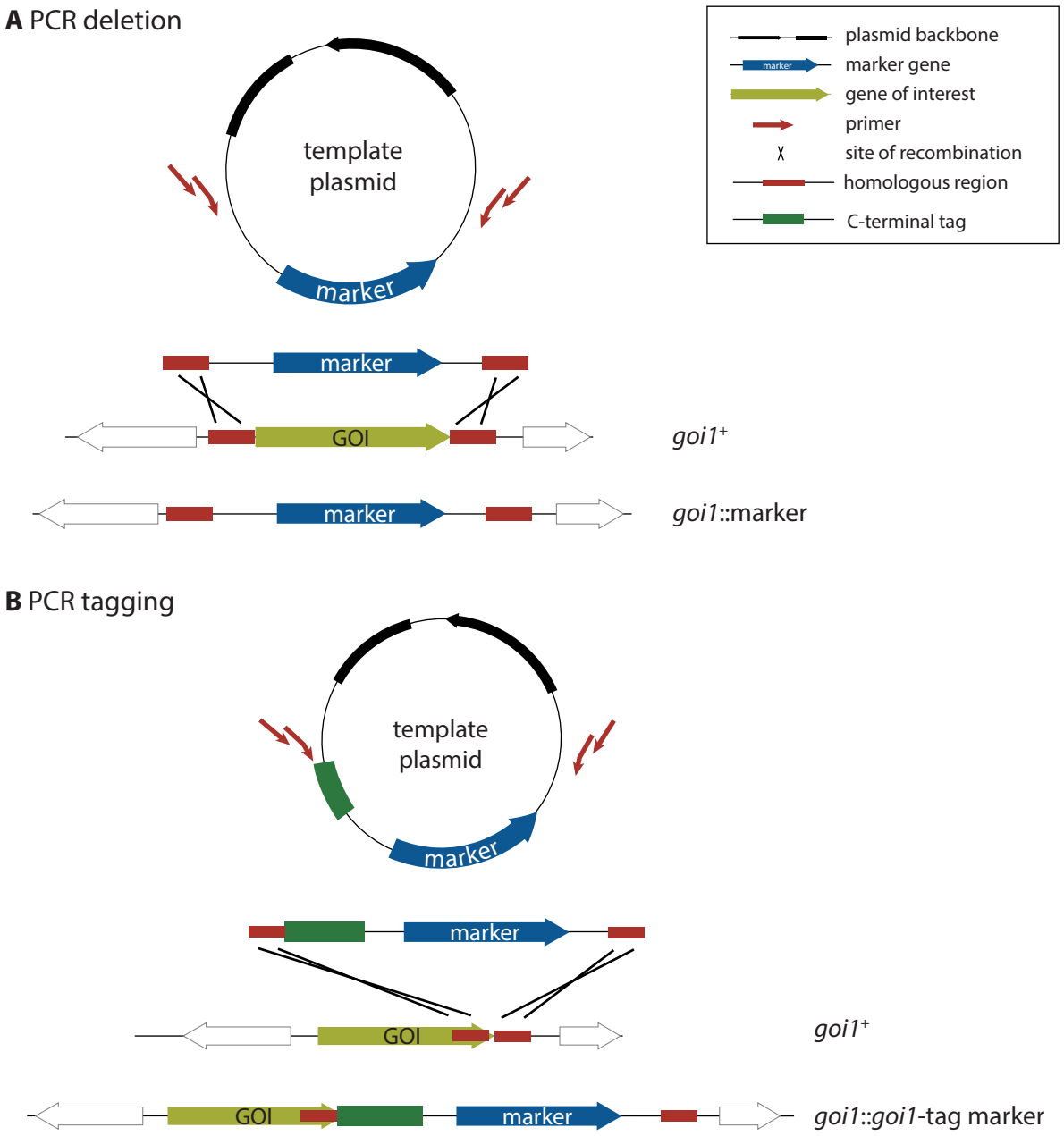

Figure 4.1: Principle of PCR based gene targeting. (A) Deletion (B) endogenous ORF tagging.

4.5.6 Plasmid integration

Plasmid integration was used to introduce a DNA sequence into the *S. pombe* genome at locus of interest. The DNA sequence of interest (e. g. a gene or operator arrays) was cloned into a plasmid carrying a *S. pombe* marker gene (see 4.5.7). Additionally, more than 400 bp homologous to the integration locus containing a unique restriction site had to be present in the plasmid. If the marker gene was an auxotrophic marker, it could serve as target integration locus as long as it contained a unique restriction site. The plasmid was linearized by a unique restriction site (section 4.1.16) and introduced into a strain lacking the marker gene as described in section 4.5.4. The plasmid integrated into the genome at the restriction site with a single crossover (see section 4.5.6 A, and Orr-Weaver et al. (1981, p 6358)).

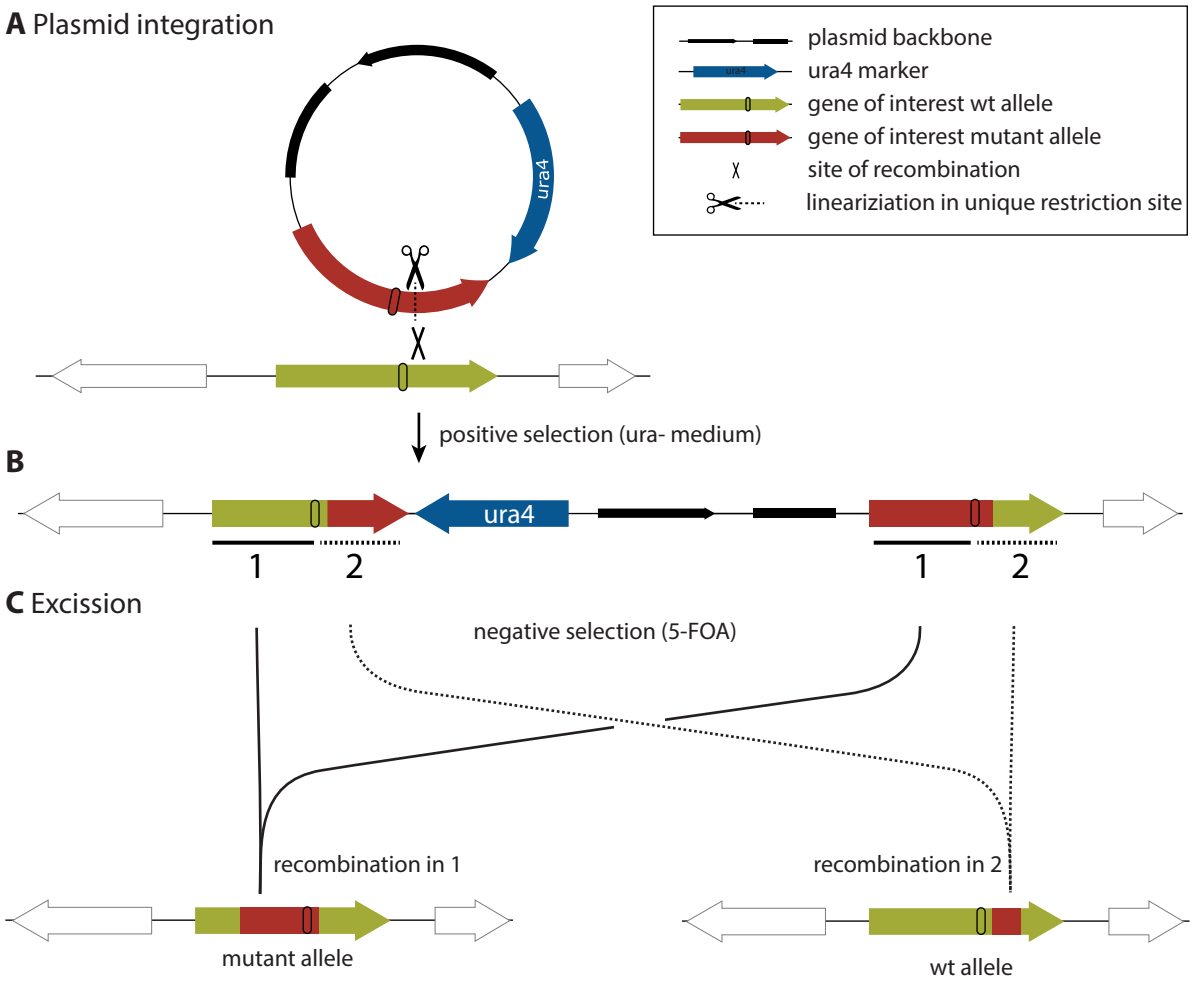

Figure 4.2: Plasmid integration and excision. (A) Diagram of An integration plasmid containing a marker gene (blue) and a homology-region (red) is linearized by restriction within the homology region (scissors). Linear plasmid will integrate into the genome by strand invasion leading to the sequence depicted in (B). The two identical regions (1 and 2 in B) created during integration can recombine at low frequency, excising the marker gene. If the marker can be negatively selected for, clones can be isolated in which the marker has been excised thought recombination. This process can be exploited to introduce genome modifications without marker gene requirement (see section 4.5.7). In this case the integrating plasmid has to bear the mutation of interest surrounded by homology region (red oval). (C) If excision occurs in the arm between mutation and marker opposite to the integration site (1 in B), the mutation of interest will be retained. The marker gene will be deleted and can therefore be used again.

4.5.7 Creation of point mutations by integration-excission strategy

To create the single point mutations in *zas1* ts FROS strains (section 2.1.3), intergation-excision strategy out was applied. The intergation-excision strategy (also called pop-in/pop-out or loop-in/loop-out strategy) is a classical mutagenesis strategy for introduction of genomic mutations with no other genomic alterations (e. g. described by Gao et al. (2014)), based on plasmid integration (see4.5.6). It utilizes a genetic marker that can be positively as well as negatively selected for. In *S. pombe*, *ura4* can be used as auxotrophic marker through complementation but can as well be negatively selected for. For negative selection, 5-fluoorotic acid (5-FOA) is added to the medium. *ura4* encodes a orotidine 5'-phosphate decarboxylase, which catalyzes 5-FOA to fluorouracil. Fuorouracil kills cells by covalently inhibiting thymidylate synthase, thereby stoping thymine synthesis and ribosomal RNA (rRNA) processing (Nislow and Giaever, 2007, p. 398). A diagram of the strategy is shown in section 4.5.6 A and B.
Zas1 was cloned into pUR19 (1826) via SacI and NotI. The resulting plasmid was used for mutagenesis PCR (section 4.1.14) to introduce *W5*, *Ts34* or *A1* mutations in the plasmid. Plasmids were linearized by PpuMI (section 4.1.16) and transformed into strain 1283 (section 4.5.4). Transformed strains were incubated in YE5S containing uracil over night, and plated on 5-FOA plates (Gao et al., 2014). Colonies appeared after 2-3 days. Because 5FOA is a known mutagen, incubation was kept as short as possible. Clones were streaked for singles colonies on YE5S. From strains which had spontaneously recombined out the *ura4* marker, genomic DNA was prepared (section 4.1.10) and the *zas1* locus was sequenced (section 4.1.5). Strains, which carried the desired mutation were stored in the collection (3693, 3717).

S. pombe markers used in this thesis

Auxotrophic markers Five auxotrophic marker genes are used in this thesis. Strains carrying inactivating mutations in auxotrophic marker genes can only grow in media supplemented with the respective nutrient. Mutations interfere with enzyme function and thereby inactivate biosynthesis of central metabolites (aas or nucleobases). All auxotrophic mutations are recessive and can only be used as markers by complementation, i. e. the gene has to be non-functional in the basis strain and a functional copy has to be reintroduced during transformation. An overview of auxotrophic markers used in this thesis can be found in section 4.5.7.

Antibiotic markers Next to auxotrophic markers, dominant antibiotic marker cassettes natMX, kanMX and hphMX are available for selection in *S. pombe*. Antibiotic marker genes encode enzymes that inactivate antibiotics by modification (phosphorylation or acetylation). In MX cassettes, expression of resistance conferring enzymes is driven by TEF promoters from *Ashbya gossypii* Wach et al. (1994).

4.5.8 Strain crossing and tetrad dissections

Crossing *S. pombe* strains

Two strains of opposite mating type were grown on YE5S agar for 24-48 h at 25 °C. Approximately equal amounts of cells were resuspended in 10 µL H_2O and the suspension was pipetted onto SPAS agar (section 4.11.9). After 24 h incubation at 25 °C, mating efficiency was monitored in a transmission light microscope. If necessary, strains were incubated with both mating types to ensure only the desired mating type was present in the original strain.

Auxotrophic marker genes			
Marker gene	Nutrient	Alleles	References
ade6	Adenine	M210 (P489L), M216 (G16D)	Ponticelli et al. (1988)
his7	Histidine	366 (H290Y)	Apolinario et al. (1993)
leu1	Leucine	32 (G46E)	Matsuyama et al. (2004)
lys1	Lysine	131	Ye and Bhattacharjee (1988)
ura4	Uracil	D18	Grimm et al. (1988)
Antibiotic resistance marker gene cassettes			
Marker gene	Enzyme	Antibiotic	References
kanMX	Aminoglycoside 3′-phosphotransferase	G418	Wach et al. (1994); Bähler et al. (1998)
natMX	Nourseothricin acetyltransferase	Nourseothricin	Krügel et al. (1988); Goldstein and McCusker (1999); Hentges et al. (2005)
hphMX	Hygromycin B phosphotransferase	Hygromycin B	Rao et al. (1983); Goldstein and McCusker (1999); Hentges et al. (2005)

Table 4.11: Overview of *S. pombe* marker genes used in this thesis.

Induction of sporulation in diploid *S. pombe* strains

The diploid strain was grown on YE5S for 24 h at 25 °C. An inoculation loop of cells were resuspended in 8 µL H_2O and the suspension was pipetted on a SPAS agar plate (section 4.11.9). The plate was incubated for 24-48 h at 25 °C. Just like mating, sporulation is inhibited at 30 °C. The fraction of sporulated cells was monitored in a transmission light microscope.

Tetrad dissection

Sporulated cells were scraped off the SPAS agar plate using a sterile pipet tip and resuspended in 150 µL water. The suspension had an OD_{200} of about 0.2-0.4. A YE5S agar plate was held at a 45° angle and the suspension was run along its top to bottom diameter. The plate was incubated at 25 °C for 12-36 h. To delay ascus digestion, the plate was stored at 4 °C for up to 2 days. Tetrad dissection was performed on a Singer instruments tetrad dissection microscope. I found that it beneficial to take only tetrads that had grown considerably after ascus digestion to make sure they were viable.

4.5.9 Replica plating

For each replica plating, a sterile velvet cloth was stretched on a replica plating stamp (EMBL workshop). The agar plate on which the cells for replica plating were growing (source plate) was stamped upside down onto the velvet with light pressure such that cells adhered to the velvet. The source plate was gently removed and the target agar plate (usually selective medium) was

stamped on the velvet, again applying light pressure to facilitate transfer of cells from velvet to agar surface. Velvets were washed with desalted water, air dried and autoclaved for reuse.

4.5.10 NaOH lysis

This is a rapid protein extraction method described in Matsuo et al. (2006). 5×10^7 cells (5 ODs) were pelleted by centrifugation at 2200 × *g* for 2 min. Cells were washed once with H_2O and resuspended in 0.3 mL H_2O. An equal volume of 0.6 M NaOH was added and the suspension was incubated for 5 min at RT to hydrolyze cell wall. The cells were pelleted at 2200 × *g* for 2 min and the supernatant was aspirated. The cell pellet was dissolved in 70 µL SDS-PAGE loading buffer (section 4.9.2) by pipetting until no cell clumps were visible. The sample was heated to 95 °C for 5 min. Cell wall and debris were pelleted by centrifugation at 20000 × *g* for 5 min. Usually 15 µL of the supernatant (corresponding to protein from 1 OD cells) were analyzed on SDS-PAGE (section 4.4.4). This extraction method was used to prepare samples for western blotting (section 4.4.7). Samples could be frozen at -20 °C for long term storage.

4.5.11 Glass bead lysis

S. pombe cells were lysed using a glass bead beater (MP Bio FastPrep-24, 6004-500) for preparation of intact chromatin (e. g. for ChIP) or medium scale protein extraction. The cell suspension was mixed with 0.2-0.5 mm ø glass beads (Sigma, G8772, stored at 16 °C) so that beads filled the tube up to the meniscus of the liquid. 1 mL glass beads accommodated around 500 µL liquid. 5 cycles of 1 min shaking at 6.5 m/s, alternated with 3 min cooling incubation on ice lysed more than 80 % of the cells. To prepare separation of lysate from glass beads, a cap-less 1.5 mL tube was inserted (bottom to bottom) in a 15 mL tube. The bottom of the screw cap tube containing the glass beads and lysed material was pierced using a Microlance needle (Beckton Dickson, 300300). Immediately after perforation, the tube was stacked on top of the 1.5 mL tube inside the 15 mL tube. The tube stack was centrifuged for 3 min in a swing bucket rotor at 4 °C at 1000 × *g* to elute the lysate.

4.5.12 Cryomilling

Cell suspension freezing Cells were pelleted and washed with 1 × PBS. The cells were resuspended in in 24 mL IP lysis buffer (section 4.9.6) per 10×10^{10} cells (1000 ODs). The suspension was snap frozen by dripping it from a 25 mL serological pipet directly into a liquid N_2 containing 500 mL beaker. The resulting spherules ("popcorn") were transferred to 50 mL falcons and stored at -80 °C.

Cryomilling The cryomill (Spex SamplePrep Freezer/Mill 6870) was filled with liquid N_2 and switched on. The grinding cyclinder was closed on one end with a metal lid. The pestle was placed into the cylinder, which was filled about one third with liquid N_2 to cool both pestle and cylinder. After all liquid N_2 was evaporated, frozen cell suspension spherules and were placed into the grinding cylinder, such that the cylinder was less than half full. The cylinder was closed with the other metal lid and loaded into the cryomill. Grinding was performed at 12 cycles per s for five 3 min pulses interrupted by 2 min pauses. The lysate powder was collected in a cooled beaker and either stored at -80 °C or processed.

Final lactose conc. (%)	30 % lactose stock (mL)	7 % lactose stock (mL)
30.0	50	0
27.125	43.75	6.25
24.25	37.5	12.5
21.375	31.25	18.75
18.5	25.0	25.0
15.625	18.75	31.25
12.75	12.5	37.5
11.025	6.25	43.75
7.0	0	50

Table 4.12: Lactose gradient solutions for preparation of a lactose gradient.

4.6 Imaging

4.6.1 Live *S. pombe* DNA staining with Hoechst 33342

2 mg/mL Hoechst 33342 (Sigma B2261) stock solution as prepared. *S. pombe* cells were culture in EMM2 liquid medium (section 4.11.1) to mid log phase. After two washing steps in H_2O cells were incubated in 1 µg/mL Hoechst 33342 on H_2O for 15 min. Cells were resuspended in EMM2 liquid medium (Hiraoka et al., 2000). A glass bottom dish was prepared as described in section 4.6.2. The cell suspension was pipetted on top of the glass surface and incubated for 10 min at RT. Non-attached cells were rinsed off using a pipette and the dish was covered with 1.5 mL EMM2. Cells were observed in an inverted fluorescence microscope (DeltaVision). Adding Hoechst 33342 to cells which had been grown in YE5S did not stain the nuclei efficiently.

4.6.2 Chromosome condensation assay

A detailed description of sample preparation and imaging conditions is published in Schiklenk et al. (2016).

Preparation of a lactose gradient

30 % w/v and 7 % w/v lactose (Merck 107657) solution were prepared in water by gentle warming in the microwave to increase lactose solubility. Solutions were cooled to RT. 30 % w/v and 7 % w/v lactose stock solutions, the nine dilutions described in table 4.12 were prepared. 1.5 mL of the 30 % solution were pipetted into a 15 mL tube and any air bubbles were eliminated. From highest to lowest concentration, 1.5 mL of each lactose solution from table 4.12 were layered in the 15 mL tube without mixing the phases. To minimize mixing of the two phases due to pipetting pressure, a cut off P1000 pipet tip was used.

Preparation of a glass bottom dish for imaging

The glass surface of a glass bottom dish (MatTek) was covered with 2 mg/mL BS-1 lectin (from *Griffonia simplicifolia*, an african climbing shrub, Sigma Aldrich L2380) solution and incubated at RT for 2 min. The BS-1 was aspirated and residual liquid was left to dry.

Enrichment of G_2 cells by lactose gradient centrifugation

Cells were grown in 50 mL liquid YE5S or appropriate medium to OD_{600} 0.3-0.7, transferred to a 50 mL tube and pelleted by centrifugation at 2200 × *g* for 2 min. The cells were washed one with 50 mL H_2O (2200 × *g*, 2 min) and resuspended in 750 µL H_2O. The suspension was loaded on top of the 7-30% lactose gradient (section 4.6.2) and centrifuged at 210 × *g* for 8 min in a swing bucket rotor with slowest acceleration and slowest deceleration. 300 µL cells were immediately aspirated from the highest density in the upper half of the gradient and transferred to a 2 mL tube containing 1 mL YE5S. The suspension was mixed and washed with liquid YE5S (2200 × *g*, 1 min). Supernatant was aspirated and the cells were resuspended in 200 µL YE5S. The suspension was pipetted to the glass surface of the glass bottom dish (prepared as above, section 4.6.2) and allowed to settle for at least 10 min. The glass was rinsed thoroughly with liquid YE5S using a 200 µL pipet. This step washed off loosely attached cells and created a cell monolayer. The dish was filled with 2 mL liquid YE5S, which had been equilibrated to the imaging temperature. The culture was incubated in the microscope environment box which had been pre-warmed to the imaging temperature for one hour prior to imaging.

Microscope imaging conditions

Imaging was either performed on a GE Healthcare API DeltaVision widefield fluorescence microscope system (sections 2.1.3, 2.1.8, 2.3.1, 2.3.2 and 2.3.6) or on an Olympus Cell^R total internal reflection fluorescence (TIRF) (sections 2.3.7 and 2.4) microscopy system in widefield mode. Both setups featured an automated stage and an environment box for temperature control during imaging experiments.

DeltaVision Samples were excited using a metal halide lamp. To attenuate the light intensity, imaging was performed with a 10 % or a 30 % neutral density filter in the light path. A full width at half maximum (FWHM) 520 nm/25 band pass filter and a 620 nm long pass filter were used to switch between excitation bands of a dual band dichroic (FWHM 520 nm/25 and 630 nm/50). Up to six stage positions were defined, that contained about 50 to 100 *S. pombe* cells. For each position 10 z-stacks were acquired with 400 nm distance between focal planes. Each position was imaged every 45 s for 1 h. In case of drift in z-direction, the stage was manually adjusted during acquisition. The order of image acquisition was xy-z-channel-position-time point. Images were acquired with a CoolSNAP camera in 2×2 pixel binning mode and SoftWoRx software.

Cell^R TIRF Samples were excited using 488 nm laser and 561 nm laser in widefield mode at 20 % laser intensity, which corresponded to about 300 µ, as measured by a photodiode (Thorlabs) from the Olympus 100 × NA 1.4 objective (fig. 4.3). Excitation bands were switched by illuminating with either 488 nm and 561 nm laser. Excitation light was reflected to the sample by a 4-band dichroic (QuadBS, Semrock, Di01-R405/488/561/635-25x36). Neither excitation filter nor emission filter were present in the light path during acquisition. For single cell condensation assay, two to three positions were chosen in which the field of view contained 50-100 cells in a monolayer. For each position 8 z-stacks were acquired with 500 nm distance between focal planes for 2 h every 15 s and 13 s, respectively. The order of image acquisition was xy-channel-z-position-timepoint. Images were acquired with a Hamamatsu Image EM CCD camera and xCELLence-RT software. Z-drift was avoided by autofocusing the sample before acquisition of z-stacks by the ZDC infrared autofocus system (Olympus).

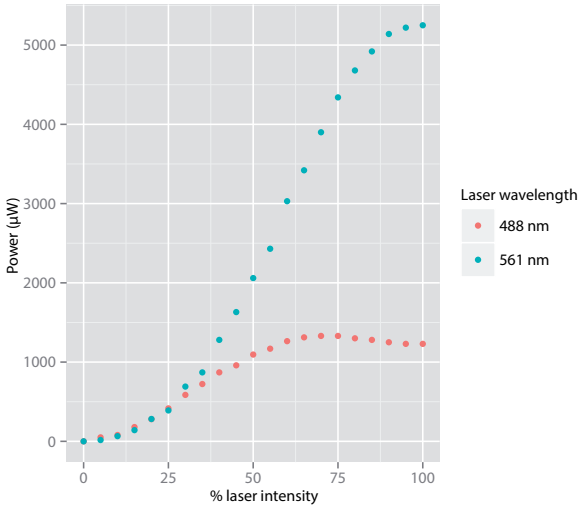

Figure 4.3: Light dose measured at the objective in for 488 nm and 561 nm laser on the Cell^{R} TIRF microscopy setup.

Data analysis Data was transferred from the microscope setup to the lab server and analyzed as described in section 2.2.

4.7 List of antibodies

Target	Host	Epitope	Source	Catalog ID	1°/2°	Conjugation	WB
V5 (PK tag)	mouse	IPNPLLGL (Dunn et al., 1999)	BIO-RAD	MCA1360	1°	-	100 ng/µL
HA 16B12	mouse	YPYDVPDY	Covance	MMS-101R	1°	-	100 ng/µL
T. brucei tubulin (TAT1)	mouse	monoclonal	Keith Gull lab		1°	-	1:1000
mouse IgG	goat	polyclonal	Jackson Research	115-035-146	2°	HRP	100 ng/µL

Table 4.13: List of antibodies. WB: Dilution used for in western blot detection (section 4.4.7). Absolute concentration of tubulin antibody was unknown.

4.8 *E. coli* strains used in this thesis

Strain name	Genotype	Purpose
DH5$_\alpha$	*fhuA2 lac(del)U169 phoA glnV44* Φ80' *lacZ(del)M15 gyrA96 recA1 relA1 endA1 thi-1 hsdR17*	plasmid amplification
stbl2	F$^-$ *endA1 glnV44 thi-1 recA1 gyrA96 relA1* (lac-proAB) mcrA (mcrBC-hsdRMS-mrr) λ$^-$	Amplification of repetitive DNA
Rosetta(DE3) pLysS	F$^-$ ompT hsdSB(RB- mB-) gal dcm λ$^($DE3 [lacI lacUV5-T7 gene 1 ind1 sam7 nin5]) pLysSRARE (cam^r)	Protein expression
DH10MultiBac^{Turbo} EmBacY	see Bieniossek et al. (2008) for details	Bacmid transposition

Table 4.14: *E. coli* strains used in this thesis

4.9 Buffers and Solutions

10 × X7 reaction buffer

Tris-HCl pH 8.8	200	mM
KCl	100	mM
$(NH_4)_2SO_4$	60	mM
$MgSO_4$	20	mM
BSA	1	mg/mL
Triton X-100	1	%

4.9.1 Agarose gel electrophoresis buffers

50 × TAE running buffer

Tris-HCl	2	M
Glacial Acetic Acid	5.75	% v/v
EDTA pH 8.0	50	mM

Tris-Acetate EDTA (TAE) is a standard buffer for agarose gel electrophoresis. TAE has advantages over the other common agarose gel electrophoresis buffer. The borate in TBE (Tris-borate EDTA) inhibits enzymatic reactions and it therefore not suitable for most gel elution experiments. Borate is less soluble in H_2O than acetate and therefore only 20 x stock solutions are feasible. TBE buffer resolves DNA fragments smaller than 2.0 kb better than TAE.

6 x DNA loading dye

Glycerol	30	%
EDTA	25	mM
Bromphenol blue	0.2	%

1 kb DNA ladder

H_2O	800	µL
6 × loading dye	200	µL
NEB 1 kb ladder (N3232L)	200	µL

4.9.2 Polyacrylamide gel electrophoresis buffers

20 x MOPS running buffer for Bis-Tris SDS-PAGE

MOPS	104.6	g
Tris Base	60.6	g
SDS	10	g
EDTA	3	g
Ad 500 mL H_2O		

MOPS can be used with Bis-Tris PA gels. MOPS resolves high molecular weight proteins (bigger 80 kDa) better than MES, but has lower separation for smaller polypeptides. It is convenient to solve the SDS in 300 mL H_2O by heating it in the microwave. If stored at 4 °C, SDS crystals may form.

20 x MES running buffer

MES	97.6	g
Tris Base	60.6	g
SDS	10	g
EDTA	3	g
Ad 500 mL H_2O		

MES resolves small molecular weight polypeptides (bigger 80 kDa) better than MOPS, but has lower separation for large proteins. Dissolve the reagents in 500 mL H_2O. The buffer is stable for 6 months if stored at 4 °C. SDS crystals may form. For PAGE, dilute this buffer to 1x with water. The pH of the 1 × solution is 7.3. Do not use acid or base to adjust the pH.

2 x Laemmli Buffer

1 M Tris-HCl pH 6.8	25	mL
SDS	5	%
Bromphenol blue	0.05	g
Glycerol (87%)	57	mL
Ad 100 mL H_2O		

Mixture was heated briefly in a microwave to solve the SDS. Before usage, 2- mercaptoethanol was added to a final concentration of 4 %, or DTT was added to a final concentration of 0.1 mM.

2 x Modified SDS-PAGE loading buffer (Matsuo et al., 2006)

Tris-HCl pH 6.8	60	mM
SDS	4	%
Bromphenol blue	0.01	%
Glycerol	5	%

Before usage 2- mercaptoethanol was added to a final concentration of 4 %.

4.9.3 Silver staining solutions

Fixation solution

Methanol	50	mL
Glacial Acetic acid	10	mL
37 % Formaldehyde sol.	50	µL
Ad 100 mL H_2O		

Staining solution

$AgNO_3$	0.1	g
37 % Formaldehyde sol.	75	µL
Ad 100 mL H_2O		

Developer solution

Na_2CO_3	6	g
37 % Formaldehyde sol.	50	µL
1 mg/mL $Na_2S_2O_3$	20	µL
Ad 100 mL H_2O		

4.9.4 Western blot buffers

Westernblot transfer buffer stock solution

Tris	3.03	$g\,L^{-1}$
Glycine	14.4	$g\,L^{-1}$
SDS	0.1	$g\,L^{-1}$
Methanol	10	% v/v

Ponceau S solution

Ponceau S	0.1	%w/v
Glacial acetic acid	5	%v/v

In WEK water.

Western blot blocking solution

Tween-20	0.05	% v/v
Milk powder	50	$g\,L^{-1}$

in 1 × PBS (EMBL media kitchen).

Western blot wash solution

0.05 % v/v Tween-20 in 1 × PBS (EMBL media kitchen).

10x TBS

250 mM Tris	30	g
KCl	2	g
NaCl	80 g	

ad 900 mL H_2O, ad pH 7.4 (ca 12 mL of 37 % HCl), ad 1 L H_2O

4.9.5 Coomassie staining

Coomassie protein staining solution

H_2O	10	mL
EtOH	90	mL
Coomassie Brilliant Blue G250	0.2	g
20% Acetic Acid sol.	100	mL

Mix in the exact order.

Coomassie fixing and destaining solution

Methanol	45	%
Acetic acid	10	%
H_2O	45	%

4.9.6 Buffers for protein purification

***E. coli* Hexa-His tag lysis buffer**

NaCl	500	mM
Tris-HCl pH 7.5	50	mM
Imidazole	20	mM
2- mercaptoethanol	5	mM
PMSF	0.1	mM
1 × cOmplete		

2- mercaptoethanol, PMSF and cOmplete protease inhibitor were added shortly before use. This is a standard His purification lysis buffer as used by Markus Hassler. EDTA or DTT must not be added to this buffer since they chelate divalent ions.

IP lysis buffer

NaCl	200	mM
Tris-HCl pH 8.0	300	mM
EDTA	5	mM
Triton-X100	0.1	% (v/v)
DTT	1	mM
PMSF	0.1	mM
2 × cOmplete		

DTT, PMSF and cOmplete protease inhibitor were added shortly before use.

4.9.7 Miniprep Kit Buffers

Buffer P1

Tris-HCl pH 8.0	50	mM
EDTA	10	mM
RNaseA	100	µg/mL

Stored at 4 °C.

Buffer P2

NaOH	200	mM
SDS	1	%

Buffer N3

Guanidine-HCl pH 4.8	4.2	M
K-Acetate	0.9	M

PE buffer

EtOH	80	%
Tris-HCl pH 7.5	20	%

4.9.8 ChIP buffers

2 x Fixation solution stock

Tris-HCl pH 8.0	50	mM
NaCl	200	mM
EDTA	2	mM
EGTA	1	mM

Formaldehyde fixation solution

2x Fixation solution stock	11	mL
37% Formaldehyde solution (Merck, 104003)	6.6	mL
H_2O	4.4	mL

ChIP buffer 1

Hepes/KOH pH 7.5	50	mM
NaCl	140	mM
EDTA	1	mM
Triton X-100	1	% v/v
Na-Deoxycholate	0.1	% w/v

ChIP buffer 2

Hepes/KOH pH 7.5	50	mM
NaCl	500	mM
EDTA	1	mM
Triton X-100	1	% v/v
Na-Deoxycholate	0.1	% w/v

ChIP buffer 3

Tris-HCl pH 8.0	50	mM
LiCl	250	mM
EDTA	1	mM
NP-40	0.5	% v/v
Na-Deoxycholate	0.5	% w/v

TES

Tris-HCl pH 8.0	50	mM
EDTA	10	mM
SDS	1	% w/v

4.10 *E. coli* media

4.10.1 *E. coli* chemical competent transformation buffer

Stock solution	Volume [mL]	Final conc. [mM]
1 M $CaCl_2$	15	15
1 M $MnCl_2$	55	55
2.5 M KCl	100	250
500 mM PIPES pH 6.7	20	5
H_2O	810	

pH should be monitored if not prepared freshly.

4.10.2 LB liquid medium

Tryptone	10	$g\,L^{-1}$
Yeast Extract	5	$g\,L^{-1}$
NaCl	5	$g\,L^{-1}$

Adjust to pH 7.4 with NaOH. Autoclave. This medium was supplied by the EMBL media kitchen.

4.10.3 2 × YT liquid medium

Tryptone	16	$g\,L^{-1}$
Yeast Extract	10	$g\,L^{-1}$
NaCl	5	$g\,L^{-1}$

Adjust to pH 7.4 with NaOH. Autoclave. This medium was supplied by the EMBL media kitchen.

4.10.4 LB agar plates

Tryptone	10	$g\,L^{-1}$
Yeast Extract	5	$g\,L^{-1}$
NaCl	5	$g\,L^{-1}$
Agar	15	$g\,L^{-1}$

Adjust to pH 7.4 with NaOH. After autoclaving cool to 55 °C, pour plates. This medium as well as ampicillin, kanamycin or chloramphenicol containing LB agar plates were supplied by the EMBL media kitchen.

4.10.5 Antibiotic stock solutions for *E. coli*

1000 ×	Ampicillin (Roth K029)	$100\,mg\,mL^{-1}$	in H_2O
1000 ×	Kanamycin (Roth T832)	$40\,mg\,mL^{-1}$	in H_2O
1000 ×	Chloramphenicol (Sigma C0378)	$34\,mg\,mL^{-1}$	in EtOH

4.11 *S. pombe* media

4.11.1 Edinburgh Minimal Medium 2 (EMM2)

KH-phthalate	3	$g\,L^{-1}$
Na_2HPO_4	2.2	$g\,L^{-1}$
NH_4Cl	5	$g\,L^{-1}$
Glucose	20	$g\,L^{-1}$
50 x Salts 4.11.7	20	$mL\,L^{-1}$
1000x Vitamins 4.11.5	1	$mL\,L^{-1}$
10 000 x Minerals 4.11.6	0.1	$mL\,L^{-1}$
as required:		
Adenine	0.225	$g\,L^{-1}$
Uracil	0.225	$g\,L^{-1}$
Lysine	0.225	$g\,L^{-1}$
Histidine	0.225	$g\,L^{-1}$
Leucine	0.225	$g\,L^{-1}$

Sterile filter before use. About pH 6.0. For plates boil 4 % agar (EMBL media kitchen) and stir, add 2 × EMM2 1 to 1 and wait for the mixture to cool down to hand warm temperature. Pour plates.

4.11.2 10 L 2 × YE5S

Yeast Extract BD 212750	100	g
Glucose	600	g
Adenine	4.5	g
Uracil	4.5	g
Lysine	4.5	g
Histidine	4.5	g
Leucine	4.5	g
Ad 10 L H_2O		

For Adenine and Uracil, make 2 L of 2.25 g/L stock solution and heat in water bath to 60 °C to facilitate solubilization. Add all other components and sterile filter.

4.11.3 Antibiotics stock solutions

Geneticin G418 1000x stock solution

Dissolve 5 g geneticin in 25 mL H_2O in a falcon tube. Sterile filter and aliquot a 1 mL in 1.5 mL tubes. Store at -20 °C. Working concentration for G418 is 200 µg per mL

Nourseothricin 1000x stock solution

Dissolve 2 g ClonNat (Nourseothricin, Werner Bioagents 5.2000) in 20 mL H_2O. aliquot a 1 mL and store at -20 °C.

Hygromycin B 1000x stock solution

200 mg/mL Hygromycin B powder (Roth, CP13.3) solved in PBS. Store at -20 .

4.11.4 MSL-N

Glucose	10	$g\,L^{-1}$
50 × Salts	20	$mL\,L^{-1}$
1000 × Vitamins	1	$mL\,L^{-1}$
10000 × Minerals	0.1	$mL\,L^{-1}$

Sterile filter before use.

4.11.5 1000 × Vitamins stock solution

Panthothenic acid	1	$g\,L^{-1}$
Nicotinic acid	10	$g\,L^{-1}$
Inositol	10	$g\,L^{-1}$
Biotin	0.01	$g\,L^{-1}$

Sterile filter before use.

4.11.6 10000 × Minerals stock solution

Boric acid	5	$g\,L^{-1}$
$MnSO_4$	4	$g\,L^{-1}$
$ZnSO_4 \cdot 7\,H_2O$	4	$g\,L^{-1}$
$FeCl_2 \cdot 6\,H_2O$	2	$g\,L^{-1}$
$MoNa_2O_4 \cdot 2\,H_2O$	2	$g\,L^{-1}$
KI	1	$g\,L^{-1}$
$CuSO_4 \cdot 5\,H_2O$	0.4	$g\,L^{-1}$
Citric acid	10	$g\,L^{-1}$

Sterile filter before use.

4.11.7 50 × Salts solution

$MgCl_2 \cdot 6\,H_2O$	52.5	$g\,L^{-1}$
$CaCl_2 \cdot 2\,H_2O$	0.735	$g\,L^{-1}$
KCl	50	$g\,L^{-1}$
Na_2SO_4	2	$g\,L^{-1}$

Sterile filter before use.

4.11.8 5-Fluoroorotic acid (5FOA) Plates

YNB without Aminoacids BD, 291940	3.5	g
Glucose	10	mg
Adenine	112.5	mg
Histidine	112.5	mg
Lysine	112.5	mg
Leucine	112.5	mg
Uracil	25.125	mg
Ad 250 mL H_2O		

Add 0.5 g 5FOA to solution and sterile filter. Melt 4 % agar (EMBL media kitchen) in a microwave cool down to 50 °C. Mix agar and 5FOA-medium and pour plates. Scorch bubbles before agar is gelled.

4.11.9 SPAS mating medium

Glucose	10	g
KH_2PO_4	1	g
Adenine	45	mg
Histidine	45	mg
Lysine	45	mg
Leucine	45	mg
Uracil	45	mg
1000 × Vitamins	1	mL
10000 × Minerals	1	mL
Ad 1 L H_2O		

Autoclave. For plates add 3 % Difco Bacto Agar.

4.11.10 EMM low Glu N-source for mating

KH-phthalate	3	g
Na_2HPO_4	2.2	g
Glutamate	1	g
Glucose	20	g
50 × Salts	20	mL
1000 × Vitamins	1	mL
10000 × Minerals	100	µL
Adenine	40	mg
Uracil	40	mg
Histidine	40	mg
Lysine	40	mg
Leucine	40	mg
Ad 1 L H_2O		

4.11.11 *S. pombe* LiAc/PEG transformation buffers

10 × TE

Tris-HCl pH 7.5	100	mM
EDTA	10	mM

1 M LiAc solution

1 M LiAc in H_2O
Autoclave.

0.1 M LiAc/TE-buffer

Tris -HCl pH 7.5	10	mM
EDTA	1	mM
LiAc	100	mM

50 % PEG stock solution

25 g PEG 3055 (MW) ad 50 mL H_2O. Sterilize by syringe filtering. Store in fridge.

4.11.12 Buffers for *S. pombe* genomic DNA extraction

SCE Buffer

Sorbitol	1	M
Na-Citrate pH 5.8	0.1	M
EDTA pH 7.6	10	mM

SDS Lysis Buffer

SDS	2	% w/v
Tris-HCl pH 9.0	0.1	M
EDTA	50	mM

4.12 List of *S. pombe* strains

Newly created strains have been modified as indicated in the 'Origin' column. PT: modification by PCR targeting (section 4.5.5) with indicated primers (left of slash) and plasmid (right of slash). LPI: linearized plasmid integration (section 4.5.6) with indicated restriction enzyme (left of slash) and plasmid (right of slash). LIO: loop-in-loop-out (section 4.5.7) with indicated restriction enzyme and plasmid. #: collection number.

Table 4.15: List of *S. pombe* strains.

#	Genotype	Origin	Created by
28	*h⁻*	972 isolate	J. Kohli
1283	*h⁺, ade6-M210, his7-366, leu1-32, lys1-131, ura4-D18*		J.-P. Javerzat
2457	*h⁺/h⁻, ade6-M210/ade6-M216*	D. Brunner lab	
2774	*h⁻, ChrI 1.95Mb::LacO-natMX, ChrI 1.5Mb::TetO-hphMX, LacI-eGFP::his7⁺, TetR-tdTom::leu1⁺, lys1-131, ura4-D18, ade6-M210*	Petrova 2012	B. Petrova
2779	*h⁻, ChrI 2.49 Mb::LacO-natMX, ChrI 1.5 Mb::TetO-hphMX, LacI-eGFP::his7⁺,TetR-tdTom::leu1⁺, lys1-131, ura4-D18, ade6-M210*	Petrova 2012	B. Petrova
2926	*h⁻, ChrI 2.49Mb::TetO-hphMX, LacO::lys1⁺, TetR-tdTom-natMX::zfs1⁺, LacI-GFP::his7⁺, lys1-131, ura4-D18, ade6-M210*	Petrova 2012	B. Petrova
2930	*h?, cut14-208, TetR-tdTom::leu1⁺, lacI-GFP::his7⁺, Chr1 2.49Mb::natMX-LacO, Chr1 1.5Mb::hphMX-TetO, ura4?, ade6-210, lys1?*	Petrova 2012	B. Petrova
3399	*h⁻, zas1-1A, LacO::lys1⁺, lacI-GFP::his7⁺, TetR-tdTom-natMX::Z-locus, ChrI 2.49Mb::HygMX-TetO, ura4-D18, ade6-210, leu1?*	Petrova 2012	B. Petrova
3693	*h⁺, zas1-W5, ade6-M210, his7-366, leu1-32, lys1-131, ura4-D18*	1283, pUR19-zas1-W5 LIO	C. Schiklenk
3717	*h⁺, zas1-Ts34, ade6-M210, his7-366, leu1-32, lys1-131, ura4-D18*	1283, pUR19-zas1-Ts34 LIO	C. Schiklenk
3766	*h?,zas1-W5, lys1⁺::LacO, his7⁺::lacI-GFP, zfs1⁺::TetR-tdTom-natMX, Chr1 2.49Mb::hphMX-TetO, ura4-D18, ade6-M210, leu1-1*	2926 x 3693	C. Schiklenk
3782	*h⁺, zas1-3x mCherry::kanMX, ade6-M210, his7-366, leu1-32, lys1-131, ura4-D18*	1283 PT: 10, 13, 19 / 1286	C. Schiklenk
3809	*h?, zas1-Ts34,lys1⁺::LacO, his7⁺::lacI-GFP, zfs1⁺::TetR-tdTom-natMX, Chr1 2.49Mb::hphMX-TetO, ura-D18, ade6-M210, leu1-1*	2926 x 3717	C. Schiklenk
3849	*h⁻ ade6::ade6⁺-Padh15-skp1-OsTIR1-natMX6 Padh15-skp1-AtTIR1-2NLS, ura4-D18*	YGRC strain FY21104	Kanke et al. 2011
3921	*h⁻, zas1⁺-HA2-IAA17-ura4, ade6⁺::Padh15-skp1-OsTIR1-natMX-Padh15-skp1-AtTIR1-2NLS,ura4-D18*	3849 PT: 10,13,19 / 1861	C. Schiklenk
3968	*h⁺, ade6-M210, his7-366, leu1-32, lys1-131*	28 x 1283	C. Schiklenk
3969	*h⁻, ura4-D18*	28 x 1283	C. Schiklenk
4005	*h⁺/h⁻, zas1⁺/Δzas1::kanMX,ade6-M210/ade6-M216*	2457 PT:10, 154, 155 / 237	C. Schiklenk
4006	*h⁺/h⁻, zas1⁺/zas1-712X::kanMX, ade6-M210/ade6-M216*	2457 PT: 10,159, 160 / 237	C. Schiklenk
4007	*h⁺/h⁻, zas1⁺/zas1-470X::kanMX, ade6-M210/ade6-M216*	2457 PT: 10, 152, 153 / 237	C. Schiklenk
4020	*h?, gcn5⁺, ChrI 2.49 Mb::LacO-natMX, ChrI 1.5 Mb::TetO-HygMX, LacI-eGFP::his7⁺, TetR-tdTomato::leu1⁺, lys1-131, ura4-D18, ade6-M210*	2779 x LY3476	Bernard Lab
4021	*h? gcn5-47, ChrI 2.49 Mb::LacO-natMX, ChrI 1.5 Mb::TetO-HygMX, LacI-eGFP::his7⁺, TetR-tdTomato::leu1⁺, lys1-131, ura4-D18, ade6-M210*	2779 x LY3476	Bernard Lab
4024	*h⁺, ade6-, zas1-470X::kanMX*	4007 tetrad dissection	C. Schiklenk
4025	*h⁻, ade6-, zas1-470X::kanMX*	4007 tetrad dissection	C. Schiklenk
4026	*h⁻, ade6-, zas1-712X::kanMX*	4006 tetrad dissection	C. Schiklenk
4027	*h⁺, ade6-, zas1-712X::kanMX*	4006 tetrad dissection	C. Schiklenk
4035	*h⁺/h⁻, zas1⁺/zas1-274X::kanMX, ade6-M210/ade6-M216*	2457 PT: 10,169, 170 / 237	C. Schiklenk
4036	*h⁺/h⁻, zas1⁺/zas1-360X::kanMX, ade6-M210/ade6-M216*	2457 PT: 10,171, 172 / 237	C. Schiklenk
4037	*h⁻, zas1-360X::kanMX, ade6-*	4036 tetrad dissection	C. Schiklenk

continued on next page.

#	Genotype	Origin	Created by
4046	*h^+/h^-, $zas1^+$/zas1-289X::kanMX, ade6-M210/ade6-M216*	2457 PT: 10,175, 176 / 237	C. Schiklenk
4047	*h^-, zas1-289X::kanMX, ade6-*	4046 tetrad dissection	C. Schiklenk
4048	*h^+, zas1-289X::kanMX, ade6-*	4046 tetrad dissection	C. Schiklenk
4083	*h^+/h^-, $zas1^+$/zas1-cDNA-natMX, ade6-M210/ade6-M216*	2457 PT: 10, 165 / 2302	C. Schiklenk
4093	*h^+/h^-, $zas1^+$/zas1-ΔZF::natMX, ade6-M210/ade6-M216*	2457 PT: 10, 165 / 2326	C. Schiklenk
4094	*h^-, zas1-Y289X::kanMX, ChrI 2.49Mb::TetO-hphMX, LacO::$lys1^+$, TetR-tdTomato-natMX::$zfs1^+$, LacI-GFP::$his7^+$, lys1-131, ura4-D18, ade6-M210*	2926 PT: 10, 175, 176 / 237	C. Schiklenk
4098	*h^+/h^-, $zas1^+$/zas1-cDNAΔ(267-282)-natMX, ade6-M210/ade6-M216*	2457 PT: 10, 165 / 2320	C. Schiklenk
4099	*h^-, zas1-cDNA-natMX, ade6-*	4083 tetrad dissection	C. Schiklenk
4100	*h^+, zas1-cDNA-natMX, ade6-*	4083 tetrad dissection	C. Schiklenk
4106	*h^-,zas1-K833X::kanMX, ChrI 2.49Mb::TetO-hphMX, LacO::$lys1^+$, TetR-tdTom-natMX::$zfs1^+$, LacI-GFP::$his7^+$, lys1-131, ura4-D18, ade6-M210*	2926 PT: 10, 220, 221 / 237	Carlo Klein
4114	*h^+/h^-, $zas1^+$/zas1-cDNAΔ(103-267)-natMX, ade6-M210/ade6-M216*	2457 PT: 10, 165 / 2353	Carlo Klein
4118	*h^+, zas1-cDNAΔ(103-267)-natMX, ade6-*	4114 tetrad dissection	C. Schiklenk
4120	*h^-, zas1-PK_6-kanMX*	28 PT: 64, 65 / 75	C. Schiklenk
4215	*h?, $cut14^+$, ura4-D18, ade6-M210, lys1-131, TetR-tdTomato::$leu1^+$, LacI-GFP::$his7^+$, ChrI 1.95 Mb::LacO-natMX, ChrI 1.5 Mb::TetO-hphMX*	2774 x LY3831	Bernard Lab
4217	*h?, cut14-208, ura4-D18, ade6-M210, lys1-131, TetR-tdTomato::$leu1^+$, LacI-GFP::$his7^+$, ChrI 1.95 Mb::LacO-natMX, ChrI 1.5 Mb::TetO-hphMX*	2774 x LY3831	Bernard Lab
4219	*h?, $gcn5^+$, ura4-D18, ade6-M210, lys1-131, TetR-tdTomato::$leu1^+$, LacI-GFP::$his7^+$, ChrI 1.95 Mb::LacO-natMX, ChrI 1.5 Mb::TetO-hphMX*	2774 x LY3456	Bernard Lab
4221	*h?, gcn5-47, ura4-D18, ade6-M210, lys1-131, TetR-tdTomato::$leu1^+$, LacI-GFP::$his7^+$, ChrI 1.95 Mb::LacO-natMX, ChrI 1.5 Mb::TetO-hphMX*	2774 x LY3456	Bernard Lab
4303	*h^+/h^-, cnd2-PK_6-kanMX/$cnd2^+$, ade6-M210/ade6-M216*	2457 PT: 125, 128, 388, 389 / 75	C. Schiklenk
4386	*h^+/h^-, ade6-M210/ade6-M216, $zas1^+$/zas1::zas1-cDNA-S281A-natMX*	2457 PT: 10, 165 / 2339	C. Schiklenk
4387	*h^+/h^-, ade6-M210/ade6-M216, $zas1^+$/zas1::zas1-cDNAΔ(P212-C254)-natMX*	2457 PT: 10, 165 / 2651	C. Schiklenk
4389	*h^+/h^-, $zas1^+$/zas1::zas1-cDNA-S281D-S282N-natMX, ade6-M210/ade6-M216*	2457 PT: 10, 165 / 2338	C. Schiklenk
4390	*h^+/h^-, ade6-M210/ade6-M216, $zas1^+$/zas1::zas1-cDNA-Δ(98-261)-natMX*	2457 PT: 10, 165 / 2650	C. Schiklenk
4415	*h^+/h^-, $zas1^+$/zas1::zas1-cDNA-V276K F280K-natMX, ade6-M210/ade6-M216*	2457 PT: 10, 165 / 2772	C. Schiklenk
4445	*h^+/h^-, $zas1^+$/zas1-590X::kanMX, ade6-M210/ade6-M216*	2457 PT: 10, 320, 321 / 273	C. Schiklenk
4446	*h^+, zas1-590X::kanMX, ade6-*	4445 tetrad dissection	C. Schiklenk
4470	*h^+/h^-, ade6-M210/ade6-M216, $zas1^+$/zas1ΔNLS (E9-R17)*	2457 PT: 10, 165 / 2771	C. Schiklenk
4477	*h^-, ura4-D18, $srk1^+$::EGFP-LacI $ura4^+$ tetR-tdTomato*	3969 LPI: AatII / 2872	C. Schiklenk
4484	*h^+/h^-, $zas1^+$/zas1::zas1Δ(103-267)-natMX, $cnd1^+/\Delta P_{cnd1}$::kanMX-P_{cnd3}-cnd1, ade6-M210/ade6-M216*	4114 PT: 348, 349, 350, 351 / 2856	C. Schiklenk
4485	*h^+/h^-, $cnd1^+/\Delta P_{cnd1}$::kanMX-P_{cnd3}-cnd1, ade6-M210/ade6-M216*	2457 PT: 348, 349, 350, 351 / 2856	C. Schiklenk
4486	*h^+/h^-, $zas1^+$/zas1::zas1(98-261)to(TEV_2PK_6)-natMX, ade6-M210/ade6-M216*	2457 PT: 10, 165 / 2823	C. Schiklenk
4487	*h^-, $zas1^+$::zas1(98-261)to(TEV_2PK_6)-natMX, ade6-*	4486 tetrad dissection	C. Schiklenk
4488	*h^+, $zas1^+$::zas1(98-261)to(TEV_2PK_6)-natMX, ade6-*	4486 tetrad dissection	C. Schiklenk
4489	*h^+, zas1::zas1Δ(103-267)-natMX, ΔP_{cnd1}::kanMX-P_{cnd3}-cnd1, ade6-*	4484 tetrad dissection	C. Schiklenk
4490	*h^-, zas1::zas1Δ(103-267)-natMX, ΔP_{cnd1}::kanMX-P_{cnd3}-cnd1, ade6-*	4484 tetrad dissection	C. Schiklenk
4503	*h^+/h^-, $cnd1^+$/cnd1-PK_6-kanMX, ade6-M210/ade6-M216*	2457 PT: 356, 357, CK14, CK16 / 75	C. Schiklenk
4504	*h^+, cnd1::cnd1-PK_6 kanMX, ade6-*	4503 tetrad dissection	C. Schiklenk
4505	*h^-, cnd1::cnd1-PK_6 kanMX, ade6-*	4503 tetrad dissection	C. Schiklenk
4507	*h^-, ura4-D18, $srk1^+$::EGFP-LacI-$ura4^+$-tetR-tdTomato, ChrI 2.49Mb::pTetO hphMX*	4477 LPI: XcmI / 2880	C. Schiklenk
4508	*h^+/h^-, $SPAC713.13^+$/ ΔSPAC713.13::kanMX, ade6-M210/ade6-M216*	2457 PT: 360, 361, 362, 363 / 237	C. Schiklenk

continued on next page.

#	Genotype	Origin	Created by
4509	*h^+/h^-, SPBC887.16$^+$/ ΔSPBC887.16::kanMX, ade6-M210/ade6-M216*	2457 PT: 364, 365, 366 / 237	C. Schiklenk
4510	*h?, ΔSPAC713.13::kanMX, ade6-*	4508 tetrad dissection	C. Schiklenk
4511	*h?, ΔSPBC887.16::kanMX, ade6-*	4509 tetrad dissection	C. Schiklenk
4542	*h^-, ura4-D18, urg1::Purg1-TEV protease-HA6-TEVsite-TEVsite-NLS-TEV protease-myc3-NLS2-Turg1 ura4$^+$::urg1$^+$*	3969 LPI: BstBI / 2917	C. Schiklenk
4543	*h^+/h^-, cnd1$^+$/cnd1-PK$_6$-kanMX, zas1$^+$/zas1-K833X::natMX, ade6-M210/ade6-M216*	4503 PT: 10, 220, 221 / 237	C. Schiklenk
4544	*h?, cnd1::cnd1-PK$_6$-kanMX, zas1$^+$, ade6-*	4543 tetrad dissection	C. Schiklenk
4545	*h?, cnd1::cnd1-PK$_6$ kanMX, zas1-K833X-natMX, ade6-*	4543 tetrad dissection	C. Schiklenk
4572	*h^+/h^-, zas1$^+$/zas1-Y289X kanMX, klf1$^+$/Δklf1::natMX*	4046 PT: 216, 217, 233, 234 / 467	C. Schiklenk
4573	*h^-, Δklf1::natMX*	4572 tetrad dissection	C. Schiklenk
4574	*h^+, Δklf1::natMX*	4572 tetrad dissection	C. Schiklenk
4575	*h^-, Δklf1::natMX, zas1-Y289X::kanMX*	4572 tetrad dissection	C. Schiklenk
4576	*h^+, Δklf1::natMX, zas1-Y289X::kanMX*	4572 tetrad dissection	C. Schiklenk
4610	*h^+/h^-, cnd2$^+$/cnd2-PK$_6$ kanMX, zas1$^+$/zas1-K833X natMX, ade6-M210/ade6-M216*	4303 PT: 10, 220, 221 / 237	C. Schiklenk
4642	*h^+/h^-, puc1-PK$_6$ kanMX/puc1$^+$, ade6-M210/ade6-M216*	2457 PT: 414, 415, 416, 420 / 75	C. Schiklenk
4643	*h^+, puc1-PK$_6$ kanMX, ade6-*	4642 tetrad dissection	C. Schiklenk
4644	*h^-, puc1-PK$_6$ kanMX, ade6-*	4642 tetrad dissection	C. Schiklenk
4648	*h^+/h^-, ade6-M210/ade6-M216, cnd1$^+$/kanMX-ΔP$_{cnd1}$*	2457 PT: 348, 349, 408, 409 / 2856	C. Schiklenk
4674	*h^+/h^-, puc1-PK$_6$ kanMX/puc1$^+$, zas1$^+$/zas1-K833X natMX, ade6-M210/ade6-M216*	4642 PT: 10, 220, 221 / 237	C. Schiklenk
4675	*h?, puc1-PK$_6$ kanMX, zas1-K833X natMX, ade6-*	4674 tetrad dissection	C. Schiklenk

4.13 List of oligonucleotides

Table 4.16: List of oligonucleotides. P- indicates 5' phosphorylation

#	Name	Sequence 5'→3'	Designed by
1	Rtz1 CDS rev-XhoI	ATTATTAAC CTCGAG TTAATCATTTCCCTTGGATAATAATTG	C. Schiklenk
2	Rtz1 3UTR rev-XhoI	ATTATTAAC CTCGAG AGAAATATTTAATAAGATGTCATAAGCTGC	C. Schiklenk
3	Rtz1B proof fw	ATTATTAAC GCGGCCGCG GTATGTTAAATGCTTCCTGCTTTCTTG	C. Schiklenk
4	Rtz1 W5 fw	CATTGTTAGCTGAG A AGCATCACTGGGAAG	C. Schiklenk
5	Rtz1 W5 rev	CTTCCCAGTGATGCT T CTCAGCTAACAATG	C. Schiklenk
6	Rtz1 AJ3 fw	TGGGCGAACAT T AAAAAATCATACAAC	C. Schiklenk
7	Rtz1 AJ3 rev	GTTGTATGATTTTTT A ATGTTCGCCCA	C. Schiklenk
8	Rtz1 Ts34 fw	GATATGTAAAAATATG A GCGAATACTGAGAATG	C. Schiklenk
9	Rtz1 Ts34 rev	CATTCTCAGTATTCGC T CATATTTTTACATATC	C. Schiklenk
10	Rtz1 S2-rev	ATTTAATAAGATGTCATAAGCTGCTATAACTTCGAGTAGATT-TATAA TCGGCATTAAATAAAATTTACCTCAGTTTATAAT	C. Schiklenk
11	Rtz1 S2-rev-syn	ATCGATGAATTCGAGCTCG AGTAAGAAAATTAAGCAAAAAATACATAAAAAGGTTACCT-GAGTTT AATAATTAATTTTTTATTCCAGAAAT	C. Schiklenk
12	Rtz1 S3-fw +T	ATTTAATAAGATGTCATAAGCTGCTAT TCCAGTTTATTCGTGTATACTAATTAACCAGTGGGCGAA-CATAAAA AAATCATACAACAATTATTATCCAAGGGAAATGAT T CGTACGCTGCAGGTCGAC	C. Schiklenk
13	Rtz1 S3-fw-syn	CCAATAATTCTCCATGTCGTACTACAGGCGTTGGATGTATTCC-CTTG GGACCTTTGTAAGTAATCACCAAA	C. Schiklenk
14	pYM16 TEV fw	TCCAGTTTATTCGTGTATACTAATTAAC GAAAATCTTTATTTTCAAGGTTCT	C. Schiklenk
15	S3	TCCGGTTCTGCTGCTAGATACC GTCGACCTGCAGCGTACG	C. Schiklenk
16	Rtz1 CDS rev-SacI	ATTATTAAC GAGCTC TTAATCATTTCCCTTGGATAATAATTG	C. Schiklenk
17	Rtz1 W5 PL rev	TCTCAGCTAACAATGGCATGGAAAC	C. Schiklenk
18	Rtz1 W5 PL fw	GAGCATCACTGGGAAGCCGAAAATT	C. Schiklenk
19	Rtz1 S3-fw 2	TCCAGTTTATTCGTGTATACTAATTAACCAGTGGGCGAA-CATAAAAA AATCATACAACAATTATTATCCAAGGGAAATGAT CGTACGCTGCAGGTCGAC	C. Schiklenk
20	Rtz promoter fw NotI	TTATTAAC GCGGCCGC GGCTTATGGGTTTTAGACCAAAG	C. Schiklenk
21	Rtz 3'UTR rev SacI	TTATTAAC GAGCTC TGCTGTAACATTTCTTACAAATGG	C. Schiklenk
22	Cut14 prom fw NotI	ATTATTAC GCGGCCGC TTGTGTAGTGAGTGCAGTACTGAT	C. Schiklenk
23	Cut14 3'UTR rev AscI	GTAATAAT GGCGCGCC ATCAACAACAAGGGTAGGAGAC	C. Schiklenk
24	pBS AscI fw	P-GTTCCCTTTAGTGAGGGTTAATTTCG	C. Schiklenk
25	pBS AscI rev	P-GGCGCGCC AAAAGCTGGGTACCGGGC	C. Schiklenk
26	seq Rtz1-Exon5 fw	GGTTCCTTTCATTTGCAGCC	C. Schiklenk
27	seq Rtz1-Exon5 rev	AAAAGTTCCCCTATGCAAAATGG	C. Schiklenk
28	seq GFP ct	GTTACAAACTCAAGAAGGACC	C. Schiklenk
29	T7	TAATACGACTCACTATAGGG	C. Schiklenk
30	M13	TGTAAAACGACGGCCAGT	C. Schiklenk
31	S2	ATCGATGAATTCGAGCTCG	C. Schiklenk
32	Exon2 rev	CTAGAAGAAAACTCGTTAATAAGC	C. Schiklenk
33	PacI Kan rev	TTATTAAC TTAATTAA TTAGAAAAACTCATCGAGCAT	C. Schiklenk
34	FseI Kan fw	TTATTAAC GGCCGGCC ACAATAAAACTGTCTGCTTACATA	C. Schiklenk
35	pBS PacI f Kan fw	TTATTAAC TTAATTAA CCGCAAAAAAGGGAATAAG	C. Schiklenk
36	pBS FseI f Kan rev	TTATTAAC GGCCGGCC TCATGACCAAAATCCCTTAAC	C. Schiklenk
37	new AJ3 fw	GGCGAACAT T AAAAAATCATACAAC	C. Schiklenk
38	new AJ3 rev	ATGATTTTTT A ATGTTCGCCCA	C. Schiklenk
39	Rtz ncRNA fw	ATCCAACGCCTGTAGTACGAC	C. Schiklenk
40	Rtz ncRNA rev	CTTAACCTTGCAACAATGGC GAGAGCT	C. Schiklenk
42	pUR19 MCS rev	GAATTCAAGCTTATCGATACCGTCGACCTCGAGGGGCCCG GTACCCAGCTTTTGGCGCGCCACTGGCCGTCGTTTTACAAC GAGAGCT	C. Schiklenk
43	pUR19 MCS fw	GAATTCCTGCAGCCCGGGGGATCCACTAGTTCTAGAGCGGC CGCCACCGCGGTGGAGCTCGGCGTAATCATGGTCATAGC AGGCATGCAAGCTTGGC	C. Schiklenk
44	cut3 L23 NotI fw	GAGAGCT GCGGCCGC GAACACAAATCTCGGCTCCGCG	C. Schiklenk
45	cut3 L23 NotI rev	GAGAGCT GCGGCCGC TATACAATTCCTTTGCGCAG	C. Schiklenk
46	cut3 M26 AscI fw	GAGAGCT GGCGCGCC CAACTCATCCTTCTCTCG	C. Schiklenk
47	cut3 M26 NotI rev	GAGAGCT GCGGCCGC TTAGAAGACAGGATATTCCG	C. Schiklenk
48	cnd3 J29 NotI fw	GAGAGCT GCGGCCGC GAGATAGACATTGTTCAACC	C. Schiklenk
49	cnd3 J29 NotI rev	GAGAGCT GCGGCCGC ACACTGAACGTACGAAAG	C. Schiklenk
50	sts5 AJ5 NotI fw	GAGAGCT GCGGCCGC CCACTTGCGTCAGGAATTC	C. Schiklenk
51	sts5 AJ5 NotI rev	GAGAGCT GCGGCCGC TTCGAGCTCCTTGGCTATG	C. Schiklenk
52	bgs4 S15 AscI fw	GAGAGCT GGCGCGCC ACCAGTTGTCTCGTGTCAC	C. Schiklenk
53	bgs4 S15 NotI rev	GAGAGCT GCGGCCGC GCGCAACCCAAACAGTCATAG	C. Schiklenk
54	cut3 ORF fw	AAAACGACGGCCAGT GGCGCGCC ATGTCTGACAAGGGCATCTTTC	C. Schiklenk
55	sts5 ORF rev	AGCTCCACCGCGGTGGCGGCCGCTCAAAACTCGA-CATTTGAAACG	C. Schiklenk
56	colE1 seq rev	CGCCTGGTATCTTTATAGTCCTG	C. Schiklenk
57	ura4 prom fw	AGCTACAAATCCCACTGGC	C. Schiklenk
58	ura4 cds fw	ATGGATGCTAGAGTATTTCAAAGC	C. Schiklenk
59	ura4 cds 3' fw	GGAAGGCATATCAGCAAAGAC	C. Schiklenk
60	sts5 ORF fw	AAAACGACGGCCAGT GGCGCGCC ATGGATGAGGAGTTTGAAAATG	C. Schiklenk
61	bgs4 rev NotI	GCGGCCGCTTTTGTGAACCAATGGGAATTC	C. Schiklenk
62	bgs4 SpeI fw	TTACGACACTAGTATCGTTCCACG	C. Schiklenk
63	cnd3 J29 rev full-length	AGCTCTC GCGGCCGC TATGTCTTTGGCAAACTTTC	C. Schiklenk

continued on next page.

#	Name	Sequence 5'→3'	Designed by
64	rtz1-fw for PK6 tagging	TCCAGTTTATTCGTGTATACTAATTAACCAGTGGGCGAACATA AAAAAATCATACAACAATTATTATCCAAGGGAAATGAT TCCGGTTCTGCTGCTAG	C. Schiklenk
65	rtz1-rev for PK6 tagging	ATTTAATAAGATGTCATAAGCTGCTATAACTTCGAGTAGATTTA TAATCGGCATTAAATAAAATTTACCTCAGTTTATAATTTA GAAAGATCTGTTTAGCTTGCC	C. Schiklenk
66	pKM40-mcm4C fw seq	CAACTGATCCTGCAACAGGA	C. Schiklenk
67	pKM40-mcm4DWrev seq	GAATCATGGCGAATTATTGGTTACG	C. Schiklenk
68	pKM40 seq 1	TAACCAAGTTTTATCTTGTTTGTC	C. Schiklenk
69	pKM40 seq 2	CCTATTTAGAGAAAGAATGCTG	C. Schiklenk
70	rtz1-IAA CT tag fw	TCCAGTTTATTCGTGTATACTAATTAACCAGTGGGCGAACATA AAAAAATCATACAACAATTATTATCCAAGGGAAATGAT CGAGCATACCCATACGATG	C. Schiklenk
71	rtz1-IAA CT tag rev	ATTTAATAAGATGTCATAAGCTGCTATAACTTCGAGTAGATTTA TAATCGGCATTAAATAAAATTTACCTCAGTTTATAATGCTTGT-GATATTGACGAAAC	C. Schiklenk
72	rtzNT1 200ups fw BlpI	AGCTCTC GCTTAGC GAACATAGCACAAATCATTTC	C. Schiklenk
73	rtzNT2 200ups rev BlpI	ATTTGTA GCTAAGC CAGATCGTAAAATCGTATGC	C. Schiklenk
74	rtzNT3 prom fw	GGCCAGT GGCGCGCC TGAACTTACTTTTTTCATAAACAC	C. Schiklenk
75	rtzNT4 cds Xho rev	GTCGAC CTCGAG GATTATTCTCAGAGTATTGTGG	C. Schiklenk
76	rtzNT5 AgeI ins fw	GAGCTAAAAG ATGACCGGT ATGTCAAATGAGGAATCTTTTAC	C. Schiklenk
77	rtzNT6 Age ins rev	CATTTGACA TACCGGTCAT CTTTTAGCTCAACTTTTACTAAG	C. Schiklenk
78	rtzNT1 long	GCTCGAGCTCTC GCTTAGC GAACATAGCACAAATCATTTC	C. Schiklenk
79	rtzNT2 long	GCTCGAGATGTGTA GCTAAGC CAGATCGTAAAATCGTATGC	C. Schiklenk
80	NT-6HA-2Presc fw	GAGCGAGTGGATG ACCGGT AGATACCCATACGATGTTCC CATTTCCACTCGCTC ACCGGT AGGACCTTGAAAAAGAACTTC	C. Schiklenk
81	NT-6HA-2Presc rev	CAAAGGACCTTGAAAAAGAACTTCCAAGCTAGA AGCGTAATCTGGAAC	C. Schiklenk
82	NT6HA-810 fw	GAGCGAGTGGATG ACCGGT TCAAGATCCACCATGCCTAGATAC	C. Schiklenk
83	NT6HA-810 rev	CATTTCCACTCGCTC ACCGGT AGATCTGGCCGGCCTGTTCC-TAGAAGATCTGGCCGGCCTGTTCCTAGA	C. Schiklenk
84	rtzNT5-A AgeI ins fw	GAGCTAAAAG ACCGGT ATGTCAAATGAGGAATCTTTTAC	C. Schiklenk
85	rtzNT6-A Age ins rev	CATTTGACAT ACCGGT CTTTTAGCTCAACTTTTACTAAG	C. Schiklenk
86	rtzNT-3mCh fw	GAGCGAGTGGATG ACCGGT ATGGTGAGCAAGGGCGAGG	C. Schiklenk
87	rtzNT-3mCh rev	GAGCGAGTGGATG ACCGGT CTTGTATAACTCGTCCATGCCA	C. Schiklenk
88	NT6HA-810 rev corr	CATCCACTCGCTC ACCGGT AGGACCTTGAAA-CAAAACTTCAAGAGGACCTTGAAACAAAACTTCAAG GGCCGGCCTAGATCTGTTC	C. Schiklenk
89	DBH fw syn	ACCTTGGCCTCTCCTGAATTGGAGGAGAAAATGGACAT-GAATCTTTTCAAGGTATACTGCATGTTTTT GGAAGTACGTAATCAATTTGAC	C. Schiklenk
90	DBH-IAA17 fw	GGAAGTACGTAATCAATTTGAC GCTAAATTCAGAAAGATGTGGGCACGA GCATACCCATACGATG	C. Schiklenk
91	DBH-IAA17 rev	AGAAAAAACAGAATAAAGCCATACAACATCAACTAAAAAG-TAAAAGCAACAGCGCAAAATTTA GCTTGTGATATTGACGAAAC	C. Schiklenk
92	DBH rev syn	CTCAAGAAGACGTGCTATAACTCCAAAAAAACATTCTAT-GACGCTCAATCAATTCTCTAATTTTCAA AGAAAAAACAGAATAAAGCCAT	C. Schiklenk
93	DBH S1	GGAAGTACGTAATCAATTTGAC GCTAAATTCAGAAAGATGTGGGCACGA TCGTACGCTGCAGGTCGAC	C. Schiklenk
94	DBH S3	AGAAAAAACAGAATAAAGCCATACAACATCAACTAAAAAG-TAAAAGCAACAGCGCAAAATTTA ATCGATGAATTCGAGCTCG	C. Schiklenk
114	rtz1 qPCR fw	AAACGTTCCCGGGCTCATAG	C. Schiklenk
115	rtz1 qPCR rev	ACACATCGCTTCTAGCAAATGC	C. Schiklenk
116	NT pipo tRNA 1 fw AscI	GAGCGAGTGGATG GGCGCGCC GAACATAGCACAAATCATTTC	C. Schiklenk
117	NT pipo tRNA 1 rev NcoI	CATCCACTCGCTC CCATGG CAGATCGTAAAATCGTATGC	C. Schiklenk
118	NT pipo tRNA 1 rev AgeI	CATCCACTCGCTC ACCGGT CAGATCGTAAAATCGTATGC	C. Schiklenk
119	NT Pnmt 2 fw NcoI	GAGCGAGTGGATG CCATGG GATC TCGCCATAAAAGACAG	C. Schiklenk
120	NT Pnmt 2 fw AgeI	GAGCGAGTGGATG ACCGGT GATC TCGCCATAAAAGACAG	C. Schiklenk
121	NT Pnmt 2 rev AgeI	CATCCACTCGCTC ACCGGT AAGACAT GATTTAACAAAGCG	C. Schiklenk
122	Presc2HA6 fw	CATCCACTCGTC GTCGAC TCTAGCTTAGAAGTTTTGTTCC	C. Schiklenk
123	Presc2HA6 rev	CATCCACTCGTC GGCGCGCC AGAAACTTTGCAGCACACTAT	C. Schiklenk
124	CT 6HA rev SacI	CATCCACTCGTC GAGCTC TCCACTTTTTAGCTAGAAGCG	C. Schiklenk
125	cnd2 CT-tag fw syn	AAAGATATATCCACCAGTTTTGCCTTTATTTGTGTTTTA-CATTTGGCGAATGAACATAATTTAGAGCTTACAA GCAACGAAGATTTTTCAGATGT	C. Schiklenk
126	cnd2 CT-tag fw S1	GCAACGAAGATTTTTCAGATGT TTTTATTAGGCCAGGTCC-TAACTTGACGACGCTAGAAGCATTAGAAAATGATGTT CGTACGCTGCAGGTCGAC	C. Schiklenk
127	cnd2 CT-tag rev S2	CACGCTAGCTAAAAGTATGCG ATGATGACTAATTAATGAT-GACCTGCATCATTTCGATTCTACACACTTTA ATCGATGAATTCGAGCTCG	C. Schiklenk
128	cnd2 CT-tag rev syn	TACGAGCTAGTGTTTTTATTATTCAAGGTAGATCAAAAAGAG-TATAATTTCCGGC-TATCTTGAAAATGATTCACGCTAGCTAAAAGTATGCG	C. Schiklenk
129	pKM40 S2 fw	CTTGGTACCGAATTCCGAGCTCGAATTCATCGATCTCGAG-GATCCAGATC	C. Schiklenk
130	pKM40 S2 rev	GATCTGGATCCTCGAGATCGATGAATTCGAGCTCGGAATTCG-GTACCAAG	C. Schiklenk
131	pKM40 S1 fw	P-CGTACGCTGCAGGTCGAC CGAGCATACCCATACGAT	C. Schiklenk

continued on next page.

#	Name	Sequence 5'→3'	Designed by
132	pKM40 S1 rev	P-ATGTACCCAATTCGCCCTA	C. Schiklenk
133	his7-locus seq fw	GACTGTTTCCTAACCAAGCAAGG	C. Schiklenk
134	his7-locus seq rev	AGTAGCTTACTTCTCAGGAGATGG	C. Schiklenk
135	ade6 3'UTR fw AscI	GAGCGAGTGGATG GGCGCGCC ATTATTCTGCATAGGCGACCATAG	C. Schiklenk
136	vct4 3' cds fw AscI	GAGCGAGTGGATG GGCGCGCC TTACTTTTGCTGCAATCAGCG	C. Schiklenk
137	rtz1-A743G fw	GCCTGATTTGAATGTAAATGTTGATC	C. Schiklenk
138	rtz1-A743G rev	CATTTACATTCAAATCAGGCTCACC	C. Schiklenk
139	AtTIR cds 5' fw AscI	GAGCGAGTGGATG GGCGCGCC ATGCAGAAGCGAATAGCCTTG	C. Schiklenk
140	AtTIR cds 5' rev	CCAGCTGAATAAACGAGAACAC	C. Schiklenk
141	OsTIR cds 5' fw NotI	GAGCGAGTGGATG GCGGCCGC ATGTCCGAGGAGGACGACG	C. Schiklenk
142	OsTIR cds 5' rev	TTGTCGAGCACCTGGTCCG	C. Schiklenk
143	OsTIR cds 3' rev NotI	GAGCGAGTGGATG GCGGCCGC TTATAGGATCTTCACGAATGGTG	C. Schiklenk
144	OsTIR cds 3' fw	CATGTATCGGTCGCTTGAAG	C. Schiklenk
146	rtz1-5UTR NotI fw	GAGCGAGTGGATG GCGGCCGC CGGTATTCCTGCTACTTCTTAG	C. Schiklenk
147	Pnmt fw NcoI	GAGCGAGTGGATG CCATGG TTATCGCCATAAAAGACAGAATA	C. Schiklenk
148	Pnmt rev AgeI	GAGCGAGTGGATG ACCGGT AGATTTAACAAAGCGACTATAAGTC	C. Schiklenk
149	GFP 3Prime fw	ATTACCTGTCCACACAATCTGC	C. Schiklenk
150	E2 Crimson fw NotI	GAGCGAGTGGATG GCGGCCGC ATGGATAGCACTGAGAACGTC	C. Schiklenk
151	E2 Crimson rev AscI	GAGCGAGTGGATG GGCGCGCC CGCCACCACCTGTTCCAG	C. Schiklenk
152	rtz-ncR-KO syn fw	AAACAAGAATTTGGGCCTCCTGTTTCCCTGTGGGTCTAT-CAAGCTTTATTTTTGATACA AGTCTTTGAATTATTTACTAGTAATCTC	C. Schiklenk
153	rtz-ncR-KO S1 fw	AGTCTTTGAATTATTTACTAGTAATCTCAAACAACACCG-GCTTGCCCAGATGTTCCACCCTAGCTAGGTAG CGTACGCTGCAGGTCGAC	C. Schiklenk
154	rtz-KO S1 fw	TGTAAGGAGTCAACTTTACCCCCACATCCTTCGACGAGAC-TAAGTGGATGTCTTAGTAAAAGTTGAGCTAAAAG CGTACGCTGCAGGTCGAC	C. Schiklenk
155	rtz-KO syn fw	AATAGTACGGTATTCCTGCTACTTCTTAGTTTCTTCCACCAT-ACTTTTCTAACACAGTAT TGTAAGGAGTCAACTTTACCCC	C. Schiklenk
156	rtz 1-1739 KO rev	CTTAATAAGTTAGCCTCTAGCATATATTATTTATAATATGAT-TACCTCAATTAAAACAGGGTGGAACATCTG ATCGATGAATTCGAGCTCG	C. Schiklenk
157	rtz 1-1739 KO syn rev	TATTCGATTCTCCAAATGTCTCTGACCGGACGGTGAGCG-CATCAGATGGAATCGCTTGACGCATGGC CTTAATAAGTTAGCCTCTAGCAT	C. Schiklenk
158	ura4 rev	TCCCAAGGTGTTTATCTATAATAG	C. Schiklenk
159	rtz1 KO764-897 Ts34 syn fw	ACTTTATAATTTAGCATGCATCTACTCAAAGACCCGTCTAACC-TATTTACAGGCTTTTGCCAAAGCTGT CACCGATCCGGTAGATGGTTC	C. Schiklenk
160	rtz1 KO764-897 Ts34 S1 fw	CACCGATCCGGTAGATGGTTC TGTAACCTCAAAAACTGTTGCACCGTTACGATATGTAAAAATA TGATAACTAAGTAA CGTACGCTGCAGGTCGAC	C. Schiklenk
161	swi6 CT-tag syn fw	GATGGAACCTTGGAAATTTATCTGACTTGGAAGAACGGTG-CAATATCTCATCATCCTAGTACTATCA CCAATAAAAAATGTCCTCAGAAG	C. Schiklenk
162	swi6 CT-tag fw	CCAATAAAAAATGTCCTCAGAAG ATGCTTCAATTTTAT-GAAAGCCACTTAACGTTCCGTGAAAATGAA CGTACGCTGCAGGTCGAC	C. Schiklenk
163	swi6 CT-tag rev	CGTCAGAAAAAAGCGAAATCT AATTTATAAACAAAAGAAAAA-GAATTTTTTAAAGGAACACAAAAAAA ATCGATGAATTCGAGCTCG	C. Schiklenk
164	swi6 CT-tag syn rev	GCATTTTTCGAGTAAGAGAACAAGAACTCATACTACGA-CACGGGACTTGATAAAAGCAATAA CGTCAGAAAAAAGCGAAATCT	C. Schiklenk
165	Prtz1 qPCR II fw	GATGAATGTACAGAAGGCTGC	C. Schiklenk
166	Prtz1 qPCR II rev	TTAGTCTCGTCGAAGGATGTG	C. Schiklenk
167	rtz1 5' fw	GGTGACCCTAGATTCTATTGCAC	C. Schiklenk
168	swi6 3Prime fw	CTATGATTCTTGGGAAGACTTGG	C. Schiklenk
169	deltaMotif fw inner	CTCGACTGGACTTACAGGGAGA TTGTACTTGTATTTT-TAAAAATAGATCTTCCATCGCCTCCTCTAGGACTATGGATTAA CGTACGCTGCAGGTCGAC	C. Schiklenk
170	deltaMotif fw outer	GATACAAGGCCTGTATCCTCGTACCCAGATGAATTAACT-CAACTTGAGTCTAATCCTGATTCATTTT CTCGACTGGACTTACAGGGAGA	C. Schiklenk
171	deltaCTDomain inner	GGTATAGATTTACTATTTTATTAATACTAA TAAACATAGGGTTCCTTTCATTTGCAGCCTAATTTCCTTG-CAATGTTTACT CGTACGCTGCAGGTCGAC	C. Schiklenk
172	deltaCTDomain outer	GCCCAATGTATGTTCCTCAGAAATGTCCTGCTACCGTTTA-CAACAATTTGTTAAATTTTTTGGA GGTATAGATTTACTATTTTATTAATACTAA	C. Schiklenk
173	rtz1-exon5 mut fw	CATGCTCAAAAGTAAATCTAAAGGAGCC	C. Schiklenk
174	rtz1-exon5 mut rev	TAGATTTACTTTTGAGCATGATAACTTTGGG	C. Schiklenk
175	rtzD287-end fw outer	GGACTATGGATGATGTCGTCCGTTGGTTATTCTCATCTG-GTAAAAGACGACAAAAA TAACTAGCTAG CGTACGCTGCAGGTCGAC	C. Schiklenk
176	rtzD287-end fw inner	TCTCGACTGGACTTACAGGGAGATTGTACTTGTATTTT-TAAAAATAGATCTTCCATCGCCTCCTCTA GGACTATGGATGATGTCGTCCGT	C. Schiklenk
177	spZAS1 5' XhoI S317	AGAGG CTCGAG TCCATCGCCTCCTCTAGGACTATGG	C. Schiklenk
178	spZAS1 5' XhoI M378	AGAGG CTCGAG ATGTATGTTCCTCAGAAATGTCCTGCTACC	C. Schiklenk
179	spZAS1 3' D897 stop BamHI	AGAGG GGATCC TCA TTA ATCATTTCCCTTG-GATAATAATTGTTGTATGATTTTTTTATGTTCG	C. Schiklenk

continued on next page.

#	Name	Sequence 5'→3'	Designed by
180	C1 NotI Prtz fw	AAAGGCATGCCGATAGGTACCTCGCGGCGGCCGCTACGATTT-TACGATCTGAACTTAC	C. Schiklenk
181	C2 Prtz AscI rev	CTGTAAAAGATTCCTCATTTGACATGGCGCGCCCTTTTAGCT-CAACTTTTACTAAGAC	C. Schiklenk
182	C3 AscI rtz1 fw	GTCTTAGTAAAAGTTGAGCTAAAAGGGCGCGCCATGTCAAAT-GAGGAATCTTTTACAG	C. Schiklenk
183	C4 rtz1 AvrII rev	GCATTAAATAAAATTTACCTCAGTTTATAATTTACCTAGGAT-CATTTCCCTTGGATAATAATTG	C. Schiklenk
184	C5 AvrII Trtz fw	CAATTATTATCCAAGGGAAATGATCCTAGGTAAATTATAAACT-GAGGTAAATTTTATTTAATGC	C. Schiklenk
185	C6 Trtz NheI rev	GTATTCTGGGCCTCCATGTCGCTAGCTTAATAGTTACTGCTTT-TATTTCTAAGAA	C. Schiklenk
186	C7 NheI nat fw	TTCTTAGAAATAAAAGCAGTAACTATTAAGCTAGCGACATG-GAGGCCCAGAATAC	C. Schiklenk
187	C8 FseI nat rev	TAGGGGTTCCGCGCACATTTAGTTGGCCGGCCATCGAT-GAATTCGAGCTCGCAGTATAGCGACCAGCATTCACATAC	C. Schiklenk
188	rtz1 dmotif 276-282 rev	P-GACATCATCCATAGTCCTAGAGGAG	C. Schiklenk
189	rtz1 dmotif 276-282 fw	P-GGTAAAAGACGACAAAAATACGAATC	C. Schiklenk
190	rtz1 dZF 25-83 rev	P-AGGGTCACCAAGTCTATGAGCC	C. Schiklenk
191	rtz1 dZF 25-83 fw	P-AATCTAAGTGAAAGACCACCTCC	C. Schiklenk
192	rtz1 3ZF outer rev	P-GTCTTGCATTGATCAAGTTG ACATAATCATGAGCAAGCACA ACATAATCATGAGCAAGCACA	C. Schiklenk
193	rtz1 3ZF inner rev	CAGAAACCAAGAAAGCAGGAAGCATTTAACATTCTACG TTCACTTAGATTTTGTTTTTGAAGATG	C. Schiklenk
194	rtz1 3ZF outer fw	P-ATTTCATGATTGAACATTTCCTG TCTTTATTCGCATTCTGTCGTAC TCTTTATTCGCATTCTGTCGTAC	C. Schiklenk
195	rtz1 3ZF inner fw	AATTTTATTCAGCTTATTAACGAGTTTTCTTTTGGTTCCG CCTCCTCAGTTCTTTCACAGC	C. Schiklenk
196	spZAS1 5 XhoI M356 fw	AGAGGT CTCGAG ATGTTTACTTTGGAATCGGTCAG	C. Schiklenk
197	pGEX6P1 rev	P-GGATCCCAGGGGCCCCTGGAAC	C. Schiklenk
198	rtz1 M357 fw	P-ATGTTTACTTTGGAATCGGTCAGC	C. Schiklenk
199	chr2-0.35Mb outer fw	TATATATAAAATTGAGCAACCATATGGGTTAGAATTATCAA-GAAAAAATTAAGACTCTTAAA GTCCGTTAACGCCATAATGCAG	C. Schiklenk
200	chr2-0.35Mb inner fw	GTCCGTTAACGCCATAATGCAG ATATTATAATTTTTTCAAT-TATTTAACAGTAAACACATTAAGCAACTA TACGATTTTACGATCTGAACTTAC	C. Schiklenk
201	chr2-0.35Mb outer rev	GTTTTTATATTCAGTGGAAGTCAGGGCTATTAGACATATG-GTAGGACAACTGATCTTTT GCTACCTTTTCGTCTTCATCT	C. Schiklenk
202	chr2-0.35Mb S2 rev	GCTACCTTTTCGTCTTCATCT TTTTTCGTAATTGTTAAGTAC-TACTTACTCTGTTATAGTACTGATTTATCCATC ATCGATGAATTCGAGCTCG	C. Schiklenk
203	rtz1 S281D-S282N fw	P-GTCCGTTGGTTATTC GATAAC GGTAAAAGACGACAAAAATACGA	C. Schiklenk
204	rtz1 S281A fw	P-GTCCGTTGGTTATTC GCT TCTGGTAAAAGACGACAAAAATACGA	C. Schiklenk
205	rtz1 S281D-S282D fw	P-GTCCGTTGGTTATTC GATGAT GGTAAAAGACGACAAAAATACGA	C. Schiklenk
206	SPBC1271.09 5' rev	AGAACCCGACCGCCCTCCTGC	C. Schiklenk
207	SPBC1271.10c 3' fw	GAAGAGGTCAGGATGGGGTTG	C. Schiklenk
208	BamHI rtz fw	GGGCGCCATG GGATCC ATGTCAAATGAGGAATCTTTTACAG ATTCGAAA GCGGCCGC	C. Schiklenk
209	rtz NotI rev	TTAATCATTTCCCTTGGATAATAATTG	C. Schiklenk
210	rtz1 delta linker R102 rev	P-TCTCTCACCTGCCTCGCTGTG	C. Schiklenk
211	rtz1 delta linker S268 fw	P-TCCTCTAGGACTATGGATGATGTC	C. Schiklenk
212	3ZF repair rev	P-GCGAATAAAGACAGGAAATGTTC	C. Schiklenk
213	3ZF repair fw	P-ATTCTGTCGTACAATTTTATTCAGC GTTCATCAAATACTAACAGTTTTAGTGG	C. Schiklenk
214	klf1 CT-tag fw inner	TAGATGGTGTTCGCATTTTGTCTAAATTAGTACAGCTTT CGTACGCTGCAGGTCGAC	C. Schiklenk
215	klf1 CT-tag fw outer	GATGTGCTGTGCCCAGCTAGATGGGGTTTGTGTAAGTC-GATCTTTCGTAGTTGTATT GTTCATCAAATACTAACAGTTTTAGTGG	C. Schiklenk
216	klf1 CT-tag rev inner	GCGTAAATTAAAACTATGGATTAGAAATAATG TAAAAAATGC-TATAATACAAGAAATCGTTCGTTATACATCCTCAAG ATCGATGAATTCGAGCTCG	C. Schiklenk
217	klf1 CT-tag rev outer	ACTAGCTTAAATAAGTTATTTCTAATGATATTCTGAACATAT-TAATCACAAATATTCAAAAT GCGTAAATTAAAACTATGGATTAGAAATAATG	C. Schiklenk
218	W760X fw inner	GAGTCAGCTCCTCGTTATGATACTC TAATTTATCATTCTTG-GTGTTATTATGTTGCTGCTCTTGTTTTATAG CGTACGCTGCAGGTCGAC	C. Schiklenk
219	W760X fw outer	CGCGATATTCCACTTCTAATGCACTTGAGATATTAGATAT-GCTTTTAAGAGAAAAAATA GAGTCAGCTCCTCGTTATGATACTC	C. Schiklenk
220	K821X fw inner	CCCTTGGGACCTTTGTAAGTAATCACC AAATCCAGTT-TATTCGTGTATACTAATTAACCAGTGGGCGAACATTAA CGTACGCTGCAGGTCGAC	C. Schiklenk
221	K821X fw outer	GCAAAAACCCAATAATTCTCCATGTCGTACTACAGGCGTTG-GATGTATT CCCTTGGGACCTTTGTAAGTAATCACC	C. Schiklenk
222	tRNA prom fw	CAATGACTTTGGAAATACATGCATAGC	C. Schiklenk
223	NheI KanMX fw	AGAGG GCTAGC GGATCCCCGGGTTAATTAAGG	C. Schiklenk
225	KanMX S2 FseI rev	ACAGT GGCCGGCC ATCGATGAATTCGAGCTCG	C. Schiklenk
226	6hisTagATG rev	P-CATGGATCCCATGGCGCCCTG	C. Schiklenk
227	rtz1 S309 fw	P-TCCGATACTGACAGTAATTTTTTGAGC	C. Schiklenk

continued on next page.

#	Name	Sequence 5'→3'	Designed by
228	rtz1 D273 fw	P-GATGATGTCGTCCGTTGGTTATTC	C. Schiklenk
229	tdTom AvrII fw	TCCATA CCTAGG TCTAGGTACCTTATGGTGAGCAAGGGCG	C. Schiklenk
230	tdTom AvrII rev	AGTAGT CCTAGG CTTGTACAGCTCGTCCATGCC	C. Schiklenk
231	klf1 CT-tag fw inner - T	GTTCATCAAATACTAACAGTTTTAGTGG TAGATGGTGTTCGCATTTTGTCTAAATTAGTACAGCTT CGTACGCTGCAGGTCGAC	C. Schiklenk
232	klf1 CT-tag tom fw inner	GTTCATCAAATACTAACAGTTTTAGTGG TAGATGGTGTTCGCATTTTGTCTAAATTAGTACAGCTT ATCCTAGGTCTAGGTACCTTATGG	C. Schiklenk
233	klf1 KO fw inner	GCTATCATTGCGTTGAATCTG TTTAATCACTATTTTTCTG-TAAAGTGAGGTTACTTGCGTTTCTTC CGTACGCTGCAGGTCGAC	C. Schiklenk
234	klf1 KO fw outer	CTTCTTTCTTATTTCTCTTTCTGAATGTATTGTCAC-GAATTTTGAATATAGGTGTTA GCTATCATTGCGTTGAATCTG	C. Schiklenk
235	cut14 CTtag fw inner	GGAATGTTTACCAATGCTAATCG ACTATTTCATGTACGATT-TATGGACGGATCATCTGTGGTACAAGCTCGC CGTACGCTGCAGGTCGAC	C. Schiklenk
236	cut14 CTtag fw outer	ACTTATTAAAACAAAGTTTAAAGGTTCTCAGTTTATTATTGT-TAGCCTTAAAGAA GGAATGTTTACCAATGCTAATCG	C. Schiklenk
237	cut14 CTtag rev inner	GACATCGGTGATAGTAAATAGTAGGAC TATACATGCGCGTATAATTCAAGTGTTTACGTTCAAATTA ATCGATGAATTCGAGCTCG	C. Schiklenk
238	cut14 CTtag rev outer	ACAACTTTAAAGAACCAAAAGTCTTGTTTTTAATGATTGGTA-GAAATATTCTTTAAATAAATTAA GACATCGGTGATAGTAAATAGTAGGAC	C. Schiklenk
239	SpeI-E2Crimson fw	TGTAA ACTAGT ATGGATAGCACTGAGAACGTC	C. Schiklenk
240	E2-crimsonRsrII rev	GTTAC TTCGGTCCG CTGGAACAGGTGGTGGCGGGC	C. Schiklenk
241	rtzY289-PK6	GGACTATGGATGATGTCGTCCGTTGGTTATTCTCATCTG-GTAAAAGACGACAAAAA TCCGGTTCTGCTGCTAG	C. Schiklenk
242	klf1 3' rev	CTAGTAAACTAGCGCAACAGCGG	C. Schiklenk
243	klf1 5' fw	AATTGCCCGCCGCGGATCCGG	C. Schiklenk
244	AscI P-ura4 fw	TGTCCA GGCGCGCC AGCTACAAATCCCACTGGC	C. Schiklenk
245	T-ura4 XhoI rev	TCCATA CTCGAG AGCTTGTGATATTGACGAAACTT	C. Schiklenk
246	FseI Kan fw	TCCATA GGCCGGCC GTTTAGCTTGCCTCGTCCCC	C. Schiklenk
247	Kan Fse rev	TGTCCA GGCCGGCC TTTTCGACACTGGATGGCGGC	C. Schiklenk
248	FseI srk1 3 fw	TCTGAA GGCCGGCC TGCTCCTAACACTGCTCAACGC	C. Schiklenk
249	srk1 3 Fse rev	TGTCCA GGCCGGCC GAGCATCATATAATTCGTATGGTTCTATC	C. Schiklenk
250	colPCR ChI1.95 rev	CGCGCGTTCGATAAGCTCTTCGGC	C. Schiklenk
251	colPCR ChI1.5 rev	CCGACTGCACCTACCTCCTCAG	C. Schiklenk
252	1miniDegr rev	P-CTTATACATACGAAGATCAATTTTGCG	C. Schiklenk
253	1miniDegr fw	P-GGTATTCCTAACCCTTTATTGGGATTAG	C. Schiklenk
254	srk1 col PCR fw	ATTCTAAGGGAGTTGATATGTGGGC	C. Schiklenk
255	rtz1 D255 fw	P-GATTGTACTTGTATTTTTAAAAATAGATCTTC	C. Schiklenk
256	rtz1 Q211 rev	P-TTGTTGAAAAGCATTGGCGG	C. Schiklenk
257	SpeI-sfGFP fw	TGCTTA ACTAGT ATGGTGGCTATGAGCAAGGGCGAGG	C. Schiklenk
258	sfGFP-RsrII rev	TGCTTA CGGACCG ACCGGTGCTGCCCTTGTACAGC	C. Schiklenk
259	BamHI rtz1 M1 fw	AATTG GGATCC ATGTCAAATGAGGAATCTTTTACAGAAAAG	C. Schiklenk
260	rtz1 S282 NheI rev	AAAGG GCTAGC TTATTA AGATGAGAATAACCAACGGACGAC	C. Schiklenk
261	rtz1 Q211 NheI rev	AAAGG GCTAGC TTATTA TTGTTGAAAAGCATTGGCGGT	C. Schiklenk
262	RsrII sfGFP fw	GTGATG CGGACCG CTATGAGCAAGGGCGAGGAGC	C. Schiklenk
263	sfGFP RsrII rev	TGCTAT CGGTCCG ACCGGTGCTGCCCTTGTACAG	C. Schiklenk
264	linker-lacI fw	P-GTGGTTCTATGGTTAAACCT GTAACGTTATACGATGTCGCAGAG	C. Schiklenk
265	E2C-RsrII-linker rev	P-CAGGTTGCAAAAATTCTTTTT CGGTCCG CTGGAACAGGTGGTGGC	C. Schiklenk
266	linker colPCR fw	TGCAACCTGGTGGTTCTATGG	C. Schiklenk
267	rtz1-deltaNLS fw	P-GGCTCATAGACTTGGTGACCCTAG	C. Schiklenk
268	rtz1-deltaNLS rev	P-CTGTAAAAGATTCCTCATTTGAC	C. Schiklenk
269	rtz1-AJ3-PK6 inner fw	CCCTTGGGACCTTTGTAAGTAATCACC AAATCCAGTT-TATTCGTGTATACTAATTAACCAGTGGGCGAACAT TCCGGTTCTGCTGCTAG	C. Schiklenk
270	rtz1-Ts34-PK6 inner fw	CACCGATCCGGTAGATGGTTC TGTAACCTCAAAAACTGTTGCACCGTTACGATATGTAAAAATA TCCGGTTCTGCTGCTAG	C. Schiklenk
271	tRNA-Gly3 fw	CGTTGCCATCGATTCGACCCGGG	C. Schiklenk
272	Rtz1 Y289 NheI rev	AAAGG GCTAGC TTATTA GTATTTTTGTCGTCTTTTACCAGATGAG	C. Schiklenk
273	Rtz1 dNLS rev corr	P-CCTGTAAAAGATTCCTCATTTGAC	C. Schiklenk
274	RtzExon3-4junct rev	TCTGAGGAACATACATTGGGCCAC	C. Schiklenk
275	BsrGI-hphMX fw	AGGATT TGTACA GGCGCGCC GACATGGAGGCCCAGAATACC	C. Schiklenk
276	hphMX-BsrGI blunt rev	P-TTA GGCGCGCC CAGTATAGCGACCAGCATTCAC	C. Schiklenk
277	rtz1 V276K F280K fw	P-AAA CGT TGG TTA AAA TCATCTGGTAAAAGACGACAAAAATACGA	C. Schiklenk
278	rtz1 V276K W278K F280K fw	P-AAA CGT AAA TTA AAA TCATCTGGTAAAAGACGACAAAAATACGA	C. Schiklenk
279	blunt PK6 fw	P-GGTATTCCTAACCCTTTGTTGGGCC	C. Schiklenk
280	AvrII PK6 fw	TGTCCA CCTAGG GGTATTCCTAACCCTTTGTTGGGCC	C. Schiklenk
281	PK6 TAA AvrII rev	TGGACA CCTAGG TTATGAGGAACCATCCAATCCAAGAAGAGGG	C. Schiklenk
282	PK6-2Presc-rev	P-AGGACCTTGAAAAAGAACTTCCAAAGGACCTTGAAAAAGAA CTTCCAATGAGGAACCATCCAATCCAAGAAGAGGG	C. Schiklenk
283	AscI ATG PK6 fw	TGTCAA GGCGCGCC ATG GGTATTCCTAACCCTTTGTTGGGCC	C. Schiklenk
284	PK6 AscI rev	TGGACA GGCGCGCC C TGAGGAACCATCCAATCCAAGAAGAGGG	C. Schiklenk
285	PK6 rfCloning fw	GGATGTCTTAGTAAAAGTTGAGCTAAAAG ATG GGTATTCCTAACCCTTTGTTGGGCC	C. Schiklenk

continued on next page.

#	Name	Sequence 5'→3'	Designed by
286	PK6 rfCloning rev	CTGTAAAAGATTCCTCATTTGACAT TGGACCCTGAAAAAGTACTTCCAAAGGACCTTGAAATAAAAC-CTCAAGTGAGGAACCATCCAATCCAAGAAGAGGG	C. Schiklenk
287	TEV2-PK6 rfCloning fw	CCTCCTCAGTTCTTTCACAGCG GTTCTC AAAACCTT-TACTTTCAAGGTTCTCAGAATTTGTATTTCCAAGGTTCT GGTATTCCTAACCCTTTGTTGGGCC	C. Schiklenk
288	TEV2-PK6 rfCloning rev	GAGGAGGCGATGGAAGATCTATT-TGAGGAACCATCCAATCCAAGAAGAGGG	C. Schiklenk
289	pLau44colPCR fw	CAGTGATAGAGAAGATGGGGGC	C. Schiklenk
290	NsiI-leu1 fw	TGTCAA ATGCAT GCGCAATTTCAACAATTCCTATGAACATCC	C. Schiklenk
291	BstEII rev	TGTCAA GGTAACC GATGTCGTAAATCAATTCCATGCTTTTGC	C. Schiklenk
292	BirA R118G fw	GCTGGCCGTGGTGGTCGGGGTCGGAAATGGTTTTCGC	C. Schiklenk
293	BirA R118G rev	CATTTCCGACCCCGACCACCACGGCCAGCCTGCTGGTATTC	C. Schiklenk
294	rtz-AvrII-LGGG-BirA fw	CATACAACAATTATTATCCAAGGGAAATGAT CCTAGG TTGGGTGGTGGC ATGAAGGATAACACCGTGCCACTG	C. Schiklenk
295	BirA-TAA-AvrII-Trtz rev	CGGCATTAAATAAAATTTACCTCAGTTTATAA CCTAGG TTA TTATTTTTCTGCACTACGCAGGGATATTTCAC	C. Schiklenk
296	ucsToTEVPK6 rf fw	GTCCACCGCCAATGCTTTTCAACAA G GTTCTC AAAACCTT-TACTTTCAAGGTTCTCAGAATTTGTATTTCCAAGGTTCT GGTATTCCTAACCCTTTGTTGGGCC	C. Schiklenk
297	BirA R118G plmd-PCR rev	P-ACCACGGCCAGCCTGCTGGTATT	C. Schiklenk
298	BirA R118G plmd-PCR fw	P-GGTCGGGGTCGGAAATGGTTTTC	C. Schiklenk
299	AvrII BirA fw	AAATGAT CCTAGG ATGAAGGATAACACCGTGCCAC	C. Schiklenk
300	BirA AvrII rev	ATAATTA CCTAGG TTATTTTTCTGCACTACGCAGGG	C. Schiklenk
301	AscI Purg1 fw	AAATCGT GGCGCGCC CTATAGCCATTCTAAACAAGCCAGC	C. Schiklenk
302	Turg1 NotI rev	GCGATA GCGGCCGC GGATATGATGTATGGTAGTAGCGCG	C. Schiklenk
303	P148 fw	P-CCTCCTCGTGTTACAATTGAAAATG	C. Schiklenk
304	E147 rev	P-TTCATTGGAAACTCGAGGATT	C. Schiklenk
305	Purg-NLS-p14 rf fw	CTTCAATTACTAAATTAGAACTAATTCAAT ATGCCAAAGAAGAAGCGTAAGGTC GCGATGCAAGCGGCCAAGAG	C. Schiklenk
306	TEV DSR rf inner rev	CGTTTAACCTGCCGTTTAAAGTTCTG TTTAAGAATGGGTTTAATACGGAGTTTAA TTA CAATTGAGTCGCTTCCTTAACTGGC	C. Schiklenk
307	DSR Turg rf outer rev	GTCTAAAACAGATGGGCAAGC GTTTAACATAAAGTTTAAGCACCTGTTTAACATTA CGTTTAACCTGCCGTTTAAAGTTCTG	C. Schiklenk
308	P212 fw	P-CCCTCAAATCAATTTCAAACG	C. Schiklenk
309	urg1Prmtr seq fw	TGACTTGCGTCGGCTATTGCC	C. Schiklenk
310	TEVtoPKrep-fw	P-TCTGAAAATTTGTATTTCCAAGGTTCTGGTATTCCT AACCCTTTGTTGGGCC	C. Schiklenk
311	TEV-F-toPK-fw	P-TCTGAAAATTTGTATTTCCAATTTTCTGGTATTCCT AACCCTTTGTTGGGCC	C. Schiklenk
312	TEVrep-rev	P-AGAACCTTGAAAGTAAAGGTTTTCAGAACCGCTGTGAAA-GAACTGAGG	C. Schiklenk
313	TEV-F-rev	P-AAATTGAAAGTAAAGGTTTTCAGAACCGCTGTGAAAG-AACTGAGGAGG	C. Schiklenk
314	Leu1 col fw	CCGCAAAAATGCCTGGTTTCG	C. Schiklenk
315	kan col rev	CATCGAGCATCAAATGAAACTGC	C. Schiklenk
316	TEVtoMyc fw	CAGTTAAGGAAGCGACTCAATTGGAACAAAAGTTAATTTCT-GAGGAAGATTTAAATGGCGAGCAAAAATTGATTAGT	C. Schiklenk
317	MycToNLS rev	CTTTTTTGGAAGGTCCTCTTCTGAGATAAGTTTCTGTTCA-GAACCGTTCAAATCTTCTTCACTAATCAATTTTTGCTCGCC	C. Schiklenk
318	NLStoTurg rev	GAATGGGTTTAATACGGAGTTTAATTATAC-CTTTCTCTTTTTCTTAGGTGATCCAACCT-TACGCTTCTTTTTTGGAAGGTCCTCTTC	C. Schiklenk
319	Y289 AvrII rev	GGCAAT CCTAGG GTATTTTTGTCGTCTTTTACCAGATG ACCATTCTTCATATGCTGAAAGC	C. Schiklenk
320	P590X inner S2 fw	ATTTGTACAATGTGAACAATGTGAATCACCATTA TAATAA CGTACGCTGCAGGTCGAC	C. Schiklenk
321	P590X outer fw	AAAATTTTGAAGTTTGGGCCGCCCAAAAACCTACGATAGAGC-CCCCA ACCATTCTTCATATGCTGAAAGC	C. Schiklenk
322	N651X inner S2	TGTTTTTGAAGCATATCAAAAATGGAACAGATGTTATTATAG-CATTTTTCTGAAT TAATAA CGTACGCTGCAGGTCGAC	C. Schiklenk
323	N651X outer	TACCCGGAATGAAATTGAGTAAACGCGAAATTGATGGCTGGT-GCTCTCT TGTTTTTGAAGCATATCAAAAATGG	C. Schiklenk
324	urg1 CDS 5 rev	CGCCATTGCACTCTGCAGGACGGC	C. Schiklenk
325	urg1 int fw	CTGAAAGAGCTACATTTAGTATGGGGC	C. Schiklenk
326	p14 rev	GAATGTTCGCCCTCTTGGCCGC	C. Schiklenk
327	cnd3 KO fw inner	GGTATGCCAGTGAGGTGCTCC TCAACTTCAGCAAAAGCAC-TAAAATTGGCATAATATAATTGTTATTGAAT CGTACGCTGCAGGTCGAC	C. Schiklenk
328	cnd3 KO fw outer	AGGGTTCATTTTTTTGTTTGCATACCCCAGCTTAACCTAC-CACTGAGAGCCAACTGTA GGTATGCCAGTGAGGTGCTCC	C. Schiklenk
329	cnd2 KO fw inner	CATATCGTTAAAGCGCGATATACG TATAGGCACACCGACTTAC-CACTTGTGAACATAAACATTTACTTAAATCA CGTACGCTGCAGGTCGAC	C. Schiklenk
330	cnd2 KO fw outer	TTATTTAGAAACTTATTTGAATCTTTATCATTTGTTGATTA-GAAAGAAATATACGG CATATCGTTAAAGCGCGATATACG	C. Schiklenk
331	cnd2 col rev	CAAAGTCCATTCGTTGACGGTG	C. Schiklenk
332	cnd3 KO rev inner	GGCTCAAAATATTGAATGATGAGGG GTTTTAGAAAC-TAGTTGTTGTAAGTAAGTTATAAAAACACAGCAACATAC ATCGATGAATTCGAGCTCG	C. Schiklenk

continued on next page.

#	Name	Sequence 5'→3'	Designed by
333	cnd3 KO rev outer	CATAAACAGGAAAGAAATAGCCAAGAACTTGCCGTAGCGCAT-GATTATCAACTGTGTTA	C. Schiklenk
334	cnd3 colPCR fw	GGCTCAAAATATTGAATGATGAGGG GACTACACCAATGGTTAGGACTTGC	C. Schiklenk
336	SV40-NLS rev	P-TTATACCTTTCTCTTTTTCTTAGGTGATC	C. Schiklenk
337	4DSR fw	P-TTAAACGTAATGTTAAACAGGTGC	C. Schiklenk
338	urg1 fw	P-TGCCCATCTGTTTTAGACGTC	C. Schiklenk
339	pLau43 seq 1	GCGGATAACAATTGAAGAAGCGGC	C. Schiklenk
340	sfGFP-NLS fw	CCAACCTTACGCTTCTTTTTTGG CTTATAAAGCTCGTCCATTCCG	C. Schiklenk
341	SV40NLStoMotif	GCCAAAGAAGAAGCGTAAGGTCGCG TCTTCCATCGCCTCCTCTAGGACTATGGATGATGT	C. Schiklenk
342	motifTosfGFP	CGTCCGTTGGTTATTCTCATC CGTCCGTTGGTTATTCTCATC TGGTAAAAGACGACAAAAATACGAATCAAGTTAC	C. Schiklenk
343	cnd3 P775 rev	ATGTCCAAGGGTGAAGAGCTAT TGATGAAGGCAAGTCAGTAGGG	C. Schiklenk
344	kanMXfw-B7	GCTAGGATACAGTTCTCACATCACATCCG	Petrova
345	pFA6 cnd3 Prom fw	CTGTCGATTCGATACTAACGCC CCCTACTACTGTGCACTCTACTACTG	C. Schiklenk
346	cnd3 Prom pFA6 rev	CTCGTTTTCGACACTGGATGGC ATTCAATAACAATTATATTATGCCAATTTTAG	C. Schiklenk
348	cnd1Prom outer fw	GTTAGTAAGAAAGTATAAATGGACCCCCACACAGGACATATAG-GTGGGGTTATTGTTTACAA	C. Schiklenk
349	cnd1Prom inner fw	GGACTACTAGAATGTAGTACGCC GGACTACTAGAATGTAGTACGCC AAATCCATCTTTTATTTCATTCGTAACATAGAAAGATTCG-GCTTTCAGTGGCCTCA	C. Schiklenk
350	cnd1NT inner rev	CGTACGCTGCAGGTCGAC GTCGGAATTTTCTTCATCATGAATG TATTTCTTTAATCTAGAAAGAAGATCCAACGACAT	C. Schiklenk
351	cnd1NT outer rev	ATTCAATAACAATTATATTATGCCAATTTTAG AATGTCCATACCGTTAACCACGGCTGTCAATCCAGCATTTTCA-CATTCAGCATAAATCGAGTCCAA	C. Schiklenk
352	sfGFPmco-li-sfGFPyco rev	GTCGGAATTTTCTTCATCATGAATG ATAGCTCTTCACCCTTGGACAT ACCTCCTGAGCCTCCACTTCCACCAGA ACCTTTGTAGAGCTCATCCATG	C. Schiklenk
353	pFR sfGFPmco fw	GAGTCGTTAATTTATATTTGTTTATTAAACTAGT ATGAGTAAAGGAGAAGAACTTTTCACTG	C. Schiklenk
354	HindIII-ChrI-2.49 fw	ATCT AAGCTT AAATTGAGCACGATCAATAACTGTAATG	C. Schiklenk
355	ChrI-2.49 HindIII rev	CAAGTGT AAGCTT GATCTGATTTAGGCAGCGCAGA	C. Schiklenk
356	cnd1 CT PK6 inner fw	GTGGTGTATGCACTTTCTTTGC TTCCTCATAAAGCC-GATAATATTCAAAAGCTCATTGACGATGGATATCATGAA	C. Schiklenk
357	cnd1 CT PK6 inner rev	TCCGGTTCTGCTGCTAGA CGTCATTCTTCTTTTTAATTAGGCAATAC TAATATACAAAG-GATTTTGAATATGTAAGATAAAGCATTAGAATTGACTTTA	C. Schiklenk
358	cnd1-3P-rev	GAAAGATCTGTTTAGCTTGCC ATGCACTTATACTCAGTATATGCCG	C. Schiklenk
359	pFR srk colPCR fw	CCTTTCTATTAGTAATGGGCCGGCCG	C. Schiklenk
360	SPAC713 KO outer fw	TCTACATTCTGCAGCTATAATTCGTAAGTACGGGTGGAGCACA-GAGTACATAT	C. Schiklenk
361	SPAC713 KO inner fw	GGATGTTGCATGCGGAAAAAGACGG GGATGTTGCATGCGGAAAAAGACGG GCGTAGTAGATTTATTATTTGCGATAGAAATATATCAACATGCC	C. Schiklenk
362	SPAC713 KO inner rev	CGTACGCTGCAGGTCGAC GGGGTGGTTGAGGAAGACGGTG AGAAGAGCGTATATTGATT-TAATTTGCCTTAGTTGCAACATATG	C. Schiklenk
363	SPAC713 KO outer rev	ATCGATGAATTCGAGCTCG CTATGAGAATGATTCTAAATGAGTATGGAAATGCACCCCACTT-TAGATCTCAGTG	C. Schiklenk
364	SPBC887.16 KO outer fw	GGGGTGGTTGAGGAAGACGGTG ATAATAAAATAACGCTTGATAGTCTTTTAAGAATTTCATTTTT CGAATACCGCCTTGTGAATTATG	C. Schiklenk
365	SPBC887.16 KO innner fw	CGAATACCGCCTTGTGAATTATG CGTAGTTTACTTGTATCTATATCGTTTCAAATTTTCATACTTC	C. Schiklenk
366	SPBC887.16 KO inner rev	CGTACGCTGCAGGTCGAC CTACTACTTGCATTAGTAACAGGGGGG TTTCATGTAGATAAC-CCTCACATACTCTCTCACGTTGACGCTGAATG	C. Schiklenk
367	SPBC887.16 KO outer rev	ATCGATGAATTCGAGCTCG TTTGAATTCTGTCTTTGCTAAAGTTATTGCTTCTCTTT CTACTACTTGCATTAGTAACAGGGGGG	C. Schiklenk
368	SPAC713 colPCR rev	AGCGAGGAAGAGAGGTATCGCCG	C. Schiklenk
369	SPAC713 colPCR fw	ATGAAGGCAAACCGAATTAGCTGGG	C. Schiklenk
370	SPBC887.16 colPCR fw	AATGCCGGTCCCCATCCCCTC	C. Schiklenk
371	SPBC887.16 colPCR rev	GCAAAGTGTCGCTGATGGACCC	C. Schiklenk
372	ChrI 2.49 colPCR fw	GCTTTCGGCTGTCGGATGCGGC	C. Schiklenk
373	pTetO colPCR	CCGCCCCTCTAGCACGGCCGG	C. Schiklenk
374	ChrI 2.49 col PCR rev	AGGTCATTTCGCGCCTCGGCGC	C. Schiklenk
375	purg TEV fw 2	CTTATCCGTTTTCTTCAATTACTAAATTAGAAC-TAATTCAATATG	C. Schiklenk
376	TEV NLS rev 2	CCAAAGAAGAAGCGTAAGGTCGCTAGTGG GGTGATCCAACCTTACGCTTCTTTTTTGG TGACCCTTGCGAGTACACCAATTCATTCATGAG	C. Schiklenk
377	Purg1ToSpCOTEV fw	TTCTTCAATTACTAAATTAGAACTAATTCAAT ATG GCTGAGTCCGGTGAATCATTATTC	C. Schiklenk
378	NLStoTEV rev	ACGTGGTCCCTTAAACAAGCTTTCTCCACCAGAAGC GACTTTGCGTTTCTTTTTAGGAGA	C. Schiklenk
379	SpCOTEVplus col fw	TTCAAACTAAAGACGGTCAATGCGG	C. Schiklenk

continued on next page.

#	Name	Sequence 5'→3'	Designed by
380	SpCOTEVplus col rev	AAACGCCATCCGGATACCCATT	C. Schiklenk
381	Prtz1ToHA RF fw	GGATGTCTTAGTAAAAGTTGAGCTAAAAG ATG TATCCCTACGACGTCCCCGACTAC	C. Schiklenk
382	TEVYToRtz	CTGTAAAAGATTCCTCATTTGACATACT ATATTG GAAGTAAAGATTCTCGCTACC	C. Schiklenk
383	pLau43-pw1	TCACAATTCACTCCGGTTTGC	C. Schiklenk
384	cnd1 col fw 2	GGTAAAATGCTGCCAAGGGAAGG	C. Schiklenk
385	modNd fw	TGGGGTGGTTCTAAAGGTAAAAAAGGTATTCCTAACC-CTTTGTTGGGCC	C. Schiklenk
386	modNd rev	TTTACCTTTAGAACCACCCCATTGAAAGTAAAGGTTTTCA-GAACCGCTG	C. Schiklenk
387	cnd1P KO rev inner	CGAGTCCAAGTCGGAATTTTCTTCATCATGAATGTATTTCTT-TAATCTAGAAAGAAGATCCAACGACAT	C. Schiklenk
388	cnd2-PK6 fw inner	ATCGATGAATTCGAGCTCG GCAACGAAGATTTTTCAGATGT TTTTATTAGGCCAGGTCC-TAACTTGACGACGCTAGAAGCATTAGAAAATGATGTT TCCGGTTCTGCTGCTAGA	C. Schiklenk
389	cnd2-PK6 rev inner	CACGCTAGCTAAAAGTATGCG ATGATGACTAATTAATGAT-GACCTGCATCATTTCGATTCTACACACTTTACTTTA GAAAGATCTGTTTAGCTTGCCT	C. Schiklenk
390	NcoI-lys1 fw	ACTGCCATGG AAACAGGATAGATATTAGAAGTCTACATAG	C. Schiklenk
391	lys1-NheI rev	TTAACC GCTAGC GGCCCTGATAGTACTCCCACAC	C. Schiklenk
392	klf1-PK6 fw inner	GTTCATCAAATACTAACAGTTTTAGTGGTAGATGGTGTTCG-CATTTTGTCTAAATTAGTACAGCTT TCCGGTTCTGCTGCTAGA	C. Schiklenk
393	klf1-PK6 rev inner	TAAATTAAAACTATGGATTAGAAATAATG TAAAAAATGC-TATAATACAAGAAATCGTTCGTTATACATCCTCAAGCTA GAAAGATCTGTTTAGCTTGCCT	C. Schiklenk
394	cnd3-PK6 fw inner	GGCGAAATTATTCCTGATACAGTGGAAG CCAACATGGAAGAC-GAGGAGGAAGTTTATGTTAAACAAGAAGAAGATCTT TCCGGTTCTGCTGCTAGA	C. Schiklenk
395	cnd3-PK6 rev inner	CTTTTATCAGTTTCTGAAAGATATGCG GAAGGGATTCCGT-GAACTTCATAGAAAGGATCTGTCTCAATTGATTTAATAA GAAAGATCTGTTTAGCTTGCC	C. Schiklenk
396	lys1-3Pfw	GAAAGTCATTGCCTTAGTCCGCGCC	C. Schiklenk
397	lys1-fw	ATCGTTCTGGTGACTTGGGCCGC	C. Schiklenk
398	cut3-PK6 fw outer	CGCAGTTTATTGTTATTTCTTTAAGAAGTAATATGTTTGAGT-TATCTTCTCGTT TGGTTGGCATTTATAAAACGGCG	C. Schiklenk
399	cut3-PK6 fw inner	TGGTTGGCATTTATAAAACGGCG AATATGACTAAGAGTGTCA-CAATCAACAACAAGGAAATACTTACAGAT TCCGGTTCTGCTGCTAGA	C. Schiklenk
400	cut3-PK6 rev inner	CATTCAGTAGCCAAAAATTCGTAAATTATTAAATATC-TAGTTTCCAATTTTCTACGTTTTTATTTGAATGTGCAGTTA GAAAGATCTGTTTAGCTTGCC	C. Schiklenk
401	cut3-PK6 rev outer	GTTTAATCTTCTCATAACATAGATTTATTAGTATGCACACTGT-GAATTATGAAACACTGA CATTCAGTAGCCAAAAATTCGTAAATTATTA	C. Schiklenk
402	cut3 col rev	GCGCAGATTTTACAGGCTTTAAAAGCGAG	C. Schiklenk
403	top2-PK6 fw inner	GGATGAACCCAGCATGCAAGA TGATTCTTTTATCGTC-GATAACGATGAGGATGTAGACGATTATGATGAGAGTGAT TCCGGTTCTGCTGCTAGA	C. Schiklenk
405	top2-PK6 rev inner	CCTACCATTTACAATGTTCATCCAAT TTTTTCAGATTGTACTG-TAAATAGCGTTTGAAAACACCAAATTTTAGAAGCTA GAAAGATCTGTTTAGCTTGCC	C. Schiklenk
406	top2-Cttag rev outer	ATATAAAATTAATAAGCTAAGTGTAATACTTAAAAAATACAT-TAATTGGAACTCGTAT CCTACCATTTACAATGTTCATCCAAT	C. Schiklenk
407	top2-3P fw col PCR	AAATAGCAGCCTCGGCGTCTGG	C. Schiklenk
408	cnd1PromoterKO rev inner	TAAATCGAGTCCAAGTCGGAATTTTC TTCATCATGAATG-TATTTCTTTAATCTAGAAAGAAGATCCAACGACAT GGCGTTAGTATCGAATCGACAGCAG	C. Schiklenk
409	cnd1PromoterKO rev outer	AAACCCAAATGTCCATACCGTTAACCACGGCTGT-CAATCCAGCATTTTCACATTCAGCA TAAATCGAGTCCAAGTCGGAATTTTC	C. Schiklenk
410	BamHI cut3 E1006 fw	AAGCG GGATCC AACACAAATCTCGGCTCCGCGAA	C. Schiklenk
411	cut3 3UTR rev AscI	TCTTCT GGCGCGCC TCCTTTGCGCAGATTTTACAGGC	C. Schiklenk
412	BamHI cut14 N962 fw	AGATT GGATCC AACATGCGTCAGTGTAGAGAGCAG	C. Schiklenk
413	cut14 3UTR rev AscI	ATACC GGCGCGCC ACATACCGTAGTCTAAGTTTCATTAGCGGC	C. Schiklenk
414	puc1 CT tag fw outer	AGGTATGCTAATGAGGAATGTACTGATTTACTGTTTTCCTCAC-TAGGCCGTATTTCTAGTATTTTA GCAAAGAAATATCCGGAACAATG	C. Schiklenk
415	puc1 CT tag rev outer	ATTACATCACTATACACTTACTTTTCTCAAG-TAAATATATAATTTTGAAAT TATATCTCCATTACATGTTTGTCTAGAAG	C. Schiklenk
416	puc1 PK6 fw inner	GCAAAGAAATATCCGGAACAATG CGCAATGGCTGCCTGGTG-CAACATGACTGAAAAGGATACTGAGCGTACTTTG TCCGGTTCTGCTGCTAGA	C. Schiklenk
417	puc1 rev col PCR	GTTCCTGATGGCCTTAATCGTGCG	C. Schiklenk
418	puc1-KO fw outer	TGAGCCTGTTTATGTCCAATTATTTTTTCTTCAGTAT-CATTTTTTTAATAATTCACTGAACTTTGAGCT GCAACTTCATCGACTGTGAAGAGC	C. Schiklenk
419	puc1-KO fw inner	GCAACTTCATCGACTGTGAAGAGC TTTTCTACTCTTTC-CTTCTCATTATTTTCAAATACCTGTCTACCCAGT CGTACGCTGCAGGTCGAC	C. Schiklenk
420	puc1 PK6 rev inner	CTCCATTACATGTTTGTCTAGAAG CATTGCAATATATATAAATCGAAGAAGAAGCAATGTTAAAGT-TAGAAAGATCTGTTTAGCTTGCC	C. Schiklenk
421	puc1 CT tag rev inner	ATATCTCCATTACATGTTTGTCTAGAAG CATTG-CAATATATATAAATCGAAGAAGAAGCAATGTTAAAGTTA ATCGATGAATTCGAGCTCG	C. Schiklenk

continued on next page.

#	Name	Sequence 5'→3'	Designed by
422	puc1 CT tag fw inner	GCAAAGAAATATCCGGAACAATG CGCAATGGCTGCCTGGTG-CAACATGACTGAAAAGGATACTGAGCGTACTTTG CGTACGCTGCAGGTCGAC	C. Schiklenk
423	puc1 col PCR fw	CCTTAATTTTCCGCCGTTGTATCGC	C. Schiklenk
424	cut14-K1080E fw	AATTGGGTCAATTTGGGAAGATAGTCTGGCAGAACTTAGTGG	C. Schiklenk
425	cut14-K1080E rev	TGCCAGACTATCTTCCCAAATTGACCCAATTTTTACATGAAT	C. Schiklenk
426	cut14-W1079A fw	TAAAAATTGGGTCAATTGCTAAAGATAGTCTGGCAGAACTTAG	C. Schiklenk
427	cut14-W1079A rev	CAGACTATCTTTAGCAATTGACCCAATTTTTACATGAATTTC	C. Schiklenk
428	cut3-K1225E fw	TCCCAAAAAATCTTGGGAAAACATATCTAACCTTTCGGGAGG	C. Schiklenk
429	cut3-K1225E rev	TAGATATGTTTTCCCAAGATTTTTTGGGAGGCATCAC	C. Schiklenk
430	cut3-W1224A fw	GCCTCCCAAAAAATCTGCTAAGAACATATCTAACCTTTCGGG	C. Schiklenk
431	cut3-W1224A rev	AGATATGTTCTTAGCAGATTTTTTGGGAGGCATCACACTAAAC	C. Schiklenk
432	cut3 trafo fw	CTATGGGCGGAAACGCAGAGCTTGAGTTAGTGGATAGTTT GGATCCGTTTTCTGAGGGGGT	C. Schiklenk
433	cut3 S rev inner	GTAACTACAAATTGTAGATACCTTCTGAAATTG ATGATGTAAACAACATATTTAATTATATACAA TATCGATGAATTCGAGCTCG	C. Schiklenk
434	cut3 outer rev	ATGCATACGATTGCAATAAATCTTTAAAAGCATTACCCAC-TAAAATATTATACTAT	C. Schiklenk
435	cut14 S rev inner	GTAACTACAAATTGTAGATACCTTCTGAAATTG GCTACAAATGACATCGACGC TAATAATAAATTTGGAAATGAT-GAGTTTACGATATTTTATACATATGAT ATCGATGAATTCGAGCTCG	C. Schiklenk
436	cut14 rev outer	CACAGAAACATCCTGTATCGATCAAAATTTTAAAACCCTACCC-TAAATATTTTTGAATAT	C. Schiklenk
437	XhoI rtz1-K220 fw	GCTACAAATGACATCGACGC AGTTCG CTCGAG AAATTACCTTCAGGACTTGATACAAGG	C. Schiklenk
438	XhoI rtz1-D251 fw	AGTTCG CTCGAG GACTTACAGGGAGATTGTACTTG	C. Schiklenk
439	cut3 Cttag S inner fw	GTTGGCATTTATAAAACGGCG AATATGACTAAGAGTGTCA-CAATCAACAACAAGGAAATACTTACAGA TCGTACGCTGCAGGTCGAC	C. Schiklenk
440	cut3 CTtag outer fw	CGCGCAGTTTATTGTTATTTCTTTAAGAAGTAATAT-GTTTGAGTTATCTTCTCGTTTG GTTGGCATTTATAAAACGGCG	C. Schiklenk
441	cut3 3 col PCR rev	CTGAGTTTAATGGGTGGGAACACC	C. Schiklenk
442	TEF-term fw	CGCCTCGACATCATCTGCCCAG	C. Schiklenk
443	cnd3 3P col PCR	GAGGGCTCAAGAGATGGAGGCG	C. Schiklenk
444	Sc SDD4 KO fw	GGCTGTATTGAGATTCTAGGACTCATCTACTATGTTTATAAT-TATAAAAAGTGACCAATAAAGCAGTGAAG CGTACGCTGCAGGTCGAC	C. Schiklenk
445	Sc SDD4 KO rev	GGCAGTTTACAAATGTTTTCATAACCATTTCATTAATCTAA-CAATAAATATGATGATTTACCAATATACGAATA ATCGATGAATTCGAGCTCG	C. Schiklenk
446	Sc SDD4 colPCR fw	ATTGCGAGATATCACATGTGCGC	C. Schiklenk
447	Sc SDD4 colPCR rev	AACCGCTTGCAGTGGGATGACC	C. Schiklenk
448	Pdis1-LacI fw	CGAGTCGTTAATTTATATTTGTTTATTAAACTAGTATG-GTAACGTTATACGATGTCGCAG	C. Schiklenk
449	lacI-linker rev	AACCATACTGCCACCGGAGGCTCCACCACTGGATCCCAGCTG-CATTAATGAATCG	C. Schiklenk
450	linker-YCOmNG fw	GCTGGGATCCAGTGGTGGAGCCTCCGGTGGCAGT ATGGTTTCTAAGGGTGAAGAAGAC	C. Schiklenk
451	YCOmNG-NLS-Tnmt rev	GAAAGAAAAACCCTAGCAGTACTGGCAAGGGAGCTAGCT-TAAACTTTACGCTTTTTCT-TAGGCTTGTACAATTCGTCCATACCCATAAC	C. Schiklenk
452	cdc13-PK6 outer fw	GCTAGTCTTTTTGTTCGTGACTGGATCAAGAAGAATTCTATC-CCTCTTGGCGATGACGCTGATGAAGATTATAC	C. Schiklenk
453	cdc13-PK6 inner fw	CGATGACGCTGATGAAGATTATAC TTTTCACAAGCAAAAACGTATACAACATGACATGAAAGAT-GAAGAATGGTCCGGTTCTGCTGCTAGA	C. Schiklenk
454	cdc13-PK6 inner rev	GAGCGCTTGAACAAGTTGGAAT ATTCACAATTGAAAGAGGTTGAGATAGTGATATGCACAATA-CACTAAATTAGAAAGATCTGTTTAGCTTGCC	C. Schiklenk
455	cdc13-PK6 outer rev	CGTTTACAGGACATTACGGTTGCTATTAGTGATAAACTAATA-CACATATAAAGAGCGCTTGAACAAGTTGGAAT	C. Schiklenk
456	cdc13 col PCR rev	CCAGCATGTACTATGCATCTGGC	C. Schiklenk
457	cdc13 col PCR fw	GGAAATGCTTGGACGTGGACCG	C. Schiklenk
458	FseI-ptr8 fw	ATATT GGCCGGCC AGAAGCTCAACGTTTGGGGCG	C. Schiklenk
459	ptr8 rev FseI	ATATA GGCCGGCC TTTGAAGGGTTTAATTCGCCG	C. Schiklenk
460	ptr8 col fw	ATGGTGGAACTCCACAGCAGG	C. Schiklenk
461	ptr8 col rev	GGGGTTTCATGCAAAAGTCCCGC	C. Schiklenk
462	lacO-2	GCGGATAACAATTCAGTCTACC	C. Schiklenk
463	lacO-1	TTATCCGCTCACAATTCTACCGCCGC	C. Schiklenk
464	lacO-3	GACCTCTAGCATAGAAAGTTC	C. Schiklenk
465	FseI-est1 fw	ATATA GGCCGGCC CAGTTGATTGCATTTTACAGACGC	C. Schiklenk
466	est1 FseI rev	ATATGGCCGGCC AGTATCATTAAACGTTACACCCG	C. Schiklenk
467	est1 col fw	CTTGCCTCAAAAAACGCGGCGC	C. Schiklenk
468	est1 col rev	ATAGGTATCAGCCATGCGCTGG	C. Schiklenk
469	lacO4	CCGCTCACAATTTTATTCACCG	C. Schiklenk
470	lacO5	GGATAACAATTAGGGGTGGGC	C. Schiklenk
191A	rtz1 dZF 25-83 fw new	P-AATCTAAGTGAAAGACTGCCACC	C. Schiklenk
B102	BamHI-Promoter-Ura4 rev	CATCAT GGATCC AACTTTGCTTTTAAACCTTTAATTTCGATC	Petrova
B138	S3 fw	CGTACGCTGCAGGTCGAC	Petrova
B139	S3 rev	ATCGATGAATTCGAGCTCG	Petrova
B16	his7 3' fw	GGGAGATGCTAAAGTTGCATG	Petrova
B166	cut14-seq5-fwd	TATCATGGGCGGTACAAGCAAA	Petrova
B167	cut14-seq6-fwd	ATCGAAACAGGAGGTTTTAATACT	Petrova
B168	cut14-seq7-fwd	ATGGTTTTGTAATATATCGATTT	Petrova
B169	cut14-seq8-fwd	AACTTTCTTTGCCGATTCAGGGGTA	Petrova
B17	his7 5' rev	CACTCTTGTTTGCACTCTGCCG	Petrova
B170	cut14-seq9-fwd	ATAGTCATTCTCGGACTTTTCCAA	Petrova
B171	cut14-se105-fwd	ATCGCGATGAATGGTCTTTATCAT	Petrova

continued on next page.

#	Name	Sequence 5'→3'	Designed by
B18	GFP 5'rev	CCGTCCAGCTCGACCAGGATGG	Petrova
B180	cnd2-NotI-fw	GAGAGGTG GCGGCCGC ATGAAAAGAGCTAGTTTAGGCG	Petrova
B181	cnd2-NotI-rev	CTCACCTC GCGGCCGC TTAAACATCATTTTCTAATGCTTCTAG	Petrova
B19	Amp-3'fw	CGGGGAGTCAGGCAACTATGG	Petrova
B195	cnd2-seq1	GCTCTCATCAGGTTCCTGTTC	Petrova
B196	cnd2-seq2	GGGAGACCTTGAATGGTATTTAC	Petrova
B197	cnd2-seq3	CAAGCTTCCCAAGTCTCATTG	Petrova
B20	Amp-5'rev	CCGCAAAAAAGGGAATAAGGGC	Petrova
B221	cnd2 S1	CAAGCAACGAAGATTTTTCAGATGTTTTTATTAGGCCAGGTC-CTAACTTGACGACGCTA-GAAGCATTAGAAAATGATGTTCGTACGCTGCAGGTCGAC	Petrova
B240	cut14-R8 fw	ACT CAT CAT TGA TGA TTT CAA ATC ATA TG	Petrova
B241	cut14-R8 rev	CAT ATG ATT TGA AAT CAT CAA TGA TGA GT	Petrova
B242	cnd2-AE9 fw	CGACATGTCGCTTCC ACGTGATGGTGAAG	Petrova
B243	cnd2-AE9 rev	CTT CAC CAT CAC GTG GAA GCG ACA TGT CG	Petrova
B247	Rtz1 CDS fw-NotI	GAGAGCT GCGGCCGC ATGTCAAATGAGGAATCTTTTAC	Petrova
B279	rtz1 rev	GGAGTAGGTCTCTCACCTGC	Petrova
B279	rtz1-seq1-rev	GGAGTAGGTCTCTCACCTGC	Petrova
B280	rtz1-seq2	GCATTTGCTAGAAGCGATG	Petrova
B281	rtz1-seq3	CGACTGGACTTACAGGGAG	Petrova
B282	rtz1-seq4	CCCTGTGGGTCTATCAAGC	Petrova
B283	rtz1-seq5	GATGGCTGGTGCTCTCTTG	Petrova
B284	rtz1-seq6	TCTACTCGAAGTTATAGCAGCTTATG	Petrova
B30	dis1 Prom fw	CTGCACAGCT GTCGAC GGCGTAACACGGCTTCTTTGCG	Petrova
B7	kanMX6	GCTAGGATACAGTTCTCACATCACATCCG	Petrova
c171	MatingType1	AGAAGAGAGAGTAGTTGAAG	Nurse Lab
c172	MatingPlus	ACGGTAGTCATCGGTCTTCC	Nurse Lab
c173	MatingMinus	TACGTTCAGTAGACGTAGTG	Nurse Lab
c256	purg1	ATAAATAAGGGAGGAAATCCATACG	Petrova
c341	cnd1 seq 5 fw	GCTGGGTATTATGGCTCGTTC	Petrova
c452	kanMX	CGATACCAGGATCTTGCCATCC	Ilaria Piazza
C47	nat fw	CGGCGGATGGGGTTCACCC	Haering
C48	MX rev	ATGCCCCTGAGCTGCGC	Haering
C75	EGFPR(225)	CTGCTTCATGTGGTCGGG	Haering
CK1	fw-SpeI-mNeonG	AGGATTACTAGTATGGTTTCTAAGGGTGAAG	C. Klein
CK10	rev-BstEIIadh1Term	AGGATTGGTGACCCCGGTAGAGGTGTGGTCAATAAG	C. Klein
CK11	fw-BamHI-mKATE	AGGATTGGATCCATGGTGAGCGAGCTGATTAAG	C. Klein
CK12	fw-cut14-seq-3	GCTCTATGATAAAGACCATTCATCGCG	C. Klein
CK13	fw-cnd1-Cttag-inner	GTGGTGTATGCACTTTCTTTGC TTCCTCATAAAGCC-GATAATATTCAAAAGCTCATTGACGATGGATATCATGAA CGTACGCTGCAGGTCGAC	C. Klein
CK14	fw-cnd1-Cttag-outer	GCCGAACGTCTGGCTGCTCGTCTTGATCGGTGTAAAACT-CAACGTCAATGGGATCAT GTGGTGTATGCACTTTCTTTGC	C. Klein
CK15	rev-cnd1-Cttag-inner	CGTCATTCTTCTTTTTAATTAGGCAATAC TAATATACAAAG-GATTTTGAATATGTAAGATAAAGCATTAGAATTGACTTTA ATCGATGAATTCGAGCTCG	C. Klein
CK16	rev-cnd1-Cttag-outer	GATCAATGAAGTTATAGTTATTAACATTCAATTCGT-TATAAAAAAGGTATACC GTCATTCTTCTTTTTAATTAGGCAATAC	C. Klein
CK17	fw-cnd3-Cttag-inner	CGAAATTATTCCTGATACAGTGGAAG CCAACATGGAAGAC-GAGGAGGAAGTTTATGTTAAACAAGAAGAAGATCTT CGTACGCTGCAGGTCGAC	C. Klein
CK18	fw-cnd3-Cttag-outer	GAAGAAAGATTAATGGAAAATGCTGAAGAGAATGAACAT-GCTGGAGCTGAAGCCATATCTGG CGAAATTATTCCTGATACAGTGGAAG	C. Klein
CK19	rev-cnd3-Cttag-inner	CTTTTATCAGTTTCTGAAAGATATGCG GAAGGGATTCCGT-GAACTTCATAGAAAGGATCTGTCTCAATTGATTTA ATCGATGAATTCGAGCTCG	C. Klein
CK2	rev-RsrII-mNeonG	AGGATTCGGTCCGCTTGTACAATTCGTCCATACC	C. Klein
CK20	rev-cnd3-Cttag-outer	GCATTGTCATCCACCTCTACCACATGTTGATGATTTGGTAAA-CAAGGTTAATCGCACTAGAGA CTTTTATCAGTTTCTGAAAGATATGCG	C. Klein
CK21	fw-SpeI-mKate2	AGGATTACTAGTATGGTGAGCGAGCTGATTAAG	C. Klein
CK23	pdis1-fw-seq	CATGCTCTGCTGGTTGTAAAC	C. Klein
CK24	rw-RsrII-mkate2-nostop	AGGATTCGGTCCGTCTGTGCCCCAGTTTGCTAG	C. Klein
CK25	fw-cnd3-seq	CGCAAGTATGCTCAAACTGGTGG	C. Klein
CK26	fw-cnd2-seq	GATGGAGAAGGACAGCTACAACTG	C. Klein
CK27	fw-cnd1-seq	CGAGCCATAATACCCAGCTGG	C. Klein
CK28	fw-ChrI-2.49-FseI	AGGATTGGCCGGCCAAATTGAGCACGATCAATAACT	C. Klein
CK29	rev-ChrI-2.49-FseI	AGGATTGGCCGGCCGATCTGATTTAGGCAGCGCAGAGC	C. Klein
CK3	fw-SpeI-sfGFPyco	AGGATTACTAGT ATGTCCAAGGGTGAAGAGC	C. Schiklenk
CK3	fw-SpeI-sfGFP	AGGATTACTAGTATGTCCAAGGGTGAAGAGC	C. Klein
CK4	rev-RsrII-sfGFPyco	AGGATT CGGTCCG CTTATAAAGCTCGTCCATTCCG	C. Schiklenk
CK4	rev-RsrII-sfGFP	AGGATTCGGTCCGCTTATAAAGCTCGTCCATTCCG	C. Klein
CK5	fw-pMaM4-370-a¿t	CGAAGGGGATACACTTGTTAATCGCATCG	C. Klein
CK6	rev-pMaM4-370-a¿t	CGATGCGATTAACAAGTGTATCCCCTTCG	C. Klein
CK7	fw-BamHI-S1-mKATE	AGGATTGGATCCCGTACGCTGCAGGTCGACATGGTGAGC-GAGCTGATTAAG	C. Klein
CK8	rev-taa-AgeI-mKATE	AGGATTACCGGTTTATCATCTGTGCCCCAGTTTGC	C. Klein
CK9	fw-AgeI-adh1term	AGGATTACCGGTGCGAATTTCTTATGATTTATGATTTTTA	C. Klein
M1	pMSG-mcs rev	CGTTCCCTAGGCTCGAGTGCCTGGCGCGCCTGAAAGCGGC-CGCCGCGAGGTACCTATCGGCATGCCTTTACATGT GAGCAAAAGGCCAG	C. Schiklenk
M10	T-adh AscI	AGGATT GGCGCGCC TGCCGGTAGAGGTGTGGTC	C. Schiklenk
M11	AvrII P-dis1	AGGATT CCTAGG AGAAACTCAAGGCGTAACACG	C. Schiklenk
M12	P-dis1 SpeI	AGGATT ACTAGT TTACATAAACAAATATAAATTAACGAC	C. Schiklenk
M13	SpeI EGFP fw	AGGATT ACTAGT ATGAGTAAAGGAGAAGAACTTTTC	C. Schiklenk
M14	EGFP RsrII rev	AGGATT CGGTCCG TAGTTCATCCATGCCATGTG	C. Schiklenk

continued on next page.

#	Name	Sequence 5'→3'	Designed by
M15	SpeI ZsGreen fw	AGGATT ACTAGT ATGGCCCAGTCCAAGCACG	C. Schiklenk
M16	ZsGreen RsrII rev	AGGATT CGGTCCG CACATTGATCCTAGCAGAAGCAC	C. Schiklenk
M17	RsrII LacI fw	AGGATT CGGACCG AA GTAACGTTATACGATGTCGC	C. Schiklenk
M18	LacI NheI rev	AGGATT GCTAGC TTAGGCAACCTTTCTCTTCT	C. Schiklenk
M19	NheI nmt terminator fw	AGGATT GCTAGC TCCCTTGCCAGTACTGCTAGG	C. Schiklenk
M2	pMSG-mcs fw	GCACTCGAGCCTAGGGAACGACTAGTGCATTCGGACCGATG-GTGCTAGCTACTAAGGCCGGCCAACT AAATGTGCGCGGAACCCCTA	C. Schiklenk
M20	nmt terminator FseI rev	AGGATT GGCCGGCC GAAGTCAAGCTCATAGACTCGG	C. Schiklenk
M20	M20 nmt terminator Fse rev	AGGATT GGCCGGCC GCATTACTAATAGAAAGGATTATTTCAC	C. Schiklenk
M21	SalI Crimson	AGGATT GTCGAC ATGGATAGCACTGAGAACGT	C. Schiklenk
M22	AscI Crimson	AGGATT GGCGCGCC CTACTGGAACAGGTGGTGG	C. Schiklenk
M23	Pdis1 fw AvrII	GCGCGCCAGGCACTCGAG CCTAGG AAAATTTGATCAAGCATGGTATTACATCG	C. Schiklenk
M24	Pdis rev SpeI	CAGTGAAAAGTTCTTCTCCTTTACTCAT ACTAG TTACATAAACAAATATAAATTAACGACTCGTATGTT	C. Schiklenk
M25	GFP fw SpeI	AACATACGAGTCGTTAATTTATATTTGTTTATGTAA ACTAGT ATGAGTAAAGGAGAAGAACTTTTCACTG	C. Schiklenk
M26	GFP rev RsrII	CTGCGACATCGTATAACGTTAC TT CGGTCCG TAGTTCATCCATGCCATGTGTAATCC	C. Schiklenk
M27	LacI fw RsrII	GATTACACATGGCATGGATGAACTA CGGACCG AA GTAACGTTATACGATGTCGCAGAGT	C. Schiklenk
M28	LacI rev NheI	TAGCAGTACTGGCAAGGGA GCTAGC TTAGGCAACCTTTCTCTTCTTCTTTGG	C. Schiklenk
M29	Nmt Term fw NheI	CCAAAGAAGAAGAGAAAGGTTGCCTAA GCTAGC TCCCTTGCCAGTACTGCTAG	C. Schiklenk
M3	PciI P-adh	AGGATT ACATGT CCTACAACAACTAAGAAAATG	C. Schiklenk
M30	Nmt Term rev FseI	CAAATAGGGGTTCCGCGCACATTTAGTT GGCCGGCC CATTACTAATAGAAAGGATTATTTCACTTCTAATTACACA	C. Schiklenk
M33	ChrIII XhoI fw	AGGATT CTCGAG ATGCCCCTGCTCGTCTTCCC	C. Schiklenk
M34	ChrIII site XhoI rev	AGGATT CTCGAG GCGCCAATGTTATCTTAAACTTCAATGC	C. Schiklenk
M35	ade6 fw AscI	AGGATTA GGCGCGCC ATGCCCCTGCTCGTCTTCCC	C. Schiklenk
M36	ade6 rev AvrII	AGGATTA CCTAGG TTGGGAACATGGTCAACGGG	C. Schiklenk
M4	P-adh SphI	AGGATT GCATGC ATATGGGCAATTCTCTTGCT	C. Schiklenk
M5	SphI TetR	AGGATT GCATGC ATATGTCTAGATTAGATAAAAGTAAAG	C. Schiklenk
M6	TetR KpnI	AGGATT GGTACC TAGACCCACTTTCACATTTA	C. Schiklenk
M7	KpnI tdTom	AGGATT GGTACC TTATGGTGAGCAAGGGCGAG	C. Schiklenk
M7b	KpnI tdTom II	AGGATT GGTACC TTATGGTGAGCAAGGGCGAGGAG	C. Schiklenk
M8	tdTom NotI	AGGATT GCGGCCGC CGCTTAGGCAACCTTTCTCTTC	C. Schiklenk
M9	NotI T-adh-Sc	AGGATT GCGGCCGC CGCCACTTCTAAATAAGCGAAT	C. Schiklenk
Z101	spZAS1 5' BamHI S317	AGAGG GGATCC TCCATCGCCTCCTCTAGGACTATGG	M. Hassler
Z102	spZAS1 5' BamHI M378	AGAGG GGATCC ATGTATGTTCCTCAGAAATGTCCTGCTACC	M. Hassler
Z103	spZAS1 3' D897 stop EcoRI	AAGGAC GAATTC TCA TTA ATCATTTCCCTTG-GATAATAATTGTTGTATGATTTTTTTATGTTCG	M. Hassler

4.14 List of plasmids

Table 4.17: List of plasmids

#	Name	origin
3	pFastBac 6HTb	Invitrogen
75	pFA6a PK6 kanMX6	Bahler et al. 1998
237	pFA6a-kanMX4	Wach et al. 1994
467	pFA6a-natMX4	Wach et al. 1994
1286	pFA6-3x mCherry-kanMX6	M. Knop Lab
1308	pNATZA31-tetR-Tomato	Y. Watanabe Lab
1695	pYM16 2TEV	this study
1861	pKM40	Kanke et al. 2011
1937	pZsGreen1-DR	P. Neveu lab
1948	pE2 Crimson	P. Neveu lab
1950	pUR-Pnmt81-zas1-noSwaI-TEV2-HA6	this study
1952	pUR-Pnmt41-zas1-noSwaI-TEV2-HA6	this study
1953	pUR-Pnmt1-zas1-noSwaI-TEV2-HA6	this study
2199	pBlueScript KS zas1-cDNA	this study
2204	pGEX6P1-zas1(261-845)	this study
2205	pGEX6P1-zas1(326-845)	this study
2279	pGEX6P1-zas1(358-845)	this study
2299	pNat zas1-Tzas-natMX	this study
2301	pET MCN HIs6-TEV-zas1(261-845)	this study
2302	pNat Pzas-zas1cDNA-Tzas-NatMX	this study
2314	pUra4 MCS 12HA-zas1	this study
2320	pNat zas1 delta 276VxxLFSS	this study
2321	pET MCN HIs6-TEV-zas1(358-845)	this study
2323	pET MCN HIs6-TEV-zas1(326-845)	this study
2325	pUra4 MCS HA6-zas1	this study
2326	pNat Pzas-zas1-cDNA-ΔZF-Tzas-natMX	this study
2338	pNat zas1-cDNA-S281D-S282N	this study
2339	pNat zas1-cDNA-S281A	this study
2340	pNat zas1-cDNA-S281D S282D	this study
2341	pFastBac HTb zas1	this study
2352	pNat zas1-cDNAΔ linker	this study
2379	pGen zas1-cDNA	this study
2389	pFastBac HTb zas1 ΔMotif	this study
2395	pGen zas1-cDNAΔlinker	this study
2396	pGen zas1-cDNAΔmotif	this study
2507	pFastBacHTb-zas1-S273-845	this study
2508	pFastBacHTb-zas1-S309-845	this study
2557	pNat Pzas-zas1cDNA-tdTomato-Tzas-natMX	this study
2562	pMSG8a	this study
2565	pMSG9A	this study
2593	pFR E2Crimson-LacI	this study
2602	pFR ura4 E2Crimson-lacI	this study
2625	pFR tetR-tdTom ura4 E2Crimson lacI	this study
2633	pFR tetR-tdTom ura4 lacI-E2Crimson srk1+	this study
2645	p3E sfGFP	this study
2650	pNat zas1-Δ102-268	this study
2651	pNat zas1-Δ211-255	this study
2652	pNat zas1-ΔZF	this study
2653	pNat zas1-ΔMotif	this study
2657	pET MCN HIs6-TEV-zas1(1-Q211)	this study
2658	pET MCN HIs6-TEV-zas1(1-S282)	this study
2750	pET MCN 6His-TEV-zas1-289	this study
2757	pLau44	Lau et al. 2003

continued on next page.

#	Name	origin
2771	pNat zas1-ΔNLS	this study
2772	pNat zas1-V276K-F280K	this study
2773	pNat zas1-V276K-W278K-F280K	this study
2776	pNat PK6-3C2-zas1 cDNA	this study
2779	pTetO hphMX	this study
2781	pNat zas1 98-261 PK6	this study
2804	pNat zas1-PRLGGG-BirA	this study
2805	pNat zas1 ucs PK6	this study
2806	pNat zas1-PRLGGG-BirA*	this study
2812	pUra4 urg1	this study
2813	pUra4 MCS	this study
2820	pUra4 Purg1 NLS p14-TEV$^+$ 8DSR Turg1	this study
2821	pUra4 Purg1 NLS p14-TEV$^+$ myc3 NLS2 8DSR Turg1	this study
2822	pNat zas1-cDNA-Δ103-147	this study
2823	pNat zas1-cDNA-(98-261)::TEV2 PK6	this study
2824	pNat zas1-cDNA-(98-261)::TEV-F2 PK6	this study
2829	pNat zas1-cDNA-(98-261)::TEV2 PK6 ΔCT	this study
2830	pNat zas1 ΔNLS	this study
2831	pNat zas1-V276K-F280K	this study
2834	pUra4 Purg1 NLS p14-TEV$^+$ myc3 NLS2 4DSR Turg1	this study
2835	pUra4 Purg1 NLS p14-TEV$^+$ myc3 NLS2 Turg1	this study
2856	pFA6a kanMX cnd3-Promoter	this study
2871	pFR sfGFP(noSpeI)-Linker-LacI ura4 srk1	this study
2872	pFR tetR-tdTom ura4 EGFP-lacI srk1	this study
2873	pFR tetR-tdTom ura4 mNeonGreen-lacI srk1	this study
2879	pFR sfGFP2-lacI ura4 srk1	this study
2880	pTetO hphMX ChrI 2.49	this study
2884	pFR tetR-tdTom ura4 sfGFP-lacI srk1	this study
2885	pFR tetR-tdTom ura4 sfGFP-sfGFP-lacI srk1	this study
2917	pUra4 Purg1 SpCOTEV$^+$-HA6-TEVsite2-NLS-TEV$^+$-myc3-NLS2 Turg1	this study
2918	pNat HATEVY-zas1	this study
2963	pTetO hphMX lys1	this study
2977	pFR Padh31 TetR-tdTom Tadh ura4	this study
2978	pFA6a cut3(D1207-end) kanMX	this study
2979	pFA6a cut14(N962-end) kanMX	this study
2980	pFR Pahd31 tetR-tdTom Tadh1 ura4 srk1	this study
2983	pFA6a cut14(N962-end)W1079A kanMX	this study
2984	pFA6a cut14(N962-end)S1077A K1080E kanMX	this study
2989	pFA6a cut14(N962-end)K1080E kanMX	this study
3054	pLau43-ΔXhoIFragment	this study
3055	pTetO hphMX est1	this study
3058	pFR lacOs	this study

List of plasmids.

4.15 Source code

4.15.1 MetadataDrift.py

```
#MetadataDrift: A plugin in the FROS tracking pipeline to correct stack format, metadata and xydrift
#author: Christoph Schiklenk

from os import listdir, path, mkdir
import re

from ij import IJ, WindowManager
from ij.io import DirectoryChooser, Opener, FileSaver
from ij.plugin import HyperStackConverter
from ij.process import StackConverter

from loci.formats.in import LIFReader, BaseTiffReader
from loci.formats import MetadataTools
from loci.plugins import BF
from loci.plugins.in import ImporterOptions

from javax.swing import JDialog, JTextField, JLabel, JButton, JFrame, JPanel, JCheckBox, JOptionPane
from javax.swing import SwingConstants, BoxLayout, BorderFactory
from java.awt import GridLayout, Dialog, Color

#Globals
RAWDIRNAME = "raw"

def roiPos(l):
    offset = max(l)
    if (abs(min(l)) <= abs(max(l))):
        return int(round(offset)), int(round(abs(max(l))))
    if (abs(min(l)) > abs(max(l))):
        return int(round(offset)), int(round(abs(min(l))))

class experiment:
    def __init__(self, date=None, strain=None, temp=None, experimentPath=None):
        if (date == None or strain == None or temp == None or experimentPath == None):
            i = initDialog()
            self.experimentPath, self.date, self.strain, self.temp, self.pxWidth, self.pxHeight, self.pxDepth, \
            self.timeInterval, self.nChannels, self.nSlices, self.nFrames = i.getData()
            self.exportMetaData()
            driftcorrect = i.getOptions()
        self.rawPath = path.join(self.experimentPath, "raw")
        # Make position instances from .dv and .dv.log pairs
        self.positionList = []
        fileList = [path.join(self.rawPath, f) for f in listdir(self.rawPath) if not f == ".DS_Store"] # .DS_Store for Mac only.
        positionID = 0
        for f in fileList:
            if path.splitext(f)[1] == ".dv": # for .dv files (DeltaVision)
                dvFilePath = f
                positionID += 1
                if path.isfile(f + ".log"):
                    logFilePath = f + ".log"
                else: logFilePath = None
                self.positionList.append(position(self, originalFilePath=dvFilePath, positionID=positionID, logFilePath=logFilePath))
            elif path.splitext(f)[1] == ".btf" or path.splitext(f)[1] == ".tif": # for big tif files from olympus TIRF
                originalFilePath = f
                positionID += 1
                p = position(self, originalFilePath=f, positionID=positionID, logFilePath=None)
                self.positionList.append(p)
                imp = Opener.openUsingBioFormats(f)
                #correct calibration
                cal = imp.getCalibration()
                cal.setTimeUnit("second")
                cal.frameInterval = float(self.timeInterval)
                cal.setUnit("micron") # set length unit
                cal.pixelWidth = float(self.pxWidth)
                cal.pixelHeight = float(self.pxHeight)
                cal.pixelDepth = float(self.pxDepth)
                #correct stack dimensions
                imp = HyperStackConverter().toHyperStack(imp, int(self.nChannels), int(self.nSlices), int(self.nFrames))
                imp.show()
                # Correct drift if
                if driftcorrect:
                    p.driftCorrect(imp, True, True)
                imp.close()

    def driftcorrectPositions(self):
        for p in self.positionList:
            print "Correcting position " + str(self.positionList.index(p)+1) + "/" + str(len(self.positionList))
            imp = p.openOriginalImage()
            p.driftCorrect(imp, True, True)

    def exportMetaData(self):
        "Saves date, strain and temp in a .csv file in an Analysis folder so that its readable for R"
        self.analysisPath = path.join(self.experimentPath, "Analysis")
        if not path.exists(self.analysisPath):
            mkdir(self.analysisPath)
        self.metaDataFilePath = path.join(self.analysisPath, "meta.csv")
        f = open(self.metaDataFilePath, "w")
        f.write("Date,Strain,Temp,pxWidth,pxHeight,pxDepth,timeInterval,nChannels,nSlices,nFrames\n")
        f.write(self.date + "," + self.strain + "," + self.temp + "," + self.pxWidth + "," + self.pxHeight + "," + \
        self.pxDepth + "," + self.timeInterval + "," + self.nChannels + "," + self.nSlices + "," + self.nFrames + "\n")
```

```
90          f.close()
91
92  class position:
93      def __init__(self, experiment, originalFilePath, positionID, logFilePath=None, dc8BitFilePath=None):
94          self.experiment = experiment
95          self.positionID = positionID
96          self.originalFilePath = originalFilePath
97          self.logFilePath = logFilePath
98          if dc8BitFilePath == None:
99              self.dc8BitFilePath = path.splitext(self.originalFilePath)[0] + "_dc.tif"
100         else:
101             self.dc8BitFilePath = path.join(path.split(self.originalFilePath)[0], dc8BitFilePath)
102         self.cellList = []
103
104     def openOriginalImage(self):
105        #open with Bio-Formats importer
106        imp = Opener().openUsingBioFormats(self.originalFilePath)
107        if imp.getBitDepth() != 8:
108            IJ.run(imp, "8-bit", "")
109        return imp
110
111     def driftCorrect(self, imp, saveResults=True, saveImage=True):
112         """This method calculates the drift of the position using turboReg in a macro wrapper,
113            saves the results and saves the drift corrected image."""
114         xDriftArray, yDriftArray = self.calculateDrift(imp, saveResults)
115         driftCorrectedImp = self.applyDriftCorrection(imp, xDriftArray, yDriftArray)
116         #save output
117         if saveImage:
118             FileSaver(driftCorrectedImp).saveAsTiffStack(self.dc8BitFilePath)
119             self.driftCorrected = True
120         imp.close()
121         IJ.freeMemory()
122
123     def calculateDrift(self, imp, save=True):
124         # close potential old results windows
125         if WindowManager.getWindow("Results"):
126             WindowManager.getWindow("Results").close()
127         imp.show()
128         IJ.runMacroFile("/Users/schiklen/codes/PipelineRefactoring/DriftMeasure_.ijm")
129         resWindow = WindowManager.getWindow("Results")
130         resTable = resWindow.getTextPanel().getResultsTable()
131         xDriftArray = resTable.getColumn(1)
132         yDriftArray = resTable.getColumn(2)
133         if save: # save drift table as .csv
134             self.driftResultsPath = path.splitext(self.dc8BitFilePath)[0] + "_drift.csv"
135             f = open(self.driftResultsPath, "w")
136             f.write("Frame,xDrift,yDrift\n")
137             for frame in range(len(xDriftArray)):
138                 f.write(str(frame) + "," + str(xDriftArray[frame]) + "," + str(yDriftArray[frame]) + "\n")
139             f.close()
140         resWindow.close(False)
141         return xDriftArray, yDriftArray
142
143     def applyDriftCorrection(self, imp, xDriftArray, yDriftArray):
144         for frame in range(imp.getNFrames()):
145             xOffset = xDriftArray[frame]
146             yOffset = yDriftArray[frame]
147             for channel in range(imp.getNChannels()):
148                 for slic in range(imp.getNSlices()):
149                     imp.getStack().getProcessor(imp.getStackIndex(channel+1, slic+1, frame+1)).translate(xOffset, yOffset) # int
150         imp.show()
151         # Create roi of minimal region and crop it
152         xOffset, xShift = roiPos(xDriftArray)
153         yOffset, yShift = roiPos(yDriftArray)
154         imp.setRoi(xOffset, yOffset, imp.getWidth()-xShift, imp.getHeight()-yShift)
155         IJ.run(imp, "Crop", "")
156         return imp
157
158 class initDialog(JDialog):
159     """initialization gui for experiment class"""
160     def __init__(self):
161         self.setModalityType(Dialog.ModalityType.APPLICATION_MODAL)
162         self.setDefaultCloseOperation(JDialog.DISPOSE_ON_CLOSE)
163
164         # GUI elements from which info is fetched
165         self.frame = JFrame("Initdialog")
166         self.dateField = JTextField("", 10)
167         self.strainField = JTextField("", 10)
168         self.tempField = JTextField("", 10)
169         self.dirField = JTextField(10)
170         self.driftcorrCB = JCheckBox("Driftcorrect", True)
171         self.xField = JTextField("", 10)
172         self.yField = JTextField("", 10)
173         self.zField = JTextField("", 10)
174         self.tField = JTextField("", 10)
175         self.slicesField = JTextField("", 10)
176         self.cField = JTextField("", 10)
177         self.nFramesField = JTextField("", 10)
178
179         # GUI layout
180         self.Panel = JPanel()
181         self.Panel.setLayout(BoxLayout(self.Panel, BoxLayout.Y_AXIS))
182         blackline = BorderFactory.createLineBorder(Color.black)
183
184         self.dirChoosePanel = JPanel(GridLayout(0,2))
```

```
185         self.dirButton = JButton("Choose dir...", actionPerformed=self.choseDir)
186         self.dirChoosePanel.add(self.dirButton)
187         self.dirChoosePanel.add(self.dirField)
188         #metadata Panel
189         self.metaDataPanel = JPanel(GridLayout(0,2))
190         self.metaDataPanel.setBorder(BorderFactory.createTitledBorder(blackline, "Metadata"))
191         self.metaDataPanel.add(JLabel("Date", SwingConstants.RIGHT))
192         self.metaDataPanel.add(self.dateField)
193         self.metaDataPanel.add(JLabel("Strain", SwingConstants.RIGHT))
194         self.metaDataPanel.add(self.strainField)
195         self.metaDataPanel.add(JLabel("Temperature (C)", SwingConstants.RIGHT))
196         self.metaDataPanel.add(self.tempField)
197         #calibration Panel
198         self.calibrationPanel = JPanel(GridLayout(0,2))
199         self.calibrationPanel.setBorder(BorderFactory.createTitledBorder(blackline, "Calibration"))
200         self.calibrationPanel.add(JLabel("Voxel width (micron)", SwingConstants.RIGHT))
201         self.calibrationPanel.add(self.xField)
202         self.calibrationPanel.add(JLabel("Voxel height (micron)", SwingConstants.RIGHT))
203         self.calibrationPanel.add(self.yField)
204         self.calibrationPanel.add(JLabel("Voxel depth (micron)", SwingConstants.RIGHT))
205         self.calibrationPanel.add(self.zField)
206         self.calibrationPanel.add(JLabel("Time interval (s)", SwingConstants.RIGHT))
207         self.calibrationPanel.add(self.tField)
208         #dimension Panel
209         self.dimensionPanel = JPanel(GridLayout(0,2))
210         self.dimensionPanel.setBorder(BorderFactory.createTitledBorder(blackline, "Image Dimensions"))
211         self.dimensionPanel.add(JLabel("Number of channels", SwingConstants.RIGHT))
212         self.dimensionPanel.add(self.cField)
213         self.dimensionPanel.add(JLabel("Number of slices", SwingConstants.RIGHT))
214         self.dimensionPanel.add(self.slicesField)
215         self.dimensionPanel.add(JLabel("Number of frames", SwingConstants.RIGHT))
216         self.dimensionPanel.add(self.nFramesField)
217         self.dimensionPanel.add(JLabel("Total number of images", SwingConstants.RIGHT))
218         self.totalNImg = JLabel("", SwingConstants.CENTER)
219         self.dimensionPanel.add(self.totalNImg)
220         #ok cancel panel
221         self.okCancelPanel = JPanel(GridLayout(0,2))
222         self.okCancelPanel.add(self.driftcorrCB)
223         self.okCancelPanel.add(JLabel(""))
224         self.cancelButton = JButton("Cancel", actionPerformed=self.close)
225         self.okButton = JButton("OK", actionPerformed=self.ok)
226         self.okCancelPanel.add(self.cancelButton)
227         self.okCancelPanel.add(self.okButton)
228         #add all sub panels to the dialog panel
229         self.Panel.add(self.dirChoosePanel)
230         self.Panel.add(self.metaDataPanel)
231         self.Panel.add(self.calibrationPanel)
232         self.Panel.add(self.dimensionPanel)
233         self.Panel.add(self.okCancelPanel)
234         self.add(self.Panel)
235         self.pack()
236         self.show()
237
238     def close(self, event):
239         self.dispose()
240
241     def choseDir(self, event):
242         d = DirectoryChooser("Choose Experiment Directory")
243         if path.isdir(d.getDirectory()):
244             self.directory = d.getDirectory()[:-1] # delete trailing / that the DirectoryChooser returns
245             self.dirField.setText(self.directory)
246             #try to parse date, strain and temp from self.directory basename
247             r = re.compile("^(?P<date>\d{6})[-_ ](?P<strain>\d{4})[-_ ](?P<temp>\d{2}).*")
248             mo = re.match(r, path.basename(self.directory))
249             if mo:
250                 self.dateField.setText(mo.group("date"))
251                 self.strainField.setText(mo.group("strain"))
252                 self.tempField.setText(mo.group("temp"))
253             else:
254                 print "No Experiment folder"
255             #Creating list of image files in folder
256             rawDir = path.join(self.directory, "raw")
257             fileList = [path.join(rawDir,f) for f in listdir(rawDir) if (f.endswith(".tif") or f.endswith(".btf"))]
258             firstImageFile = fileList[0]
259             iO = ImporterOptions()
260             iO.setVirtual(True)
261             iO.setId(firstImageFile)
262             imp = BF.openImagePlus(iO)[0]
263             #interface for correction of dimensions
264             width, height, nChannels, nSlices, nFrames = imp.getDimensions()
265             totalNImg = nChannels*nSlices*nFrames
266             self.totalNImg.setText(str(totalNImg))
267             vxWidth = imp.getCalibration().pixelWidth
268             vxHeight = imp.getCalibration().pixelHeight
269             vxDepth = imp.getCalibration().pixelDepth
270             interval = imp.getCalibration().frameInterval
271             #interface for correction of calibration
272             if imp.getDimensions():
273                 self.xField.setText(str(vxWidth))
274                 self.yField.setText(str(vxHeight))
275                 self.zField.setText(str(vxDepth))
276                 self.tField.setText(str())
277                 self.slicesField.setText(str(nSlices))
278                 self.nFramesField.setText(str(nFrames))
279                 self.cField.setText(str(nChannels))
```

```
    def ok(self, event):
        if "" in (self.dateField.getText(), self.strainField.getText(), self.tempField.getText(), self.dirField.getText()):
            JOptionPane.showMessageDialog(self ,"Please complete all fields.")
        else:
            self.dispose()

    def getData(self):
        return self.directory, self.dateField.getText(), self.strainField.getText(), self.tempField.getText(), str(self.xField.getText()), \
        str(self.yField.getText()), str(self.zField.getText()), str(self.tField.getText()), str(self.cField.getText()), \
        str(self.slicesField.getText()), str(self.nFramesField.getText())

    def getOptions(self):
        return self.driftcorrCB.isSelected()

# M A I N
experiment()
```

4.15.2 DriftcorrectHeadless ImageJ macro

ImageJ macro language script wrapper for TurboReg

```
//Driftcorrect headless mode

/*
 * A 2D drift correction macro for multichannel multislide stacks
 * by Christoph Schikenk, schiklen@embl.de
 */


macro "DriftCorrectHeadless_" {

    startout = 0;
        REFCH = 0;
        ipos = 0; // imaged position currently processed
        ch = 0;
        frame = 0;
        slice = 0;
        directapply = true;
        crop = true;
        splitch = false;
        setrefch = false;

        //take the only window thats open
        title = getTitle();
        openimage = getImageID();

        setBatchMode(true);
        measure_driftcorrect(openimage); // false is for folder-mode = false
        selectImage(openimage);
        apply_driftcorrect(openimage, crop);
        setBatchMode(false);

print("I'm done.");
} // end Macro


// ------ function definitions -------

function measure_driftcorrect(dcstack) // add arg. refchannel
{
    if (isOpen(dcstack) != true) //check that target-window open
        exit("The stack you want to correct for drift is not open!");

    else
    {
        selectImage(dcstack);
        Stack.getDimensions(w, h, chn, sln, frn);
        filename = getInfo("image.filename");
        dcresultsx = newArray(frn+1);
        dcresultsy = newArray(frn+1);

        if (chn > 1 && setrefch == true)
        {
               channelsel = newArray(chn);
               for (i = 0; i < chn; i++)
                   {channelsel[i] = i;}
            refchannel = REFCH;
            Stack.setChannel(refchannel);
        }

        if (sln > 1)
        {
               cenSl = sln/2; // go to central Z-postition. dirty here! needs to be rounded up! cenSl: central slice
               write("Moving to slice " + cenSl + " of " + sln);
               Stack.setSlice(cenSl); // better: z-projection (but which mode? avg/max/min/stdev). make selectable in dialog.
               run("Reduce Dimensionality...", " frames keep");
               dcstack = getImageID(); //
               selectImage(dcstack); // select new window with the reduced timepoint
               Stack.setFrame(0); // set to first time frame - for StackReg as reference
               write("Starting driftcorrect calculation on position " + ipos + ", slide " + cenSl);
        }

        for (frame = 0; frame <= frn; frame++)
        {
            selectImage(dcstack);
            Stack.setFrame(frame);
            run("Duplicate...", "title=sourceimage");
            frame1 = "sourceimage"; // a frame in a sequence

            selectImage(dcstack);
            Stack.setFrame(frame + 1); // select next frame.
            run("Duplicate...", "title=targetimage");
            frame2 = "targetimage"; // next frame in the sequence

            selectWindow(frame1);
            width = getWidth();
            height = getWidth();

            run("TurboReg ",
                "-align "
                + "-window " + frame1 + " "// Source (window reference).
                + " 0 0 " + (width - 1) + " " + (height - 1)
```

```
                + " -window " + frame2 + " "// Target (window reference).
                + " 0 0 " + (width - 1) + " " + (height - 1)
                + " -translation"
                + " " + (width / 2) + " " + (height / 2)
                + " " + (width / 2) + " " + (height / 2)
                + " -hideOutput"
            );

            sourceX0 = getResult("sourceX", 0); // First line of the table.
            sourceY0 = getResult("sourceY", 0);
            targetX0 = getResult("targetX", 0);
            targetY0 = getResult("targetY", 0);

            xoffset = sourceX0 - targetX0; // calculate offsets in respect to previous image.
            yoffset = sourceY0 - targetY0;
            xoffsetsum = xoffsetsum + xoffset; // x and yoffsetsums: value each frame has to be aligned in respect to first frame.
            yoffsetsum = yoffsetsum + yoffset;
            dcresultsx[frame] = xoffsetsum; // saving results for each frame in arrays
            dcresultsy[frame] = yoffsetsum;

            print("Frame " + frame + " - x: " + xoffsetsum + " y: " + yoffsetsum);

            selectWindow(frame1);
            close();
            selectWindow(frame2);
            close();

        } // closes for (frame = 0; frame <= driftcorfrn; frame++);
    } //closes else

        if (sln > 1)
        {
                selectImage(dcstack);
                close();
        }

        print("Done calculating drift");

    // transferring results to results-table
        run("Clear Results");
        for (i = 0; i < dcresultsx.length; i++)
        {
                setResult("Frame", i, i);
                setResult("X-offsetsum", i, dcresultsx[i]);
                setResult("Y-offsetsum", i, dcresultsy[i]);
    }
    absolute_max(dcresultsx); // absolute maxfunction
    setResult("X-max", 0, absolute_max(dcresultsx));
    setResult("X-start", 0, startout);
    absolute_max(dcresultsy);
    setResult("Y-max", 0, absolute_max(dcresultsy));
    setResult("Y-start", 0, startout);
    updateResults();
    selectWindow("Results");
        // saves resultstable as a file.
    filename1 = split(filename, ".");
    imagedir = getInfo("image.directory");
    saveAs("Results", imagedir + filename1[0] + "_drift.tsv");

setBatchMode(false);

} // end of function




// End of code
```

4.15.3 CellExciser.py

```
# CellExciser: A plugin for ImageJ to isolate cells via ROIs
# author: Christoph Schiklenk
# email: schiklen@embl.de

from javax.swing import JButton, JFrame, JPanel, JLabel, JTextField, JScrollPane
from javax.swing import SwingConstants, WindowConstants, BoxLayout
from java.awt import Component, GridLayout, Color
import re
import copy

from os import path, listdir
from os import makedirs as mkdir
from java.awt.event import KeyEvent, KeyAdapter, MouseEvent, MouseAdapter
from ij.plugin import Zoom
from ij.plugin import Duplicator
from ij.plugin.frame import RoiManager
from ij.gui import Overlay, YesNoCancelDialog
from ij.io import OpenDialog, Opener
from ij import WindowManager
from ij import IJ

#Globals
G_saveSubFold = "cutout"

class Menue(object):
    def __init__(self):
        self.counter = 1
        self.olay = Overlay()
        self.od = OpenDialog("Open movie", "")
        self.path = self.od.getDirectory()
        self.filename = self.od.getFileName()
        self.position = self.getPosition(self.path, self.filename)
        regex = re.compile('(?P<prefix>.+)(?P<suffix>\.tif|\.dv|\.btf)$')
        if regex.match(self.filename):
            self.imp = Opener.openUsingBioFormats(self.path + self.filename)
            self.fnPrefix = regex.match(self.filename).group('prefix')
        self.imp.show()
        # check if there is an existing overlay file and load it!
        olre = re.compile(self.fnPrefix+'.zip')
        self.filelist = listdir(self.path)
        for ol in self.filelist:
           if olre.match(ol):
               print olre.match(ol).group()
               try:
                   rm = RoiManager.getInstance()
                   rm.runCommand("reset")
                   Opener().openZip(self.path + olre.match(ol).group())
                   IJ.run("From ROI Manager", "")
               except AttributeError:
                   Opener().openZip(self.path + olre.match(ol).group())
                   IJ.run("From ROI Manager", "")
                   rm = RoiManager.getInstance()
                   rm.runCommand("Show All with labels")
                   rm = RoiManager.getInstance()
        self.frame = JFrame("CellExciser", size=(200,200))
        self.frame.setLocation(20,120)
        self.Panel = JPanel(GridLayout(0,1))
        self.frame.add(self.Panel)
        self.nameField = JTextField("p" + str(self.position) + "_c",15)
        self.Panel.add(self.nameField)
        self.cutoutButton = JButton("Add to ROI list",actionPerformed=self.cut)
        self.Panel.add(self.cutoutButton)
        self.delOlButton = JButton("Clear ROI list",actionPerformed=self.delOverlay)
        self.Panel.add(self.delOlButton)
        self.saveOlButton = JButton("Save ROI list",actionPerformed=self.saveOverlay)
        self.Panel.add(self.saveOlButton)
        self.quitButton = JButton("Quit script",actionPerformed=self.quit)
        self.Panel.add(self.quitButton)
        self.frame.pack()
        WindowManager.addWindow(self.frame)
        self.show()
        IJ.setTool("freehand")

    def getPosition(self, imagePath, filename):
        fileList = listdir(imagePath)
        regex = re.compile('(?P<prefix>.+)(?P<suffix>\.tif|\.dv|\.btf)$')
        imagesInFolder = [path.splitext(f)[0] for f in fileList if regex.match(f)]
        unique = sorted(list(set(imagesInFolder)))

        if filename + ".zip" in fileList:
            openOl(path, filename)

        return unique.index(path.splitext(filename)[0]) + 1

    def show(self):
        self.frame.visible = True

    def setCounter(self):
        self.counter += 1

    # 'get' functions
    def getImp(self):
```

```
93          return self.imp
94
95      def getCounter(self):
96          return self.counter
97
98      def getFrame(self):
99          return self.frame
100
101     def getPath(self):
102         return self.path
103
104     def getTextField(self):
105         return self.nameField.text
106
107     # ROI functions
108
109     def getOverlay(self):
110         return self.olay
111
112     def cut(self, event):
113         imp = self.imp
114         roi = self.imp.getRoi()
115         if roi != None:
116             newRoi = roi.clone()
117             from ij.plugin import Duplicator
118             Dup = Duplicator().run(imp, 1, imp.getNChannels(), 1, imp.getNSlices(), 1, imp.getNFrames())
119             newRoi.setLocation(0,0)
120             Dup.setRoi(newRoi)
121             Dup.setTitle(self.getTextField() + str(self.getCounter()))
122             Dup.show()
123             self.setCounter()
124             # add roi to overlay
125             self.olay.add(roi)
126             imp.setOverlay(self.olay)
127             # show cell number
128             imp.getOverlay().drawLabels(True)
129             self.saveOverlay()
130             #imp.deleteRoi()
131
132             saveFolder = path.join(path.split(path.dirname(self.getPath()))[0], G_saveSubFold)
133             if not path.exists(saveFolder):
134                 print "Making directory " + saveFolder
135                 mkdir(saveFolder)
136             savePath = path.join(saveFolder, (Dup.getTitle()+".tif"))
137             print savePath
138             IJ.saveAs(Dup, ".tiff", savePath)
139             print "Saved as " + savePath
140             Dup.close()
141             event.consume()
142
143
144     def delOverlay(self, event):
145         IJ.run(self.imp, "Remove Overlay", "")
146         self.olay.clear()
147         self.counter = 1
148         self.imp.show()
149
150     def saveOverlay(self):
151         if self.olay != []:
152             self.rm = RoiManager.getInstance()
153             if self.rm == None:
154                 rm = RoiManager()
155             #rm.runCommand("reset")
156             IJ.run(self.imp, "To ROI Manager", "")
157             print "Saving overlay as " + self.path+ self.fnPrefix+".zip"
158             rm.runCommand("Save", self.path+self.fnPrefix+".zip")
159             rm.close()
160
161
162     def quit(self, event):
163         if self.olay != None:
164             yncd = YesNoCancelDialog(self.frame, "Save overlay?", "Save overlay?")
165             if yncd.yesPressed():
166                 self.saveOverlay(None)
167         WindowManager.removeWindow(self.frame)
168         self.frame.dispose()
169         self.getImp().close()
170
171 # M A I N
172
173 Men = Menue()
```

4.15.4 BatchPreProcessor.py

```
# Batch extension for Kotas dot segmenting script PreProcessing
# authors: Christoph Schiklenk (schiklen@embl.de), Kota Miura (CMCI) (miura@embl.de)

from os import listdir, makedirs, path
import re
from ij.plugin.filter import Filler as CO
from emblcmci.foci3Dtracker import PreprocessChromosomeDots as PPC
from ij.plugin import ChannelSplitter as CS
from ij.plugin import RGBStackMerge as StackMerge
from ij.io import DirectoryChooser, Opener
from ij.process import ImageConverter
from ij import IJ, WindowManager

# Globals
G_saveSubFold = "ppcd"
G_saveFilePrefix = "ppcd_"

class batchPreprocessor:
    def __init__(cutOutDir):
        saveFolder = path.join(path.split(path.dirname(cutOutDir))[0], G_saveSubFold)
        regEx = re.compile('(?!ppcd_)(?P<prefix>.+).tiff?$', re.IGNORECASE)
        self.moFileList = [] # match object File list
        for fileName in listdir(cutOutDir):
            if regEx.match(fileName): # if matches RE, add to list
                moFileList.append(regEx.match(fileName))
        if moFileList == []:
            IJ.showMessage("Input Exception", "No unprocessed images found in the directory you selected.")
            raise IOError("No unpocessed TIFFs found in this folder.")
        for image in moFileList:
            print "Processing cell " + image.group() + " (" + str(moFileList.index(image)+1) + "/" + str(len(moFileList)) + ")"
            IJ.log("Processing cell " + image.group() + " (" + str(moFileList.index(image)+1) + "/" + str(len(moFileList)) + ")")
             # open Image
            imp = Opener().openImage(path + image.group())
            roi = imp.roi
            imps = CS.split(imp)
            ppc = PPC()
            for aimp in imps:
                ppc.setImp(aimp)
                ppc.run()
                if roi != None:
                    aimp.setRoi(roi)
                    for n in range(1, aimp.getImageStackSize()+1):
                        aimp.getImageStack().getProcessor(n).fillOutside(roi)
                    aimp.killRoi()
            final = StackMerge.mergeChannels(imps, False)
            final.copyScale(imp) # copyscale from .copyscale
            if not path.exists(saveFolder):
                makedirs(saveFolder)
            fileName = G_saveFilePrefix + image.group('prefix')
            IJ.saveAs(final, ".tiff", path.join(saveFolder, fileName) ) # saveAs(ImagePlus imp, java.lang.String format, java.lang.String path)
            print "Successfully saved", G_saveFilePrefix + image.group('prefix')
            IJ.log("Successfully saved " + G_saveFilePrefix + image.group('prefix') + ".tif")
            for win in WindowManager.getIDList():
                imp = WindowManager.getImage(win)
                imp.close()
        print "Finished."
        IJ.log("Finished pre-processing.")

# M A I N
# select directory that is to be processed via dialog
p = DirectoryChooser("DotSeg Preprocess Batch Extension - Please choose directory containing the images").getDirectory()
saveFolder = path.join(path.split(path.dirname(p))[0], G_saveSubFold)

# create list of match objects of .tiff files in directory
regEx = re.compile('(?!ppcd_)(?P<prefix>.+).tiff?$', re.IGNORECASE)
moFileList = [] # match object File list
for fileName in listdir(p):
   if regEx.match(fileName): # if matches RE, add to list
      moFileList.append(regEx.match(fileName))

if moFileList == []:
   IJ.showMessage("Input Exception", "No unprocessed images found in the directory you selected.")
   raise IOError("No unpocessed TIFFs found in this folder.")

for image in moFileList:
   print "Processing cell " + image.group() + " (" + str(moFileList.index(image)+1) + "/" + str(len(moFileList)) + ")"
   IJ.log("Processing cell " + image.group() + " (" + str(moFileList.index(image)+1) + "/" + str(len(moFileList)) + ")")
   imp = Opener().openImage(p + image.group()) # open Image
   roi = imp.roi
   imps = CS.split(imp)
   ppc = PPC()
   for aimp in imps:
      ppc.setImp(aimp)
      ppc.run()
      if roi != None:
         aimp.setRoi(roi)
         for n in range(1, aimp.getImageStackSize()+1):
            aimp.getImageStack().getProcessor(n).fillOutside(roi)
         aimp.killRoi()
   final = StackMerge.mergeChannels(imps, False)
   final.copyScale(imp) # copy calibrations (pixel sizes and time)
   if not path.exists(saveFolder):
```

```
93        makedirs(saveFolder)
94     fileName = G_saveFilePrefix + image.group('prefix')
95     IJ.saveAs(final, ".tiff", path.join(saveFolder, fileName) )
96     print "Successfully saved", G_saveFilePrefix + image.group('prefix')
97     IJ.log("Successfully saved " + G_saveFilePrefix + image.group('prefix') + ".tif")
98     for win in WindowManager.getIDList():
99        imp = WindowManager.getImage(win)
100       imp.close()
101 print "Finished."
102 IJ.log("Finished pre-processing.")
```

4.15.5 BatchMeasurement.py

```
# Batch plugin for Kotas dot segmenting script
# by Christoph Schiklenk (schiklen@embl.de)

from os import listdir, makedirs
from os import path as pth
import pickle
import os, re, math
import time.clock
from ij.plugin.filter import Filler as CO
from emblcmci.foci3Dtracker import PreprocessChromosomeDots as PPC
from ij.plugin import ChannelSplitter as CS
from ij.plugin import RGBStackMerge as StackMerge
from emblcmci.foci3Dtracker import AutoThresholdAdjuster3D as ATA
from ij.io import DirectoryChooser, Opener
from ij.process import ImageConverter
from ij.text import TextWindow
from ij import IJ, WindowManager

from emblcmci.foci3Dtracker import Measure

# GLOBALS
G_saveSubFold = "meas" # name of the subfolder that is suppodes to contain the result values and images

class cell(object):
    def __init__(self, frameList): # should be constructed based on path.
        self.frameList = frameList # here: sort by framenumber!

    def exportData(self, exportFilePath):
        "A method to export xyz coordinates in microns, distances and all as .csv file"
        f = open(exportFilePath, "w")
        # write column names
        f.write("Frame,Timepoint,Distance,ch0x,ch0y,ch0z,ch0vol,ch1x,ch1y,ch1z,ch1vol\n")
        for frame in self.frameList:
            frameNumber = str(frame.getFrameNo())
            timepoint = str(frame.getTime())
            distance = str(frame.getDistance()) # is always z-corrected distance in microns
            ch0Dot, ch1Dot = frame.getDots()
            ch0x, ch0y, ch0z = ch0Dot.getXYZ()
            ch0vol = str(ch0Dot.getVol())
            ch1x, ch1y, ch1z = ch1Dot.getXYZ()
            ch1vol = str(ch1Dot.getVol())
            line = frameNumber + "," + timepoint + "," + distance + "," + str(ch0x) + "," + str(ch0y) + "," + str(ch0z) + "," + ch0vol + \
            "," + str(ch1x) + "," + str(ch1y) + "," + str(ch1z) + "," + ch1vol + "\n"
            f.write(line)
        f.close()

    def serialize(self, saveFilePath):
        """Serialization function not in use"""
        f = open(saveFilePath, "w")
        pickle.dump(self, f)
        f.close()

class fr:
    def __init__(self, frame, distance, ch0DotList, ch1DotList):
        self.frame = int(float(frame))
        self.time = round((timeInterval * float(frame)), 1)
        if distance == None: # No distance -> at least one dot is missing.
            self.distance = "NA"
            if ch0DotList == None:
                self.ch0Dot = dot(0, self.frame, "NA", "NA", "NA", "NA", "NA", "NA")
            else: # not the case yet since reading is based on distance table
                self.ch0Dot = ch0DotList
            if ch1DotList == None:
                self.ch1Dot = dot(1, self.frame, "NA", "NA", "NA", "NA", "NA", "NA")
            else: # not the case yet since reading is based on distance table
                self.ch1Dot = ch1DotList
        else:
            # the distance from the distance table (kota)
            self.distance_kota_m = round((calibration.pixelWidth * float(distance)), 5)
            self.distance_kota_p = float(distance)
            self.distance = self.distance_kota_m
            # own distance calculation: first x y z lengths to microns (made isotropic), then distance
            self.ch0Dot = ch0DotList
            self.ch1Dot = ch1DotList
            self.m_distance = self.calculateDistance(self.ch0Dot, self.ch1Dot)
            self.m_distance_p = self.m_distance/calibration.pixelWidth # my/(my/px) = px
            # own distance calculation: first make isotropic in px, then calculate distance in px, then to microns
            x_ch0px, y_ch0px, z_ch0px = self.ch0Dot.getXYZpx()
            x_ch1px, y_ch1px, z_ch1px = self.ch1Dot.getXYZpx()
            zFactor = calibration.pixelDepth/calibration.pixelWidth
            z_ch0pxCorr = zFactor * z_ch0px
            z_ch1pxCorr = zFactor * z_ch1px
            self.p_distance = math.sqrt( math.pow((x_ch0px-x_ch1px),2.0)
                                + math.pow((y_ch0px-y_ch1px),2.0)
                                + math.pow((z_ch0pxCorr-z_ch1pxCorr),2.0) )
            self.p_distance_m = self.p_distance * calibration.pixelWidth

    def __repr__(self): # defines the print output.
        return "Frametime " + str(self.time)

    def getFrameNo(self):
        return self.frame
```

```
93
94      def getDots(self):
95          return self.ch0Dot, self.ch1Dot
96
97      def getDistance(self):
98          return self.distance
99
100     def getDistances(self):
101         return self.distance_kota_p, self.distance_kota_m, self.m_distance_p, self.m_distance, self.p_distance, self.p_distance_m
102
103     def getTime(self):
104         return self.time
105
106     # static method to calculate distance between two dot objects.
107     @staticmethod
108     def calculateDistance(dot1, dot2):
109         x1, y1, z1 = dot1.getXYZ()
110         x2, y2, z2 = dot2.getXYZ()
111         if ((dot1.getXYZ() != ("NA", "NA", "NA")) or dot2.getXYZ() != ("NA", "NA", "NA")):
112             distance = math.sqrt( math.pow((x1-x2),2.0) +
113                                   math.pow((y1-y2),2.0) +
114                                   math.pow((z1-z2),2.0) )
115             return distance
116         else:
117             return "NA"
118
119 class dot(object):
120     def __init__(self, ch, frame, dotID, vol, x, y, z, intden):
121         self.ch = ch
122         self.frame = int(float(frame))
123         try:
124             self.dotID = int(float(dotID))
125             self.vol = int(float(vol))
126             self.xPx = x
127             self.yPx = y
128             self.zPx = z
129             self.x = round((calibration.pixelWidth * float(x)), 5)
130             self.y = round((calibration.pixelHeight * float(y)), 5)
131             self.z = round((calibration.pixelDepth * float(z)), 5) # "%.5f" %
132         except ValueError: # if is "NA"
133             self.dotID = "NA"
134             self.vol = "NA"
135             self.x = "NA"
136             self.y = "NA"
137             self.z = "NA"
138
139     def getFrame(self):
140         return self.frame
141
142     def getVol(self):
143         return self.vol
144
145     def getXYZ(self):
146         return self.x, self.y, self.z
147
148     def getXYZpx(self):
149         return float(self.xPx), float(self.yPx), float(self.zPx)
150
151 class dot2(object):
152     def __init__(self, ch, frame, dotID, vol, x, y, z, intden):
153         self.ch = ch
154         self.frame = int(frame)
155         try:
156             self.dotID = dotID
157             self.vol = vol
158             self.xPx = x
159             self.yPx = y
160             self.zPx = z
161             self.x = round((calibration.pixelWidth * float(x)), 5)
162             self.y = round((calibration.pixelHeight * float(y)), 5)
163             self.z = round((calibration.pixelDepth * float(z)), 5) # "%.5f" %
164         except ValueError: # if is "NA"
165             self.dotID = "NA"
166             self.vol = "NA"
167             self.x = "NA"
168             self.y = "NA"
169             self.z = "NA"
170
171     def getFrame(self):
172         return self.frame
173
174     def getVol(self):
175         return self.vol
176
177     def getXYZ(self):
178         return self.x, self.y, self.z
179
180     def getXYZpx(self):
181         return float(self.xPx), float(self.yPx), float(self.zPx)
182
183 def tableToDots(lines, ch):
184     """Parser for .tsv files to dot objects."""
185     dotList = []
186     for l in lines[1:len(lines)-1]: #skip first line because its the col headings
187         i, frame, dotID, vol, x, y, z, intden = l.split("\t")
```

```
188         dotList.append(dot(ch, frame, dotID, vol, x, y, z, intden))
189     return dotList
190
191 def dotListToSingle(dotList):
192     if len(dotList) > 1:
193        return dotList.pop()
194     if len(dotList) == 1:
195        return dotList.pop()
196     if len(dotList) == 0:
197        return None
198
199 class bm:
200     """Benachmark class to monitor calculation times"""
201     def __init__(self, fileName, start, stop, width, height, nSlices, nFrames):
202         self.fileName = fileName
203         self.start = str(start)
204         self.stop = str(stop)
205         self.width = str(width)
206         self.height = str(height)
207         self.nSlices = str(nSlices)
208         self.nFrames = str(nFrames)
209
210 class benchmarkList(list):
211     def __init__(self):
212         pass
213
214     def addBenchmark(self, bm):
215         self.append(bm)
216
217     def exportCsv(self, fileName):
218         f = open(fileName, 'w')
219         f.write("FileName,start,stop,width,height,nSlices,nFrames\n")
220         for bm in self:
221             f.write(",".join([bm.fileName, bm.start, bm.stop, bm.width, bm.height, bm.nSlices, bm.nFrames]) + "\n")
222         f.close()
223
224 # M A I N
225 inputDir = DirectoryChooser("DotSeg Preprocess Batch Extension - Please choose directory containing the images").getDirectory()
226 saveFolder = pth.join(pth.split(pth.dirname(inputDir))[0], G_saveSubFold)
227 print "Will save results in folder ", saveFolder
228
229 bml = benchmarkList()
230
231 regEx = re.compile('ppcd_(?P<name>p\d+_c\d+).tif$', re.IGNORECASE) # create list of match objects of .tif files in directory
232 moFileList = [] # match object File list
233 for fileName in listdir(inputDir):
234     if regEx.match(fileName): # if matches RE, add to list
235         moFileList.append(regEx.match(fileName))
236 print "Will process files ", moFileList
237
238 if moFileList == []:
239     IJ.showMessage("Input Exception", "Directory does not contain any preprocessed images.")
240     raise IOError("Input Exception: Directory does not contain any preprocessed images.")
241
242 if not pth.exists(saveFolder): # check if directory for analysis-files is present
243     makedirs(saveFolder)
244
245 for image in moFileList:
246     benchmarkStart = time.clock()
247     print "starting with cell " + image.group() + " " + "("+ str(moFileList.index(image)) + "/" + str(len(moFileList)) + ")"
248      # open Image
249     imp = Opener().openImage(inputDir + image.group())
250     # read calibration for distance conversion in microns.
251     calibration = imp.getCalibration()
252     pxWidth = calibration.pixelWidth
253     zfactor = calibration.pixelDepth / calibration.pixelWidth
254     timeInterval = round(calibration.frameInterval)
255     # split channels
256     splitCh = CS.split(imp)
257     # set autothresholdadjuster options
258     ata = ATA()
259     ata.showPlot(True)
260     ata.setSilent(False)
261     ata.setScale(imp)
262     # perform segmentation and measurement
263     ata.segAndMeasure(splitCh[0], splitCh[1])
264
265     #close all unnecessary windows.
266     WindowManager.getImage("binProjMerged").close()
267     WindowManager.getWindow("Statistics_Distance").close()
268     WindowManager.getWindow("Statistics_Ch0").close()
269     WindowManager.getWindow("Statistics_Ch1").close()
270
271     # 20140926 added by Kota Miura
272     linkedArray = ata.getLinkedArray()
273     frameList = []
274     for focipair in linkedArray:
275             ch0Obj = focipair.ch0dot
276             ch1Obj = focipair.ch1dot
277             if (ch0Obj is not None) and (ch1Obj is not None):
278                 ch0dot = dot2(0, ch0Obj.getTimepoint(), 1, ch0Obj.size, ch0Obj.centroid[0], ch0Obj.centroid[1], ch0Obj.centroid[2], ch0Obj.int_dens)
279                 ch1dot = dot2(1, ch1Obj.getTimepoint(), 1, ch1Obj.size, ch1Obj.centroid[0], ch1Obj.centroid[1], ch1Obj.centroid[2], ch1Obj.int_dens)
280                 distance = Measure.returnDistanceZfact(ch0Obj, ch1Obj, zfactor)
281                 frameList.append(fr(focipair.timepoint, distance, ch0dot, ch1dot))
282     # fill up table with FROSless frames.
```

```
    presentFrames = [f.getFrameNo() for f in frameList]
    missingFrames = [f for f in range(max(presentFrames)) if f not in presentFrames]

    for f in missingFrames:
        frameList.append(fr(f, None, None, None))
    #sort by frame
    frameList.sort(key=lambda x: x.getFrameNo())
    c = cell(frameList)
    # write to file.
    c.exportData(saveFolder +"/val_" + image.group('name') + ".csv")
    # save Z-projection image with marked dots
    detDots = WindowManager.getImage("DetectedDots")
    detDots.copyScale(imp)
    IJ.saveAs(detDots, ".tiff", saveFolder + "/zi_"+image.group('name')) # save the overlay with connecting line
    print "Saving as " + image.group('name')
    detDots.close()
    # stop the time for benchmarking
    benchmarkStop = time.clock()
    bml.addBenchmark(bm(image.group('name'), benchmarkStart, benchmarkStop, imp.getWidth(), imp.getHeight(), imp.getNSlices(), imp.getNFrames()))

bml.exportCsv(saveFolder + "/benchmarkList.csv")
print "Saved benchmark list"
IJ.log("Finished")
```

4.15.6 QualityControl.py

```
# Quality control Plugin for the FROS position pipeline
# author: Christoph Schiklenk
# email: schiklen@embl.de

from javax.swing import JButton, JFrame, JPanel, JLabel, JTextArea, JScrollPane, JProgressBar, JRadioButton, ButtonGroup
from javax.swing import SwingConstants, WindowConstants
from java.awt import Component, Dimension, GridLayout
import re, random, os, sys, glob
from java.awt.event import ActionListener, KeyEvent, KeyAdapter, MouseEvent, MouseAdapter, WindowFocusListener
from ij.plugin import Zoom
from ij import WindowManager, IJ, ImagePlus
from ij.text import TextWindow, TextPanel
from ij.io import DirectoryChooser

# go through frames with arrowleft ()
# 0: anaphase Onset
# q: delete measurement

# Globals
G_SAVESUBDIR = "qc-meas"
G_OPENSUBDIR = "meas"

def bigRound(x, base):
    return int(base * round(float(x)/base))


# Eventlistener classes
class ListenToKey(KeyAdapter):
    def keyPressed(self, event):
        eventSrc = event.getSource()
        cT = eventSrc.getParent() #panel is the parent, canvas being component.
        if event.getKeyCode() == 37 and cT.getSelectionEnd() > 0: # KeyCode 37 : arrowLeft
            cT.setSelection(cT.getSelectionEnd()-1, cT.getSelectionEnd()-1)
        if event.getKeyCode() == 39 and cT.getSelectionEnd() < cT.getLineCount(): # KeyCode 39 : arrowRight
            cT.setSelection(cT.getSelectionEnd()+1, cT.getSelectionEnd()+1)
        cT.changeFrame()
        if event.getKeyCode() == 48: # Anaphase Onset Def. KeyCode 48 : 0
            cT.setAnaphase()
        if event.getKeyCode() == 81: # KeyCode 81: q
            cT.delVal()
        # Prevent further propagation of the key event:
        #event.consume()


class ListenToMouse(MouseAdapter):
    def mouseClicked(self, event):
        event.getSource().getParent().changeFrame()
        #event.consume()


class twFocusListener(WindowFocusListener):
    def windowGainedFocus(self, e):
        tw = e.getWindow()
        #e.consume()

    def windowLostFocus(self, e):
        print e.getWindow()
        #e.consume()


class cell:
    def __init__(self, csvPath):
        self.csvPath = csvPath
        self.openDir, self.filename = os.path.split(self.csvPath)
        csvRE = re.compile( os.path.join('(?P<mainDir>.*)', '(?P<strain>.*)', G_OPENSUBDIR ,'val_p(?P<position>\d+)_c(?P<cell>\d+).csv') )
        pathMO = re.match(csvRE, csvPath)
        self.mainDir = pathMO.group('mainDir')
        self.strain = pathMO.group('strain')
        self.position = int(pathMO.group('position'))
        self.cellNo = int(pathMO.group('cell'))
        self.measTifPath = os.path.join(self.openDir, "zi_p%i_c%i.tif" %(self.position, self.cellNo))
        self.qcCsvPath = os.path.join(self.mainDir, self.strain, G_SAVESUBDIR, "qc_val_p%i_c%i.csv") %(self.position, self.cellNo)
        self.isProcessed()
        self.anaphaseOnset = None
        self.annotation = None

    def isProcessed(self):
        if os.path.exists(self.qcCsvPath):
            self.processed = True
        else:
            self.processed = False

    def hasTif(self):
        if os.path.exists(self.measTifPath):
            self.processed = True
        else:
            self.processed = False

    def getAnOn(self):
        return self.anaphaseOnset

    def setAnOn(self, anaphaseOnset):
```

```
93          self.anaphaseOnset = anaphaseOnset
94
95      def annotate(self, annotation):
96          self.annotation = annotation
97
98      def getAnnotation(self):
99          return self.annotation
100
101     def getMeasTifPath(self):
102         return self.measTifPath
103
104     def getQcCsvPath(self):
105         return self.qcCsvPath
106
107     def getCsvPath(self):
108         return self.csvPath
109
110
111 class MenueFrame(JFrame, ActionListener, WindowFocusListener):
112     def __init__(self):
113         self.mainDir = ""
114         self.setTitle("Dots Quality Check")
115         self.setSize(250, 300)
116         self.setLocation(20,120)
117         self.addWindowFocusListener(self)
118
119         # GUI
120         self.Panel = JPanel(GridLayout(0,1))
121         self.add(self.Panel)
122         self.openNextButton = JButton("Open Next Random", actionPerformed=self.openRandom)
123         self.Panel.add(self.openNextButton)
124         self.saveButton = JButton("Save", actionPerformed=self.save, enabled=False)
125         self.Panel.add(self.saveButton)
126         self.cropButton = JButton("Crop values from here", actionPerformed=self.cropVals)
127         self.Panel.add(self.cropButton)
128         self.DiscardButton = JButton("Discard cell", actionPerformed=self.discardCell)
129         self.Panel.add(self.DiscardButton)
130         self.quitButton = JButton("Quit script",actionPerformed=self.quit)
131         self.Panel.add(self.quitButton)
132
133         annoPanel = JPanel()
134         self.wtRButton = JRadioButton("wt", actionCommand="wt")
135         self.wtRButton.addActionListener(self)
136         self.defectRButton = JRadioButton("Defect", actionCommand="defect")
137         self.defectRButton.addActionListener(self)
138         annoPanel.add(self.wtRButton)
139         annoPanel.add(self.defectRButton)
140         self.aButtonGroup = ButtonGroup()
141         self.aButtonGroup.add(self.wtRButton)
142         self.aButtonGroup.add(self.defectRButton)
143         self.Panel.add(annoPanel)
144
145         self.ProgBar = JProgressBar()
146         self.ProgBar.setStringPainted(True)
147         self.ProgBar.setValue(0)
148         self.Panel.add(self.ProgBar)
149
150         self.pathLabel = JLabel("-- No main directory chosen --")
151         self.pathLabel.setHorizontalAlignment( SwingConstants.CENTER )
152         self.Panel.add(self.pathLabel)
153
154         WindowManager.addWindow(self)
155         self.show()
156
157     # B U T T O N M E T H O D S
158     def openRandom(self, event):
159         import glob, os
160         if self.mainDir == "":
161             self.mainDir = DirectoryChooser("Random QC - Please choose main directory containing ctrl and test folders").getDirectory()
162             self.pathLabel.setText("MainDir: " + os.path.basename(os.path.split(self.mainDir)[0]))
163         try:
164             self.cT.closeWindows()
165         except AttributeError:
166             pass
167         finally:
168             inFiles = glob.glob(os.path.join(self.mainDir, "*", "meas", "val_*.csv")) # glob.glob returns list of paths
169             uncheckedCells = [cell(csvPath) for csvPath in inFiles if cell(csvPath).processed == False]
170             if len(uncheckedCells) > 0:
171                 self.cell = random.choice(uncheckedCells)
172                 #update progressbar
173                 self.ProgBar.setMaximum(len(inFiles)-1)
174                 self.ProgBar.setValue(len(inFiles)-len(uncheckedCells))
175                 # open imp and resultstable
176                 self.cT = correctionTable(self.cell, self)
177                 # delete previous Radiobutton annotation
178                 self.wtRButton.setSelected(False)
179                 self.defectRButton.setSelected(False)
180             else:
181                 print "All cells measured!"
182
183     def save(self, event):
184         savepath = self.cell.getQcCsvPath()
185         anaphase = self.cell.getAnOn()
186         timeInterval = self.cT.getImp().getCalibration().frameInterval
187         annotation = self.getAnnotation()
```

```
        position = str(self.cell.position)
        cellIndex = str(self.cell.cellNo)
        import os
        if not os.path.exists(os.path.split(savepath)[0]): # check if save folder present.
            os.makedirs(os.path.split(savepath)[0]) # create save folder, if not present
        f = open(savepath, "w")
        f.write("Position,Cell,Phenotype,Frame,Time,Anaphase,Distance,ch0x,ch0y,ch0z,ch0vol,ch1x,ch1y,ch1z,ch1vol\n")
        for i in range(self.cT.getLineCount()):
            frame, distance, a = self.cT.getLine(i).split("\t")
            corrFrame = str(int(frame)-int(anaphase))
            time = "%.f" % (round(timeInterval) * int(corrFrame))
            if distance == "NA":
                ch0x, ch0y, ch0z, ch0vol, ch1x, ch1y, ch1z, ch1vol = ("NA," * 7 + "NA\n").split(",")
            else:
                ch0x, ch0y, ch0z, ch0vol, ch1x, ch1y, ch1z, ch1vol = self.cT.getXYZtable()[i]
            f.write(position + "," + cellIndex + "," + annotation + "," + corrFrame + "," + time + "," + anaphase + "," + distance + \
            "," + ch0x + "," + ch0y + "," + ch0z + "," + ch0vol + "," + ch1x + "," + ch1y + "," + ch1z + "," + ch1vol)
        f.close()
        print "Successfully saved!"

    def cropVals(self, event):
        """this function deletes all values with frame bigger than current cursor"""
        for line in range(self.cT.getSelectionEnd(), self.cT.getLineCount(), 1):
            frame, distance, AOCol = self.cT.getLine(line).split("\t")
            self.cT.setLine(line, frame + "\tNA" + "\t" + AOCol)

    def discardCell(self, event):
        import os
        if not os.path.exists(os.path.split(self.cell.getQcCsvPath() )[0]): # check if save folder present.
            os.makedirs(os.path.split(self.cell.getQcCsvPath() )[0]) # create save folder, if not present.
        f = open(self.cell.getQcCsvPath() ,"w")
        # Write dummy header.
        f.write("Position,Cell,Phenotype,Frame,Time,AnOn,Distance,ch0x,ch0y,ch0z,ch0vol,ch1x,ch1y,ch1z,ch1vol\n")
        f.close()
        print "Discarded cell - saved dummy"

    def quit(self, event):
        try:
            self.cT.closeWindows()
        finally:
            from ij import WindowManager
            WindowManager.removeWindow(self)
            self.dispose()

    # Methods implementing ActionListener interfaces:
    def actionPerformed(self, e):
        # this function is called when RadioButtons are changed
        self.cell.annotate( e.getSource().getActionCommand() )
        self.setSaveActive()

    def windowGainedFocus(self, e):
        pass

    def windowLostFocus(self, e):
        pass

    def getAnnotation(self):
        return self.aButtonGroup.getSelection().getActionCommand()

    def getMainDir(self):
        return self.mainDir

    def setSaveActive(self):
        if (self.cell.getAnnotation() != None and self.cell.getAnOn() != None):
            self.saveButton.setEnabled(True)
            self.show()

    def setSaveInactive(self):
        self.saveButton.setEnabled(False)
        self.show()

    def setMainDir(self, path):
        self.mainDir = path
        self.pathLabel.setText("MainDir: " + os.path.basename(os.path.split(self.mainDir)[0]))


class correctionTable(TextPanel):
    """A class that displays an imagePlus and a resultstable. Resultstable and imp are linked in such a
     way that click on a table row shows the imps respective timeframe."""
    def __init__(self, cell, mF, title="Results"):
        # Call constructor of superclass
        TextPanel.__init__(self)
        # pass menue for setting save active/inactive
        self.cell = cell
        self.mF = mF
        # Create a window to show the content in
        self.window = JFrame()
        self.window.add(self)
        self.window.setTitle(title)
        # Add event listeners for keyboard and mouse responsiveness
        self.addKeyListener(ListenToKey())
        self.addMouseListener(ListenToMouse())
        self.imp = self.openImp(self.cell.getMeasTifPath())
        csvFile = open(self.cell.getCsvPath())
        lines = csvFile.readlines()
```

```
        heads = lines.pop(0)
        self.setColumnHeadings("Frame\tDistance\tAnaphase")
        self.XYZtable = []
         # load file lines in textPanel.
        for line in lines:
            frame, timepoint, dist, ch0x, ch0y, ch0z, ch0vol, ch1x, ch1y, ch1z, ch1vol = line.split(",")
            self.append(frame + "\t" + dist + "\t" )
            self.XYZtable.append((ch0x, ch0y, ch0z, ch0vol, ch1x, ch1y, ch1z, ch1vol))
        self.setSelection(0,0)
        self.changeFrame()
        self.mF.setSaveInactive()
        self.requestFocus()
        self.window.setSize(Dimension(220, 600))
        x = int(self.imp.getWindow().getLocation().getX()) + int(self.imp.getWindow().getWidth()) + 10
        self.window.setLocation(x, int(self.imp.getWindow().getLocation().getY()) )
        self.window.show()

    # Event driven methods
    def changeFrame(self):
        if self.getSelectionEnd() >= 0:
            frame, dist, AOCol = self.getLine(self.getSelectionEnd()).split("\t")
            self.imp.setSlice(int(frame)+1)

    def setAnaphase(self):
        frame, Distance, x = self.getLine(self.getSelectionEnd()).split("\t")
        #set anaphase onset
        self.cell.setAnOn(frame)
        for i in range(self.getLineCount()): # very unelegantly solved, but it works.
            blFr, blDist, blAOCol = self.getLine(i).split("\t")
            self.setLine(i, blFr + "\t" + blDist + "\t")
            frame, distance, AOCol = self.getLine(self.getSelectionEnd()).split("\t") # get old line
            self.setLine(self.getSelectionEnd(), frame + "\t" + distance + "\tX")
        # setFocus back to tw,tp
        self.mF.setSaveActive()
        print "Anaphase set to", self.cell.getAnOn()

    def delVal(self):
        frame, distance, AOCol = self.getLine(self.getSelectionEnd()).split("\t")
        self.setLine(self.getSelectionEnd(), frame + "\tNA" + "\t" + AOCol)

    # other methods
    def openImp(self, path):
        # opens associated tif file
        imp = ImagePlus(path)
        imp.show()
        imp.getWindow().setLocationAndSize(280, 120, imp.getWidth()*4, imp.getHeight()*4)
        return imp

    def getImp(self):
        return self.imp

    def getXYZtable(self):
        return self.XYZtable

    def closeWindows(self):
        self.imp.changes = False
        self.imp.close()
        from ij import WindowManager
        WindowManager.removeWindow(self.window)
        self.window.dispose()

# M A I N
random.seed()
mF = MenueFrame()
```

4.15.7 Trackfinder.py

```
# dot tracking function for cell class
# cell class is list of frame objects
# author: Christoph Schiklenk
# email: schiklen@embl.de

from os import listdir, path, mkdir
from operator import attrgetter
from itertools import chain
import math, pickle, re, weakref
from ij.io import DirectoryChooser

# substituting from itertools import permutations
# because import is not working
# from python documentation:
def permutations(iterable, r=None):
    pool = tuple(iterable)
    n = len(pool)
    r = n if r is None else r
    if r > n:
        return
    indices = range(n)
    cycles = range(n, n-r, -1)
    yield tuple(pool[i] for i in indices[:r])
    while n:
        for i in reversed(range(r)):
            cycles[i] -= 1
            if cycles[i] == 0:
                indices[i:] = indices[i+1:] + indices[i:i+1]
                cycles[i] = n - i
            else:
                j = cycles[i]
                indices[i], indices[-j] = indices[-j], indices[i]
                yield tuple(pool[i] for i in indices[:r])
                break
        else:
            return


class dot(object):
    def __init__(self, ch, frame, x, y, z, vol):
        self.ch = ch
        self.frame = int(float(frame))
        self.prevDot = None
        self.nextDot = None
        self.trackID = None
        self.isStart = False
        self.isEnd = False
        try:
            self.vol = int(float(vol))
            self.x = float(x)
            self.y = float(y)
            self.z = float(z)
        except ValueError: # if is "NA"
            self.vol = "NA"
            self.x = "NA"
            self.y = "NA"
            self.z = "NA"

    def __repr__(self):
        return "Dot in frame " + str(self.frame) + " at " + str(self.x) + "/" + str(self.y) + "/" + str(self.z)

    def getXYZ(self):
        return self.x, self.y, self.z

    def getVol(self):
        return self.vol

    def getFrame(self):
        return self.frame

    def getNextDot(self):
        return self.nextDot

    def getPrevDot(self):
        return self.prevDot

    def linkWithDot(self, dot):
        # TODO: check, if prevDot /nextDot get overwritten!
        if dot != self:
            if dot.getFrame() > self.frame:
                self.nextDot = dot
            elif dot.getFrame() < self.frame:
                self.prevDot = dot
            else: # dot.getFrame() == self.frame
                print "sameframe"

            if self not in [dot.prevDot, dot.nextDot]:
                dot.linkWithDot(self)

    def getTrackID(self):
        return self.trackID

```

```
    def setTrackID(self, ID):
        self.trackID = ID

    def setStart(self, z):
        self.isStart = z

    def setEnd(self, z):
        self.isEnd = z


class frame:
    def __init__(self, frame, time, distance, ch0DotList, ch1DotList):
        self.frame = int(float(frame))
        self.time = float(time)
        self.distance = distance
        self.ch0DotList = ch0DotList
        self.ch1DotList = ch1DotList

    def getDotListCh0(self):
        return self.ch0DotList

    def getDotListCh1(self):
        return self.ch1DotList

    @staticmethod
    def calculateDistance(dot1, dot2):
        x1, y1, z1 = dot1.getXYZ()
        x2, y2, z2 = dot2.getXYZ()
        if ((dot1.getXYZ() != ("NA", "NA", "NA")) or dot2.getXYZ() != ("NA", "NA", "NA")):
            distance = math.sqrt( math.pow((x1-x2),2.0) +
                                  math.pow((y1-y2),2.0) +
                                  math.pow((z1-z2),2.0) )
            return distance
        else:
            return "NA"


class cell:
    def __init__(self, positionID, cellID, phenotype, anaphaseOnset, frameList):
        self.positionID = positionID
        self.cellID = cellID
        self.phenotype = phenotype
        self.AnaphaseOnset = anaphaseOnset
        self.frameList = frameList

    def getParameters(self):
        return self.positionID, self.cellID, self.phenotype, self.AnaphaseOnset

    def exportAsCsv(self, outPutPath):
        out = open(outPutPath, "w")
        out.write("Position,Cell,Phenotype,Frame,Time,Anaphase,Distance,ch0x,ch0y,ch0z,ch0vol,ch1x,ch1y,ch1z,ch1vol,Ch0TrackID,Ch1TrackID\n")
        for f in self.frameList:
            if len(f.getDotListCh0()) == 0:
                out.write( ",".join(map(str, [self.positionID, self.cellID, self.phenotype, f.frame, f.time, self.AnaphaseOnset, f.distance, \
                "NA", "NA", "NA", "NA", "NA", "NA", "NA", "NA", "NA"])) + "\n" )
            for d0, d1 in zip(f.getDotListCh0(), f.getDotListCh1()):
                ch0x, ch0y, ch0z = d0.getXYZ()
                ch1x, ch1y, ch1z = d1.getXYZ()
                ch0vol = d0.getVol()
                ch1vol = d1.getVol()
                ch0TrackID = d0.getTrackID()
                ch1TrackID = d1.getTrackID()
                out.write( ",".join(map(str, [self.positionID, self.cellID, self.phenotype, f.frame, f.time, self.AnaphaseOnset, f.distance, \
                ch0x, ch0y, ch0z, ch0vol, ch1x, ch1y, ch1z, ch1vol, ch0TrackID, ch1TrackID])) + "\n" )
        out.close()


class connection(list):
    "A list of EXACTLY 2 dot objects."
    def __init__(self, dot1, dot2):
        list.__init__(self, [dot1, dot2])
        self.distance = frame.calculateDistance(dot1, dot2)

    def __repr__(self):
        return "Connection of distance " + str(self.distance)

    def getDistance(self):
        return self.distance

    def linkDots(self):
        self[0].linkWithDot(self[1]) # links both dots


class connectionList(list):
    def __init__(self, *connections): # overwrites list's __init__
        list.__init__(self, *connections)
        self.distanceSum = sum( [e.getDistance() for e in self] ) # better to use math.fsum here, but was not able to import.

    def addConnection(self, connection):
        self.append(connection)
        self.distanceSum += connection.getDistance()

    def getDistanceSum(self):
        return self.distanceSum

```

```
    def __repr__(self):
        return "Global distance sum " + str(self.distanceSum)


def findShortestCombination(dotListFrame1, dotListFrame2):
    # find shortest global distance combination.
    # combine both in a list of lists and sort by length of the list. This step is important to find all combinations later.
    cList = [dotListFrame1, dotListFrame2]
    cList.sort(key=len) # shortest list first
    # the following stuff could be a oneliner but then nobody understands it. That's why its long.
    # make all possible combinations between both frames.
    globalConnectionCombinations = [zip(x, cList[0]) for x in permutations(cList[1], len(cList[0]))]
    possibleConnections = []
    for g in globalConnectionCombinations:
       # for each connection combination unpack each dots combination tuple and make a connection object out of it.
        cl = connectionList([connection(*c) for c in g])
        possibleConnections.append(cl)
    # of all the possible commections, find the global connectionList in which the sum of distances is minimum:
    shortestCombination = min(possibleConnections, key=lambda x: x.getDistanceSum() )
    return shortestCombination

def findNextNearest(startFrame, nextFrame):
    # first channel
    startFrameDots = startFrame.getDotListCh0()
    nextFrameDots = nextFrame.getDotListCh0()
    shortestConnectionCombination = findShortestCombination(startFrameDots, nextFrameDots)
    for connection in shortestConnectionCombination:
        connection.linkDots()
    # second channel
    startFrameDots = startFrame.getDotListCh1()
    nextFrameDots = nextFrame.getDotListCh1()
    shortestConnectionCombination = findShortestCombination(startFrameDots, nextFrameDots)
    for connection in shortestConnectionCombination:
        connection.linkDots()

def makeTrack(startDot, trackID):
    startDot.setTrackID(trackID)
    nextDot = startDot.getNextDot()
    if nextDot != None:
        makeTrack(nextDot, trackID)

def parse(table):
    # convert read file string into objects list.
    frameList = []
    frameIndices = [int(row.split(",")[3]) for row in table[1:(len(table)+1)]]
    maxNFrames = range(min(frameIndices), max(frameIndices))
    positionID = None
    cellID = None
    phenotype = None
    for fI in maxNFrames:
        # subset all lines that have the same frame value
        frameRows = [row for row in table if row.split(",")[3] == str(fI)]
        dotListCh0 = []
        dotListCh1 = []
        postitionID, cellID, phenotype, fra, time, anaphaseOnset, distance, ch0x, ch0y, ch0z, ch0vol, ch1x, ch1y, ch1z, ch1vol = frameRows[0].split(",")

        for line in frameRows:
            positionID, cellID, phenotype, fra, time, anaphaseOnset, distance, ch0x, ch0y, ch0z, ch0vol, ch1x, ch1y, ch1z, ch1vol = line.split(",")
            if ch0x != "NA":
                dotListCh0.append(dot(0, fra, ch0x, ch0y, ch0z, ch0vol))
            else:
                dotListCh0 = []
            if ch1x != "NA":
                dotListCh1.append(dot(1, fra, ch1x, ch1y, ch1z, ch1vol))
            else:
                dotListCh1 = []
        f = frame(fra, time, distance, dotListCh0, dotListCh1)
        frameList.append(f)
    c = cell(positionID, cellID, phenotype, anaphaseOnset, frameList)
    return c


# M A I N
wd = DirectoryChooser("Chose Directory").getDirectory()
r = re.compile("qc_val_p\d+_c\d+\.csv")
for fname in listdir(wd):
    print fname
    if r.match(fname) == None:
        continue
    f = open(path.join(wd, r.match(fname).group(0)), "r")
    table = f.readlines()
    f.close()
    if len(table) == 1: # table is empty: is a dummy
        continue # go to next iterator

    c = parse(table)

    # make links.
    for firstFrame, secondFrame in zip(c.frameList, c.frameList[1:]):
        findNextNearest(firstFrame, secondFrame)

    # make tracks.
    # Channel 0
    weakRefDotList = [] # make a flat list of weak copies of all dots in one channel
    for f in c.frameList:
```

```
        if len(f.getDotListCh0()) > 0:
            for d in f.getDotListCh0():
                weakRefDotList.append(weakref.ref(d))
    ID = 0
    while len(weakRefDotList) > 0:
        earliestDot = min(weakRefDotList, key=lambda x: x().getFrame) # find the earliest dot in the filteredList
        if earliestDot().getTrackID() != None: # if dot has a track ID already
            weakRefDotList.remove(earliestDot) # dont use it as a start point
        elif earliestDot().getTrackID() == None:
            makeTrack(earliestDot(), ID) # makeTrack and delete from list
            weakRefDotList.remove(earliestDot)
            ID += 1

    #Channel 1
    weakRefDotList = [] # make a flat list of weak copies of all dots in one channel
    for f in c.frameList:
        if len(f.getDotListCh1()) > 0:
            for d in f.getDotListCh1():
                weakRefDotList.append(weakref.ref(d))
    ID = 0
    while len(weakRefDotList) > 0:
        earliestDot = min(weakRefDotList, key=lambda x: x().getFrame) # find the earliest dot in the filteredList
        if earliestDot().getTrackID() != None: # if dot has a track ID already
            weakRefDotList.remove(earliestDot) # dont use it as a start point
        elif earliestDot().getTrackID() == None:
            makeTrack(earliestDot(), ID) # makeTrack and delete from list
            weakRefDotList.remove(earliestDot)
            ID += 1

    # TODO: seal track gaps: by global nearest neighbour
    # 1. set isStart, isEnd
    # -------**----- -------*------ -----*-----
    # ------------- -------*------ ----*------
    # if there is only one track, easy!

    # export as .csv with column order:
    outPutDir = path.join(path.split(path.split(wd)[0])[0], "tracked")
    outFileName = "t_"+r.match(fname).group(0)
    if not path.exists(outPutDir):
        mkdir(outPutDir)
    outPutPath = path.join(outPutDir, outFileName)
    c.exportAsCsv(outPutPath)

print "Finished script"
```

4.15.8 CurveAnalysis.R

```
#Chromosome Condensation Curve Analysis
#author: Christoph Schiklenk
#Version 11.3
#refactored 2015


#TODO: implement date, strain, temp, condition extraction from data extraction pipeline

# Imports ---------------------------------------------------------------
library("dplyr", "ggplot2")

# Input grab function ---------------------------------------------------
#grab user input on strain and date.
inputGrab <- function(s) {
  message(s)
  input <- readLines(n = 1)
  input
}


# Themes for ggplot -----------------------------------------------------
require(ggplot2) # load ggplot2
theme_overview <- theme(
  axis.text = element_text(size=rel(1.0), colour="darkgrey"),
  axis.title.x = element_text(size=rel(1.2), hjust=1),
  axis.title.y = element_text(size=rel(1.2), hjust=1),
  complete = FALSE
)

theme_fit <- theme(
  axis.text = element_text(size=rel(1.2), colour="darkgrey"),
  axis.title.x = element_text(colour="black", angle=0, size=rel(1.2), hjust=0.5, vjust=-0.5),
  axis.title.y = element_text(colour="black", angle=90, size=rel(1.2), hjust=0.5, vjust=0.2),
  complete = FALSE
)


# M A I N ---------------------------------------------------------------

# organize input and output dirs
setwd(dirname(getwd())) # wd has to be experiment Dir
importDir <- file.path(getwd(), "tracked") # import from this path
saveDir <- file.path(getwd(), "Analysis") # create subdirectory "Analysis" to save all results in
dir.create(saveDir, showWarnings = TRUE)

# read in files
trackedFiles <- list.files(path=importDir, recursive=T, pattern="t_qc_val_*")
setwd(importDir)
df <- do.call("rbind", lapply(trackedFiles, read.csv, header = TRUE)) #this is the data.frame that contains all the raw data
setwd(saveDir)

#read in metadata. only works with 00-8bitizer V2
if (file.exists(file.path(saveDir, "meta.csv"))){
  meta <- read.csv(file=file.path(saveDir, "meta.csv"), header=TRUE, sep=",")
  date <- meta$Date
  strain <- meta$Strain
  temp <- meta$Temp
} else {
  date <- as.factor(inputGrab("Enter date:"))
  strain <- as.factor(inputGrab("Enter strain:")) # change in inputgra(strain, "enter strain") and check with "missing" in inputgrab function.
  temp <- as.numeric(inputGrab("Enter temperature:")) # must be integer!
}

qcer <- as.factor(inputGrab("Enter QualityController:"))

#set analysisDate
analysisDate <- date()

filenameString <- paste(date, strain, temp ,sep="_")

df <- mutate(df, Date=date, Strain=strain, Temp=temp, analysisDate=analysisDate)
write.csv(x=df, row.names=FALSE, file=file.path(saveDir, paste(filenameString,"_raw.csv",sep="")))

#calculate the number of cells
NCells <- nrow(plyr::count(df[,c(1,2)]))

# summarize by timepoint: mean, standard deviation, median and count of observations (n).
df.timeGroup <- group_by(df, Time)
timeSummary <- dplyr::summarise(df.timeGroup,
                            N = length(Distance[!is.na(Distance)]), # count the observations per timepoint
                            mean.Distance = mean(Distance, na.rm=TRUE), # rename to mean.Distance
                            sd.Distance = sd(Distance, na.rm=TRUE), # rename to sd.Distance
                            median.Distance = median(Distance, na.rm=TRUE), # rename to median.Distance
                            se.Distance = sd.Distance/sqrt(N) #rename to se.Distance
                            )
timeSummary <- mutate(timeSummary, Date=date, Strain=strain, Temp=temp, analysisDate=analysisDate, qcer=qcer)
# save means
write.csv(x=timeSummary, row.names=FALSE, file=file.path(saveDir, paste(filenameString,"_summary.csv",sep="")))

# raw plot --------------------
rawPlot <- ggplot(data=df, aes(x=Time, y=Distance)) +
  geom_point(size=rel(3), colour="#3A778D", alpha=0.3) + # plot raw points
```

```
  geom_line(data=timeSummary, aes(x=Time, y=mean.Distance), colour="black") + #plot averages
  guides(fill=FALSE) +
  geom_vline(xintercept = 0, colour="red") +
  coord_cartesian(ylim=c(0,3.5)) +
  labs(x="Time / s", y="Distance / micron") +
  scale_x_continuous("Time / s", expand=c(0,0), limits=c(-50*42,50*42),
                     breaks=seq(from=-2000, to=2000, by=1000),
                     labels=c("-2000","-1000","Anaphase \n Onset","1000","2000")) +
  annotate(geom="text",label=paste("N = ", NCells, sep=""), size=rel(8), x=-2000, y=3.15, hjust=0) +
  theme_overview
print(rawPlot)
ggsave(filename=file.path(saveDir, paste(filenameString,"_rawPlot.pdf",sep="")), plot=rawPlot)


# single cell plot
ggplot(data=df, aes(x=Time, y=Distance)) +
  geom_point(size=rel(3), colour="#3A778D", alpha=0.3) + # plot raw points
  guides(fill=FALSE) +
  geom_vline(xintercept = 0, colour="red") +
  coord_cartesian(ylim=c(0,2.1)) +
  labs(x="Time / s", y="Distance / microns") +
  scale_x_continuous("Time / s", expand=c(0,0), limits=c(-50*42,50*42),
                     breaks=seq(from=-2000, to=2000, by=1000),
                     labels=c("-2000","-1000","Anaphase \n Onset","1000","2000")) +
  annotate(geom="text",label=paste("N = ", NCells, sep=""), size=rel(8), x=-2000, y=3.15, hjust=0) +
  facet_wrap(Position ~ Cell)

sdPlot <- ggplot(data=timeSummary, aes(x=Time, y=mean.Distance)) +
  geom_ribbon(aes(x=Time, ymin=mean.Distance-sd.Distance, ymax=mean.Distance+sd.Distance), fill="#3A778D", alpha=0.2) +
  geom_point(size=rel(3), colour="darkblue") +
  geom_line() +
  guides(fill=FALSE) +
  geom_vline(xintercept = 0, colour="red") +
  scale_x_continuous("Time / s", expand=c(0,0), limits=c(-50*42,50*42),
                     breaks=seq(from=-2000, to=2000, by=1000),
                     labels=c("-2000","-1000","Anaphase \n Onset","1000","2000")) +
  ylim(0, max(timeSummary$mean.Distance+timeSummary$sd.Distance, na.rm=TRUE)) +
  labs(x="time", y="Distance / microns") +
  annotate(geom="text",label=paste("N = ", NCells, sep=""), x=-1750, y=max(timeSummary$mean.Distance+timeSummary$sd.Distance, na.rm=TRUE)) +
  theme_overview
print(sdPlot)
ggsave(filename=file.path(saveDir, paste(filenameString,"_sdPlot.pdf",sep="")), plot=sdPlot)

# Fitting to timepoint averages ----------------------------------------------

t <- dplyr::filter(timeSummary, Time >= -1000 & Time <= 0)
fd <- data.frame(x = t$Time, y = abs(t$mean.Distance))

# defining the sigmoid function as supposed to be fitted, see Petrova et al 2013, p 986, paragraph "Mathematical data fit"
sigmoid <- function(x, k, a, b, offset){ # k: difference between asymptotes, a: decay rate, b: ~inflection point, offset: lower asymptote
  k/(1+exp(a*x+b)) + offset
}

# the nls function needs estimated starting parameters to converge towards a solution.
make.start.parameters <- function(){
  return(list(a = runif(1, min=0, max=0.2),
              b = runif(1, min=2, max=8),
              k = runif(1, min=0, max=2),
              offset = runif(1, min=0, max=2)))
}

# do the fitting.
i = 0
while(i < 100000){
  fit <- NULL
  fit <- nls(formula = y ~ I(sigmoid(x, k, a, b, offset)),
      data = fd,
      start = make.start.parameters(),
      trace = FALSE,)
  if(!is.null(fit)) break
  i = i + 1
}

fit
# export the fitting results
fitResults <- data.frame(t(coef(fit)))
fitResults <- mutate(.data=fitResults, Date=date, Strain=strain, Temp=temp, analysisDate=analysisDate, qcer=qcer)
write.csv(x=fitResults, file=file.path(saveDir, paste(filenameString,'_fit.csv',sep='')))

print(NCells)
```

4.15.9 R script for experiment-to-experiment variation analysis

```
# plotting wt condensation curves at different temperatures, July 2016
# Author: Christoph Schiklenk
# Email: schiklen@embl.de

library("ggplot2")
library("dplyr")
library("magrittr")
library("tidyr")

# Data import
# -----------

rawFiles <- list.files(path=getwd(), recursive=T, pattern="_raw.csv")
raw.df <- do.call("rbind", lapply(rawFiles, read.csv, header = TRUE))
write.csv(raw.df, file="wtTempRaw.csv")
#delete all NAs because they can hinder analysis
raw.df <- subset(raw.df, !is.na(raw.df$Distance))

#count N cells per experiment
raw.df.group.experiment <- dplyr::group_by(.data=raw.df, analysisDate)
NcellsTable <- dplyr::summarise(.data=raw.df.group.experiment,
                            date=as.Date(as.character(unique(Date)), format="%y%m%d"),
                            strain=unique(Strain),
                            temp=unique(Temp),
                            nCells = length( unique( paste(Position, Cell) ) ) )

ggplot(NcellsTable, mapping=aes(x=factor(temp), y=nCells )) + geom_boxplot(outlier.size=0, color="grey") +
  geom_jitter() + facet_wrap(~strain) + coord_cartesian(ylim=c(0,85)) +
  xlab("Temperature [C]") +
  ylab("N analyzed mitoses") + theme_bw()


#calculate time summaries/means
summary.df <- group_by(raw.df, Time, Strain, Date, analysisDate, Temp) %>%
  summarise(mean.distance = mean(Distance),
            sd.distance = sd(Distance),
            N = length(Distance) )

# calculate average distance at anaphase onset
# --------------------------------------------

anaphaseOnset.dist <- group_by(raw.df, Strain, Temp, Date, analysisDate) %>%
  filter(Time==0) %>%
  summarise(avg.anaphaseOnset.Distance = mean(Distance), sd.anaphaseOnset.Distance = sd(Distance))
G2.dist <- group_by(raw.df, Strain, Temp, Date, analysisDate) %>%
  filter(Time <= -750) %>%
  summarise(avg.G2.Distance = mean(Distance), sd.G2.Distance = sd(Distance))
rawDistances <- merge(anaphaseOnset.dist, G2.dist, by=c("Strain", "Temp", "analysisDate"))

# Plot averaged data
# ------------------

#plot the by time point means
strainWrap <- ggplot(data=summary.df, mapping=aes(x=Time, y=mean.distance, group=analysisDate)) +
  geom_line(aes(color=factor(Temp)) ) +
  geom_vline(x=0, color="black") +
  xlim(c(-1300, 2200)) +
  ylim(c(0, 2.2)) +
  ylab("Distance [micron]") + xlab("Time [s]") +
  facet_wrap(~ Strain)
print(strainWrap)
ggsave(filename="strainWrap.pdf", plot=strainWrap, width=16.2, height=6, unit="in") # 6 x 16.2 inch

# F I T S
# -------

# find condensation start by fit slope threshold.
findCondStart <- function(fit.Obj, slope.threshold=-0.0002, t.min=-1000, t.max=-135){
  fit.slopes <- data.frame(predict(fit.Obj, x=seq(t.min,t.max,by=1), deriv=0 ),
                       stD=predict(fit.Obj, x=seq(t.min,t.max,by=1), deriv=1 )$y,
                       ndD=predict(fit.Obj, x=seq(t.min,t.max,by=1), deriv=2 )$y)
  names(fit.slopes) <- c("Time", "dist", "stD", "ndD")
  cond_start <- max( subset(fit.slopes, subset=fit.slopes$stD >= slope.threshold)$Time )
  return(as.numeric(cond_start))
}

summary.df.byExperiment <- group_by(summary.df, Date, analysisDate, Strain, Temp)
# do the fits
fits.by.experiment <- do( summary.df.byExperiment, fits = smooth.spline(x=.$Time, y=.$mean.distance, w=.$N) )
# join with earlier results
summary.df.byExperiment <- inner_join(x=fits.by.experiment, y=rawDistances, by=c("Strain", "Temp", "analysisDate"))
# extract the values from the fits for each experiment
fits.val.individual <- summarise( summary.df.byExperiment,
    Strain = Strain,
    Temp = Temp,
    Date = Date,
    avg.G2.Distance = avg.G2.Distance,
    avg.anaphaseOnset.Distance = avg.anaphaseOnset.Distance,
    fit.anaphaseOnset.Distance = as.numeric(predict(fits, x=0)$'y'),
    compaction.dist = avg.G2.Distance - fit.anaphaseOnset.Distance,
    t.condensation.start = findCondStart(fits),
    dist.condensation.start = predict(fits, x=t.condensation.start)$'y',
```

```
    min.condensation.slope = min( predict(fits, x=seq(t.condensation.start, 0, by=1), deriv=1)$y ),
    avg.condensation.slope = mean(predict(fits, x=seq(t.condensation.start, 0, by=1), deriv=1)$y ),
    dist.50p = (0.5*compaction.dist) + avg.anaphaseOnset.Distance,
    t.50 = min( predict(fits, x=seq(-1200, 0, by=1))$'x'[predict(fits, x=seq(-1200, 0, by=1))$y <= dist.50p] ),
    min.fit.Dist = min( predict(fits, x=seq(0, 2000, by=1), deriv=0 )$y ),
    t.min.fit.Dist = predict(fits, x=seq(0, 2000, by=1))$'x'[predict(fits, x=seq(0, 2000, by=1))$y==min.fit.Dist],
    avg.decon.slope = mean(predict(fits, x=seq(0, 2000, by=1), deriv=1)$y )
  )
# output the results
write.csv(fits.val.individual, file="fitsVal_ind.csv", row.names=FALSE)

#summarize and calculate statistics on values from the fits for each experiment
statistics <- group_by(fits.val.individual, Strain, Temp) %>%
  summarise(mean.G2.Dist = mean(avg.G2.Distance),
            sd.G2.Dist = sd(avg.G2.Distance),
            mean.t.condStart = mean(t.condensation.start),
            sd.t.condStart = sd(t.condensation.start),
            mean.condStart.Dist = mean(dist.condensation.start),
            sd.condStart.Dist = sd(dist.condensation.start),
            mean.condensation.slope.nm.s = mean(avg.condensation.slope)*1000, # in nm/s
            sd.condensation.slope.mn.s = sd(avg.condensation.slope)*1000, # in nm/s
            mean.Dist.50p = mean(dist.50p),
            sd.Dist.50p = sd(dist.50p),
            mean.t.50 = mean(t.50),
            sd.t.50 = sd(t.50),
            mean.anaphOnset.Dist = mean(avg.anaphaseOnset.Distance),
            sd.anaphOnset.Dist = sd(avg.anaphaseOnset.Distance),
            mean.min.fit.Dist = mean(min.fit.Dist),
            sd.min.fit.Dist = sd(min.fit.Dist),
            mean.min.t = mean(t.min.fit.Dist),
            sd.min.t = sd(t.min.fit.Dist),
            mean.decon.slope.nm.s = mean(avg.decon.slope)*1000,
            sd.decon.slope.nm.s = sd(avg.decon.slope)*1000
            )

# Plot the fits and the averages
# ----------------------------
fit.dist.for.plot <- do(fits.by.experiment,
                      data.frame(
                        analysisDate = .$analysisDate,
                        Date=.$Date,
                        Strain=.$Strain,
                        Temp=.$Temp,
                        fit.time = seq(-1000, 2000, by=5),
                        fit.distance = predict(.$fits, x=seq(-1000, 2000, by=5))$'y',
                        fit.slope = predict(.$fits, x=seq(-1000, 2000, by=5), deriv=1)$'y') )

fits.plot <- ggplot() +
  geom_line(data=fit.dist.for.plot,
            mapping=aes(x=fit.time, y=fit.distance, group=analysisDate, color=factor(Temp)) ) +
  geom_errorbar(data=statistics, size=1,
                mapping=aes(x=mean.min.t, ymin=mean.min.fit.Dist-sd.min.fit.Dist, ymax=mean.min.fit.Dist+sd.min.fit.Dist)) +
  geom_errorbarh(data=statistics, size=1,
                 mapping=aes(x=mean.min.t, y=mean.min.fit.Dist, xmin=mean.min.t-sd.min.t, xmax=mean.min.t+sd.min.t)) +
  geom_vline(x=0, color="black") +
  geom_errorbar(data=statistics, size=1,
                mapping=aes(x=mean.t.condStart, ymin=mean.condStart.Dist-sd.condStart.Dist, ymax=mean.condStart.Dist+sd.condStart.Dist )) +
  geom_errorbarh(data=statistics, size=1,
                 mapping=aes(y=mean.condStart.Dist, x=mean.t.condStart,
                             xmin=(mean.t.condStart-sd.t.condStart), xmax=(mean.t.condStart+sd.t.condStart)) ) +
  xlim(c(-1300, 2200)) +
  ylim(c(0, 2.2)) +
  ylab("Distance [micron]") + xlab("Time [s]") +
  facet_wrap(~ Strain)
print(fits.plot)
ggsave(filename="fitsStrainWrap.pdf", plot=fits.plot, width=16.2, height=6, unit="in")

# output the results
statistics <- format(statistics, digits=3)
write.csv(x=statistics, file="wtTempCondensStatistics.csv", row.names=FALSE)



# plot condensation rates for fig
ggplot(data=fits.val.individual, aes(x=as.factor(Strain), y=abs(avg.condensation.slope) )) +
  geom_point(aes(color=as.factor(Temp)), size=4 ) + facet_wrap(~Temp) +
  ylab("condensation rate in micron/s") + xlab("Strain") + ylim(c(0,0.002))

#plot decondensation rates for figure
ggplot(data=fits.val.individual, aes(x=as.factor(Strain), y=abs(avg.decon.slope) )) +
  geom_point(aes(color=as.factor(Temp)), size=4 ) + facet_wrap(~Temp) +
  ylab("condensation rate in micron/s") + xlab("Strain") #+ ylim(c(0,0.002))

# plot the first derivative for fun.
slopesubset <- subset(fit.dist.for.plot, fit.time <= 0)
ggplot(data=slopesubset, mapping=aes(x=fit.time, y=fit.slope, color=as.factor(Temp), group=analysisDate)) +
  geom_line() + facet_wrap(~Strain) + xlab("Time s") + ylab("slope microns/s")

# plot the distribution of FROS distances in 2779 in G2.
singleTimePointBeforeCond <- filter(summary.df, Strain==2774 && Time< (-600) )
mostData <- max(singleTimePointBeforeCond$N)
stbc <- filter(singleTimePointBeforeCond, N==mostData )
distAtSTBC <- filter(raw.df, (Time==stbc$Time & analysisDate==stbc$analysisDate))
ggplot(data=distAtSTBC, mapping=aes(x=Distance)) + geom_bar() + theme_bw())
```

4.15.10 Modeling of underlying causes of shallow condensation curves

```
# a script to simulate outcome of average condensation curves
# from either when underlying

library("ggplot2")
library("dplyr")

# k: difference between asymptotes, a: decay rate, b: ~inflection point, offset: value of lower asymptote
sigmoid <- function(x, k, a=0.015, b, offset){
  k/(1+exp(a*x+b)) + offset
}



# this function returns a slightly randomized paramlist
# k = difference between asymptotes

makeParamList <- function(time.min= -1000, time.max=50, nReps=20, time.by=2, b.min, b.max, a=0.015){
  modD <- data.frame()
  n.points <- ((abs(time.min)+abs(time.max)) / time.by ) +1
  for (c.id in 1:nReps ) {
    n <- data.frame(
      Time = seq(from=time.min, to=time.max, by=time.by),
      k = rep( runif(n=1, 0.73, max=0.79), times=n.points ),
      a = rep( a, times=n.points ),
      b = rep( runif(n=1, min=b.min, max=b.max), times=n.points ),
      offset = rep( runif(n=1, min=0.48, max=0.52), times=n.points),
      id = c.id)
    n$distance <- sigmoid(n$Time, n$k, n$a, n$b, n$offset)
    modD <- rbind(modD, n)
  }
  return(modD)
}

mod.delay <- makeParamList(b.min=4, b.max=10)
mod.delay$delay <- "APCdelay"

mod.wt <- makeParamList(b.min=3.7, b.max=4.3)
mod.wt$delay <- "wt"

mod.shallow <- makeParamList(b.min=3.7, b.max=4.3, a=0.008)
mod.shallow$delay <- "kinetics"

mo <- rbind(mod.delay, mod.wt, mod.shallow)
mo$delay <- factor(mo$delay, levels=c("wt", "APCdelay","kinetics"))

modelPlot <- ggplot() + coord_cartesian(ylim=c(0,1.5)) +
  geom_line(data=mo, aes(x=Time, y=distance, group=id), alpha=0.4) +
  facet_wrap(~delay, ncol=1) + theme_classic()

#calculate the averages

mo.g.time <- group_by(mo, Time, delay)
mo.avg.dist <- summarise(mo.g.time,
                         distance = mean(distance))

averagePlot <- ggplot(data=mo.avg.dist, aes(x=Time, y=distance)) +
  coord_cartesian(ylim=c(0,1.5)) + geom_line(size=1) +
  facet_wrap(~delay, ncol=1) + theme_classic()
```

List of Figures

List of Tables

Appendix

4.16 *SPAC713.13* and *SPAC887.16* are not essential

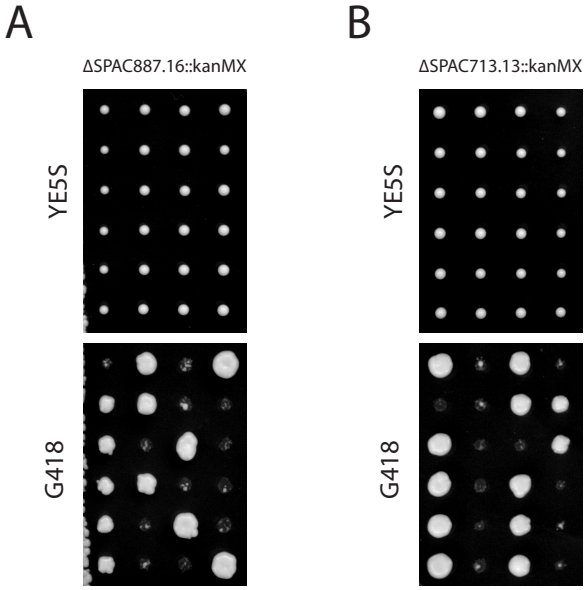

Figure 4.4: SPAC713.13 and SPAC887.16 are not essential. Top row: Tetrad dissection on YE5S, bottom row: top row replica plated to YE5S containing G418. (A) Tetrad dissection of strain 4509, genotype h^+/h^-, *SPAC713.13*$^+$*/ΔSPAC713.13::kanMX, ade6-M210/ade6-M216* (B) Tetrad dissection of strain 4508, genotype h^+/h^-, *SPBC887.16*$^+$*/ΔSPBC887.16::kanMX, ade6-M210/ade6-M216.* Haploid ΔSPBC887.16::kanMX cells

Acknowledgements

I thank Christian Häring for giving me the opportunity to do a PhD in his lab and for showing me how to manage a research project completely independently. I thank the Häring lab members Yuri Frosi, Markus Hassler, Marc Kschonsak, Indra Shaltiel, Jin Wang, Shveta Bisht for helpful discussions and kicker, coffee and cake-breaks. In this context, I specifically thank Markus and Marc for playing I thank Boryana Petrova for initial introduction to the CCA and showing me the basics of working with *S. pombe*. I thank Toby Gibson, for being a brilliant scientist with insight and intuition. Toby made the right prediction at the right time in my PhD. I especially thank the media kitchen employees - Magdalena Gierlach and team - for tremendous help in preparing media and the lab kitchen employees for cleaning and autoclaving countless glassware and reaction tubes. The core facilities and the technical support at EMBL made some otherwise impossible experiments possible. ALMF-members Marko Lampe, Stefan Terjung and Christian Tischer for helping me with the microscopes and keeping them running. Kota Miura told me to learn Phython and showed me the next step when I was lost in image processing and analysis. I thank the Genomics core facility (in particular Vladimir Benes and Bianka Baying) for advice, the library preparation tutorial and sequencing and the Genome Biology Computational Support (Charles Girardot and Jelle Scholtalbers) for help with analysis of the ChIP seq data. I thank Proteomics core facility members Mandy Rettel for mass spectrometry service. I thank my first student Maria Saez-Garcia for a tremendous amount of cloning. My second student Carlo Klein was very productive, had many ideas and great skill (both bench and kicker!) that was central to the implementation of the single cell condensation assay. Thank you, Carlo!

I thank my fellow PhD student Gustavo Quintas de Medeiros for sharing some of the writing process and music. I thank all the friends I have found at EMBL. I also thank Marcus Heisler and his Jazz Club and Lab Rat members for letting me play in their band. A special thanks to The Signals Tobi Tornrös, Luggi Richter and Nils Norlin for filling the sparse free time and relatively stressless fulfillment of my favorite hobby. I thank my flat mates Camilla Godlee, Norina Poppe, Hamster and Leo Kiss for nice and entertaining, but sometimes troublesome times in the flat. I thank Christina Wenz for understanding and patience during stressful times. Most of all, I thank my parents and grand parents. They have supported me in every situation and I am endlessly grateful for all they have done for me. Without them this work would not have been possible.

Bibliography

E. Abbe. Beiträge zur Theorie des Mikroskops und der mikroskopischen Wahrnehmung, 1873. ISSN 0176-7364.

S. Abe, K. Nagasaka, Y. Hirayama, H. Kozuka-Hata, M. Oyama, Y. Aoyagi, C. Obuse, and T. Hirota. The initial phase of chromosome condensation requires Cdk1-mediated phosphorylation of the CAP-D3 subunit of condensin II. Genes & Development, 25(8):863–874, apr 2011. ISSN 0890-9369. doi: 10.1101/gad.2016411. URL `http://genesdev.cshlp.org/cgi/doi/10.1101/gad.2016411`.

Y. Adachi, M. Luke, and U. K. Laemmli. Chromosome assembly in vitro: topoisomerase II is required for condensation. Cell, 64(1):137–48, jan 1991. ISSN 0092-8674. doi: doi: 10.1016/0092-8674(91)90215-K. URL `http://www.ncbi.nlm.nih.gov/pubmed/1846085`.

E. Afgan, D. Baker, M. van den Beek, D. Blankenberg, D. Bouvier, M. Čech, J. Chilton, D. Clements, N. Coraor, C. Eberhard, B. Grüning, A. Guerler, J. Hillman-Jackson, G. Von Kuster, E. Rasche, N. Soranzo, N. Turaga, J. Taylor, A. Nekrutenko, and J. Goecks. The Galaxy platform for accessible, reproducible and collaborative biomedical analyses: 2016 update. Nucleic Acids Research, 44(W1):W3–W10, jul 2016. ISSN 1362-4962. doi: 10.1093/nar/gkw343.

B. Alberts, A. Johnson, J. Lewis, D. Morgan, M. Raff, K. Roberts, and P. Walter. Molecular Biology of the Cell. Garland Science, 5th edition, 2014. ISBN 978-0-8153-4524-4.

S. J. Altschuler and L. F. Wu. Cellular Heterogeneity: Do Differences Make a Difference? Cell, 141(4):559–563, 2010. ISSN 00928674. doi: 10.1016/j.cell.2010.04.033.

N. Aono, T. Sutani, T. Tomonaga, S. Mochida, and M. Yanagida. Cnd2 has dual roles in mitotic condensation and interphase. Nature, 417(May):197–202, 2002. ISSN 0028-0836. doi: 10.1038/417197a.

E. Apolinario, M. Nocero, M. Jin, and C. S. Hoffman. Cloning and manipulation of the Schizosaccharomyces pombe his7 +gene as a new selectable marker for molecular genetic studies. Current Genetics, 24(6):491–495, dec 1993. ISSN 0172-8083. doi: 10.1007/BF00351711. URL `http://link.springer.com/10.1007/BF00351711`.

P. Arumugam, S. Gruber, K. Tanaka, C. H. Haering, K. Mechtler, and K. Nasmyth. ATP Hydrolysis Is Required for Cohesin's Association with Chromosomes. Current Biology, 13 (22):1941–1953, nov 2003. ISSN 09609822. doi: 10.1016/j.cub.2003.10.036. URL http://linkinghub.elsevier.com/retrieve/pii/S0960982203008042.

O. T. Avery, C. M. Macleod, and M. McCarty. STUDIES ON THE CHEMICAL NATURE OF THE SUBSTANCE INDUCING TRANSFORMATION OF PNEUMOCOCCAL TYPES: INDUCTION OF TRANSFORMATION BY A DESOXYRIBONUCLEIC ACID FRACTION ISOLATED FROM PNEUMOCOCCUS TYPE III. The Journal of experimental medicine, 79(2):137–58, feb 1944. ISSN 0022-1007. doi: 10.1084/jem.79.2.137.

J. Bähler, J.-Q. Wu, M. S. Longtine, N. G. Shah, A. Mckenzie III, A. B. Steever, A. Wach, P. Philippsen, and J. R. Pringle. Heterologous modules for efficient and versatile PCR-based gene targeting inSchizosaccharomyces pombe. Yeast, 14(10):943–951, jul 1998. ISSN 0749503X. doi: 10.1002/(SICI)1097-0061(199807)14:10⟨943::AID-YEA292⟩3.0.CO;2-Y.

A. L. Bak, J. Zeuthen, and F. H. Crick. Higher-order structure of human mitotic chromosomes. Proceedings of the National Academy of Sciences of the United States of America, 74(4): 1595–9, apr 1977. ISSN 0027-8424. doi: 10.1073/pnas.74.4.1595.

S. Bandyopadhyay, M. Mehta, D. Kuo, M.-K. Sung, R. Chuang, E. J. Jaehnig, B. Bodenmiller, K. Licon, W. Copeland, M. Shales, D. Fiedler, J. Dutkowski, A. Guenole, H. van Attikum, K. M. Shokat, R. D. Kolodner, W.-K. Huh, R. Aebersold, M.-C. Keogh, N. J. Krogan, and T. Ideker. Rewiring of Genetic Networks in Response to DNA Damage. Science, 330(6009): 1385–1389, dec 2010. ISSN 0036-8075. doi: 10.1126/science.1195618.

M. Baumgartner, B. Dutrillaux, N. Lemieux, A. Lilienbaum, D. Paulin, and E. Viegas-Péquignot. Genes occupy a fixed and symmetrical position on sister chromatids. Cell, 64 (4):761–6, feb 1991. ISSN 0092-8674. doi: http://dx.doi.org/10.1016/0092-8674(91)90505-S.

C. Bieniossek, T. J. Richmond, and I. Berger. MultiBac: Multigene baculovirus-based eukaryotic protein complex production. Current Protocols in Protein Science, (February):1–26, 2008. ISSN 19343655. doi: 10.1002/0471140864.ps0520s51.

W. Burger and M. J. Burge. Digital image processing: an algorithmic introduction using Java. Springer Science, 2008. ISBN B011DAXG56.

S. Cai, L. N. Weaver, S. C. Ems-McClung, and C. E. Walczak. Kinesin-14 family proteins HSET/XCTK2 control spindle length by cross-linking and sliding microtubules. Molecular Biology of the Cell, 20(5):1348–59, mar 2009. ISSN 1939-4586. doi: 10.1091/mbc.E08-09-0971.

B. Chen, L. A. Gilbert, B. A. Cimini, J. Schnitzbauer, W. Zhang, G.-W. Li, J. Park, E. H. Blackburn, J. S. Weissman, L. S. Qi, and B. Huang. Dynamic imaging of genomic loci in living human cells by an optimized CRISPR/Cas system. Cell, 155(7):1479–91, dec 2013. ISSN

1097-4172. doi: 10.1016/j.cell.2013.12.001. URL http://www.ncbi.nlm.nih.gov/pubmed/24360272.

T. M. K. Cheng, S. Heeger, R. A. G. Chaleil, N. Matthews, A. Stewart, J. Wright, C. Lim, P. a. Bates, and F. Uhlmann. A simple biophysical model emulates budding yeast chromosome condensation. eLife, 4:e05565, apr 2015. ISSN 2050-084X. doi: 10.7554/eLife.05565.

N. Chenouard, I. Smal, F. de Chaumont, M. Maška, I. F. Sbalzarini, Y. Gong, J. Cardinale, C. Carthel, S. Coraluppi, M. Winter, A. R. Cohen, W. J. Godinez, K. Rohr, Y. Kalaidzidis, L. Liang, J. Duncan, H. Shen, Y. Xu, K. E. G. Magnusson, J. Jaldén, H. M. Blau, P. Paul-Gilloteaux, P. Roudot, C. Kervrann, F. Waharte, J.-Y. Tinevez, S. L. Shorte, J. Willemse, K. Celler, G. P. van Wezel, H.-W. Dan, Y.-S. Tsai, C. Ortiz de Solórzano, J.-C. Olivo-Marin, and E. Meijering. Objective comparison of particle tracking methods. Nature Methods, 11 (3):281–9, mar 2014. ISSN 1548-7105. doi: 10.1038/nmeth.2808. URL http://www.ncbi.nlm.nih.gov/pubmed/24441936.

S. Cuylen, J. Metz, and C. H. Haering. Condensin structures chromosomal DNA through topological links. Nature structural & molecular biology, 18(8):894–901, aug 2011. ISSN 1545-9985. doi: 10.1038/nsmb.2087. URL http://www.ncbi.nlm.nih.gov/pubmed/21765419.

S. Cuylen, J. Metz, A. Hruby, and C. H. Haering. Entrapment of chromosomes by condensin rings prevents their breakage during cytokinesis. Developmental Cell, 27(4):469–78, nov 2013. ISSN 1878-1551. doi: 10.1016/j.devcel.2013.10.018. URL http://www.ncbi.nlm.nih.gov/pubmed/24286828.

M. M. DeAngelis, D. G. Wang, and T. L. Hawkins. Solid-phase reversible immobilization for the isolation of PCR products. Nucleic Acids Research, 23(22):4742–4743, nov 1995. ISSN 0305-1048. doi: 10.1093/nar/23.22.4742.

H. Dinkel, K. Van Roey, S. Michael, M. Kumar, B. Uyar, B. Altenberg, V. Milchevskaya, M. Schneider, H. Kühn, A. Behrendt, S. L. Dahl, V. Damerell, S. Diebel, S. Kalman, S. Klein, A. C. Knudsen, C. Mäder, S. Merrill, A. Staudt, V. Thiel, L. Welti, N. E. Davey, F. Diella, and T. J. Gibson. ELM 2016–data update and new functionality of the eukaryotic linear motif resource. Nucleic Acids Research, 44(D1):D294–300, jan 2016. ISSN 1362-4962. doi: 10.1093/nar/gkv1291.

C. Dunn, A. O'Dowd, and R. E. Randall. Fine mapping of the binding sites of monoclonal antibodies raised against the Pk tag. Journal of immunological methods, 224(1-2):141–50, apr 1999. ISSN 0022-1759. doi: 10.1016/S0022-1759(99)00017-4.

E. J. DuPraw. Evidence for a 'folded-fibre' organization in human chromosomes. Nature, 209 (5023):577–81, feb 1966. ISSN 0028-0836. doi: 10.1038/209577a0.

J. M. Eeftens, A. J. Katan, M. Kschonsak, M. Hassler, L. de Wilde, E. M. Dief, C. H. Haering, and C. Dekker. Condensin Smc2-Smc4 Dimers Are Flexible and Dynamic. Cell reports, 14 (8):1813–8, mar 2016. ISSN 2211-1247. doi: 10.1016/j.celrep.2016.01.063.

T. Eide, C. Carlson, K. A. Taskén, T. Hirano, K. Taskén, and P. Collas. Distinct but overlapping domains of AKAP95 are implicated in chromosome condensation and condensin targeting. EMBO Reports, 3(5):426–432, 2002. ISSN 1469221X. doi: 10.1093/embo-reports/kvf089.

J. Feng, T. Liu, and Y. Zhang. Using MACS to identify peaks from ChiP-seq data. Current Protocols in Bioinformatics, (SUPPL. 34):1–14, 2011. ISSN 19343396. doi: 10.1002/0471250953.bi0214s34.

R. D. Finn, A. Bateman, J. Clements, P. Coggill, R. Y. Eberhardt, S. R. Eddy, A. Heger, K. Hetherington, L. Holm, J. Mistry, E. L. L. Sonnhammer, J. Tate, and M. Punta. Pfam: the protein families database. Nucleic Acids Research, 42(Database issue):D222–30, jan 2014. ISSN 1362-4962. doi: 10.1093/nar/gkt1223.

W. Flemming. Zur Kenntnis der Zelle und ihrer Teilung-Erscheinungen. Schr. Nat. Wiss. Ver. Schlesw.-Holst., 3(1):23–27, 1878.

S. L. Forsburg and P. Nurse. Identification of a Gl-type cyclin puc1 + in the fission yeast Schizosaccharomyces pombe. Nature, 351(6323):245–248, may 1991. ISSN 0028-0836. doi: 10.1038/351245a0. URL `http://www.ncbi.nlm.nih.gov/pubmed/1828291http://www.nature.com/doifinder/10.1038/351245a0`.

S. L. Forsburg and P. Nurse. Analysis of the Schizosaccharomyces pombe cyclin puc1: evidence for a role in cell cycle exit. Journal of Cell Science, 107:601–13, mar 1994. ISSN 0021-9533. URL `http://www.ncbi.nlm.nih.gov/pubmed/8006074`.

P. S. Foundation. Jython: Python for the Java Platform. URL `www.jython.org`.

M. I. Fousteri and A. R. Lehmann. A novel SMC protein complex in Schizosaccharomyces pombe contains the Rad18 DNA repair protein. The EMBO Journal, 19(7):1691–1702, apr 2000. ISSN 14602075. doi: 10.1093/emboj/19.7.1691.

D. K. Fygenson, E. Braun, and A. Libchaber. Phase diagram of microtubules. Physical review. E, Statistical physics, plasmas, fluids, and related interdisciplinary topics, 50(2):1579–1588, aug 1994. ISSN 1063-651X.

J. Gao, F. Kan, J. L. Wagnon, A. J. Storey, R. U. Protacio, M. K. Davidson, and W. P. Wahls. Rapid, efficient and precise allele replacement in the fission yeast Schizosaccharomyces pombe. Current genetics, 60(2):109–19, may 2014. ISSN 1432-0983. doi: 10.1007/s00294-013-0406-x. URL `http://www.ncbi.nlm.nih.gov/pubmed/24026504`.

S. M. Gasser, T. Laroche, J. Falquet, E. Boy de la Tour, and U. K. Laemmli. Metaphase chromosome structure. Involvement of topoisomerase II. Journal of molecular biology, 188

(4):613–29, apr 1986. ISSN 0022-2836. doi: 10.1016/S0022-2836(86)80010-9. URL http://www.ncbi.nlm.nih.gov/pubmed/3016287.

A. Goffeau, B. G. Barrell, H. Bussey, R. W. Davis, B. Dujon, H. Feldmann, F. Galibert, J. D. Hoheisel, C. Jacq, M. Johnston, E. J. Louis, H. W. Mewes, Y. Murakami, P. Philippsen, H. Tettelin, and S. G. Oliver. Life with 6000 genes. Science, 274(5287):546, 563–7, oct 1996. ISSN 0036-8075. doi: 10.1126/science.274.5287.546.

A. L. Goldstein and J. H. McCusker. Three new dominant drug resistance cassettes for gene disruption in Saccharomyces cerevisiae. Yeast (Chichester, England), 15(14):1541–53, oct 1999. ISSN 0749-503X. doi: 10.1002/(SICI)1097-0061(199910)15:14⟨1541::AID-YEA476⟩3.0.CO;2-K. URL http://www.ncbi.nlm.nih.gov/pubmed/10514571.

J. J. Griese, G. Witte, and K.-P. Hopfner. Structure and DNA binding activity of the mouse condensin hinge domain highlight common and diverse features of SMC proteins. Nucleic Acids Research, 38(10):3454–65, jun 2010. ISSN 1362-4962. doi: 10.1093/nar/gkq038.

C. Grimm, J. Kohli, J. Murray, and K. Maundrell. Genetic engineering of Schizosaccharomyces pombe: A system for gene disruption and replacement using the ura4 gene as a selectable marker. MGG Molecular & General Genetics, 215(1):81–86, 1988. ISSN 00268925. doi: 10.1007/BF00331307.

C. H. Haering and S. Gruber. SnapShot: SMC Protein Complexes Part I. Cell, 164(1-2): 326–326.e1, 2016. ISSN 1097-4172. doi: 10.1016/j.cell.2015.12.026.

C. H. Haering, J. Löwe, A. Hochwagen, and K. Nasmyth. Molecular architecture of SMC proteins and the yeast cohesin complex. Molecular Cell, 9(4):773–88, apr 2002. ISSN 1097-2765. doi: 10.1016/S1097-2765(02)00515-4. URL http://www.ncbi.nlm.nih.gov/pubmed/11983169.

C. H. Haering, A.-M. Farcas, P. Arumugam, J. Metson, and K. Nasmyth. The cohesin ring concatenates sister DNA molecules. Nature, 454(7202):297–301, jul 2008. ISSN 1476-4687. doi: 10.1038/nature07098. URL http://www.ncbi.nlm.nih.gov/pubmed/18596691.

I. M. Hagan, A. Grallert, and V. Simanis. Cell Cycle Synchronization of Schizosaccharomyces pombe by Centrifugal Elutriation of Small Cells. Cold Spring Harbor Protocols, 2016(6), jun 2016. ISSN 1940-3402. doi: 10.1101/pdb.prot091231.

J. Hayles, V. Wood, L. Jeffery, K.-L. Hoe, D.-U. Kim, H.-O. Park, S. Salas-Pino, C. Heichinger, and P. Nurse. A genome-wide resource of cell cycle and cell shape genes of fission yeast. Open biology, 3(5):130053, may 2013. ISSN 2046-2441. doi: 10.1098/rsob.130053. URL http://www.pubmedcentral.nih.gov/articlerender.fcgi?artid=3866870{&}tool=pmcentrez{&}rendertype=abstract.

P. Hentges, B. Van Driessche, L. Tafforeau, J. Vandenhaute, and A. M. Carr. Three novel antibiotic marker cassettes for gene disruption and marker switching in Schizosaccharomyces pombe. Yeast (Chichester, England), 22(13):1013–9, oct 2005. ISSN 0749-503X. doi: 10.1002/yea.1291.

T. Hirano. Condensins: organizing and segregating the genome. Current Biology, 15(7):R265–75, apr 2005. ISSN 0960-9822. doi: 10.1016/j.cub.2005.03.037. URL `http://www.ncbi.nlm.nih.gov/pubmed/15823530`.

T. Hirano. Review Condensin-Based Chromosome Organization from Bacteria to Vertebrates. Cell, 164(5):847–857, 2016. ISSN 0092-8674. doi: 10.1016/j.cell.2016.01.033.

T. Hirano, R. Kobayashi, and M. Hirano. Condensins, chromosome condensation protein complexes containing XCAP-C, XCAP-E and a Xenopus homolog of the Drosophila Barren protein. Cell, 89(4):511–21, may 1997. ISSN 0092-8674.

Y. Hiraoka, T. Toda, and M. Yanagida. The NDA3 gene of fission yeast encodes beta-tubulin: a cold-sensitive nda3 mutation reversibly blocks spindle formation and chromosome movement in mitosis. Cell, 39(2 Pt 1):349–58, dec 1984. ISSN 0092-8674. URL `papers2://publication/uuid/B94D4CD6-874E-4612-AA12-EB696FD3B504http://www.ncbi.nlm.nih.gov/pubmed/6094012`.

Y. Hiraoka, D.-Q. Ding, A. Yamamoto, C. Tsutsumi, and Y. Chikashige. Characterization of fission yeast meiotic mutants based on live observation of meiotic prophase nuclear movement. Chromosoma, 109(1-2):103–109, apr 2000. ISSN 0009-5915. doi: 10.1007/s004120050417. URL `http://link.springer.com/10.1007/s004120050417`.

T. Hirota, D. Gerlich, B. Koch, J. Ellenberg, and J.-M. Peters. Distinct functions of condensin I and II in mitotic chromosome assembly. Journal of Cell Science, 117(Pt 26):6435–45, dec 2004. ISSN 0021-9533. doi: 10.1242/jcs.01604.

D. F. Hudson, P. Vagnarelli, R. Gassmann, and W. C. Earnshaw. Condensin is required for nonhistone protein assembly and structural integrity of vertebrate mitotic chromosomes. Developmental cell, 5(2):323–36, aug 2003. ISSN 1534-5807. doi: 10.1016/S1534-5807(03)00199-0.

O. Iwasaki, H. Tanizawa, K.-D. Kim, Y. Yokoyama, C. J. Corcoran, A. Tanaka, E. Skordalakes, L. C. Showe, and K.-i. Noma. Interaction between TBP and Condensin Drives the Organization and Faithful Segregation of Mitotic Chromosomes. Molecular Cell, 59(5):755–67, sep 2015. ISSN 1097-4164. doi: 10.1016/j.molcel.2015.07.007.

M. Johnson, I. Zaretskaya, Y. Raytselis, Y. Merezhuk, S. McGinnis, and T. L. Madden. NCBI BLAST: a better web interface. Nucleic Acids Research, 36(Web Server issue):W5–9, jul 2008. ISSN 1362-4962. doi: 10.1093/nar/gkn201. URL `http://www.ncbi.nlm.nih.gov/pubmed/18440982http://www.pubmedcentral.nih.gov/articlerender.fcgi?artid=PMC2447716`.

M. Kanke, K. Nishimura, M. Kanemaki, T. Kakimoto, T. S. Takahashi, T. Nakagawa, and H. Masukata. Auxin-inducible protein depletion system in fission yeast. BMC cell biology, 12(1):8, jan 2011. ISSN 1471-2121. doi: 10.1186/1471-2121-12-8. URL http://www.pubmedcentral.nih.gov/articlerender.fcgi?artid=3048574{&}tool=pmcentrez{&}rendertype=abstract.

D.-U. Kim, J. Hayles, D. Kim, V. Wood, H.-O. Park, M. Won, H.-S. Yoo, T. Duhig, M. Nam, G. Palmer, S. Han, L. Jeffery, S.-T. Baek, H. Lee, Y. S. Shim, M. Lee, L. Kim, K.-S. Heo, E. J. Noh, A.-R. Lee, Y.-J. Jang, K.-S. Chung, S.-J. Choi, J.-Y. Park, Y. Park, H. M. Kim, S.-K. Park, H.-J. Park, E.-J. Kang, H. B. Kim, H.-S. Kang, H.-M. Park, K. Kim, K. Song, K. B. Song, P. Nurse, and K.-L. Hoe. Analysis of a genome-wide set of gene deletions in the fission yeast Schizosaccharomyces pombe. Nature biotechnology, 28(6):617–23, jun 2010. ISSN 1546-1696. doi: 10.1038/nbt.1628.

K.-D. Kim, H. Tanizawa, O. Iwasaki, and K.-i. Noma. Transcription factors mediate condensin recruitment and global chromosomal organization in fission yeast. Nature genetics, (August): 1–12, aug 2016. ISSN 1546-1718. doi: 10.1038/ng.3647.

K. Kimura and T. Hirano. ATP-dependent positive supercoiling of DNA by 13S condensin: A biochemical implication for chromosome condensation. Cell, 90(4):625–634, 1997. ISSN 00928674. doi: 10.1016/S0092-8674(00)80524-3.

M. C. King, T. G. Drivas, and G. Blobel. A network of nuclear envelope membrane proteins linking centromeres to microtubules. Cell, 134(3):427–38, aug 2008. ISSN 1097-4172. doi: 10.1016/j.cell.2008.06.022. URL http://linkinghub.elsevier.com/retrieve/pii/S0092867408007745http://www.ncbi.nlm.nih.gov/pubmed/18692466http://www.pubmedcentral.nih.gov/articlerender.fcgi?artid=PMC2617791.

N. Kireeva, M. Lakonishok, I. Kireev, T. Hirano, and A. S. Belmont. Visualization of early chromosome condensation: a hierarchical folding, axial glue model of chromosome structure. The Journal of cell biology, 166(6):775–85, sep 2004. ISSN 0021-9525. doi: 10.1083/jcb.200406049.

C. Klein. Towards an Improved Quantitative Chromosome Condensation Assay in Fission Yeast. Master thesis, University of Kassel, 2015.

A. Klug. Letter from Aaron Klug to Francis Crick, 1977. URL https://profiles.nlm.nih.gov/ps/access/SCBBQS.pdf.

R. D. Kornberg and J. O. Thomas. Chromatin structure; oligomers of the histones. Science, 184(4139):865–8, may 1974. ISSN 0036-8075. URL http://www.ncbi.nlm.nih.gov/pubmed/4825888.

H. Krügel, G. Fiedler, I. Haupt, E. Sarfert, and H. Simon. Analysis of the nourseothricin-resistance gene (nat) of Streptomyces noursei. Gene, 62(2):209–17, 1988. ISSN 0378-1119. doi: 10.1016/0378-1119(88)90559-8. URL http://www.ncbi.nlm.nih.gov/pubmed/2835292.

T. Kruitwagen, A. Denoth-Lippuner, B. J. Wilkins, H. Neumann, and Y. Barral. Axial contraction and short-range compaction of chromatin synergistically promote mitotic chromosome condensation. eLife, 4(12):7250–7, dec 2015. ISSN 2050-084X. doi: 10.7554/eLife.10396.

M. Kschonsak and C. H. Haering. Shaping mitotic chromosomes: From classical concepts to molecular mechanisms. BioEssays, 37(7):755–66, jul 2015. ISSN 1521-1878. doi: 10.1002/bies.201500020.

J. R. Lakowicz. Principles of Fluorescence Spectroscopy. 2006. ISBN 978-0-387-31278-1 (Print) 978-0-387-46312-4 (Online). doi: 10.1007/978-0-387-46312-4.

S. G. Landt, G. K. Marinov, A. Kundaje, P. Kheradpour, F. Pauli, S. Batzoglou, B. E. Bernstein, P. Bickel, J. B. Brown, P. Cayting, Y. Chen, G. DeSalvo, C. Epstein, K. I. Fisher-Aylor, G. Euskirchen, M. Gerstein, J. Gertz, A. J. Hartemink, M. M. Hoffman, V. R. Iyer, Y. L. Jung, S. Karmakar, M. Kellis, P. V. Kharchenko, Q. Li, T. Liu, X. S. Liu, L. Ma, A. Milosavljevic, R. M. Myers, P. J. Park, M. J. Pazin, M. D. Perry, D. Raha, T. E. Reddy, J. Rozowsky, N. Shoresh, A. Sidow, M. Slattery, J. A. Stamatoyannopoulos, M. Y. Tolstorukov, K. P. White, S. Xi, P. J. Farnham, J. D. Lieb, B. J. Wold, and M. Snyder. ChIP-seq guidelines and practices of the ENCODE and modENCODE consortia. Genome research, 22(9):1813–31, sep 2012. ISSN 1549-5469. doi: 10.1101/gr.136184.111.

P. R. Langer-Safer, M. Levine, and D. C. Ward. Immunological method for mapping genes on Drosophila polytene chromosomes. Proceedings of the National Academy of Sciences of the United States of America, 79(14):4381–5, jul 1982. ISSN 0027-8424.

B. Langmead and S. L. Salzberg. Fast gapped-read alignment with Bowtie 2. Nature Methods, 9(4):357–9, apr 2012. ISSN 1548-7105. doi: 10.1038/nmeth.1923. URL http://www.ncbi.nlm.nih.gov/pubmed/22388286http://www.pubmedcentral.nih.gov/articlerender.fcgi?artid=PMC3322381.

I. Lassadi, A. Kamgoué, I. Goiffon, N. Tanguy-le Gac, and K. Bystricky. Differential Chromosome Conformations as Hallmarks of Cellular Identity Revealed by Mathematical Polymer Modeling. PLOS Computational Biology, 11(6):e1004306, 2015. ISSN 1553-7358. doi: 10.1371/journal.pcbi.1004306. URL http://dx.plos.org/10.1371/journal.pcbi.1004306.

I. F. Lau, S. R. Filipe, B. Søballe, O. A. Økstad, F. X. Barre, and D. J. Sherratt. Spatial and temporal organization of replicating Escherichia coli chromosomes. Molecular Microbiology, 49(3):731–743, 2003. ISSN 0950382X. doi: 10.1046/j.1365-2958.2003.03640.x.

C. Lelong, M. Chevallet, S. Luche, and T. Rabilloud. Two-Dimensional Electrophoresis Protocols. Methods in Molecular Biology, 519:339–350, 2009. doi: 10.1007/978-1-59745-281-6. URL http://www.springerlink.com/index/10.1007/978-1-59745-281-6.

W. Li, Y. Hu, S. Oh, Q. Ma, D. Merkurjev, X. Song, X. Zhou, Z. Liu, B. Tanasa, X. He, A. Y. Chen, K. Ohgi, J. Zhang, W. Liu, and M. G. Rosenfeld. Condensin I and II Complexes License Full Estrogen Receptor α-Dependent Enhancer Activation. Molecular Cell, 59(2): 188–202, jul 2015. ISSN 1097-4164. doi: 10.1016/j.molcel.2015.06.002.

Z. Liang, D. Zickler, M. Prentiss, F. S. Chang, G. Witz, K. Maeshima, and N. Kleckner. Chromosomes Progress to Metaphase in Multiple Discrete Steps via Global Compaction/Expansion Cycles. Cell, 161(5):1124–1137, 2015a. ISSN 00928674. doi: 10.1016/j.cell.2015.04.030. URL http://linkinghub.elsevier.com/retrieve/pii/S0092867415004869.

Z. Liang, D. Zickler, M. Prentiss, F. S. Chang, G. Witz, K. Maeshima, and N. Kleckner. Chromosomes Progress to Metaphase in Multiple Discrete Steps via Global Compaction/Expansion Cycles. Cell, 161(5):1124–1137, 2015b. ISSN 00928674. doi: 10.1016/j.cell.2015.04.030.

E. Lieberman-Aiden, N. L. van Berkum, L. Williams, M. Imakaev, T. Ragoczy, A. Telling, I. Amit, B. R. Lajoie, P. J. Sabo, M. O. Dorschner, R. Sandstrom, B. Bernstein, M. A. Bender, M. Groudine, A. Gnirke, J. Stamatoyannopoulos, L. A. Mirny, E. S. Lander, and J. Dekker. Comprehensive mapping of long-range interactions reveals folding principles of the human genome. Science, 326(5950):289–93, oct 2009. ISSN 1095-9203. doi: 10.1126/science.1181369. URL http://www.ncbi.nlm.nih.gov/pubmed/19815776http://www.pubmedcentral.nih.gov/articlerender.fcgi?artid=PMC2858594.

M. Linkert, C. T. Rueden, C. Allan, J. M. Burel, W. Moore, A. Patterson, B. Loranger, J. Moore, C. Neves, D. MacDonald, A. Tarkowska, C. Sticco, E. Hill, M. Rossner, K. W. Eliceiri, and J. R. Swedlow. Metadata matters: Access to image data in the real world, 2010. ISSN 00219525.

D. Llères, J. James, S. Swift, D. G. Norman, and A. I. Lamond. Quantitative analysis of chromatin compaction in living cells using FLIM-FRET. The Journal of cell biology, 187(4): 481–96, nov 2009. ISSN 1540-8140. doi: 10.1083/jcb.200907029.

M. S. Longworth, A. Herr, J. Y. Ji, and N. J. Dyson. RBF1 promotes chromatin condensation through a conserved interaction with the Condensin II protein dCAP-D3. Genes and Development, 22(8):1011–1024, 2008. ISSN 08909369. doi: 10.1101/gad.1631508.

K. Maeshima and U. K. Laemmli. A two-step scaffolding model for mitotic chromosome assembly. Developmental Cell, 4(4):467–80, apr 2003. ISSN 1534-5807.

A. Magalska, A. Schellhaus, D. Moreno-Andrés, F. Zanini, A. Schooley, R. Sachdev, H. Schwarz, J. Madlung, and W. Antonin. RuvB-like ATPases Function in Chromatin Decondensation at the End of Mitosis. Developmental Cell, 31(3):305–318, 2014. ISSN 15345807.

doi: 10.1016/j.devcel.2014.09.001. URL http://linkinghub.elsevier.com/retrieve/pii/S1534580714005875.

M. Mandelkern, J. G. Elias, D. Eden, and D. M. Crothers. The dimensions of DNA in solution. Journal of molecular biology, 152(1):153–61, oct 1981. ISSN 0022-2836. doi: 10.1016/0022-2836(81)90099-1.

S. Marguerat, A. Schmidt, S. Codlin, W. Chen, R. Aebersold, and J. Bähler. Quantitative analysis of fission yeast transcriptomes and proteomes in proliferating and quiescent cells. Cell, 151(3):671–83, oct 2012. ISSN 1097-4172. doi: 10.1016/j.cell.2012.09.019. URL http://www.pubmedcentral.nih.gov/articlerender.fcgi?artid=3482660{&}tool=pmcentrez{&}rendertype=abstract.

Y. Matsuo, K. Asakawa, T. Toda, and S. Katayama. A Rapid Method for Protein Extraction from Fission Yeast. Bioscience, Biotechnology, and Biochemistry, 70(8):1992–1994, 2006. ISSN 0916-8451. doi: 10.1271/bbb.60087. URL http://joi.jlc.jst.go.jp/JST.JSTAGE/bbb/60087?from=CrossRef.

T. Matsusaka, N. Imamoto, Y. Yoneda, and M. Yanagida. Mutations in fission yeast Cut15, an importin alpha homolog, lead to mitotic progression without chromosome condensation. Current Biology, 8(18):1031–4, sep 1998. ISSN 0960-9822. doi: 10.1016/S0960-9822(07)00425-3.

A. Matsuyama, A. Shirai, Y. Yashiroda, A. Kamata, S. Horinouchi, and M. Yoshida. pDUAL, a multipurpose, multicopy vector capable of chromosomal integration in fission yeast. Yeast, 21(15):1289–1305, 2004. ISSN 0749503X. doi: 10.1002/yea.1181.

A. Matsuyama, R. Arai, Y. Yashiroda, A. Shirai, A. Kamata, S. Sekido, Y. Kobayashi, A. Hashimoto, M. Hamamoto, Y. Hiraoka, S. Horinouchi, and M. Yoshida. ORFeome cloning and global analysis of protein localization in the fission yeast Schizosaccharomyces pombe. Nature Biotechnology, 24(7):841–7, jul 2006. ISSN 1087-0156. doi: 10.1038/nbt1222. URL http://www.ncbi.nlm.nih.gov/pubmed/16823372.

D. McCarthy, C. Minner, H. Bernstein, and C. Bernstein. DNA elongation rates and growing point distributions of wild-type phage T4 and a DNA-delay amber mutant. Journal of molecular biology, 106(4):963–81, oct 1976. ISSN 0022-2836. doi: 10.1016/0022-2836(76)90346-6. URL http://www.ncbi.nlm.nih.gov/pubmed/789903.

M. D. McDowall, M. A. Harris, A. Lock, K. Rutherford, D. M. Staines, J. Bähler, P. J. Kersey, S. G. Oliver, and V. Wood. PomBase 2015: updates to the fission yeast database. Nucleic Acids Research, 43(Database issue):D656–61, jan 2015. ISSN 1362-4962. doi: 10.1093/nar/gku1040. URL http://www.ncbi.nlm.nih.gov/pubmed/25361970http://www.pubmedcentral.nih.gov/articlerender.fcgi?artid=PMC4383888.

E. M. Medina, J. J. Turner, R. Gordân, J. M. Skotheim, and N. E. Buchler. Punctuated evolution and transitional hybrid network in an ancestral cell cycle of fungi. eLife, 5:1–23, 2016. ISSN 2050-084X. doi: 10.7554/eLife.09492. URL http://elifesciences.org/lookup/doi/10.7554/eLife.09492.

T. E. Melby, C. N. Ciampaglio, G. Briscoe, and H. P. Erickson. The symmetrical structure of structural maintenance of chromosomes (SMC) and MukB proteins: long, antiparallel coiled coils, folded at a flexible hinge. The Journal of cell biology, 142(6):1595–604, sep 1998. ISSN 0021-9525. doi: 10.1083/jcb.142.6.1595. URL http://www.ncbi.nlm.nih.gov/pubmed/9744887http://www.pubmedcentral.nih.gov/articlerender.fcgi?artid=PMC2141774.

M. Meselson and F. W. Stahl. The replication of DNA in Escherichia coli. Proceedings of the National Academy of Sciences, 44(7):671–682, jul 1958. ISSN 0027-8424. doi: 10.1073/pnas.44.7.671.

C. Michaelis, R. Ciosk, and K. Nasmyth. Cohesins: Chromosomal proteins that prevent premature separation of sister chromatids. Cell, 91:35–45, 1997. ISSN 00928674. doi: 10.1016/S0092-8674(01)80007-6.

T. Mizuguchi, G. Fudenberg, S. Mehta, J.-M. Belton, N. Taneja, H. D. Folco, P. FitzGerald, J. Dekker, L. Mirny, J. Barrowman, and S. I. S. Grewal. Cohesin-dependent globules and heterochromatin shape 3D genome architecture in S. pombe. Nature, 516(7531):432–5, dec 2014. ISSN 1476-4687. doi: 10.1038/nature13833. URL http://www.nature.com/doifinder/10.1038/nature13833http://www.ncbi.nlm.nih.gov/pubmed/25307058http://www.pubmedcentral.nih.gov/articlerender.fcgi?artid=PMC4465753.

F. Mora-Bermúdez and J. Ellenberg. Measuring structural dynamics of chromosomes in living cells by fluorescence microscopy. Methods, 41(2):158–167, feb 2007. ISSN 10462023. doi: 10.1016/j.ymeth.2006.07.035. URL http://www.ncbi.nlm.nih.gov/pubmed/17189858http://linkinghub.elsevier.com/retrieve/pii/S1046202306001733.

F. Mora-Bermúdez, D. Gerlich, and J. Ellenberg. Maximal chromosome compaction occurs by axial shortening in anaphase and depends on Aurora kinase. Nature Cell Biology, 9(7):822–31, jul 2007. ISSN 1465-7392. doi: 10.1038/ncb1606. URL http://www.ncbi.nlm.nih.gov/pubmed/17558394.

C. Mülhardt. Der Experimentator Molekularbiologie/Genomics. Springer Berlin Heidelberg, Berlin, Heidelberg, 6 edition, 2009. ISBN 978-3-642-34635-4. doi: 10.1007/978-3-642-34636-1. URL http://link.springer.com/10.1007/978-3-642-34636-1.

K. B. Mullis and F. A. Faloona. Specific synthesis of DNA in vitro via a polymerase-catalyzed chain reaction. Methods in enzymology, 155(C):335–50, 1987. ISSN 0076-6879. doi: 10.1016/0076-6879(87)55023-6. URL http://www.ncbi.nlm.nih.gov/pubmed/3431465.

K. Nagasaka, M. J. Hossain, M. J. Roberti, J. Ellenberg, and T. Hirota. Sister chromatid resolution is an intrinsic part of chromosome organization in prophase. Nature cell biology, 18(6):692–9, jun 2016. ISSN 1476-4679. doi: 10.1038/ncb3353.

N. Nakazawa, R. Mehrotra, M. Ebe, and M. Yanagida. Condensin phosphorylated by the Aurora-B-like kinase Ark1 is continuously required until telophase in a mode distinct from Top2. Journal of Cell Science, 124(Pt 11):1795–807, jun 2011. ISSN 1477-9137. doi: 10.1242/jcs.078733. URL http://www.ncbi.nlm.nih.gov/pubmed/21540296.

N. Naumova, M. Imakaev, G. Fudenberg, Y. Zhan, B. R. Lajoie, L. a. Mirny, and J. Dekker. Organization of the mitotic chromosome. Science, 342(6161):948–53, nov 2013. ISSN 1095-9203. doi: 10.1126/science.1236083. URL http://www.ncbi.nlm.nih.gov/pubmed/24200812.

G. Neurohr and D. W. Gerlich. Assays for mitotic chromosome condensation in live yeast and mammalian cells. Chromosome research, 17(2):145–54, jan 2009. ISSN 1573-6849. doi: 10.1007/s10577-008-9010-1. URL http://www.ncbi.nlm.nih.gov/pubmed/19308697.

K. Nishimura, T. Fukagawa, H. Takisawa, T. Kakimoto, and M. Kanemaki. An auxin-based degron system for the rapid depletion of proteins in nonplant cells. Nature Methods, 6(12):917–22, dec 2009. ISSN 1548-7105. doi: 10.1038/nmeth.1401. URL http://www.nature.com/nmeth/journal/v6/n12/abs/nmeth.1401.htmlhttp://www.ncbi.nlm.nih.gov/pubmed/19915560.

Y. Nishino, M. Eltsov, Y. Joti, K. Ito, H. Takata, Y. Takahashi, S. Hihara, A. S. Frangakis, N. Imamoto, T. Ishikawa, and K. Maeshima. Human mitotic chromosomes consist predominantly of irregularly folded nucleosome fibres without a 30-nm chromatin structure. The EMBO Journal, 31(7):1644–1653, 2012. ISSN 0261-4189. doi: 10.1038/emboj.2012.35. URL http://dx.doi.org/10.1038/emboj.2012.35.

C. Nislow and G. Giaever. 17 Chemical Genomic Tools for Understanding Gene Function and Drug Action. In Methods in Microbiology, volume 36, chapter 17, pages 387–709. 2007. ISBN 0123694787. doi: 10.1016/S0580-9517(06)36017-5. URL http://linkinghub.elsevier.com/retrieve/pii/S0580951706360175.

M. H. H. Nørholm. A mutant Pfu DNA polymerase designed for advanced uracil-excision DNA engineering. BMC biotechnology, 10:21, jan 2010. ISSN 1472-6750. doi: 10.1186/1472-6750-10-21.

F. Notta, S. Zandi, N. Takayama, S. Dobson, O. I. Gan, G. Wilson, K. B. Kaufmann, J. McLeod, E. Laurenti, C. F. Dunant, J. D. McPherson, L. D. Stein, Y. Dror, and J. E. Dick. Distinct routes of lineage development reshape the human blood hierarchy across ontogeny. Science (New York, N.Y.), 351(6269), jan 2016. ISSN 1095-9203. doi: 10.1126/science.aab2116.

K. Okazaki and O. Niwa. mRNAs encoding zinc finger protein isoforms are expressed by alternative splicing of an in-frame intron in fission yeast. DNA research, 7(1):27–30, feb 2000. ISSN 1340-2838. URL http://www.ncbi.nlm.nih.gov/pubmed/10718196.

A. L. Olins and D. E. Olins. Spheroid chromatin units (v bodies). Science, 183(4122):330–2, jan 1974. ISSN 0036-8075. URL http://www.ncbi.nlm.nih.gov/pubmed/4128918.

I. Onn, N. Aono, M. Hirano, and T. Hirano. Reconstitution and subunit geometry of human condensin complexes. The EMBO journal, 26(4):1024–34, feb 2007. ISSN 0261-4189. doi: 10.1038/sj.emboj.7601562. URL http://www.pubmedcentral.nih.gov/articlerender.fcgi?artid=1852836{&}tool=pmcentrez{&}rendertype=abstracthttp://www.ncbi.nlm.nih.gov/pubmed/17268547http://www.pubmedcentral.nih.gov/articlerender.fcgi?artid=PMC1852836.

T. Ono, A. Losada, M. Hirano, M. P. Myers, A. F. Neuwald, and T. Hirano. Differential contributions of condensin I and condensin II to mitotic chromosome architecture in vertebrate cells. Cell, 115(1):109–21, oct 2003. ISSN 0092-8674. URL http://www.ncbi.nlm.nih.gov/pubmed/14532007.

T. Ono, Y. Fang, D. L. Spector, and T. Hirano. Spatial and temporal regulation of Condensins I and II in mitotic chromosome assembly in human cells. Molecular Biology of the Cell, 15 (7):3296–308, jul 2004. ISSN 1059-1524. doi: 10.1091/mbc.E04-03-0242.

T. L. Orr-Weaver, J. W. Szostak, and R. J. Rothstein. Yeast transformation: a model system for the study of recombination. Proceedings of the National Academy of Sciences of the United States of America, 78(10):6354–8, oct 1981. ISSN 0027-8424. doi: 10.1073/pnas.78.10.6354.

J. R. Paulson and U. K. Laemmli. The structure of histone-depleted metaphase chromosomes. Cell, 12(3):817–28, nov 1977. ISSN 0092-8674. doi: 10.1016/0092-8674(77)90280-X.

F. Payre, P. Buono, N. Vanzo, and A. Vincent. Two types of zinc fingers are required for dimerization of the serendipity delta transcriptional activator. Molecular and cellular biology, 17(6):3137–45, jun 1997. ISSN 0270-7306. URL http://www.ncbi.nlm.nih.gov/pubmed/9154812http://www.pubmedcentral.nih.gov/articlerender.fcgi?artid=PMC232166.

X. Peng, R. K. M. Karuturi, L. D. Miller, K. Lin, Y. Jia, P. Kondu, L. Wang, L.-S. Wong, E. T. Liu, M. K. Balasubramanian, and J. Liu. Identification of cell cycle-regulated genes in fission yeast. Molecular Biology of the Cell, 16(3):1026–42, mar 2005. ISSN 1059-1524. doi: 10.1091/mbc.E04-04-0299. URL http://www.ncbi.nlm.nih.gov/pubmed/15616197http://www.pubmedcentral.nih.gov/articlerender.fcgi?artid=PMC551471.

J. Petersen and P. Russell. Growth and the Environment of Schizosaccharomyces pombe. In Fission Yeast: A Laboratory Manual, pages 13–29. Cold Spring Harbor Laboratory Press, mar 2016. doi: 10.1101/pdb.top079764. URL http://www.ncbi.nlm.nih.gov/pubmed/26933253.

B. Petrova. In Vivo Analysis of Chromosome Condensation in Schizosaccharomyces pombe. PhD thesis, Ruperto-Carola University of Heidelberg, 2012.

B. Petrova, S. Dehler, T. Kruitwagen, J.-K. Hériché, K. Miura, and C. H. Haering. Quantitative analysis of chromosome condensation in fission yeast. Molecular and cellular biology, 33(5):984–98, mar 2013. ISSN 1098-5549. doi: 10.1128/MCB.01400-12. URL `http://www.pubmedcentral.nih.gov/articlerender.fcgi?artid=3623070{&}tool=pmcentrez{&}rendertype=abstracthttp://www.ncbi.nlm.nih.gov/pubmed/23263988`.

R. Phillips, J. Kondev, and J. Theriot. Physical Biology of the Cell. Garland Science, 1st edition, 2009. ISBN 978-0-8153-4163-5.

I. Piazza. Structural and biochemical analysis of the non-SMC sub-complex of condensin. PhD thesis, Ruperto-Carola University of Heidelberg, 2013.

I. Piazza, C. H. Haering, and A. Rutkowska. Condensin: crafting the chromosome landscape. Chromosoma, apr 2013. ISSN 1432-0886. doi: 10.1007/s00412-013-0405-1. URL `http://www.ncbi.nlm.nih.gov/pubmed/23546018`.

I. Piazza, A. Rutkowska, A. Ori, M. Walczak, J. Metz, V. Pelechano, M. Beck, and C. H. Haering. Association of condensin with chromosomes depends on DNA binding by its HEAT-repeat subunits. Nature structural & molecular biology, 21(6):560–8, jun 2014. ISSN 1545-9985. doi: 10.1038/nsmb.2831. URL `http://www.ncbi.nlm.nih.gov/pubmed/24837193`.

A. L. Pidoux and R. C. Allshire. Kinetochore and heterochromatin domains of the fission yeast centromere. Chromosome research : an international journal on the molecular, supramolecular and evolutionary aspects of chromosome biology, 12(6):521–34, 2004. ISSN 0967-3849. doi: 10.1023/B:CHRO.0000036586.81775.8b.

E. Piskadlo, R. A. Oliveira, E. Piskadlo, and R. A. Oliveira. Novel insights into mitotic chromosome condensation. F1000Research, 5:1807, 2016. ISSN 2046-1402. doi: 10.12688/f1000research.8727.1. URL `http://f1000research.com/articles/5-1807/v1`.

M. Poirier, S. Eroglu, D. Chatenay, and J. F. Marko. Reversible and irreversible unfolding of mitotic newt chromosomes by applied force. Molecular biology of the cell, 11(1):269–76, jan 2000. ISSN 1059-1524.

M. G. Poirier and J. F. Marko. Mitotic chromosomes are chromatin networks without a mechanically contiguous protein scaffold. Proceedings of the National Academy of Sciences of the United States of America, 99(24):15393–7, nov 2002. ISSN 0027-8424. doi: 10.1073/pnas.232442599.

A. S. Ponticelli, E. P. Sena, and G. R. Smith. Genetic and Physical Analysis of the M26 recombination hotspot of Schizosaccharomyces pombe. Genetics, pages 491–497, 1988.

R Core Team. R: A Language and Environment for Statistical Computing. Vienna, Austria, 2015.

R. N. Rao, N. E. Allen, J. N. Hobbs, W. E. Alborn, H. A. Kirst, and J. W. Paschal. Genetic and enzymatic basis of hygromycin B resistance in Escherichia coli. Antimicrobial agents and chemotherapy, 24(5):689–95, nov 1983. ISSN 0066-4804. doi: 10.1128/AAC..Updated.

R. Remak. Ein Beitrag zur Entwicklungsgeschichte der krebshaften Geschwuelste. Dtsch. Klin., 6, 1854.

N. Rhind, Z. Chen, M. Yassour, D. A. Thompson, B. J. Haas, N. Habib, I. Wapinski, S. Roy, M. F. Lin, D. I. Heiman, S. K. Young, K. Furuya, Y. Guo, A. Pidoux, H. M. Chen, B. Robbertse, J. M. Goldberg, K. Aoki, E. H. Bayne, A. M. Berlin, C. A. Desjardins, E. Dobbs, L. Dukaj, L. Fan, M. G. FitzGerald, C. French, S. Gujja, K. Hansen, D. Keifenheim, J. Z. Levin, R. A. Mosher, C. A. Müller, J. Pfiffner, M. Priest, C. Russ, A. Smialowska, P. Swoboda, S. M. Sykes, M. Vaughn, S. Vengrova, R. Yoder, Q. Zeng, R. Allshire, D. Baulcombe, B. W. Birren, W. Brown, K. Ekwall, M. Kellis, J. Leatherwood, H. Levin, H. Margalit, R. Martienssen, C. A. Nieduszynski, J. W. Spatafora, N. Friedman, J. Z. Dalgaard, P. Baumann, H. Niki, A. Regev, and C. Nusbaum. Comparative functional genomics of the fission yeasts. Science, 332(6032):930–6, may 2011. ISSN 1095-9203. doi: 10.1126/science.1203357.

P. W. Rigby, M. Dieckmann, C. Rhodes, and P. Berg. Labeling deoxyribonucleic acid to high specific activity in vitro by nick translation with DNA polymerase I. Journal of molecular biology, 113(1):237–51, jun 1977. ISSN 0022-2836. doi: 10.1016/0022-2836(77)90052-3.

S. M. Rubin. Deciphering the retinoblastoma protein phosphorylation code. Trends in biochemical sciences, 38(1):12–9, jan 2013. ISSN 0968-0004. doi: 10.1016/j.tibs.2012.10.007.

Y. Saka, T. Sutani, Y. Yamashita, S. Saitoh, M. Takeuchi, Y. Nakaseko, and M. Yanagida. Fission yeast cut3 and cut14, members of a ubiquitous protein family, are required for chromosome condensation and segregation in mitosis. The EMBO journal, 13(20):4938–52, oct 1994. ISSN 0261-4189. URL `http://www.pubmedcentral.nih.gov/articlerender.fcgi?artid=395434{&}tool=pmcentrez{&}rendertype=abstract`.

A. Sakai, K. Hizume, T. Sutani, K. Takeyasu, and M. Yanagida. Condensin but not cohesin SMC heterodimer induces DNA reannealing through protein-protein assembly. The EMBO journal, 22(11):2764–75, jun 2003. ISSN 0261-4189. doi: 10.1093/emboj/cdg247.

S. J. Scharf, G. T. Horn, and H. a. Erlich. Direct cloning and sequence analysis of enzymatically amplified genomic sequences. Science, 233(4768):1076–8, sep 1986. ISSN 0036-8075. doi: 10.1126/science.3461561. URL `http://www.ncbi.nlm.nih.gov/pubmed/3461561`.

C. Schiklenk, B. Petrova, and C. H. Haering. Measuring mitotic chromosome condensation quantitatively in live fission yeast cells by fluorescence microscopy. In K. Yokomori and

K. Shirahige, editors, Cohesin and Condensin. Humana Press, New York, 2016. ISBN 978-1-4939-6545-8. doi: 10.1007/978-1-4939-6545-8. URL http://www.springer.com/us/book/9781493965434.

J. Schindelin, I. Arganda-Carreras, E. Frise, V. Kaynig, M. Longair, T. Pietzsch, S. Preibisch, C. Rueden, S. Saalfeld, B. Schmid, J.-Y. Tinevez, D. J. White, V. Hartenstein, K. Eliceiri, P. Tomancak, and A. Cardona. Fiji: an open-source platform for biological-image analysis. Nature Methods, 9(7):676–82, jul 2012. ISSN 1548-7105. doi: 10.1038/nmeth.2019. URL http://www.pubmedcentral.nih.gov/articlerender.fcgi?artid=3855844{&}tool=pmcentrez{&}rendertype=abstract.

A. Schleiffer, S. Kaitna, S. Maurer-Stroh, M. Glotzer, K. Nasmyth, and F. Eisenhaber. Letter to the Editor Kleisins : A Superfamily of Bacterial and Eukaryotic. Molecular Cell, 11:571–575, 2003.

A. J. Schoeffler and J. M. Berger. Recent advances in understanding structure-function relationships in the type II topoisomerase mechanism. Biochemical Society transactions, 33(Pt 6):1465–70, dec 2005. ISSN 0300-5127. doi: 10.1042/BST20051465.

M. Shimanuki, L. Uehara, T. Pluskal, T. Yoshida, A. Kokubu, Y. Kawasaki, and M. Yanagida. Klf1, a C2H2 zinc finger-transcription factor, is required for cell wall maintenance during long-term quiescence in differentiated G0 phase. PLoS ONE, 8(10):e78545, jan 2013. ISSN 1932-6203. doi: 10.1371/journal.pone.0078545. URL http://www.pubmedcentral.nih.gov/articlerender.fcgi?artid=3805531{&}tool=pmcentrez{&}rendertype=abstract.

X. Shu, N. C. Shaner, C. A. Yarbrough, R. Y. Tsien, and S. J. Remington. Novel chromophores and buried charges control color in mFruits. Biochemistry, 45(32):9639–47, aug 2006. ISSN 0006-2960. doi: 10.1021/bi060773l. URL http://www.ncbi.nlm.nih.gov/pubmed/16893165.

N. Siddappa, A. Avinash, M. Venkatramanan, and U. Ranga. Regeneration of commercial nucleic acid extraction columns without the risk of carryover contamination. BioTechniques, 42(2):186–192, feb 2007. ISSN 0736-6205. doi: 10.2144/000112327. URL http://www.biotechniques.com/article/000112327.

F. Sievers, A. Wilm, D. Dineen, T. J. Gibson, K. Karplus, W. Li, R. Lopez, H. McWilliam, M. Remmert, J. Söding, J. D. Thompson, and D. G. Higgins. Fast, scalable generation of high-quality protein multiple sequence alignments using Clustal Omega. Molecular systems biology, 7(1):539, 2011. ISSN 1744-4292. doi: 10.1038/msb.2011.75. URL http://msb.embopress.org/content/7/1/539.abstracthttp://www.ncbi.nlm.nih.gov/pubmed/21988835http://www.pubmedcentral.nih.gov/articlerender.fcgi?artid=PMC3261699.

D. E. Smith, S. J. Tans, S. B. Smith, S. Grimes, D. L. Anderson, and C. Bustamante. The bacteriophage straight phi29 portal motor can package DNA against a large internal force. Nature, 413(6857):748–52, oct 2001. ISSN 0028-0836. doi: 10.1038/35099581.

URL http://www.nature.com/nature/journal/v413/n6857/abs/413748a0.htmlhttp://www.ncbi.nlm.nih.gov/pubmed/11607035.

A. F. Straight, A. S. Belmont, C. C. Robinett, and A. W. Murray. GFP tagging of budding yeast chromosomes reveals that protein-protein interactions can mediate sister chromatid cohesion. Current Biology, 6(12):1599–1608, 1996. ISSN 09609822. doi: 10.1016/S0960-9822(02)70783-5.

J. E. Stray and J. E. Lindsley. Biochemical analysis of the yeast condensin Smc2/4 complex: an ATPase that promotes knotting of circular DNA. The Journal of biological chemistry, 278(28):26238–48, jul 2003. ISSN 0021-9258. doi: 10.1074/jbc.M302699200.

J. E. Stray, N. J. Crisona, B. P. Belotserkovskii, J. E. Lindsley, and N. R. Cozzarelli. The Saccharomyces cerevisiae Smc2/4 condensin compacts DNA into (+) chiral structures without net supercoiling. The Journal of biological chemistry, 280(41):34723–34, oct 2005. ISSN 0021-9258. doi: 10.1074/jbc.M506589200.

A. V. Strunnikov, V. L. Larionov, and D. Koshland. SMC1: an essential yeast gene encoding a putative head-rod-tail protein is required for nuclear division and defines a new ubiquitous protein family. The Journal of cell biology, 123(6 Pt 2):1635–48, dec 1993. ISSN 0021-9525.

A. V. Strunnikov, E. Hogan, and D. Koshland. SMC2, a Saccharomyces cerevisiae gene essential for chromosome segregation and condensation, defines a subgroup within the SMC family. Genes & development, 9(5):587–99, mar 1995. ISSN 0890-9369. doi: 10.1101/gad.9.5.587.

T. Sutani and M. Yanagida. DNA renaturation activity of the SMC complex implicated in chromosome condensation. Nature, 388(6644):798–801, aug 1997. ISSN 0028-0836. doi: 10.1038/42062.

T. Sutani, T. Yuasa, T. Tomonaga, N. Dohmae, K. Takio, and M. Yanagida. Fission yeast condensin complex: essential roles of non-SMC subunits for condensation and Cdc2 phosphorylation of Cut3/SMC4. Genes & development, 13(17):2271–83, sep 1999. ISSN 0890-9369.

T. Sutani, T. Sakata, R. Nakato, K. Masuda, M. Ishibashi, D. Yamashita, Y. Suzuki, T. Hirano, M. Bando, and K. Shirahige. Condensin targets and reduces unwound DNA structures associated with transcription in mitotic chromosome condensation. Nature Communications, 6:7815, jul 2015. ISSN 2041-1723. doi: 10.1038/ncomms8815.

K. Tada, H. Susumu, T. Sakuno, and Y. Watanabe. Condensin association with histone H2A shapes mitotic chromosomes. Nature, 474(7352):477–83, jun 2011. ISSN 1476-4687. doi: 10.1038/nature10179. URL http://www.ncbi.nlm.nih.gov/pubmed/21633354.

M. E. Tanenbaum, L. a. Gilbert, L. S. Qi, J. S. Weissman, and R. D. Vale. A protein-tagging system for signal amplification in gene expression and fluorescence imaging. Cell, 159(3):635–46, oct 2014. ISSN 1097-4172. doi: 10.1016/j.cell.2014.09.039. URL http://dx.doi.org/

10.1016/j.cell.2014.09.039http://www.ncbi.nlm.nih.gov/pubmed/25307933http://www.pubmedcentral.nih.gov/articlerender.fcgi?artid=PMC4252608.

P. Thévenaz, U. E. Ruttimann, and M. Unser. A pyramid approach to subpixel registration based on intensity. IEEE transactions on image processing : a publication of the IEEE Signal Processing Society, 7(1):27–41, jan 1998. ISSN 1057-7149. doi: 10.1109/83.650848. URL http://www.ncbi.nlm.nih.gov/pubmed/18267377.

H. Thorvaldsdóttir, J. T. Robinson, and J. P. Mesirov. Integrative Genomics Viewer (IGV): high-performance genomics data visualization and exploration. Briefings in bioinformatics, 14(2):178–92, mar 2013. ISSN 1477-4054. doi: 10.1093/bib/bbs017. URL http://www.ncbi.nlm.nih.gov/pubmed/22517427http://www.pubmedcentral.nih.gov/articlerender.fcgi?artid=PMC3603213.

E. Toselli-Mollereau, X. Robellet, L. Fauque, S. Lemaire, C. Schiklenk, C. Klein, C. Hocquet, P. Legros, L. N'Guyen, L. Mouillard, E. Chautard, D. Auboeuf, C. Haering, and P. Bernard. Nucleosome eviction in mitosis assists condensin loading and chromosome condensation. The EMBO Journal, pages 1–17, jun 2016. ISSN 1460-2075. doi: 10.15252/embj.201592849.

P. T. Tran, L. Marsh, V. Doye, S. Inoué, and F. Chang. A mechanism for nuclear positioning in fission yeast based on microtubule pushing. The Journal of cell biology, 153(2):397–411, apr 2001. ISSN 0021-9525. doi: 10.1083/jcb.153.2.397. URL http://jcb.rupress.org/content/153/2/397.shorthttp://www.ncbi.nlm.nih.gov/pubmed/11309419http://www.pubmedcentral.nih.gov/articlerender.fcgi?artid=PMC2169469.

F. Uhlmann. Open questions: Chromosome condensation - why does a chromosome look like a chromosome? BMC biology, 11(January):9, jan 2013. ISSN 1741-7007. doi: 10.1186/1741-7007-11-9.

F. Uhlmann, F. Lottspeich, and K. Nasmyth. Sister-chromatid separation at anaphase onset is promoted by cleavage of the cohesin subunit Scc1. Nature, 400(6739):37–42, jul 1999. ISSN 0028-0836. doi: 10.1038/21831.

F. Uhlmann, D. Wernic, M. a. Poupart, E. V. Koonin, and K. Nasmyth. Cleavage of cohesin by the CD clan protease separin triggers anaphase in yeast. Cell, 103(3):375–386, 2000. ISSN 00928674. doi: 10.1016/S0092-8674(00)00130-6.

K. Umesono, Y. Hiraoka, T. Toda, and M. Yanagida. Visualization of chromosomes in mitotically arrested cells of the fission yeast Schizosaccharomyces pombe. Current genetics, 7(2):123–8, apr 1983. ISSN 0172-8083. doi: 10.1007/BF00365637. URL http://www.ncbi.nlm.nih.gov/pubmed/24173154.

F. van den Ent and J. Löwe. RF cloning: A restriction-free method for inserting target genes into plasmids. Journal of Biochemical and Biophysical Methods, 67(1):67–74, apr 2006.

ISSN 0165022X. doi: 10.1016/j.jbbm.2005.12.008. URL http://linkinghub.elsevier.com/retrieve/pii/S0165022X06000029.

A. C. J. Vas, C. A. Andrews, K. Kirkland Matesky, and D. J. Clarke. In vivo analysis of chromosome condensation in Saccharomyces cerevisiae. Molecular Biology of the Cell, 18 (February):557–568, 2007. ISSN 1059-1524. doi: 10.1091/mbc.E06.

R. Virchow. Cellular-Pathologie. 1855.

A. Wach, A. Brachat, R. Pöhlmann, and P. Philippsen. New heterologous modules for classical or PCR-based gene disruptions in Saccharomyces cerevisiae. Yeast, 10:1793–1808, 1994. ISSN 0749-503X. doi: 10.1002/yea.320101310.

J. C. Wang. Cellular roles of DNA topoisomerases: a molecular perspective. Nature reviews. Molecular cell biology, 3(6):430–40, jun 2002. ISSN 1471-0072. doi: 10.1038/nrm831.

J. D. Watson and F. H. Crick. Molecular structure of nucleic acids; a structure for deoxyribose nucleic acid. Nature, 171(4356):737–8, apr 1953. ISSN 0028-0836. doi: 10.1038/171737a0.

H. Wickham. ggplot2: elegant graphics for data analysis. Springer New York, 2009. ISBN 978-0-387-98140-6.

H. Wickham and R. Francois. dplyr: A Grammar of Data Manipulation. 2015. URL http://cran.r-project.org/package=dplyr.

B. J. Wilkins, N. A. Rall, Y. Ostwal, T. Kruitwagen, K. Hiragami-hamada, M. Winkler, Y. Barral, W. Fischle, and H. Neumann. A Cascade of Histone Modifications in Mitosis. Science, 77(6166):77–80, jan 2014. ISSN 0036-8075. doi: 10.1126/science.1244508. URL http://www.ncbi.nlm.nih.gov/pubmed/24385627.

V. Wood, R. Gwilliam, M.-A. Rajandream, M. Lyne, R. Lyne, A. Stewart, J. Sgouros, N. Peat, J. Hayles, S. Baker, D. Basham, S. Bowman, K. Brooks, D. Brown, S. Brown, T. Chillingworth, C. Churcher, M. Collins, R. Connor, A. Cronin, P. Davis, T. Feltwell, A. Fraser, S. Gentles, A. Goble, N. Hamlin, D. Harris, J. Hidalgo, G. Hodgson, S. Holroyd, T. Hornsby, S. Howarth, E. J. Huckle, S. Hunt, K. Jagels, K. James, L. Jones, M. Jones, S. Leather, S. McDonald, J. McLean, P. Mooney, S. Moule, K. Mungall, L. Murphy, D. Niblett, C. Odell, K. Oliver, S. O'Neil, D. Pearson, M. A. Quail, E. Rabbinowitsch, K. Rutherford, S. Rutter, D. Saunders, K. Seeger, S. Sharp, J. Skelton, M. Simmonds, R. Squares, S. Squares, K. Stevens, K. Taylor, R. G. Taylor, A. Tivey, S. Walsh, T. Warren, S. Whitehead, J. Woodward, G. Volckaert, R. Aert, J. Robben, B. Grymonprez, I. Weltjens, E. Vanstreels, M. Rieger, M. Schäfer, S. Müller-Auer, C. Gabel, M. Fuchs, A. Düsterhöft, C. Fritzc, E. Holzer, D. Moestl, H. Hilbert, K. Borzym, I. Langer, A. Beck, H. Lehrach, R. Reinhardt, T. M. Pohl, P. Eger, W. Zimmermann, H. Wedler, R. Wambutt, B. Purnelle, A. Goffeau, E. Cadieu, S. Dréano, S. Gloux, V. Lelaure, S. Mottier, F. Galibert, S. J. Aves, Z. Xiang, C. Hunt,

K. Moore, S. M. Hurst, M. Lucas, M. Rochet, C. Gaillardin, V. A. Tallada, A. Garzon, G. Thode, R. R. Daga, L. Cruzado, J. Jimenez, M. Sánchez, F. del Rey, J. Benito, A. Domínguez, J. L. Revuelta, S. Moreno, J. Armstrong, S. L. Forsburg, L. Cerutti, T. Lowe, W. R. McCombie, I. Paulsen, J. Potashkin, G. V. Shpakovski, D. Ussery, B. G. Barrell, P. Nurse, and L. Cerrutti. The genome sequence of Schizosaccharomyces pombe. Nature, 415(6874):871–80, feb 2002. ISSN 0028-0836. doi: 10.1038/nature724.

V. Wood, M. a. Harris, M. D. McDowall, K. Rutherford, B. W. Vaughan, D. M. Staines, M. Aslett, A. Lock, J. Bähler, P. J. Kersey, and S. G. Oliver. PomBase: a comprehensive online resource for fission yeast. Nucleic Acids Research, 40(Database issue):D695–9, jan 2012. ISSN 1362-4962. doi: 10.1093/nar/gkr853.

B. Xiao, J. Spencer, A. Clements, N. Ali-Khan, S. Mittnacht, C. Broceño, M. Burghammer, A. Perrakis, R. Marmorstein, and S. J. Gamblin. Crystal structure of the retinoblastoma tumor suppressor protein bound to E2F and the molecular basis of its regulation. Proceedings of the National Academy of Sciences of the United States of America, 100(5):2363–8, mar 2003. ISSN 0027-8424. doi: 10.1073/pnas.0436813100.

T. Yamada, K.-i. Mizuno, K. Hirota, N. Kon, W. P. Wahls, E. Hartsuiker, H. Murofushi, T. Shibata, and K. Ohta. Roles of histone acetylation and chromatin remodeling factor in a meiotic recombination hotspot. The EMBO journal, 23(8):1792–803, apr 2004. ISSN 0261-4189. doi: 10.1038/sj.emboj.7600138.

C. Yanisch-Perron, J. Vieira, and J. Messing. Improved M13 phage cloning vectors and host strains: nucleotide sequences of the M13mp18 and pUC19 vectors. Gene, 33(1):103–19, jan 1985. ISSN 0378-1119. URL `http://www.ncbi.nlm.nih.gov/pubmed/2985470`.

Z. H. Ye and J. K. Bhattacharjee. Lysine biosynthesis pathway and biochemical blocks of lysine auxotrophs of Schizosaccharomyces pombe. Journal of bacteriology, 170(12):5968–70, dec 1988. ISSN 0021-9193.

Y. Zhang, T. Liu, C. A. Meyer, J. Eeckhoute, D. S. Johnson, B. E. Bernstein, C. Nusbaum, R. M. Myers, M. Brown, W. Li, and X. S. Liu. Model-based analysis of ChIP-Seq (MACS). Genome biology, 9(9):R137, 2008. ISSN 1474-760X. doi: 10.1186/gb-2008-9-9-r137.

M. Zofall and S. I. S. Grewal. RNAi-mediated heterochromatin assembly in fission yeast. Cold Spring Harbor Symposia on Quantitative Biology, 71:487–96, 2006. ISSN 0091-7451. doi: 10.1101/sqb.2006.71.059.

D. Zongker. Chicken Chicken Chicken : Chicken Chicken. Annals of Improbable Research, 12 (5), 2006.